105

THE MECHANICAL EFFECTS OF SHORT-CIRCUIT CURENTS IN OPEN AIR SUBSTATIONS

(Rigid and Flexible Bus-Bars)

CIGRE Study Committee 23 (Substations)
Working Group 23-11 (Substations and Environnement)
ESCC Task Force (Effects of Short-Circuit Currents)

Vo:ume 1
An UPDATED REVISION
OF THE CIGRE BROCHURE OF 1987

Volume 2
Data Base OF REFERNCE Tests

April 1996

cigré

CIGRE Study Commitee 23 "Substations" set up the Task Force "Effects of Short-Circuit Currents" (ESCC TF) in Paris in 1992, The Task force is affiliated to Working Group 23-11 "Substations and Environnement".
The Primary objective of the ESCC TF is to update the knowledge on calculation methods for the mechanical effects of short-circuit currents in high voltage open air substations.
The Work of ESCC TF started out from the basis of the CIGRE Technical Brochure "The Mechanical Effects of Short-Circuit Currents in Open Air Substations" prepared by former CIGRE Working Group 23.02 "Effects of High Currents" and published in 1987.

IEC Technical Comitee 73 "Short-Circuit Currents" (IEC TC 73) was set up in 1972 in Stockholm with the scope "to prepare international recommendations for standardized procedures for the calculation of short-circuit currents, and also the thermal, and mechanical effects".
In 1988 IEC Publication 865 "Calculation of the effects of Short-Circuit Currents" could be presented as the first international standard on the assessment of Short-Circuit effects and Short-Circuit strength.

The first edition of IEC 865 as well as of the CIGRE brochure represented the knowledge of 1987 and had limitations in their application. In the Meantime a revision of both seemed indicated and possible. IEC TC 73 presented its second edition 865-1 " Short-Circuit Currents - Calculation of the Effects" in 9.1993 and CIGRE SC23 is now in the position to present the second edition of the Technical Brochure. These new editions together are to be considered as the today knowledge of the field.

The new CIGRE brochure is in two volumes. The first volume deals with simplified and applicable methods for determining mechanical short-circuit stresses and respective design, it is the uptated revision of the former CIGRE brochure of 1987. The second volume can be considered as an application guide to IEC 865-1.

We would like to express our high appreciation for the excellent work of the scientists and engineers who have participated in this project, not forgetting Z. Nartowski, who was the convenor of CIGRE WG 23-02 that produced the first edition of the brochure in 1987.

The Chairman of CIGRE SC23 and IEC TC73, as well as the Convenor of CIGRE WG 23-11 are expressing their hope that the good co-operation in this field will be continued by further, similarly coordinated future activities.

May 1996

C. Dubanton
Chairman of
CIGRE SC23

D. Oeding
Chairman of
IEC TC73

H. Böhme
Convenor of
CIGRE WG 23.11

CIGRE Study Committee 23 (Substations)
Working Group 23-11 (Substations and Environment)
ESCC Task Force (Effects of Short-Circuit currents)

The Mechanical Effects of Short-Circuit Currents in Open Air Substations (Rigid and Flexible Bus-Bars)

Volume 1 :

An updated revision of the CIGRE brochure of 1987

prepared in coordination with :

Technical Committee N°73 (Short-Circuit Currents) of the
International Electrotechnical Commission, Geneva.

April 1996

CONTENTS

		Page
	PREFACE	1
1	INTRODUCTION	
1.1	Short-circuit Currents	4
1.2	Short-Circuit Current Forces	5
1.3	Mechanical Short-Circuit	6
1.3.1	General Phenomena	6
1.3.2	Installations with Rigid Conductors	8
1.3.3	Installations with Flexible Conductors	8
1.4	Substations Characteristics	9
2	TESTING AND MEASUREMENT	
2.1	Introduction	14
2.2	Tests and Experiments	14
2.2.1	Proving Tests	14
2.2.2	Experimental Tests	14
2.2.3	Calculation and Experimental Tests	15
2.3	Types of Short-Circuit Tests	15
2.3.1	Line-to-Line and Three-Phase Short-Circuit	15
2.3.2	Autoreclosure	15
2.3.3	Short-Circuit after initially successful autoreclosure	16
2.3.4	Two-phase Followed by Three-phase Short-Circuit	16
2.3.5	Short-Circuit Initiation and Duration	16
2.4	Testing Arrangements	16
2.5	Measurements	16
2.5.1	Methods and Equipment	16
2.5.2	Data Registration and Processing	18
2.5.3	Measuring Points and Calibration	19
2.6	Mechanical Tests on Insulators	20
2.6.1	Structure-mechanical Properties and Characteristics	21
2.6.2	Withstand Limits	21
2.6.3	Type and Acceptance Tests on Insulators	22
2.6.4	Special Tests on Insulators	22
2.6.5	Material Tests on Specimens	22
2.7	Conclusions	22
3	RIGID BUS SYSTEMS	
3.1	Introduction	23
3.2	Electromagnetic Short-Circuit Forces	23
3.3	Dynamic Response of the System	25
3.4	Calculation Methods	27
3.4.1	Simplified Methods	28
3.4.2	Advanced Methods	30
3.5	Parametric Studies	31
3.5.1	Electrical Parameters	31
3.5.2	Mechanical Parameters	32
3.6	Conclusions	33

Page

4 FLEXIBLE BUS SYSTEMS

4.1 Introduction 34
4.1.1 Simple Method 34
4.1.2 Advanced Methods 34
4.1.3 Bundled Conductor Pinch Effect Calculation 35
4.2 Short-Circuit Tensile Force, Drop Force and Horizontal Displacement-Simple calculation Method 35
4.2.1 General Information 35
4.2.2 Conductor Movement and Tensile Forces 36
4.2.3 Maximum Swing-Out Angle and Angle at the End of the Short-Circuit Current Flow 37
4.2.4 Short-Circuit Tensile Force F_t 41
4.2.5 Drop Force F_f 42
4.2.6 Horizontal Span Displacement and Minimum Air Clearance 43
4.2.7 Extension on Strained Conductors 43
4.2.8 Young's Modulus for Stranded Conductors 44
4.3 Bundled Conductor Pinch Effect Calculation 45
4.3.1 Introduction 45
4.3.2 Pinch Force-Simple Calculation Method 46
4.3.2.1 General Information 46
4.3.2.2 Physical model for regular n-conductor bundles 47
4.3.2.3 Electromagnetic force 48
4.3.2.4 Clashing of sub-conductors 50
4.3.2.5 Non-clashing of sub-conductors 50
4.3.2.6 Dynamic overswing factor 51
4.3.3 Design load 52
4.4 Advanced Calculation Methods 53
4.5 Parameter Analysis 55
4.5.1 Introduction and General Parameters 55
4.5.2 Effects on Tensile Forces F_t and F_f 58
4.5.3 Effects on Deflections 60
4.5.4 Pinch Effects 61
4.5.5 Applications 64

5 GUIDELINES FOR DESIGN

5.1 Introduction 68
5.2 Arrangements 68
5.2.1 Special Aspects of Strain Bus Arrangements 68
5.2.2 Connections to Apparatus 69
5.2.3 Droppers to Apparatus 70
5.2.4. Design of Jumpers 70
5.3 Loads and load combinations 71
5.3.1 Conductors and Insulators 72
5.3.2 Supporting Structures 74
5.4 Conductor Displacement and Temporary Air Clearances 76
5.4.1 Introduction 76
5.4.2 Conductor Displacement 77

6 GENERAL CONCLUSION 80

7 REFERENCES 81

APPENDIX: Calculation of Forces in a Right Angle Bend 88
References 90

THE MECHANICAL EFFECTS OF SHORT-CIRCUIT CURRENTS IN OPEN AIR SUBSTATIONS

An updated revision of the CIGRE brochure of 1987

PREFACE

This revision of the earlier CIGRE brochure, published in 1987 by Study Committee 23, Working Group 23-02, has been written by task force ESCC (Effects of Short-Circuit Currents) of the present CIGRE Working Group 23-11.

Although the text is based on the former brochure, some parts of which explicitly remain unchanged, other sections have been fully modified, and others canceled because they are no longer relevant.

Up-to-date knowledge on short-circuit mechanical effects in open-air substations has logically increased in the last ten years, so that new simplified and advanced methods can now be used with a larger range of applications and better efficiency.

This knowledge will be published in CIGRE in several steps :

- this first step is a full revision of the former brochure, with an updated simplified method. This document supports understanding of the present IEC (TC 73) 865-1. Also new recommendations have been detailed for uprating, refurbishment and new design of open-air substations.
- together with this document, another CIGRE brochure is being published, detailing more than 40 experimental tests, including data and oscillogramms of measured results. This document is an aid for designer to develop an understanding of the physical phenomena, to apply corresponding data in simple methods developed by IEC, and lastly to apply the data for advanced computation methods to validate these methods.
- another CIGRE brochure is under progress inside the ESCC task force to make a new step forward in the determination of actual design loads on structures by taking into account structural dynamics aspects [134, 137, 138, 140], to investigate loads on apparatus connected to the main bus by short flexible connections, to detail comparisons between tests and experiments by advanced methods, to detail recent short-circuit tests on flexible structures, to prepare new design recommendations and to give proposals for safety factor policy. The new brochure will also include DC auxiliary installations.

The short-circuit current levels in HV and EHV networks have been increasing considerably in recent decades and further increases may be expected in some countries in the future. High levels of short-circuit current in substations result in high mechanical stresses and in the case of flexible conductors, displacements on bus systems, connections to apparatus, substation equipment and bus supports.

The subject of this brochure is the mechanical effects of short-circuit currents in HV and EHV open air, conventional substations. The aim of this document is to give design engineers practical information about short-circuit phenomena and calculation methods and to give guidelines for design. The brochure shall serve as a guide for the design engineer, specialized in the problems of substation short-circuit design. It contains little theoretical information. The information included in the brochure is as complete as possible.

In this document, the term "RIGID" busbar is in fact typical aluminium tube on supporting insulators. Of course, this kind of bus has some stiffness (which is taken into account) and is not supposed to be infinitely stiff or rigid.
What is termed "FLEXIBLE" busbar is in fact typical stranded cable (single or bundled) which is fixed to supporting structures by tension and supporting insulators. Generally the bending stiffness can be neglected, except for small span lengths (typical short connection between two apparatuses).

This brochure deals only with open-air substations. GIS substations could also be

subjected to short-circuit mechanical effects, but in that case the interaction with the envelope is not negligible and such applications are outside the scope of this document.

The revision of the brochure has been written by the members of ESCC task force "Effects of High Currents". This task force was composed of both electrical and mechanical specialists, representing theory, research and design.

An alphabetical list of the authors of this brochure follows:

G. Declercq	EDF, France
O. Deter	VEW, Germany
M. El Adnani	Univ. Semlalia, Morocco
G. Ford	Ontario Hydro, Canada
J.L. Lilien (Convener)	Univ. of Liège, Belgium
W. Meyer	Univ. Erlangen-Nürnberg, Germany
A.M. Miri	Univ. Karlsruhe, Germany
R. Nordin	Vattenfall Utveckling AB, Sweden
A. Polevoy	The Israël Electric Corp. Ltd, Israël
N. Stein (Secretary)	FGH, Germany
D. Tsanakas	University Patras, Greece

ESCC task force wishes to acknowledge the large amount of work prepared by Wolfgang Meyer from University of Erlangen-Nürnberg, who described the simplified method developed in his department in coordination with IEC TC 73.

We have reproduced here after, the preface of the former CIGRE brochure published in 1987, to recognize the tremendous amount of work performed by the members of the old CIGRE WG 23-02 and especially the good coordination obtained by Dr. Z. Nartowski from Energoprojekt (Poland) who chaired the former 23-02 WG.

ABSTRACT The mechanical effects of short-circuit currents in open air conventional HV and EHV substations are the subjects of this brochure. In particular, the electromagnetic forces and the resulting stresses appearing in bus systems of both types of conductors, rigid (tubular) and flexible (stranded), are considered.

General descriptions of the phenomena are presented first. Simplified calculation methods are described in order to explain the present IEC (TC73) 865-1 document. Finally, guidelines for design are given which take into consideration both mechanical stresses and conductor displacements caused by short-circuit current.

KEYWORDS Short-circuit, Mechanical effect, Substation, Bus system, Calculation, Design, uprating, refurbishment.

Copies of this brochure can be purchased from:

CIGRE CENTRAL OFFICE
3-5, rue de Metz
F - 75010 Paris, France
Telephone : + 33 (1) 42 46 50 85
Fax : + 33 (1) 42 46 58 27

as from 21st October 1996 :

CIGRE CENTRAL OFFICE
21, rue d'Artois
75008 Paris, France

For further information contact:

N. Stein
FGH
Postfach 810169
D-68201 Mannheim
Germany

1. INDRODUCTION

1.1 Short-Circuit Currents

The calculation of short-circuit currents in AC. systems with nominal voltages up to 245 kV is described in detail in IEC Publication 909 [40], "Short-Circuit calculation in three-phase AC systems.

As shown in Figs. 1.1a and b, short-circuit currents consist of an aperiodic decaying component and a periodic oscillating component. If their amplitudes remain constant during the short-circuit, as in Fig. 1.1a, this is generally known as a far-from-generator short-circuit. If their amplitude decays as in Fig. 1.1b, this is known as a near-to generator short-circuit.

a)

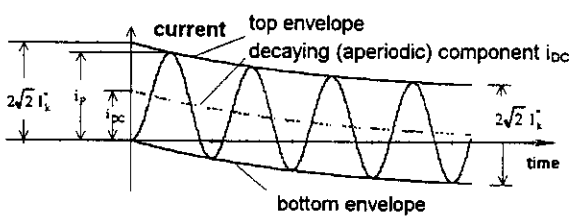

b)

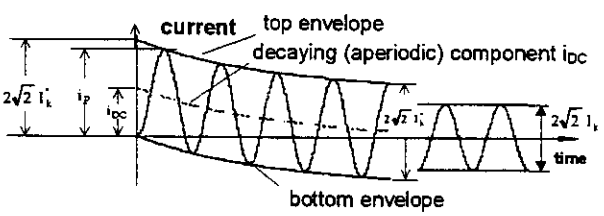

Fig 1.1 Short-Circuit current, schematic diagram [40]

a) far-from-generator
b) near-to-generator
I''_k initial symmetrical short-circuit current
i_p peak short-circuit current
i_{DC} DC (aperiodic) component of short-circuit
I_{DC} initial value of the aperiodic component i_{DC}

A short-circuit current having no AC component decay is defined by

$$i(t) = \sqrt{2} I''_k \left[\sin(\omega t + \varphi_u - \gamma_z) + \sin(\gamma_z - \varphi_u) e^{-t/\tau} \right] \quad (1.1)$$

where φ_u is the voltage phase angle related to the instant at which the fault appears and γ_z is the impedance angle. I''_k can be calculated as described in [40, section 1].

A short-circuit current having an AC component decay is defined by

$$i(t) = \sqrt{2} \left[I_k(t) \sin(\omega t + \varphi_u - \gamma_z) + I''_k \sin(\gamma_z - \varphi_u) e^{-t/\tau} \right] \quad (1.2)$$

where $I_k(t)$ is the time-variable symmetrical short-circuit current (root mean square). It is calculated according to [40, Fig. 16] with decrement factors μ for t = 0.02; 0.05; 0.10 and 0.25 s, based on the usual generator data.

The decrement factor depends on the location of the short-circuit relative to the generator concerned. Therefore, in IEC Publication 865-1, the mechanical loading by short-circuit currents is calculated without decrement factors, i.e. with $I_k(t) = I''_k$ constant.

Fig. 1.2 provides an overview of the main types of short-circuit. A diagram of their quantities is given in [40, Fig. 11]. The equation

$$I''_{k2} = \frac{\sqrt{3}}{2} I''_{k3} \quad (1.3)$$

always applies to the initial symmetrical short-circuit current in the case of a balanced three-phase short-circuit and a line-to-line short-circuit without an earth connection.

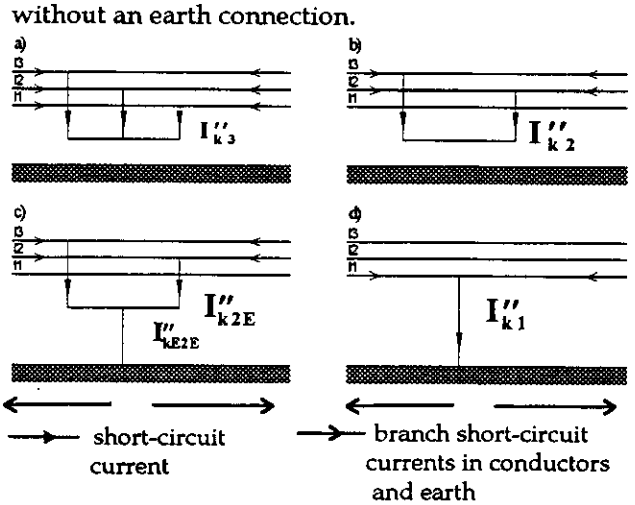

Fig. 1.2: Characterization of short-circuits and their currents [40]. The direction of current arrows has been chosen arbitrarily.

a) balanced three-phase short-circuit
b) line-to-line short-circuit without earth connection
c) line-to-line short-circuit with earth connection
d) line-to earth short-circuit

The peak value i_p of the short-circuit current is reached in the worst case after about one half cycle from the occurrence of the short-circuit at zero voltage. If the short-circuit current flows through a series circuit R+jX consisting of resistance R and reactance X = ω L, then

$$i_p = \kappa\sqrt{2} I''_k \qquad (1.4)$$

and

$$\kappa = 1{,}02 + 0{,}98\, e^{-3R/X} \qquad (1.5)$$

The peak value i_p in radial and meshed networks can be evaluated according to [40] with sufficient accuracy.

Maximum initial symmetrical short-circuit currents I''_k can be expected:

voltage level	I''_k (rms)
123 ... 170 kV	40 kA
245 ... 300 kV	40 kA
362 ... 525 kV	80 kA

1.2 Short-Circuit Current Forces

Short-Circuit currents induce forces in, and deflections of, the current carrying elements (section 1.3). In Fig. 1.3, a conductor carrying current $i_1(t)$ in a magnetic field created by another conductor carrying current $i_2(t)$ undergoes an electromagnetic force defined by the differential

$$d^2 \vec{F}_1 = \frac{\mu_0}{4\pi} i_1(t) i_2(t) \frac{d\vec{s}_1 \times (d\vec{s}_2 \times \vec{a}_{21})}{a_{21}^3} \qquad (1.6)$$

Note that we do not have the reciprocity associated with considering only conductor elements, and that ferromagnetic areas must be represented by their equivalent boundary currents.

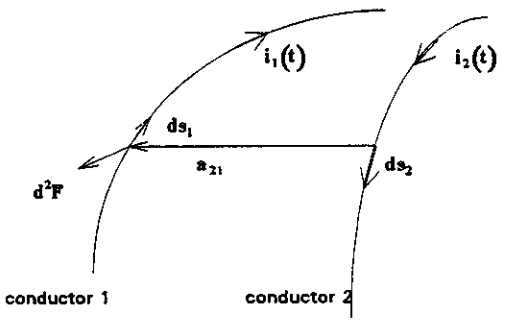

Fig. 1.3: Elementary force d^2F created on conductor 1 by conductor 2.

If, for example, n conductors lie parallel in one plane, the force per unit length is given by the simple algebraic equation

$$F_1 = \frac{\mu_0}{2\pi} i_1(t) \sum_n \frac{i_n(t)}{a_n} \qquad (1.7)$$

a_n : effective distance,
and where 2 parallel conductors are located a distance 'a' apart

$$F_1 = \frac{\mu_0}{2\pi} i_1(t) i_2(t) \frac{l}{a} \qquad (1.8)$$

Where l = the current carrying length.
In other cases, equation (1.6) has to be applied, e.g. for the calculation of edge forces on flexible conductors.

Currents flowing in the same direction produce attractive forces, while opposing currents produce repelling forces.

Equations (1.6 to 1.8) contain the products of time-variable currents. If each current consists only of a DC component and an AC component of frequency f, harmonics of order 0, f and 2 f can be expected in the force spectrum. A more detailed example can be seen in Fig. 3.2.

In the case of installations with rigid conductors, the distances a_n can be considered to be constant; with flexible conductors $a_n(t)$ changes significantly with time. For configurations with three rigid conductors lying parallel in one horizontal plane, Fig. 1.4 a,b shows the force characteristic on the outer conductors and the center conductor during a three-phase short-circuit. Fig. 1.4c shows the force characteristic during a line-to-line short-circuit. The angle of short-circuit initiation selected for φ_u is that which leads to the highest instantaneous force value.

During a symmetrical three-phase short-circuit as illustrated in Fig. 1.4a & b, it is clear that:

- the highest force peak occurs on the center conductor, the steady-state mean is zero
- the peak values are slightly lower on the outer conductors than on the center conductor, the steady-state mean force can have a significant value.

- the force characteristics during a line-to-line short-circuit, illustrated in Fig. 1.4c, are similar to those occurring on the outer conductor during a three-phase short-circuit illustrated in Fig. 1.4b.

Rigid conductors in installations with voltages of 123 kV and higher have natural frequencies which are considerably lower than 50 Hz. Therefore, the mechanical stress follows the force peaks with a delay. The three-phase short-circuit leads to the highest peak forces and sets the pattern for such installations.

For flexible conductors, the line-to-line short-circuit between center and outer conductor is decisive because it results in the smallest air clearances.

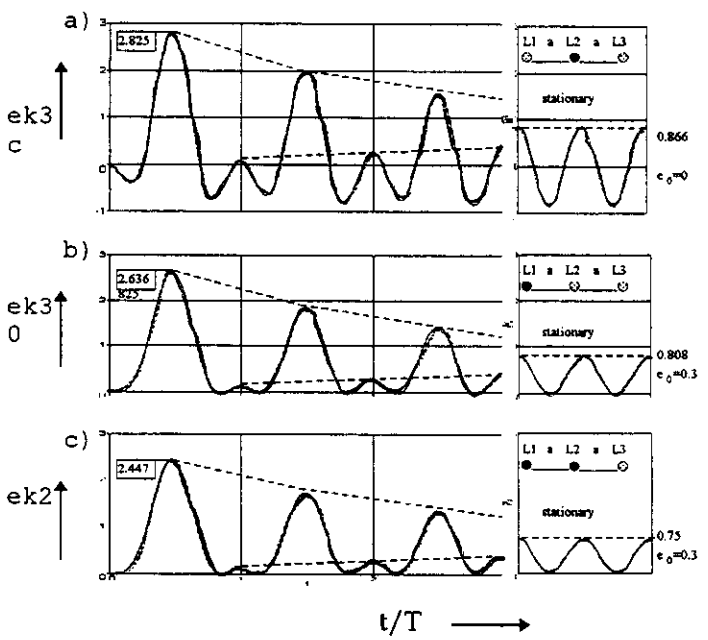

Fig. 1.4 Relative force $e_x(t)$ per unit length (see also Chapter 3.2), worst case, for different phases and short-circuits, when R/X=0.07 [5].

$$F'(t) = \frac{\mu_0}{2\pi a} \cdot \left(\sqrt{2} I''_{k3}\right)^2 \cdot e_x(t)$$

a) balanced three-phase short-circuit, center conductor L2
b) balanced three-phase short-circuit, outer conductor L1 or L3
c) line to line short-circuit

——— complete time functions
– – – envelop of the time functions according to equation (1.10)

Single phase line-to-earth short-circuit currents cause, in many cases, minor stresses due to the large distances to the return path and therefore may be disregarded, except for bundled conductor configurations and special arrangements of busbars with mixed phases.

1.3 Mechanical Short-Circuit Effects

1.3.1 General Phenomena

These effects are the manifestations of the response of the bus system to the exciting short-circuit current forces described in section 1.2. When rating substations in HV systems, the following mechanical quantities and procedures are decisive for short-circuits.

In installations with rigid conductors:

- Bending stresses in the conductors can produce undesirable deformations.
- Forces acting on the connections of the conductors with the insulators impose stress on the fittings and hardware.
- Bending moments are usually highest on the bases of the insulators and substructures and can lead to breakage.

In installations with flexible conductors:

- Tensile forces in the conductors, including their terminations and associated hardware, can lead to damage.
- Forces in the insulators and their substructures can cause yielding or insulator breakage.
- Swing-out of elastically and thermally expanded conductors during short-circuits can be the cause of secondary short-circuits.

For rigid conductors, the systems of equations for calculating the stresses are linear. The different stress components may be superimposed; hence mechanical resonance of conductors at higher harmonic orders must also be considered. For flexible conductors, the systems of equations required to represent the mechanical response of practical bus systems are obviously nonlinear; superposition is not possible. Table 1.1 outlines the most important short-circuit force phenomena.

Short-circuits cause rigid conductors to vibrate and flexible conductor spans to swing or rotate. The quotient:

$$\frac{f_c}{f} = \frac{\text{lowest significant mechanical frequency of conductor}}{\text{electrical frequency of the system}}$$

is an important parameter for all types of motion. Where $f_c / f >> 1$, the stress is proportional to the exciting force. Where $f_c / f << 1$, the stresses are lower, except for harmonic resonances in the case of rigid conductors, and can, in many cases, be further reduced by rapid short-circuit current interruption [32]. Short-Circuit duration T_k is also given by switchgear and protection design and must be considered together (see section 3.5) in normal circumstances or after a tripping on switchgear or protection devices.

In the case of rigid conductors, if the bending moment is measured along the insulator, a slightly curved characteristic is obtained because of inertia [20]. Experience shows that serious damage to busbars, dimensioned in this way, can be avoided.

Table 1.1
Short-Circuit Force Phenomena in HV Installations
with Parallel Conductors Arranged in One Plane

Effect	Installations with	
	rigid conductors	flexible conductors
fc<<f applies for	high voltage	all voltages
Stressing of supports and conductors	by bending moments	by tensile conductor forces
Deflection	small	large
Conductor bending deformation	small	none
Critical short-circuit	three-phase	line to line; three phase short-circuit causes similar force
Conductor subjected to highest stress	outer conductor (high voltage)	-
Voltage phase angle φ_u after voltage zero in the observed conductor, leading to highest peak forces	center conductor L2: $\varphi_u = +75°$ outer conductor L1: $\varphi_u = +165°$ outer conductor L3: $\varphi_u = +75°$	at zero voltage
Effect of three-phase rapid reclosure	significant	swing amplification
Physical model for simplified calculation Method	bending beam [5], section 3.4.1	pendulum [68,104] section 4.3.2
fc of conductor refers to	fundamental components of bending oscillations	swing-out period of pendulum

1.3.2 *Installations with Rigid Conductors*

In outdoor switchgear installations the conductors are usually arranged in one plane [11]. In the case of HV and EHV installations with rigid conductors, the heaviest stresses associated with three-phase short-circuits can be expected on the outer conductors (Eq. 3.1). These stresses occur at approximately the moment of maximum conductor deflection.

The lowest significant mechanical frequency f_c of rigid conductors is typically 2 to 10 Hz in HV installations and is calculated as defined in [39, eq. 16]. In order to deal with installations of all voltage ratings, the force calculations related to rigid conductors, listed in section 3 according to [39], are based on peak short-circuit current i_p for a three-phase short-circuit. Factors exist which describe the dynamic properties of the system excited by the short-circuit current forces under worst case conditions. For mechanical resonances, the harmonic components f and 2f of the exciting force spectrum must also be considered.

1.3.3 *Installations with Flexible Conductors*

The equivalent frequency f_c of installations with flexible conductors during short-circuit can be approximated by comparison with a mathematical pendulum

$$f_c = \frac{1}{2\pi}\sqrt{\frac{\text{Resultant force/unit length cause by gravity and current}}{\text{mass of conductor/unit length} \times \text{conductor sag}}}$$

The equivalent swing-out frequency is lower before than after the short-circuit. The magnitude (in Hz) may be estimated by $f_c = 0.56/\sqrt{\text{sag in meters}}$. In installations with flexible conductors, $f_c / f << 1$ is also valid for small spans, and therefore, the stress calculations are based on the root mean square value of the current I_{rms}. In the case of brief short-circuit durations in particular, this value may be significantly higher than the value of the initial symmetrical short-circuit current I''_k

$$I_{rms} = \sqrt{1 + m}\, I''_k \qquad (1.9)$$

Factor m is shown in Fig. 4.4 according to [39, Fig. 12a] and represents the influence of the DC component on the rms value of the short-circuit current.

When using advanced methods for stress calculations, the nonlinearities require step-by-step methods. The step size may be extended without significant loss of accuracy by omitting the periodic components of the exciting force spectrum. By means of the monotonous decreasing exciting current

$$I_{mon2}(t) = I''_{k2}\sqrt{a_2 + b_2\, e^{-2t/\tau}} \qquad (1.10a)$$

$$I_{mon3}(t) = I''_{k3}\sqrt{a_3 + b_3\, e^{-2t/\tau}} \qquad (1.10b)$$

an equivalent current force acting on the outer conductors may be defined. In the case of line-to-line short-circuits, $a_2 = 1$, $b_2 = 2$; in the case of three-phase short-circuits, $a_3 = 1.5$, $b_3 = 3.232$ with conductor distance 2a according to [5]. These latter factors are valid for outer phase only. For the central bus force, a3 = 0 and b3 = 3.464 (also with conductor distance 2a). The ratio

$$r = \frac{\text{current force per unit length}}{\text{mass per unit length} \cdot g_n}$$

is another important parameter for flexible conductors [78].

In installations with flexible conductors, the stresses occurring in line-to-line short-circuits and balanced three-phase short-circuits are approximately equal. However, for line-to-line short-circuits, conductor swing-out typically results in limiting minimum clearances, (i.e. when adjacent conductors carrying short-circuit current move towards one another after the short-circuit). In the case of a balanced three-phase short-circuit, the center conductor moves only slightly because its inertia and the alternating bi-directional forces which act on it.

Tensile force maxima that are shown in Fig. 1.5: for bundled conductors is F_{pi} soon after short-circuit inception [12], is F_t during the short-circuit after about $f_c \cdot t \approx 0.25$ and is F_f after the short-circuit when the conductor returns near to its initial position. Times t_{pi}, t_t and t_f in Fig. 1.5 usually lie so far apart that they allow the associated maximum stresses to be calculated separately. This makes it possible to apply simplified methods; the unlikely case that bundled conductors would be in the positions of t_t or t_f at precisely the instant of three-phase automatic reclosing can be disregarded.

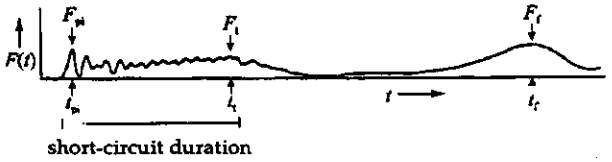

F_{pi} Pinch force
F_t Short-circuit
F_f Drop force
Short -circuit tensile force
Twin bundled slack conductors

Fig. 1.5a Measured tensile force of a flexible conductor bundle during and after a line to line short-circuit

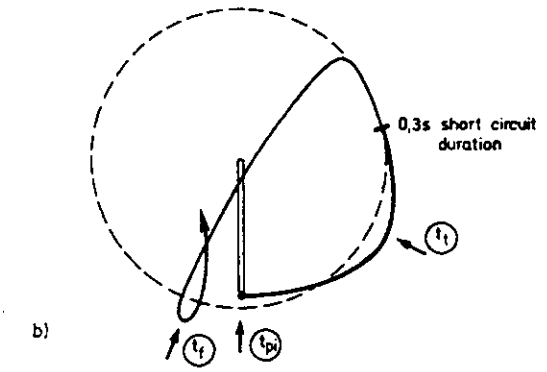

Fig. 1.5b Movement of a flexible conductor during and after a line-to-line short-circuit (schematic)

1.4 Substation Characteristics

The flow of short-circuit current within substations, is particularly important for bus system design. In general, there are two possible locations of faults which influence the distribution of short-circuit current flow in substations: inside the substation and outside the substation.

A fault inside a substation, on a busbar, results in the highest short-circuit current. The fault current level on many of the bus sections will frequently be lower than the total fault current; however in some specific fault situations (for example, at the ends of the busbars) the full addition of all fault currents supplying the fault from connected lines, transformers, etc. will occur.
In the case of a fault outside the substation (for example, in the line or bay connecting a current source) the short-circuit current flowing through any substation part (excepting the faulted bay) is reduced. This is the most common case as a result of the frequency of faults in overhead lines.

Usually the design engineer considers the short-circuit current value on the busbars and assumes the nearest higher standard level value as the base for the short-circuit withstand design of the substation. In substations uprating, the exact calculated short-circuit current value, and the results of the short-circuit current path analysis, may be taken into consideration.

The mechanical effects of short-circuit currents may cause substation failure (in particular insulator breakage). Such failures appear very rarely but are very dangerous for the stability and reliability of the power system. Therefore, designers must ensure substation security against short-circuit effects. To do so, they must have a good understanding of the phenomena and have available calculation methods which make it possible to design the short-circuit capability of substations.

In this brochure, conventional open-air substations are taken into consideration. This type of substation accounts for the majority of existing substations, and will continue to be the design of choice for a considerable number of new substations.

To analyze the mechanical effects of short-circuit currents in substations, we must consider in particular the following components.

- o conductors with their accessories
- o insulators
- o supporting structures.

The other components of substations, such as apparatus, are not considered here because utilities specify a short-circuit withstand and the inherent resistance of the apparatus is guaranteed by the manufacturer.

Short-Circuit mechanical effects within substations depend, in particular, on the types of conductors used for the busbars of the substation and the connections in the bays, namely: rigid conductors (tubes) or flexible ones (cables). The mechanical effects of short-circuit currents in such bus systems, already presented in section 1.3, are quite different in both cases.

As is usual for the analysis of complex phenomena, some typical elementary representative arrangements must be chosen. They do not represent all possible substation configurations; but usually suffice for practical design purposes. The typical elementary arrangement used in substations with rigid conductors is presented in Fig. 1.6. It is part of a three phase busbar.

A substation is usually designed with similar modules. The number of spans varies, and sometimes spans of uneven lengths are used. In some cases it is also necessary to calculate the forces at bus corners, A-frames and right-angle bends. Problems dealing with rigid conductors are discussed in Chapters 3 and 5.

The design of substations with flexible conductors, as shown for example in Fig. 1.7, is much more complicated. The most common arrangements, three-phases in flat and parallel configuration, are presented in Fig. 1.8 [139]. We distinguish here two arrangement cases, which are discussed in this brochure.

- o Case A: horizontal strain bus connected by insulator chains to steel structures (usually portals). Assumed to have no connections with apparatus or structures.
- o Case C: horizontal connection between components

Other cases like :

- o Case B: vertical dropper between strained bus and apparatus
- o Case D: jumpers connecting two strained conductor sections.
- o Case A+B : horizontal strain bus with dropper connections to apparatuses.
- o Case E : end-span droppers (classical or spring loaded)
- o Case F : first span to overhead line

will be documented in the next brochure which is under preparation by the task force. Nevertheless some experimental results are detailed in this brochure for reference cases available at the present time.

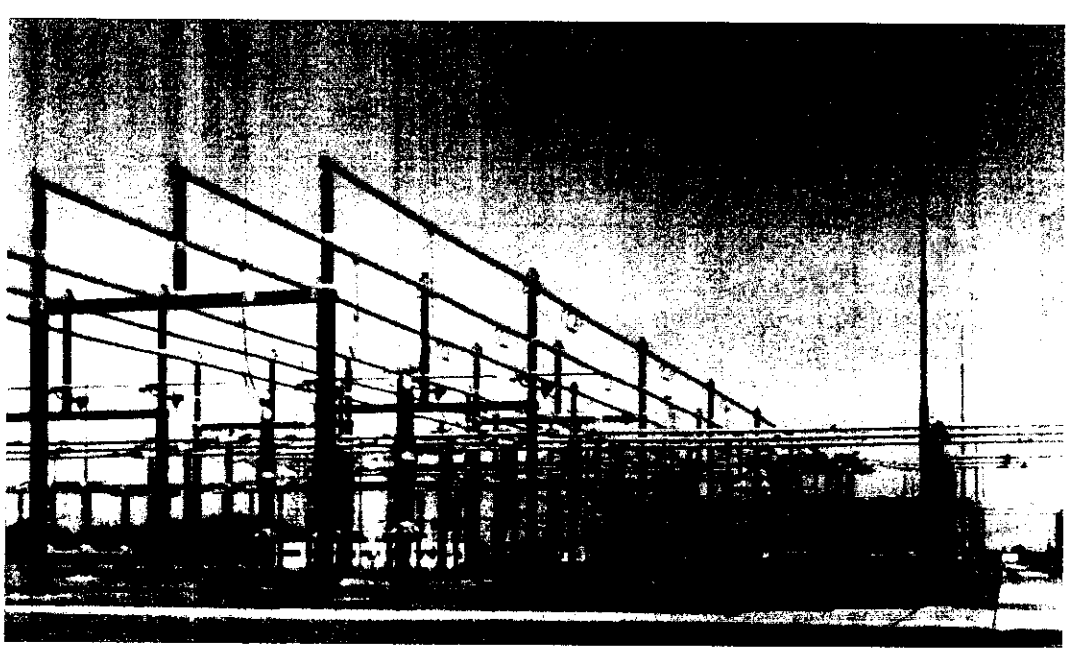

Fig.1.6: Typical arrangement used in substations with rigid conductors

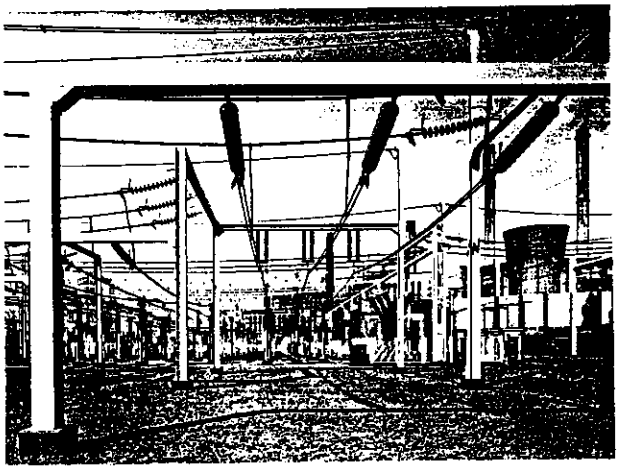

Fig. 1.7 Typical arrangement used in substations with flexible conductors

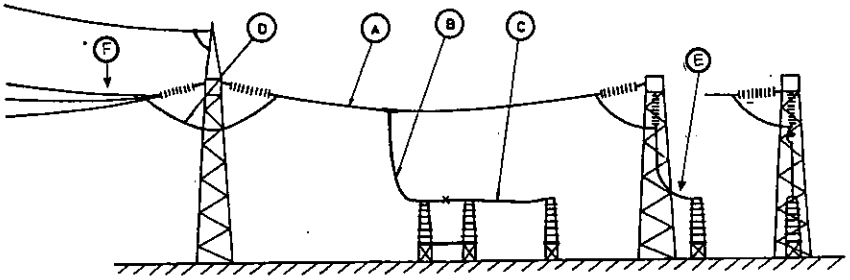

Fig. 1.8 Flexible bus configurations for calculation and tests

- o Case A: horizontal strain bus connected by insulator chains to steel structures
- o Case B: vertical dropper between strained bus and apparatus
- o Case C: horizontal connection between components
- o Case D : jumper connecting two strained onductor sections
- o Case E : end-span droppers (classical or spring loaded)
- o Case F : first span to overhead line

	Rated Voltage (kV)		
	123	245	420
Substations with rigid conductors			
Bay width - (m)	7..10	14..16	20..26
Distance between phases - a(m)	2..2.5	4..8	4.5..10
Busbars span length l (m)	7..20	5..22	8..22
Substations with flexible conduct.			
Bay width (m)	7..10	14..16	20..26
Distance between phases - a(m)	2..2.5	4	5.5..10
Busbars span length - l (m)	7..40	15..45	20..85
Bundled conduct.			
Number of sub-conductors n_s	1..2	1..4	1..4
Distance between subcond. a_s (m)	0.08..0.15	0.08..0.4	0.08..0.6
Distance between spacers - l_s (m)	2..5	2..8	2..30

Table 1.2
Typical Dimensions of Open Air Outdoor Substations

The transition span between the terminating tower of an overhead line and the line entrance portal of the substation is another specific case, not analyzed in this brochure. The flexible conductors used in the above listed cases may be simple cable or bundles, composed of two or more cables. Bundled conductor arrangements are sometimes used to meet ampacity and radio noise (caused by corona) requirements.

The mechanical effects of short-circuit current in the above arrangements depend not only on short-circuit current conditions, but also to a great degree on the geometrical dimensions of the substations and various mechanical parameters which characterize the substation components. These are briefly described in Table 1.2 and 1.3 in reference to conductors (rigid and flexible), insulators (post insulators and insulator chains) and supporting structures.

Rigid conductors (tubes) are usually made from aluminum alloy of great mechanical strength and relatively low electrical resistivity. Rigid bus conductors have typical outer diameters in the range 50-300 mm with wall thickness of 4-12 mm. The maximum tube length is typically 20 m. It is possible to weld the tubes together to obtain very long (some tens of meters) uniform conductors; but such a solution is not usually practical for substation maintenance. The tubes are fixed to post insulators and apparatus by clamps, which are of rigid, hinged or sliding types. Because of their high stiffness and low mass, rigid bus typically vibrates easily [6,55].

The bending mode frequency f_c depends on span length, tube dimensions and the type of fixation.

Steel reinforced, aluminum conductors (ACSR) and aluminum alloy conductors (AAC) are usually used for flexible conductors (cables). Conductor cross-section A ranges from 200 to 1600 mm^2, diameter d from 16 to 52 mm, and mass per unit length m' from 0.5 to 4 kg/m. The span length l, for case A is usually from 10 to 60 m; however, Case C ranges to about 15 m. The jumper length is typically from about 3.5 m for 123 kV substations to about 15 m for the 420 kV substations. In case A, the full span length l between supports must be distinguished from the conductor span length l_c between the end points of insulator chains. As well, the short-circuit current carrying span length, l_F, may be only a part of the conductor length l_c.

Bundled conductors are composed of two to four or more conductors placed with the distance between subconductors a_s, where $0.08 \leq a_s \leq 0.60$ m. This distance is maintained by spacers placed at intervals along the bundle, and the distance between spacers l_s, ranges from 2 to 30 m.

Strained conductors (case A) are usually designed with an initial static stress of relatively low value (in relation to overhead lines) in the order of 10-20 N/mm^2. This is only a small percentage (less than 10%) of the nominal rupture conductor strength. The total sag b (the sum of the cable sag b_c and the insulator string sag component b_i) under this tension amounts to about 3% of the span length. For the maximum permissible temperature of conductors (for example 80 °C), the sag is about 30% greater than the initial sag. In some countries, springs in series with the conductors are used to maintain constant sag, independent from conductor temperature.

Slack conductors, case C, have a still lower stress. The sag in this case amounts to about 8% of the span length. The rigid and flexible conductors in case C are fixed on post insulators. The main mechanical parameters of post insulators are given in Table 1.3. Some parameters, such as natural vibration frequencies and damping, are rarely provided by manufacturers. However, the most important parameter in the design is the choice of insulator cantilever strength.

Strained flexible conductors (case A) are connected to the steel supporting structures (usually portals) with insulator strings or chains. These consist of cap and pin porcelain or glass insulators or long rod porcelain insulators. Insulator chains may be single or doubled in either parallel or V arrangements. The V configuration effectively reduces the horizontal deflection of the fixation point of the strained conductors under short-circuit conditions. The most important mechanical parameters of insulator chains are given in Table 1.3. Note that the rupture strengths of insulator chains are similar to those of conductors.

Typical Data

		Rated Voltage (kV)		
		123	245	420
Post insulators				
Height	m	1..1.7	2.1..2.5	3.15..4.5
Mass	kg	35..200	120..400	250..650
Minimum failing load:				
cantilever strength	kN	4..16	8..16	8..16
Stiffness	N/mm	300..2500	40..200	40..140
First natural frequency	Hz	20..60	7..14	4..12
Damping - log decr	%	2	2	2
Insulator chains				
Length	m	2	3	5
Mass	kg	100..150	120..180	200..300
Rupture strength	kN	70..120	120..240	240..530
Supporting structures for flexible bus (gantries)				
height	m	5..6	8..10	12..15
Stiffness	N/mm	150..1300	500..800	600..3500
first natural frequency	Hz	3..6	3..5	1..4

Table 1.3
Post Insulators, Insulator Chains and Supporting Insulator

Steel supporting structures are typically of two types: portals for strained conductors and columns supporting post insulators or apparatus. These structures, usually made from latticed or solid webbed steel, are described in section 5.3.2.

The mechanical behaviour of such structures is characterized by their spring constant and their mechanical frequency.

Calculation methods for rigid conductors are presented in Chapter 3 and for flexible conductors in Chapter 4. Design guidelines for both cases are given in Chapter 5.

2. TESTING AND MEASUREMENTS

2.1 INDRODUCTION

In recent years, it has been evident that more approaches to calculation based assessment of short-circuit effects are necessary and practical. However, only two methods have essentially remained: (1) the standardized rules of IEC 865, that have been formed the European Standard and (2) the Finite-Element Method (FEM). While the majority of the individual methods in IEC 865 have been developed on the basis of a combination of theoretical studies with extensive experimental test programs, the practical proper application of the FEM, by skilled and experienced engineers, also requires a framework of testing results in the particular field of application.

Testing in this context means full-scale short-circuit tests on original size sections of substations.

For the pure test of short-circuit strength of a particular design, the test result may ultimately be restricted to the question of withstand of the specific design under specific short-circuit conditions. However, to obtain the test results required for the validation of advanced calculation models using FEM techniques, testing must necessarily consist of a wide scale of measurements describing, on the one hand the effects of fully defining short-circuit tests performed for a full range of parameters for the configuration being studied. For the present purposes the latter extensive testing techniques are attributed 'Experimental Tests', and the less extensive and complicated situation 'Proving Tests'.

The collection of test data collected by CIGRE 23.11 ESCC-TF /../ issued at the same time as this brochure is intended to serve as a guide for the sophisticated testing needed for experimental tests, as well as a reference for the application of FEM.

It may be practical in some cases to enlarge the scope - and thus get more detailed answers - of simple proving tests by foreseeing measurements of the kind described earlier. In this way designers can, in supplement to calculation, not only receive a verification of the required withstand capability, but also a contribution to optimal design and a better estimate of reliability.

This chapter reviews the various short-circuit arrangements and in particular the appropriate experimental and measuring techniques.

2.2 TESTS AND EXPERIMENTS

Contrary to rules for apparatus, design requirements regarding short-circuit strength typically leave the choice of method, testing or calculation, unspecified. In the case of testing it is important to distinguish between the two general types of tests, namely 'proving tests' and 'experimental tests', depending on the objective pursued.

2.2.1 *Proving Tests*

Proving tests are typically full scale tests on a substation, or part thereof, usually performed in a testing laboratory to demonstrate the ability of the structure to withstand a specific set of loads. No special measurements are required to achieve this purpose.

2.2.2 *Experimental Tests*

Experimental tests usually involve full-scale tests on a substation, or part thereof, generally performed in a testing laboratory. Such tests are required for the design development, proof of validity and with regard to FEM, the proper application of the calculation method. Experimental tests are necessarily combined with extensive measurements to achieve their objective.
Open air substations, though common, are usually of unique design. This type of substation is therefore not sufficiently numerous that the significant expenditures for generalized type or proving tests, can be justified. If the decision between calculation and tests was simply a question of the costs of applying the method, full scale tests (e.g. [25, 30, 31]) would not be needed. However, the choice between calculation and/or testing in each case is governed by overall economic considerations, taking into account:

- the costs of the tests and/or calculations,
- the number of identical and/or similar installations,
- the significance of design errors relative to the costs of the complete installation(s), taking into account unjustified safety

margins due to uncertainties and the immediate and long-term consequences of failure(s).

The advantages of testing to develop, confirm, validate calculation methods are obvious. The objectives for testing are obviously fulfilled in full scale tests. However, reduced scale testing is sometimes carried out because of limitations on test capability or other constraints. General uncertainty remains with scale model tests deriving from the unavoidable complexities and deviations between the behaviour and responses of the model and full scale configurations.

The obvious advantage of calculation as compared with testing is that the influence of parameter variation can be studied with substantially less effort and cost.

The ultimate proving test or calculation validation is, of course, on site testing - possibly with reduced short-circuit para-meters. This is difficult to achieve in practice, though at least one example with full short-circuit values is given in the literature [14].

2.2.3 *Calculation and Experimental Tests*

All calculation methods introduced for the short-circuit design of bus systems, whether they are so-called simple methods (IEC 865) or detailed structural analysis methods (FEM) require the results of:

(a) tests to assess the static and dynamic, eventually the thermal characteristics and also the withstand limits of the components,

(b) and most important, full scale tests on typical substation arrangements, combined with extensive measurements

- to prove the validity and limits of calculation methods through a variety of single cases covering the field of application,
- to solve problems which are peculiar to the detailed calculation methods (FEM), in that the correct development of such modelling requires the experience of calculations in comparison with measured data from full scale testing.

For these purposes, a really complete and detailed set of data describing the geometrical/structure/mechanical parameters of the complete installation tested and of its individual components is absolutely essential. Without such data a test will represent the singular case, in fact be an enlarged proving test, but will be worthless for the original more general purpose.

2.3 TYPES OF SHORT-CIRCUIT TESTS

In general, the following short-circuit tests are relevant and can be performed for a range of current magnitudes and durations.

2.3.1 *Line-to-Line and Three-Phase Short-Circuit*

All possible types of short-circuits can occur in substations; but both line-to-line and three-phase short-circuits are of most concern from a structural design point of view. As indicated in Fig. 1.4 (Chapter 1), equation (3.4) and (3.5), the maximum magnetic forces on the outer phases generated by three-phase short-circuit have the same time pattern as those generated by line-to-line short-circuit, but they have higher amplitudes. Therefore, the effects of three-phase short-circuit faults can be simulated by two-phase short-circuit testing. The equivalent value of line-to-line short-circuit current to achieve the same force, the asymmetry factor remaining the same, is

$$I_{K2} = 0.808^{1/2}\, I_{K3} = 0.9\, I_{K3}$$

2.3.2 *Autoreclosure*

Unsuccessful autoreclosure leads to a second short-circuit current which may result in a more severe test because the reclosure may occur before the dynamics of the initial fault have damped out.

The duration of the first and of the second short-circuit as well as the pause between the two can vary. The worst case (maximum stress) for a given pause between the two short-circuits occurs when the first short-circuit is terminated at a moment where the mechanical oscillation is at its maximum to the outward, and the second short-circuit is initiated at a maximum of the same oscillation in the opposite direction. Within the practical range, the duration of the pause is of less importance with rigid conductors, the damping of the oscillation being usually low.

With stranded conductors the worst case can be expected for an interval of a half period of the mechanical oscillation.

2.3.3 *Short-Circuit after initially successful autoreclosure*

It is a real possibility with flexible busses, particularly with droppers and jumpers, that the usually very large and consistent movements of the conductors after fault clearing, may lead to close approach or even contact between phase conductors. If this occurs at or after theoretically successful reclosure, the phases are then again energized, this may produce a new short-circuit condition.

2.3.4 *Two-phase Followed by Three-phase Short-Circuit*

In some cases, three-phase short-circuits do not occur spontaneously, but start as a two-phase short-circuit which changes to a three-phase. This case could result in a severe condition with doubling effects similar to the case of the unsuccessful autoreclosure, (2.3.2).

2.3.5 *Short-Circuit Initiation and Duration*

The initiation of individual short-circuit currents - asymmetry -, their duration and effects are discussed in sections 1.3 and 3.5. The worst case for the moment of minimum clearance, is a function more of the pause duration rather than the original short-circuit duration itself, which for the case of unsuccessful autoreclosure, is given above.

2.4 TESTING ARRANGEMENTS

An open air substation is a complex electro-mechanical system which includes bus systems with flexible or rigid conductors, jumpers and dropper connections between components and between lower and upper bus systems, insulators and structures including the apparatus such as discon-nectors, circuit breakers, earthing switches and instrument transformers (Fig. 1.8). To determine the real dynamic behaviour and effects of loads and stresses due to short-circuits full scale testing with very good simulation of parts of the particular sub-stations, including its apparatus, is - from the technical point of view alone - the most practical and reliable method which can be recommended [24, 25, 30, 31, 81, 83].

Mechanical, electrical, thermal and power arc testing of components can be carried out within such a test set-up. In addition, mechanical and electrical testing of a particular piece of apparatus according to IEC or other specifications is also possible.

Testing, especially full scale tests of simulated real parts of substations, has become attractive with the development of laboratory facilities having the capability to perform such realistic full scale tests. Recent papers [24, 25, 30, 31, 81, 83] review the results of full scale tests and compare them with calculations of the short-circuit current stresses on conductors, structures and apparatus. The authors report on the extensive tests performed on original parts of substations and measurements of the dynamic stresses.

In addition to extensive tests, references [7, 25] and [31] compare the results of various tests and measurements with those from calculations according to advanced methods. Their conclusion is that most accurate calculations can be carried out by advanced calculation methods (FEM).

Finally attention is called to the very comprehensive collection of test data newly issued by CIGRE 23.11 ESCC-TF [The mechanical effects of short-circuit currents in open air substation-rigid or flexible bus-bar-, Data Base of reference tests]

2.5 MEASUREMENTS

2.5.1 *Methods and Equipment*

The problems of measurement are mainly related to the fact that, in order to effectively carry out such measurements, the required multi-channel measuring systems (consisting of transducers of mechanical into electrical quantities - e.g. strain gauges, load cells -, amplifiers*), recording equipment and the required connections and wiring) have to operate in an environment of very high electromagnetic interference. This interference is produced by the very high test currents, supply voltages of some 10 kV and the well known interference generated by current making and

breaking operations required by the secondary test equipment.

*) Special strain-gauge amplifiers also supply the voltage for the one diagonal of the Wheatstone bridge beside the amplification of the bridge output signal from the other diagonal.

Practical experience [2, 30] shows that the simplest and easiest method to avoid electromagnetic interference and establish a potential separation between mechanical/electrical transducers and the follow-up units is to employ modulated carrier-frequency systems. A carrier frequency of 5 kHz allows measurements of frequency components up to about 1 kHz, which is usually quite sufficient.

Isolation of the measuring equipment from transducers that have to operate at high-voltage, is not the only advantage of transformer based potential separation that the carrier-frequency technique makes possible. Available amplifier and recording equipment is generally not designed to be used under the extreme environmental conditions associated with short-circuit testing. Usually in-line potential separation and hence channel separation of single-ended devices is required to avoid earth loops, which form an important source of electromagnetic interference.

DC systems may also be used, but require a much more complicated technology to achieve the same effect. No significant experience exists to date, of the use of DC or piezo systems in this field of application.

General guidelines which should be observed to minimize interference and/or to protect personnel and the measuring equipment at the same time are listed below. More detailed advice can be found in the literature [2, 30, 103]:

- Locate instrumentation as far as possible from the source(s) of interference.

- Use full-bridge arrangements of strain gauges to get symmetric wiring and connections; not all gauges need be active. Transducers are usually full bridge.

- Magnetic and electric shielding of transducers, cable connections and equipment is generally not too important for carrier-frequency operated instrumentation, as this type of equipment suppresses service frequency phenomena.

- Select suitable single earthing point(s) for measuring circuit(s), shielding and equipment. The selection generally involves considering the circuitry of the (multi-channel) equipment to avoid multiple earthing points and earth loops.

- The distances between amplifiers and transducers are usually rather long. This may lead to problems of voltage differences between earthed parts at the two ends during a short-circuit test, and especially on occurrence of the necessary switching operations.

  Note in particular that transducers have only weak insulation between active parts and the metallic body. It is therefore of advantage, if no potential separation by other means is possible, to provide transducers at electrically remote earthed positions (e.g. steel structures) with some insulation between the body and this remote-earth potential.

- Select suitable wiring and cabling with respect to conductor and screen arrangement, in terms of cross-section and arrangement of the individual conductors in the cable (twisting, weaving, &c), e.g. the symmetric starfour type cable for connecting the re-commended four-branch full Wheatstone bridge - 1 symmetric pair of conductors for feeding, the other for measurement.

- Establish a suitable arrangement of measuring cables, e.g. direction, elimination of excessive lengths, and so on.

- If the measuring system contains more than one element with single ended in- or output, those elements must be arranged very close to each other and with very short connections in order to avoid earth loops.

- Potential separation for measurements on high-voltage potential has been established with isolation transformers for the carrier frequency for voltages up to some 10 to 20 kV. One transformer is used for feeding the required full bridge, a second for the bridge output signal.

Figure 2.1 gives a practical example of such a device that, is oil insulated and has been tested up to 12 kV.

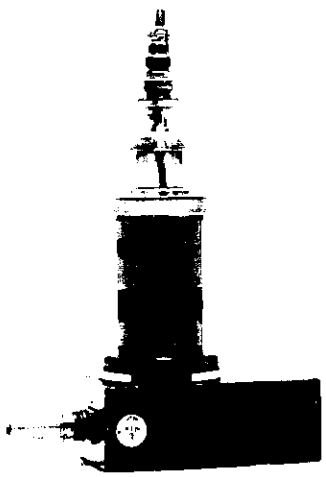

Fig. 2.1 Isolation transformer

- Potential separation between HV and units at ground potential using other means, e.g. fibre optics, require the main part of the measuring chain - the amplifier - battery operated on high potential. Only sensors at practically identical potentials may then be used with the usual multi-channel amplifiers.

  Fibre optics may be used for the connection amplifier to recording units. Galvanic separation (with the choice of multiple earthing points) and avoiding interference on this, possibly long, signal path can be of advantage.

- Last, but not least, the following should be considered: During a short-circuit test the maximum voltage above earth of an earthed test set-up is only the rather low voltage drop along that part of the whole circuit as long as no separation of the current path occurs. In that case, which in short-circuit testing can, of course, not be excluded, the full driving voltage may appear at the energized parts and at the measuring equipment installed there. Reliable potential separation must be guaranteed for this case.

The quantities to be measured on a rigid bus system are generally bending stresses on post insulators, steel supports, tubular conductors and are measured by directly applied strain-gauges.

The calibration of post-insulator and support constraints is preferably done in terms of a bending force instead of strain values.
In the case of flexible conductor arrange-ments, the tension(s) in (sub)conductors and suspension insulators, as well as the stress propagation within steel structures such as portals a various points down to their foundation are the most interesting and important measuring quantities. Forces can be measured by means of force transducers or with strain gauges applied onto an appropriate connecting part. Material stresses must be measured with directly applied strain gauges.

The measurement of displacements, particularly in the case of flexible conductors, is also an important issue. For smaller displacements, electro-optical displacement transducers, ultrasonic position sensors, or electrical displacement transducers can be used with the device itself grounded.

Accelerometers have to be mounted on the movable element, e.g. a conductor. The possible length of their electrical connections may limit the size of the displacement that can be measured; a rigid conductor would pose no problem, but a flexible conductor could. If used immediately on a part carrying the short-circuit current, a nearby and fully rated connection to earth should be provided to protect personnel and the rest of the measuring equipment.

High-speed film cameras and high-speed videography may be used, for small and larger distances from the object. Potential separation is inherent. A recording speed of over 1000 pictures per second, which is readily available for both systems - though at quite different price levels -, is the maximum required. In many cases, e.g. when observing the overall movement of stranded conductors, a lower recording speed of a few hundred pictures per second will be sufficient.

2.5.2 Data Registration and Processing

Conventional registration techniques such as galvanometer-type oscillographs and/or tape recorders may, of course, still be used. Yet, transient recorders operated via computers and a final registration/storage on magnetic/ magnetic-optical media allows much better and easier evaluation and processing of the measured data.

2.5.3 *Measuring Points and Calibration*

Measuring transducers and strain gauge bridges should be placed on conductors and components where maximum stresses are to be expected and/or particularly on sensitive locations where stresses cannot be easily predicted.

Industrially manufactured transducers normally need not be calibrated by the user. Means to reproduce the original calibration of the manufacturer are available from the same manufacturer or that of the amplifiers. The same means are to be used for self-installed strain gauge applications that are intended to measure material strain. Self-installed sensing devices, that are intended to measure forces, e.g. tension, or material constraints in terms of forces, e.g. bending force, have to be calibrated by application of the respective quantity. Linearity and re-peatability should be checked by applying a cycle of different values over the required range. Strain gauge bridges on post insulators and steel supports, for instance, can be calibrated as illustrated in Figure 2.2.

This kind of measurement on post insulators, both separate and together with the steel supporting structure is necessary to obtain the static and dynamic characteristics such as stiffness and eigenfrequencies. Accurate values for these data are necessary as prerequisite for calculation of dynamic stresses and strength.

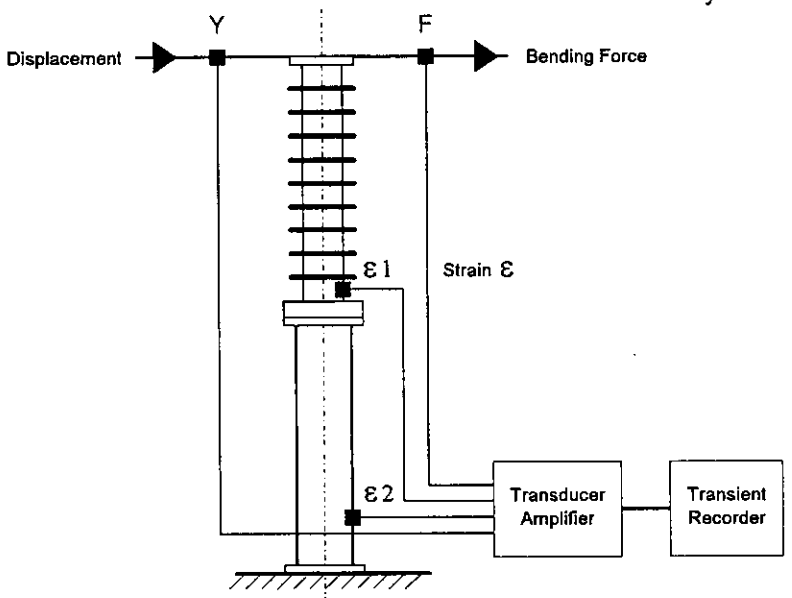

Figure 2.2

-Strain gauge measurement of insulator and support constraints: $\varepsilon = f(F)$
-Measurement of stiffness: $Y = f(F)$
-Measurement of first eigenfrequency and damping
at sudden release of bending force: $Y(t)$ and / or $\varepsilon = f(t)$

As the post insulators are particularly sensitive components of rigid bus systems and of shorter connections of stranded conductors, the determination of their strength and dynamic behaviour is very important. Some results of investigations on post insulators and their strength are given in [26,141,142]. From the static F_{st} according to Fig. 2.2 and displacement Y_{st}, the static stiffness of post insulators can be determined. Measurement of the dynamic response force F_d, for which the frequency may vary, can serve to determine the natural mechanical frequency of the system

If dynamic calibration is not possible, then the mechanical frequencies of insulators can be determined from the static calibration as follows. From static measurements according to Fig. 2.2 we obtain.

$$C = \frac{F_{st}}{Y_{st}} \qquad (2.1)$$

The static deflection of a beam according to Fig. 2.3 can be calculated according to

$$Y_{st} = \frac{F_{st} \cdot l_i^3}{3EJ_0} \cdot \frac{1}{v} \qquad (2.2)$$

From equations (2.1) and (2.2), we obtain

$$EJ_o = \frac{C \cdot l_i^3}{3} \cdot \frac{1}{v} \tag{2.3}$$

The mechanical harmonic frequencies of a beam according to Fig. 2.3 can generally be calculated according to

$$f_n = \frac{\gamma_n^2}{2\pi \cdot l_i^2} \cdot \sqrt{\frac{EJ_o}{m_i}} \tag{2.4}$$

where

$$J_0 = \frac{\pi}{64} \cdot d_{max}^4 \tag{2.5}$$

$$m_i = p \cdot \frac{\pi}{4} \cdot d_{max}^2 = \frac{M_i}{l_i} \cdot \frac{3}{v^2 + v + 1} \tag{2.6}$$

Substituting equations (2.3) and (2.6) in (2.4) gives

$$f_n = \frac{\gamma_n^2}{2\pi} \cdot \sqrt{\frac{C}{M_i} \cdot (v + 1 + \frac{1}{v})} \tag{2.7}$$

where:

γ_n = Eigenvalues according to fig. 2.3c

C = spring constant according to Eqn.(2.1)

M_i = total mass of insulator column in kg

v = d_{min}/d_{max}

2.6 MECHANICAL TESTS ON INSULATORS

In open air substations, insulators are the most fragile components in terms of short-circuit stresses. this is, of course, a result of the lack of a plastic phase (yield) prior to destructive material elongation (strain) or fracture in the case of ceramics or glass.

Strain insulators, as typically employed in substations, do not experience problems in this respect since their loadings are usually much less than their ratings. (Strain insulators with ratings in the same order as the breaking strength of the conductors are readily and economically available.) This cannot be said of post insulators subjected to bending loads in the case of short-circuit. These are typically used in substations for rigid bus supports; but also for disconnectors, breakers, arrestors, measuring transformers, transformer bushings and GIS bushings.

The cross-sections required to withstand a given bending load increase rapidly with the voltage level as the bending moment is proportional to post height or length of the cantilever arm.
Narrower margins of safety have to be tolerated in this case because of the high cost and limited strength capabilities of post insulators. This puts an increased importance on the need for accurate calculation techniques and detailed knowledge of the material properties and mechanical characteristics of post insulators and their support structures.

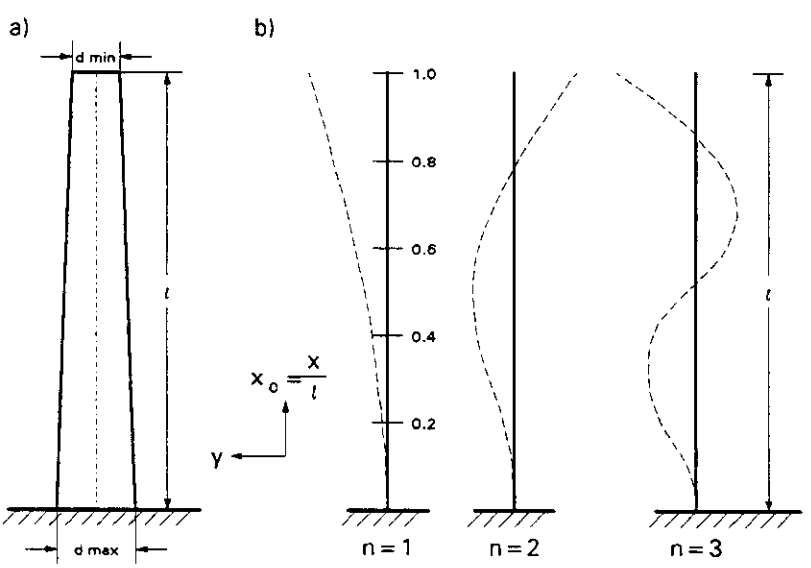

c)

d_{min}/d_{max}	n: 1	1	3	4	5
1.000	1.87510	4.69409	7.85476	10.99554	14.13717
.950	1.83681	4.62351	7.74892	10.85177	13.95464
.900	1.79751	4.55114	7.64037	10.70424	13.76731
.850	1.75710	4.47681	7.52886	10.55265	13.57477
.800	1.71548	4.40037	7.41413	10.39662	13.37656
.750	1.67255	4.32159	7.29588	10.23573	13.17213
.700	1.62814	4.24026	7.17375	10.06949	12.96086
.650	1.58210	4.15608	7.04732	9.89731	12.74199

Fig. 2.3:Eigenvalues of a beam with clamped and free ends (γ_n) with diameters at the ends d_{max} and d_{min} respectively

a) Beam (clamped-free)

b) Some modes of oscillation

c) Eigenvalues γ_n (n = mode number)

2.6.1 *Structure-mechanical Properties and Characteristics*

There is no need to describe details of the assessment of the properties, listed below, of the individual structural parts and their materials. These data are obviously indispensable for modelling insulators:

- geometrical form) > mass distribution
- mass density)
- masses
- Young's moduli

The static and the dynamic performance of insulator models can be checked against measurements of stiffness and eigenfrequency characteristics as discussed in section 2.5. Only in the case of the actual loading, i.e. bedding, need be considered. Measurements of stiffness and eigenfrequency can, and should, be done in the same test set-up (Fig. 2.2). These may relate to just one value of displacement corresponding to one value of static bending force applied. The value of this force and of the corresponding displacement shall be approximately equal to those applied in routine testing. (The so-called hammer method to determine eigenforms usually delivers somewhat too high frequency values for the first eigenform because the exciting force applied is not in that range, i.e. too low.) These measurements can be done together by releasing the insulator in the deflected position (first eigenform) to oscillate into zero position (first eigenfrequency).

Similar measurements and tests on other components and combinations of components subjected to dynamic bending forces, for example steel columns, towers, portals, cross arms, etc., are possible and are increasingly useful the more complex the structure considered.

2.6.2 *Withstand Limits*

When one has obtained, by some method, estimates of the short-circuit loads and/or stress values, they must be compared with estimates of the permissible loads and stresses. Testing is of particular importance in establishing the strength of insulators, and the dynamic, as opposed to the static, nature of the short-circuit loading must be considered. For most practical cases, the assumption of quasi-static insulator behaviour may be adequate to allow operation within permissible bending loads.

Beyond the quasi-static case, actual material stresses must be compared with permissible values. Tests are indispensable in assisting the development and proof of methods to assess material stresses for the short-circuit range of the general dynamic case. In addition, both material strength properties and the overall strengths of insulators can be expected to display considerable statistical variability. Therefore, the number of tests needed to establish withstand values must consider statistical significance requirements.

Based on the above, three types of tests can be identified:

a) Type and acceptance tests on insulators
b) Special tests on insulators
c) Material tests on specimens.

2.6.3 *Type and Acceptance Tests on Insulators*

The only strength data that the manufacturer supplies is the „Minimum Breaking Load" (MBL) of an insulator. This can be considered as a guaranteed value for static loading which is generally derived from statistical test results [35]. The statistical basis for the MBL is not defined by standards, varies considerably, and is usually not provided by the manufacturer. The higher the voltage level, i.e. the cost of an insulator, the oftener this value is checked in acceptance tests on individual lots of insulators. These full-load acceptance tests give a good indication of the quality control consistency achieved and the maximum achievable level of safety.

2.6.4 *Special Tests on Insulators*

Mechanical tests as described in [26, 27, 53], involving extensive strain-gauge and displacement measurements and comparison of static and representative short-circuit insulator loadings, can contribute considerably to the assessment of insulator response to different loadings and the parameters that influence it. Such studies on real insulators, can support or confirm the applicability of material specimen measurements. These tests have brought forth important results that must have influence on the further studies in stress assessment and the practical solution of the problem of strength assessment.

Due to stress concentrations (usually at the points of highest global stress), it is necessary to apply stress-concentration factors (>1), which are particular to the insulator type and location in the insulator, to derive discrete stress values from the bending moment and the core diameter. Further static and dynamic tests, to define stress-concentration factors more precisely are highly recommended.

2.6.5 *Material Tests on Specimens*

The costs of tests on full-size insulators, as described above, whether destructive or not, are so high that it is evident that only the minimum required data will be obtained. As with the application of other materials, e.g. metals, designers have to rely to an extent on strength values derived from tests on material specimens [99, 101].

2.7 CONCLUSIONS

Laboratory tests, especially full-scale tests on sections of a real substation set-up, are justified in some cases. The values of the short-circuit loading and design strength can be varied and an optimal and reliable design obtained. In addition, the electrical, mechanical and thermal testing of the particular components and apparatus can provide beofained combined to reduce the total cost of the testing.
Measurement data obtained during such tests provide supplementary technical information, which is useful in confirming and extending the capabilities of calculation methods.

Yet, the greatest importance of full-scale tests lies in their indispensibility for the validation and application of detailed computing methods (FEM) and the validation of the simple methods, that usually have to be developed under the application of the more detailed methods together with the tests.

3 RIGID BUS SYSTEMS

3.1 Introduction

An arrangement of rigid busbars in one plane is commonly used in modern HV and EHV open air substations. The structure must be strong enough to withstand the significant mechanical stresses created by short-circuit current flow. These stresses appear in the tubular conductors and in the supporting structures typically composed of porcelain insulators and steel substructures.

The verification of calculation methods used for design, and recommendations for proper design procedures were the tasks of CIGRE the now defunct Working Group 23.02. This Working Group published its first report describing measurement methods and a preliminary comparison of test results in 1973 [2]. At the 1976 CIGRE Session, a second report on comparison of calculated and measured values was presented [3]. Lastly, the results of a full comparison between calculated and measured values was presented in [4]. This comparison showed satisfactory consistency of results thereby confirming the accuracy of several calculation methods. Parametric studies and conclusions regarding simplified calculation methods were published in [5] and computer aided approaches in [8]. The results of CIGRE WG 23.02 investigations have been incorporated in IEC 865 (1986) [39] and were taken over to IEC 865-1 (1993) [107] with some modifications. [108] gives examples for calculation with the simplified method.

3.2 Electromagnetic Short-Circuit Forces

Figure 3.1 shows the conductors L1, L2, L3 and the reference directions of the electromagnetic short-circuit forces. The worst case time functions of the forces per unit length acting on conductors L1 or L3 during a three-phase short-circuit $F'_{L1}(t) = F'_{L3}(t)$ are given by (3.1a), on the conductor L2 $F'_{L2}(t)$ by (3.1b)

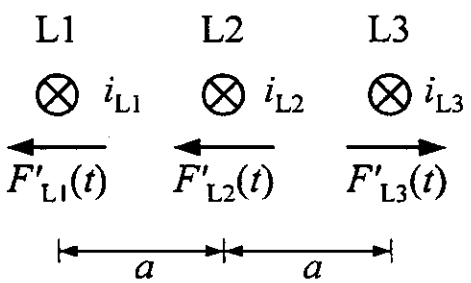

Figure 3.1: Conductor arrangement and reference directions

$$F'_{L1}(t) = F'_{L3}(t) = C' \cdot \frac{\sqrt{3}}{2}\left\{\frac{\sqrt{3}}{4} - \frac{1}{2}\cos(2\omega t - 2\gamma) + e^{-t/\tau}\left[\cos(\omega t - 2\gamma) - \frac{\sqrt{3}}{2}\cos\omega t\right] + e^{-2t/\tau}\left[\frac{\sqrt{3}}{4} - \frac{1}{2}\cos 2\gamma\right]\right\} = C' \cdot e_{L1}(t) = C' \cdot e_{L3}(t) \quad (3.1a)$$

$$F'_{L2}(t) = C' \cdot \frac{\sqrt{3}}{2}\left[-\cos(2\omega t - 2\gamma) + 2e^{-t/\tau}\cos(\omega t - 2\gamma) - e^{-2t/\tau}\cos 2\gamma\right] = C' \cdot e_{L2}(t) \quad (3.1b)$$

and for a line-to-line short circuit $F'_2(t)$ by (3.1c):

$$F'_2(t) = C' \cdot \frac{3}{4}\left[\frac{1}{2} - \frac{1}{2}\cos(2\omega t - 2\gamma) + 2e^{-t/\tau}\sin(\omega t - \gamma)\sin\gamma + e^{-2t/\tau}\sin^2\gamma\right] = C' \cdot e_2(t) \quad (3.1c)$$

where,

$$C' = \frac{\mu_0}{2\pi a} \cdot \left(\sqrt{2} I''_{k3}\right)^2 \quad (3.2)$$

the reference force per unit length,

$\gamma = \arctan X/R$ the impedance angle

X/R reactance to resistance ratio

$$\tau = \frac{L}{R} = \frac{X}{\omega R}$$ the time constant (3.3)

The above functions (3.1) are obtained if the short-circuit is initiated at the following angles after zero of the voltage in phase L1 with $\nu = 0, 1, 2, \ldots$:

- Three-phase short circuit

  L1: $\frac{11\pi}{12} \pm \nu\pi$

  L2: $\frac{5\pi}{12} \pm \nu\frac{\pi}{2}$

  L3: $\frac{5\pi}{12} \pm \nu\pi$

  Thus worse case time function (3.1a) do not occur simultaneously for phase L1 and L3
- Line-to-line short circuit between L2 and L3

  $\frac{\pi}{2} \pm \nu\pi$

  (means zero voltage on both phase L2 and L3)

Figure 1.4 shows the electromagnetic forces according to (3.1). The peak forces are proportional to the square of the factor κ for the peak short-circuit current, see (1.4):

- Three-phase short-circuit, conductor L1 or L3

$$F'_{L1P} = F'_{L3P} = \frac{3+2\sqrt{3}}{8} \cdot C'\kappa^2 = 0{,}808 \cdot C'\kappa^2 \quad (3.4)$$

- Three-phase short-circuit, conductor L2

$$F'_{L2P} = \frac{\sqrt{3}}{2} \cdot C'\kappa^2 = 0{,}866 \cdot C'\kappa^2 \quad (3.5)$$

- Line-to-line short-circuit

$$F'_{L2P} = 0{,}750 \cdot C'\kappa^2 \quad (3.6)$$

The functions (3.1a) to (3.1c) can be broken down into partial functions with different mechanical effects

$$e(t) = \underbrace{e_0 + e_{2\omega}(t)}_{\text{steady state}} + \underbrace{e_g(t) + e_\omega(t)}_{\text{decaying}} \quad (3.7)$$

where

e_0 a constant term (arithmetic mean of $e(t)$ in the steady state)

$e_{2\omega}$ undamped oscillation at double the electrical frequency

e_g exponential term, decaying with a time constant $\tau/2$

e_ω oscillation with electrical frequency, decaying with a time constant τ

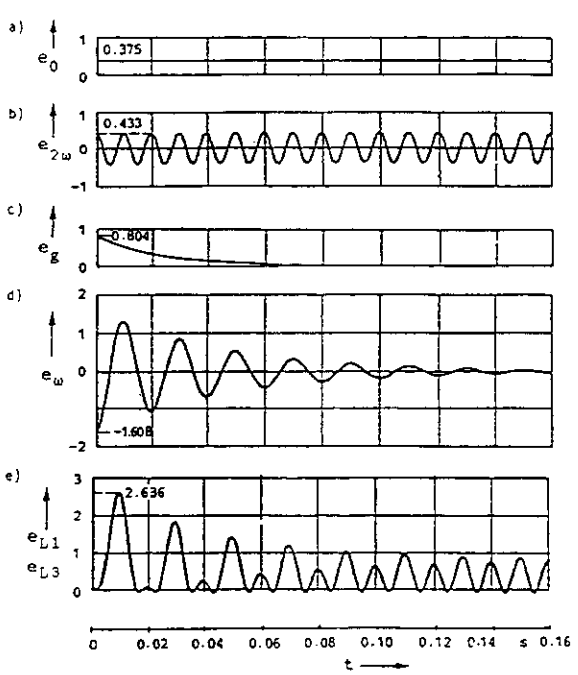

Figure 3.2: Force $e_{L1}(t) = e_{L2}(t)$ according to (3.1a) related to reference force C' for conductors L1 and L2 and the component according to (3.7). $R/X = 0{,}07$ [5]

a) e_0 = constant term

b) $e_{2\omega}$ = undamped oscillation at double the electrical frequency

c) e_g = exponential term, decaying with time constant $\tau/2$

d) e_ω = oscillation with electrical frequency, decaying with time constant τ

e) $e_{L1}(t) = e_{L2}(t) = e_0 + e_{2\omega}(t) + e_g + e_\omega(t)$

Figure 3.2 shows the components of the electromagnetic force according to (3.1a) and (3.7) for the outer conductors L1 and L3.

Table 3.1 gives the maxima of the related electromagnetic forces in (3.1) as well as their components in (3.7).

Table 3.1: Maxima of the related electromagnetic forces and their components

Function	Ratio R/X	Maxima (momentary values)		
		Three-phase short circuit		Line-to-line short circuit
		L2	L1, L3	
e	0	3,464	3,232	3
	0,07	2,825	2,636	2,447
e_0	any	0	0,375	0,375
$e_{2\omega}$	any	0,866	0,433	0,375
e_ω	0	1,723	1,616	1,500
	0,07	1,715	1,608	1,493
e_g	0	0,866	0,808	0,750
	0,07	0,858	0,804	0,746

The time pattern of the forces in Figure 1.4 and investigations of the partial functions in Table 3.1 enable the following comparisons [5]:

a) Comparison of line-to-line short-circuit force, Figure 1.4c, with three-phase short-circuit forces on conductors L1 and L3, Figure 1.4b:

- The constant terms e_0 are of equal magnitude.
- The maxima of all other partial functions are somewhat smaller in the case of the line-to-line short- circuit.
- However, the time patterns of the resultant short-circuit forces are very similar. In the case

of a line-to-line short-circuit, the maxima are 7% smaller than three-phase short-circuit values for all R/X, both for the transient as well as the steady state.

b) Comparison of the force on conductor L2, Figure 1.4a, with forces on conductors L1 and L3, Figure 1.4b, during a three-phase short-circuit:

- The constant term e_0 is of considerable magnitude for conductors L1 and L3 but zero for con ductor L2.
- The maximum of the steady-state double frequent term $e_{2\omega}$ for conductor L2 is twice that for conductors L1 and L3. The maxima of the frequency term e_ω and the exponential term e_g are somewhat larger for L2 than for L1 and L3.
- The time patterns for the resultant forces vary markedly; however, the conductor L2 maximal are only 7% greater for all R/X than the conductors L1 and L3 maxima, both for the transient and the steady state.

It follows from a) that the line-to-line short-circuit stress is somewhat smaller than the three-phase short-circuit stress of the conductors and sub-structures of the outer phases L1 and L3. The line-to-line short circuit needs no further investigations.

Measurement of phase-to-phase short-circuit stresses is more convenient than for three-phase short-circuit stresses; however, the information given by measured data from phase-to-phase tests can be applied to phases L1 and L3 for the three-phase short-circuit condition, but not to phase L2 (see also Chapter 2).

It follows from b) that although the momentary maxima of the forces on L2 are larger than those on L1 and L3, it cannot be determined which phase is stressed the most on the basis of the exciting forces alone. For this purpose, account must also be taken of the mechanical frequencies of the arrangements.

3.3 Dynamic Response of the System

The dynamic effects of the electromagnetic force can be described with the aid of factors:

$$\left.\begin{matrix} v_F(t) \\ v_\sigma(t) \end{matrix}\right\} = \frac{\text{Stress in dynamic case}}{\text{Stress in static case}}$$

where
$v_F(t)$ factor for insulator stress
$v_\sigma(t)$ factor for conductor stress

For static reference values, the electromagnetic force is assumed to be constant and equal to its maximum momentary value. The maximum momentary values of $v_F(t)$ and $v_\sigma(t)$ are characterized in the following paragraphs by V_F and V_σ. The dynamic behaviours of structures during short-circuit, for a range of structural frequencies, are illustrated in Figures 3.3 and 3.4 due to the forces of Figure 1.4.

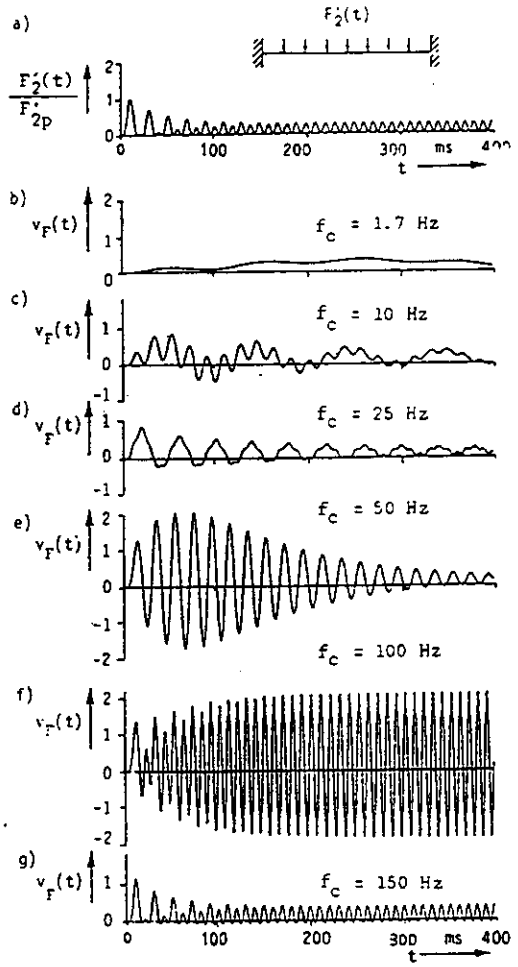

Figure 3.3: Electromagnetic force per unit length for line-to-line short circuit $F'_2(t)$ related to the peak value F'_{2p} (figure a) and coefficient $v_F(t)$ for different mechanical fundamental frequencies f_c (figures b to g). R/X = 0,07; Λ = 0,2 [1, Appendix IV]

If the frequency of the mechanical fundamental oscillation or of a mechanical harmonic oscillation

is equal to the simple or the double electrical frequency, resonance enhancements of the stress will occur. Figure 3.3 shows the factor $v_F(t)$ for line-to-line short-circuits for the mechanical fundamental eigenfrequencies f_c = 1,7 Hz, 10 Hz, 25 Hz, 50 Hz, 100 Hz and 150 Hz. A comparison of Figure 3.2a with Figures 3.2b to 3.2g shows that the time function of the dynamic insulator stress is similar to that of the acting force for only the higher mechanical fundamental frequencies f_c > 150 Hz. For mechanical frequencies $f_c \geq 250$ Hz, there is a practical coincidence of the two time functions and the maximum value of factors V_F and V_σ are approximately equal ($V_F = V_\sigma >> 1$). For low mechanical frequencies and frequencies out of the resonance ranges, $V_F < 1$ and $V_\sigma < 1$. This comparison also shows that even if the maximum instantaneous value of the electromagnetic force occurs approximately 10 ms after the appearance of the fault, the maximum value of the dynamic stress occurs for f_c < 150 Hz much later and depends on the mechanical fundamental frequency.

In Figure 3.3c, $f_c / f = 10/50 = 0.2$. For f_c / f = 0.185, there is a resonance of the third harmonic oscillation with the 50 Hz term of the electromagnetic force. But the 50 Hz harmonic oscillation is also excited for the value $f_c / f = 0.2$, which is close to the resonance value. Figure 3.3e shows the 50 Hz resonance of the mechanical fundamental frequency. Because the term $e_\omega(t)$ of the electromagnetic force is decaying, the corresponding factor $v_F(t)$ also decays after it reaches its maximum value.

Figure 3.3f shows that for the 100 Hz resonance, where the magnitude of the term $e_{2\omega}(t)$ is constant, the maximum instantaneous values of the factor $v_F(t)$ are limited to a maximum value which depends on the value of the mechanical damping decrement Λ. Without damping, these values would increase linearly with time.

The dynamic effects of the electromagnetic force terms of Figure 1.4 are very different and do not result from the maximum instantaneous values of these terms.

Figure 3.4 shows the factors V_σ, for conductors with both ends fixed, as a function of the ratio f_c / f during a three-phase short-circuit, for phases L1 or L3. In order to compare the different curves, factors $V_{\sigma 0}$, $V_{\sigma 2\omega}$, $V_{\sigma g}$, $V_{\sigma\omega}$, and $V_{\sigma 0+g}$ are related to the same static value as the factor V_σ. From comparison of Figures 3.4 and 3.3, it is clear that, especially in the low mechanical frequency range (typically for HV and EHV structures $0.02 < f_c / f < 0.2$), the dynamic effect of short-circuit forces cannot be estimated from the maximum instantaneous values. For example, $f_c / f = 0.1$ corresponds to $V_{\sigma 0}/V_{\sigma 2\omega} = 27.8$ even though the maximum instantaneous value of $e_{2\omega max}$ is greater than e_0, $e_0/e_{2\omega max} = 0.866$.

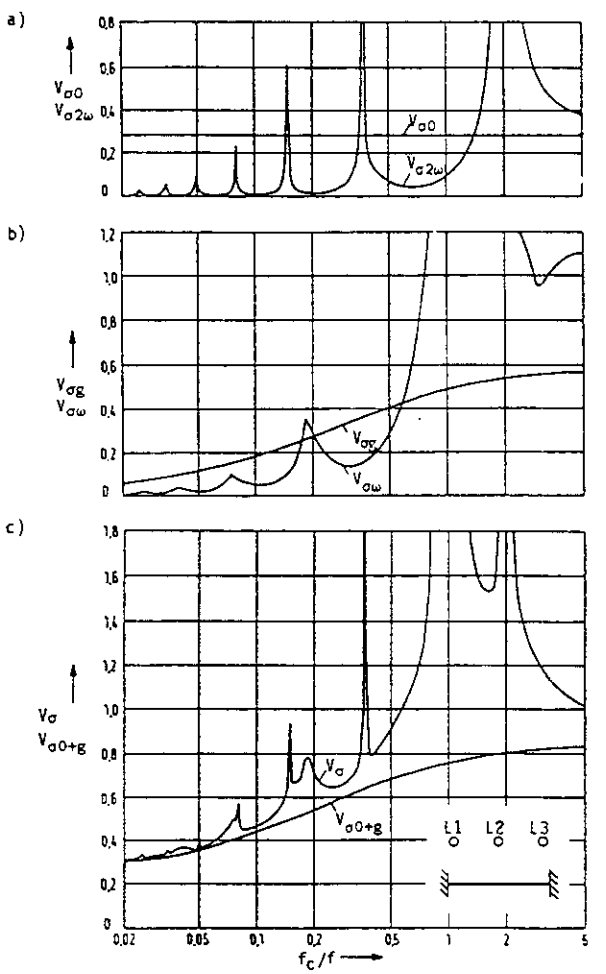

Figure 3.4: Factors V_σ for dynamic stress of the conductors for different time functions of electromagnetic forces of Figure 3.3 [74]

a) $V_{\sigma 0}$ when only e_0 is acting,
$V_{\sigma 2\omega}$ when only $e_{2\omega}(t)$ is acting.
b) $V_{\sigma g}$ when only $e_g(t)$ is acting,
$V_{\sigma\omega}$ when only $e_\omega(t)$ is acting.
c) $V_{\sigma 0+g}$ when only $e_0 + e_g(t)$ is acting,
$V_{\sigma\omega}$ when $e_{L1}(t) = e_0 + e_{2\omega}(t) + e_g(t) + e_\omega(t)$ is acting.

Factors $V_{\sigma 0}$ and $V_{\sigma 2\omega}$ are independent of the ratio R/X. The term $e_{2\omega}(t)$ causes enhancements in the 100 Hz resonance ranges. The effect of this term outside the resonance ranges and for low mechanical frequencies is very small. Figure 3.4b shows the effect of the terms $e_g(t)$ and $e_\omega(t)$ on the factor $V_{\sigma g}$ and $V_{\sigma\omega}$ for $R/X = 0.07$. These factors depend on the ratio R/X. Figure 3.4c illustrates that in the range of the usual HV and EHV structures and outside the resonance ranges, almost all of the dynamic stress is due to the terms $e_0 + e_g(t)$. These results are also valid for the corresponding factors V_F.

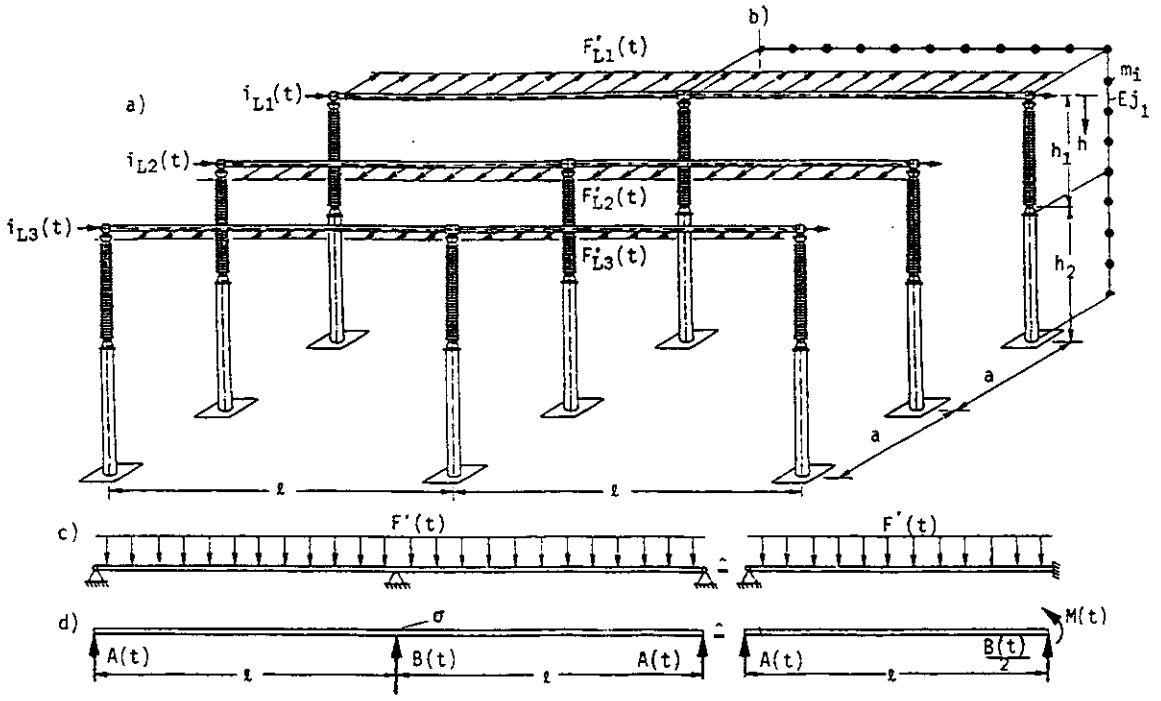

Figure 3.5: Three-phase rigid bus system with two spans, continuous tubes
- a) Physical arrangement
- b) Model for numerical calculation methods; m_i mass element, E Young's modulus, J moment of inertia
- c) Model considering the insulators and the supports as rigid
- d) Forces and moments at the conductor supporting points

3.4 Calculation Methods

Bus structures with rigid conductors consist of parallel conductors, supported by insulators and their substructures (that is, beams within the terms of mechanics), as illustrated in Figure 3.5. Time variant electromagnetic forces act on the conductors during short-circuits; and the whole structure performs forced oscillations for the short-circuit duration and free oscillations after clearing of faults. Different dynamic deflections and stresses (usually bending stresses) appear at every point of the structure. The maximum bending stress in the conductors and in the insulators is of particular interest.

Currently, two classes of methods are in general use:
- simplified methods based on simplified models (e.g. modified static) which yield fast estimates of real results suitable for everyday design purposes.
- advanced methods based on relatively realistic models, which are more cumbersome to use but which can be used to give accurate results for complex configurations

Methods of the first group are especially useful for hand calculation; but should be programmed for design purposes. They are relatively easy and presently are the most commonly used design methods. Application of the advanced methods is computer aided. They are especially useful in cases where more precise knowledge of the busbars or supporting structure responses to short-circuit current forces is required.

3.4.1 *Simplified Methods*

Description

These methods are modified static methods [1, 5, 39, 45, 49, 56]. A simplified calculation can be performed in the following two steps:

1. Static Calculation - for rigid supports, stress values and deflections can be easily determined by well-known static analysis methods. The electromagnetic force per unit length is assumed to be constant and equal to its absolute maximum according to (3.5) in the case of three-phase short-circuits and (3.6) in the case of line-to-line short-circuits.

2. Dynamic Calculation - the dynamic stress values are obtained by multiplication of the static stress values with factors V_F for the insulator stress and V_σ for the conductor stress; the deflection can be calculated in the same way, if desired, using the factor V_σ for approximation (V_F and V_σ were defined in section 3.3.).

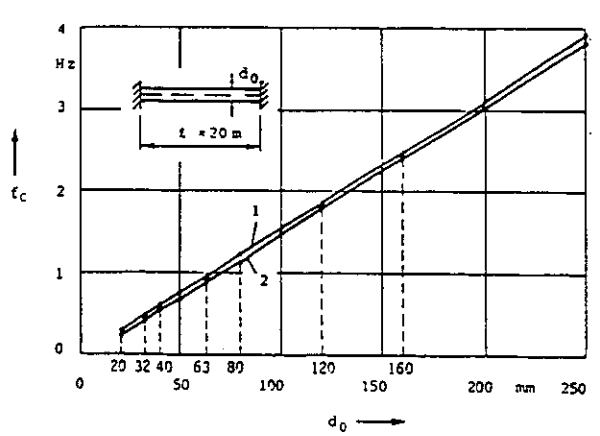

Figure 3.6: Fundamental eigenfrequencies f_c of stiff aluminum tubular busbars, fixed at both ends, l = 20 m, as a function of outer diameter D [5]. (3.8) is used to calculate f_c

1 - smallest standardized wall thickness
2 - largest standardized wall thickness

Note: As the frequency is inversely proportional to the square of the length l, the values for other lengths can be obtained from Figure 3.6 by simple conversion with l^2. The fundamental frequencies for different boundary conditions can also be obtained simply: If the conductor is supported at one end and fixed on the other, the frequencies are to be multiplied by factor 0,689, and by factor 0,441 if both ends are simply supported, see also Table 3.2.

The parametric studies carried out in [5] show that the most important parameter for the calculation of the dynamic short-circuit stress is the mechanical fundamental frequency. In the case of rigid supports, the mechanical fundamental frequency f_c can be easily determined from (3.8) or Figure 3.6; whereas for elastic supports, special computer programs are used. In publications [75, 84] a method is developed to calculate the fundamental mechanical frequency, in the case of elastic supports, without computer programs, using curves [84]. As discussed in [5] conventional high-voltage substations can be assumed to have rigid supports.

The mechanical relevant natural frequency f_c for bending can be calculated with

$$f_c = \frac{\gamma}{2\pi l^2}\sqrt{\frac{EJ}{m'}} \qquad (3.8)$$

where
E Young's modulus
J second moment of the area
m' mass per unit length
l maximum distance between two adjacent supports

γ is a factor dependent on the type and number of supports and given in Table 3.2.

For the type the supports, it is necessary to distinguish between simple and fixed supports. A simple support permits an angular movement at the point of support whereas a fixed support does not permit angular movement. If for $n \geq 2$ the conductor is not continuous but cut in the clamps, the n spans shall be handled as n mechanically single decoupled spans.

Table 3.2: Factors α, β and γ

Type of beam and support		Factor α	$M_{max,el}$ elastic / locus	$M_{max,pl}$ plastic	Factor β	Factor γ
Single span beam	A and B: simple supports 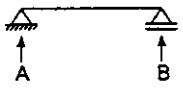	A: 0.5 B: 0.5	$\frac{Fl}{8}$ / $l/2$	$\frac{Fl}{8}$	1	1,57
	A: fixed support B: simple support 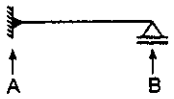	A: 0.625 B: 0.375	$\frac{Fl}{8}$ / A	$\frac{Fl}{11}=\beta\frac{Fl}{8}$	$\frac{8}{11}$	2,45
	A and B: fixed supports 	A: 0.5 B: 0.5	$\frac{Fl}{12}$ / A, B	$\frac{Fl}{16}=\beta\frac{Fl}{8}$	$\frac{8}{16}$	3,56
Continuous beam with equidistant simple supports	two spans 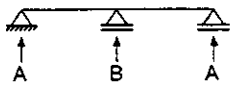	A: 0.375 B: 1.25	$\frac{Fl}{8}$ / B	$\frac{Fl}{11}=\beta\frac{Fl}{8}$	$\frac{8}{11}$	2,45
	three or more spans 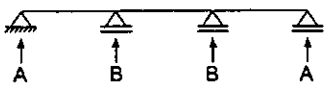	A: 0.4 B: 1.1	$\frac{Fl}{8}$ / B	$\frac{Fl}{11}=\beta\frac{Fl}{8}$	$\frac{8}{11}$	3,56

Three-phase automatic reclosing at the worst time with respect to the mechanical vibration of high-voltage test bus, increases the stress significantly as compared to the case without automatic reclosing [1, 18, 19]. Such increases range up to 95%. The results of parametric studies covering the whole range of relevant natural frequencies are given in [63]. The maximum stress increases can be determined with the aid of the factor V_r:

$$V_r = \frac{\text{dynamic stress with automatic reclosing}}{\text{dynamic stress without automatic reclosing}}$$

Figures 3.7a and 3.7b show the factors V_F, V_σ and V_r, which are proposed in [5] and which form the basis of the simplified method IEC 865-1 [109]. The development of this simplified calculation method is based on extensive parametric studies using several numerical and analytical methods [5] and measurements [3, 4].

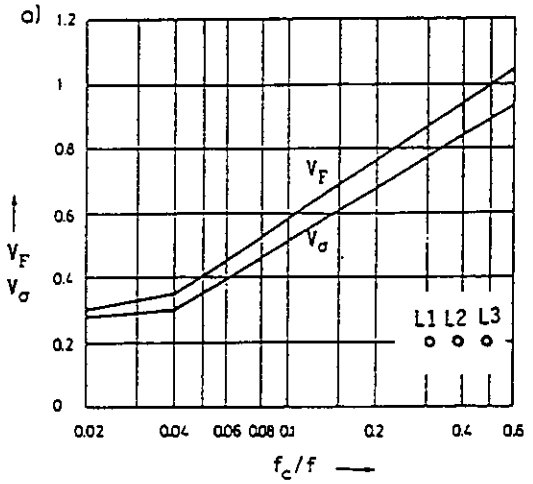

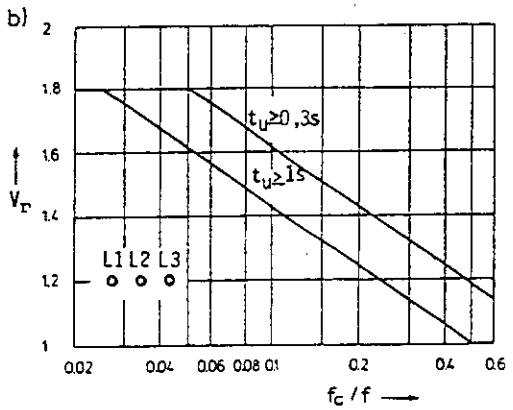

Figure 3.7: Factors V_F, V_σ and V_r for calculating of dynamic stress [4]

a) Factors V_F and V_σ; $0{,}035 \leq R/X \leq 0{,}17$ i. e. $\kappa \geq 1{,}6$. Factors for $R/X \geq 0{,}17$ are given in [74]

b) Factor V_r, t_u is the dead time.

The stress can be effectively reduced if the short-circuit duration is considerably less than half the period of the mechanical fundamental frequency. Curves for V_F and V_σ for practical use are developed in [77, 82] and given in [32, 82].

The short-circuit forces on the supports are given by

$$F_d = V_F V_r \alpha F_m \tag{3.9}$$

where $F_m = F'_{L2p} l$ according to (3.5) for a three-phase system or according to (3.6) for a single-phase system. The factor α is dependent on the type and number of supports. α follows from the rules of statics and is different for inner and outer supports and given in Table 3.2.

The axial forces in the conductors are disregarded and therefore only bending forces exist which lead to the stress in the conductor:

$$\sigma_m = V_\sigma V_r \beta \frac{F_m l}{8Z} \tag{3.10}$$

Z is the section modulus of the conductor. Factor β has a value 1 for a single span beam with simple supports where the highest moment is in the middle of the span, and is the reference arrangement, Table 3.2. In the other cases, it is reached in the ends at A and/or B. Table 3.2 gives the maximum acting moments $M_{max,el}$ in the conductor when the conductor material is in the elastic range. The force can be increased as long as the stress in the fixed ends or in the inner supports is, in the whole cross section, equal to the yield point σ_F. Then the cross section is full plastic. We get a plastic hinge in the clamps, the corresponding acting moment is $M_{max,pl}$ in Table 3.2 [109], and is the ratio related to the reference arrangement.

Further increasing the force leads to plasticity also in a cross section within the span when the yield point σ_F is reached there. This highest possible load is called realistic ultimate load. The corresponding acting moment M_{rul} is equal to the reacting inner moment:

$$M_{rul} = qZ\sigma_F \tag{3.11}$$

with the factor of plasticity q. q differs for the various profiles. For rectangular profile q = 1.5, for circular profile and q = 1.7 for tubes

$$q = 1{,}7 \frac{1-(1-2s/D)^3}{1-(1-2s/D)^4} \tag{3.12}$$

With these assumptions, the conductor is assumed to withstand the short-circuit force when

$$\sigma_m \leq q R_{p0,2} \tag{3.13}$$

with the stress corresponding to the yield point $R_{p0,2}$.

3.4.2 *Advanced Methods*

General remarks

The application of advanced methods requires the use of computers. The relevant computer programs are typically developed by specialists in numerical analysis, rather than by HV and EHV substations design engineers. Therefore substation design engineers require general information regarding which computer methods may be applied and the corresponding results to be expected; and computer specialists require brief information about the substation bus problems and recommendations concerning the proper choice of the method and programs.

In [6] mechanical and mathematical models of busbar structures are presented, as well as a general classification of possible solution methods. Since the problem can be treated as a linear problem of transient structural dynamics, a variety of methods may be applied. The following is a summary of [8] and [4].

Mechanical and mathematical models

Real bus structures can be reasonably modeled by a frame consisting of bars, uniform (conductors, steel pillars) or non-uniform (support insulators), with distributed or concentrated masses. Mechanical and electrical data required in calculations and to characterize these bars (stiffness, mass, eigenfrequencies) are established from their geometry and material properties, if known, and if not from experimental measurements.

If any data are missing, one may use as a first approximation, relations between traction, torsion and bending properties corresponding to circular cross-sections. Note that by neglecting some special effects (for example, local loss of stability in tubular rigid conductors), the mechanical effects caused by short-circuit currents in HV and EHV substations may be described with sufficient accuracy for engineering purposes, by the simple linear theory of dynamic structures. In addition, the study of earthquake effects may be considered by a similar approach.

Due to physical assumptions, real structures are represented by a space frame consisting of a certain number of similar bars subjected to bending, tension and torsion. In engineering practice, a whole space frame is sometimes simplified to one beam [52]. In such a case, the analytical approach is very effective. Further, subsequent simplifications may be introduced; for example, one concentrated mass (ordinary differential equation) or massless beam (static solution only). The models form a theoretical base for the simplified methods which may be used to find a rough approximation of real results.

Solution approaches

Two basic problems of dynamic nature are usually considered:

1. Free vibrations where eigenfrequencies and eigenforms are required.

2. Transient problems, which are the main point of interest in this chapter.

An attempt at a general classification of solution approaches is presented in Figure 3.10 [8].

Finite element methods with step-by-step time integration are presently in most common use because of their numerous advantages, viz.: generality, commercially available software, etc. Because of the linearity of the problem, some general purpose computer programs for dynamic analysis of structures may be successfully applied for calculations of mechanical effects in HV and EHV substation bus systems. Cost savings for analysis may be achieved in practical design cases where configurations and structural data are standardized and relatively simplified, medium accuracy and specially oriented programs may be applied.

Acceptable results can be obtained with four element representations of insulators and eight element models for conductors, (although the influence of discretization is perceivable). More elements are needed when the lowest frequency is less than 3 Hz or when the possibility of resonance exists.

3.5 Parametric Studies

Parametric studies have been carried out by analytical and numerical methods [5, 32, 74]. The influence of electrical and mechanical parameters on the dynamic short-circuit stress throughout the range of relevant natural frequencies was determined, namely:

- time functions of the electromagnetic forces
- short-circuit duration
- unsuccessful automatic reclosing

- mechanical resonances
- mechanical damping
- boundary conditions for the conductor

- elasticity of the support structures
- unequal distances between supports
- number of spans

3.5.1 *Electrical Parameters*

The worst case time functions of the electromagnetic forces of conductor L2 are very different from conductors L1 or L3, (see Figure 3.2). From the electromagnetic forces and investigation of their dynamic effects, it follows that [5]:

- In the range $f_c / f > 1$ (typical of medium and low-voltage busbars structures), the conductor and insulator stress is greater for phase L2 than for phases L1 and L3.

- In the range $f_c / f < 1$ (ranges of resonance with $2f$ being ignored), the stress for L2 is considerably smaller than that for L1 or L3. In HV

and EHV substation range, it is up to about 50% smaller, although the momentary maxima of the electromagnetic force are even greater for L2 than for L1 or L3.

- When the short-circuit duration $T_k \leq 0.1$ s, phase L2 stress in the HV and EHV busbars range $f_c / f \leq 0.2$ is always lower than phases L1 and L3 stress.

- The line-to-line short-circuit stress is somewhat smaller than the three-phase short-circuit stress in the conductors and insulators of the outer phases L1 and L3. Measurement of line-to-line short-circuit stresses is more convenient than for three-phase short-circuit stresses; however, the information, given by measured data from lineto-line tests, can be applied to phases L1 and L3 for the three-phase short-circuit condition, but not to phase L2 (see also Chapter 2).

The time functions of the electromagnetic forces also depend on the ratio R/X (1a), (1b), (3). The V_F and V_σ curves for $R/X = 0.035$ ($\kappa = 1.90$), and $R/X = 0.150$ ($\kappa = 1.64$) cover the usual HV and EHV structure range. Significant differences only arise in the resonance ranges and only slight deviations occur outside these ranges [5].

Resonance enhancements are reduced if the short-circuit duration is restricted. The stress outside the resonance ranges can effectively be reduced only if the short-circuit duration is considerably less than half the period of the mechanical relevant natural frequency. Curves for V_F and V_σ for practical use are developed in [77, 82] and given in [32, 82].

In three-phase automatic reclosing on HV and EHV test stations, considerable increases in stress, compared with the case without automatic reclosing, have been measured [1, 18, 19]. Such increases range to 95%. The results of parametric studies covering the whole range of relevant mechanical natural frequencies are given in [63]. Maximum stress increases can be determined according to [107] with the aid of the factor V_r which is also given in subsection 3.4.1.

3.5.2 *Mechanical Parameters*

Resonance damping and boundary conditions

The influence of mechanical resonance's, mechanical damping and boundary conditions at the ends of buses can be summarized as follows [5]:

- Apart from the fundamental oscillation resonance's, harmonic oscillation resonance's also affect the dynamic stress. These cannot be taken into account with a model of a one or two mass oscillator. Resonance enhancements are generally lower for conductor stress than for insulator stress.

- Mechanical damping is only of major significance in the resonance ranges; outside these ranges it is very slight, even with the comparatively high logarithmic damping decrement $\Lambda = 0.2$. For tubular busbars the value $\Lambda = 0.05$ is appropriate [55]. Mechanical damping can be ignored apart from the case of three-phase automatic reclosing. In numerical calculation methods, stability considerations may well make it worthwhile to take damping into account; however in this case, the calculation should be performed with a small damping value so that any resonance present can be discerned.

- Different boundary conditions for the conductor ends cause shifts in the resonance ranges. Outside these ranges the stresses alter only slightly.

Supports, number of spans and unequal distances

Investigations performed on typical high-voltage arrangements with different mechanical properties of the supports and different boundary con ditions [5, 61] show:

- Elastic supports cause a shift in the harmonic oscillation resonance's [75] and a reduction of the resonance enhancements as compared to the rigid support arrangements. The stress outside these resonance ranges, above all in the mechanical relevant natural frequency range $f_c / f \leq 0.1$, is not significantly influenced by the elasticity of the supports.
- The maximum dynamic bending moment in the supports increases approximately linearly with distance h [20]. For Figure 3.5 the maximum bending moment at the base of the insulators is $A_{max} h_1$ or $B_{max} h_1$ and at the base of the substructures correspondingly $A_{max}(h_1+h_2)$ or $B_{max}(h_1 + h_2)$.

- Investigation shows that the influence of the number of spans n is not large if $n > 3$; therefore multispan arrangements can be suitably represented by three spans.

- Arrangements with unequal distances between supports can generally be treated with sufficient accuracy if all spans are assumed to have the largest occurring distance between supports. Thereby, at most, the end insulators are stressed as severely as the inner insulators. Very short distances between supports, measuring less than 20% of adjacent distances between supports, are best avoided. If this is not possible, the conductors can be decoupled by means of flexible joints.

3.6 Conclusions

The simplified calculation method as presented and according to [107] is feasible and expedient for design purposes in most cases. This method is based on extensive parametric studies using numerical and analytical methods and was verified by measurements in HV and EHV substations carried out by WG 23.02. The application of the IEC 865-1 method is easy and the accuracy for most practical structures is adequate.

Advanced methods are needed mainly for:

- parametric and sensitivity studies
- optimum design of standard structures
- computations for unusual structures
- computations for uprating existing substations for higher short-circuit currents

Advanced methods offer the primary advantage that complex structures may be analyzed in detail including both the busbars and the support structure. When structural data are accurately known, high and controlled calculation accuracy may be achieved. However, in practical situations, data for foundations, insulators and joints are not well known and additional measurements may be needed to ensure accurate final results. General purpose programs for structural dynamics may be adapted for bus system design, and as well, various specific, less costly programs have been developed which allow fast computations for cases which are not too complex.

Assumed boundary conditions for the bus system and other structural data are inevitably imprecise and that this can cause considerable deviations in calculation results for mechanical frequencies and stresses. In order to achieve reliable results, the model data should be varied within the range of possible inaccuracies. In practice, typical substations have a large number of bus arrangements; therefore, such sensitivity studies must be performed. Simplified methods such as IEC 865-1 calculation method has the advantage to give access "instantaneously" to these boundary conditions effects. In fact, it is quite obvious that the maximum stress will occur near the clamped fixation adjacent to two free supported (hinge) support. So that both simplified and/or advanced calculations will be performed on a three span arrangement with the same distances between supports (the largest one) with alternative free rotation and a rigid one. The maximum will occur as indicated earlier. In practice, a hinge is used to reduce thermal expansion stresses. The presence of supports (insulator, supporting structure) generally decrease the stress, compared to fixed point, except if resonance's occur (which is only possible in the voltage range up to 170 kV). In fact the resonance with the high frequencies of the electromagnetic loading is only possible for insulators and these could have such high natural frequencies (50/60 Hz) only for voltage level up to 170 kV.

4 FLEXIBLE BUS SYSTEMS

4.1. Introduction

The analysis of flexible busbar systems is much more complicated than that of rigid bus systems because the structures experience significant displacements in response to the short-circuit forces. The short-circuit forces also depend on the displacements of the conductors and this results in a highly nonlinear behaviour. As well, the complete conductor, insulator and support structure system must be considered in the analysis. During the 70's, the members and experts of WG 23.02 began development of methods, for example using finite element methods to calculate the dynamic response of flexible busbar systems to short-circuits. In addition to the use of advanced methods, extensive efforts were expended to develop simple solution methods which would give good estimates of the results for parameter and sensitivity analysis.

As a result, several methods for the calculation of short-circuit effects in busbars with flexible conductors have been developed which differ very significantly in terms of the models used to represent the bus systems, the numerical calculation techniques, their capabilities and complexity [119]. Most of the calculation methods used computer programs, which presented different options, capabilities and computer requirements. The methods are divided into three classes, namely, simplified, medium and advanced. Due to the rapid development in computer technology, medium methods were left in the background. Powerful advanced methods for example, finite element methods, are available on workstations and PC's and allow the calculation of complete structures. Simple methods are nevertheless useful and necessary in design of substations for typical design cases and parameter sensitivity investigations. They have the advantage to be used very quickly (some few seconds) compared to advanced method (some minutes on up to date workstations).

The typical bus configurations to be analyzed have been classified as described in Section 1.4 and Figure 1.8

After the termination of WG 23.02, investigations in this area of technology continued independantly and since 1992 they have been included in WG 23.11. This chapter provides an update on the present status of the various classes of calculation methods for flexible bus systems.

4.1.1 Simplified Method

This class of calculation methods uses simplified analytic representations of bus short-circuit effects which can be accommodated with hand calculation and/or pocket calculators. For economic substation design, personal computers are used with programs including all the equations, diagrams and tables of the methods. They include also the calculation of the normal load and allow parameter investigations in a very short time to find the optimum in design.

Simplified methods typically give maximum values and no information about the time history or evolution of the phenomena. These methods require only general data, for example span length, static tension, distance between phases, structure stiffness, cable data, short-circuit current and duration. The method as standardized in IEC 865-1 is derived in subsection 4.2.

Cases C, D, and pure case A without droppers can be accommodated. The method provides the tensile forces generated by the swing out and falling down motions of the span, the horizontal displacement of the span, the tensile force caused by the pinch effect of bundled conductors and a maximum tensile force to be considered for design dimensioning.

4.1.2 Advanced Methods

Another approach is the accurate modelling of the structure using finite element modelling for the conductors and supporting structures. Using such methods to compute the dynamic response of the structures, including their nonlinear behaviour, it is possible to obtain highly accurate results, limited only by the degree of detail used in the modelling and the availability of reliable basic structural data. As with the rigid bus case, with some adaptations, several general purpose finite element programs can be used.

These methods can be applied to any structural configuration and forcing function including, for bus design, cases A to F as well as case A+B. Space and time integrations can be performed to any degree of accuracy, limited only by the computational time available. However, analysis of bundle conductor pinch effect is not available

from all programs and requires substantial computer time, particularly if it is included with swing effects in a global calculation. This subject is discussed in greater detail in section 4.4.

The accuracy obtained by advanced methods is of course related to the accuracy of the available data. Some of these data are generally not known with precision, which therefore leads to a need to also use some parametrical approachs. For example, the stiffness of the apparatus or the exact lengths of droppers, etc, are sometimes difficult to obtain. In addition, for the general design situation, the structures may exist only on paper at the design stage when detailed structural data are required, and the results tend to be sensitive to the data in some cases. Conservative hypothesis can be tested based f. e. using simple analysis methods. The typical data required includes, for example, configuration data for the bus, droppers, support structures, connections, material elasticity, mass, heat capacity, expansion coefficients, time variation of short-circuit current and so on. Nondestructive measurements on partly installed structures can improve the situation, by giving better knowledge of such parameters including the stiffness and dynamic behaviour of the components of the structure.

The time history of tension and displacement for all components of the structure (cable, supports, droppers, apparatus) are obtained from the results of finite element analysis. Step-by-step computations provide sets of structural data for the complete structural response as a function of time. The views of the deformed structure during the process facilitate the understanding of exactly what happens to bus systems during and after short circuits. Design loads, for example, maximum bending moments can be easily obtained by postprocessing analysis.

4.1.3 Bundled Conductor Pinch Effect Calculation

As with other aspects of bus analysis, a range of methods is used to analyze bundled conductor pinch effect, using simple, medium or advanced methods [112, 119]. Because pinch effects occur more rapidly than swing effects, following initiation of a short-circuit, pinch effects are commonly analyzed separately from swing effects. This phenomenon and the methods for its analysis, are described more completely in section 4.4; however simple or medium methods require only a few seconds on a typical desk top personal computer. Pinch effect can also be calculated at the same time as swing effects if an advanced method is used. In this case the computer time will be increased; but the whole problem will be solved at the same time.

As with analysis of the other short-circuit bus effects, the accuracy of calculation results depends on the accuracy of the data. In the case of bundle pinch, a particularly important factor is the equivalent dynamic spring rate of the hardware connections, support insulators and apparatus. For advanced methods, hardware is used in the modelling, thus intrinsically taken into account. But for simple method, empirical values can be used. As with the previously described short-circuit effect calculation methods, bundle pinch calculations require similar data. But in addition, stiffness and frequency of supporting structure, number of subspans, bundle spacing, sub-conductor diameter are particularly important parameters.

The primary results of bundle pinch effect calculations are peak tension in the conductors and the compression forces on spacers. The time history is also available with advanced methods.

The following sections provide more detailed descriptions of simple and advanced methods for swing effect calculations. In addition, bundle pinch effects are described.

4.2. Short-circuit Tensile Force, Drop Force and Horizontal Displacement — Simplified Calculation Method

4.2.1 General Information

Stranded conductors used in substation bus systems are assumed to have no flectural strenth and are therefore normally under tensile force only and in static equilibrum with the load imposed by their own weight. As long as gravity represents the only load, the conductors of the span are on vertical planes on which their anchor points are located. The smaller the sag, the larger the tensile force. For the simplified method of calculating mechanical short-circuit effects, this premise also applies for short spans and large conductor cross sections, but it gives good results for longer spans and low cross sections, too. As

well, bundles with two or more sub-conductors are assumed to behave approximately the same as single conductors of equivalent cross section and mass. These calculations are not affected by the pinch effect of bundles. The simple method for calculation of the tensile force due to the pinch is described in section 4.4.2.

In the following paragraphs, methods for calculation of the tensile forces and conductor displacement due to the short-circuit forces acting on the main-conductors are derived. References to clauses, equations and figures of IEC 865-1 [107] are marked by an asterix (*).

The equations derived apply for span lengths up to approximately 60 m and ratios of sag to span length of approximately 8%. For longer spans, the movement of the conductor can result in lower stresses than calculated using the equations in this chapter. They apply for horizontal spans in side-by-side configuration. Other configurations can result in lower tensile forces. However, because of the complicated computation involved, use of the given equations is recommended for calculating these cases also as a first approximation.

The short-circuit duration T_{kl} depends on the system protection time, which is a variable depending on system design requirements and statistical effects that occur during the service life of a substation. In practice, designers commonly assume that short-circuits occur with variable durations and estimate the "worst case" from analysis of historical operating records. If the short-circuit duration T_{kl} is not known, the simple method produces the worst case result corresponding to the specified short-circuit current level. The calculation of the short-circuit currents should be based on IEC 909 [40].

Automatic reclosing is not considered in the method; but tests show that higher forces can occur during or after the second short-circuit current [130]. Therefore additional investigations may be required.

4.2.2 *Conductor Movement and Tensile Forces*

Figure 4.1 shows a simplified view of the conductor movement caused by short-circuit forces. In the case of a balanced three-phase short-circuit, the outer phase conductors L1 and L3 swing outwardly from the steady state position and the center conductor L2 moves only slightly because of its inertia and the alternating bidirectional forces acting on it. In the case of a line-to-line short-circuit, for example between the phases L1 and L2, both conductors swing initially outwards then inwards in synchronism.

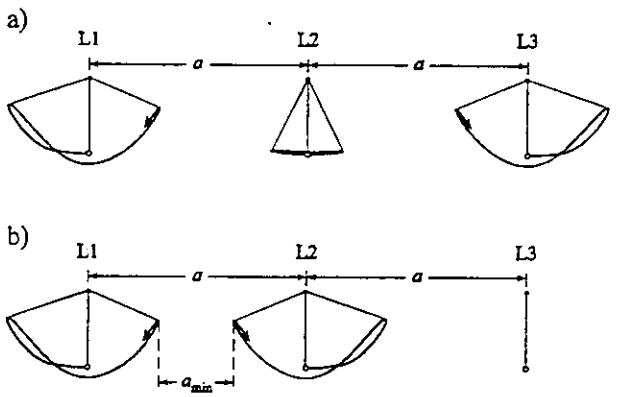

Figure 4.1: Conductor movement due to short-circuit currents
a) during and after a three-phase short-circuit
b) during and after a line-to-line short-circuit

The stresses occuring in line-to-line short-circuits and balanced three-phase short-circuits are approximately equal. However, for line-to-line short-circuits, conductor swing out typically results in decreasing minimum clearances a_{min} when the adjacent conductors carrying short-circuit current move towards one another after the short circuit current has cleared. Consequently the short-circuit tensile force F_t, the drop force F_f and the horizontal displacement b_h are calculated for line-to-line short circuits. In the case of short circuits far from sources of generation, $I''_{k2} = \sqrt{3}/2 I''_{k3}$ [40].

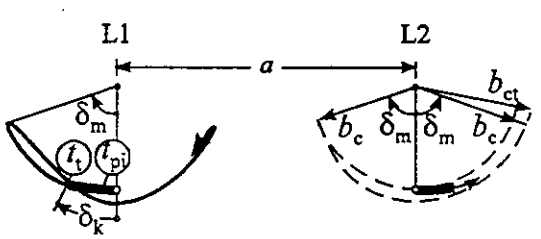

a) Oscillation of the span at $\delta_m < 70°$

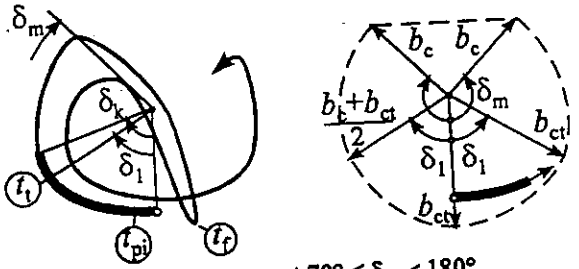

b) Oscillation of the span at $70° \le \delta_m < 180°$

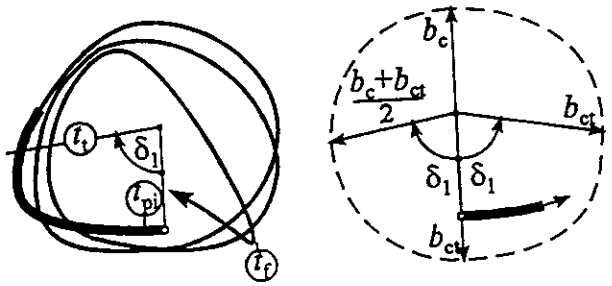

c) Oscillation of the span at $180° \le \delta_m$

Figure 4.2: Short-circuit location curves in the middle of the span for two adjacent phases in the case of a line-to-line short circuit in L1 and L2

left side: movement of the conductor

right side: surface area required

locus during current flow
locus after current flow

Figure 4.2 shows a more detailed view of the three typical conductor movements when a line-to-line fault occures between conductors L1 and L2. In this case the maximum swing-out angle δ_m is the decisive parameter:

- $\delta_m < 70°$: The span is displaced until the first reversal point is reached at δ_m and then returns to the steady-state position with damped oscillations. During or at the end of the short circuit, the short-circuit tensile force F_t is at its maximum and the sag b_{ct} at δ_m.
- $70° \le \delta_m < 180°$: The span is displaced and drops down from the position indicated by δ_m in the direction of the suspension points. At the end of the first fall at the time t_f, the drop force F_f is at its maximum, as is the sag.
- $\delta_m \ge 180°$: The electromagnetic forces accelerate the span so much, that it rotates once or several times, until the stored energy is exhausted. At the bottom of the curves, tensile-force peaks of approximately the same order as the maximum drop force F_f may occur at approximately equal intervals corresponding to the natural frequency of the span. The sag reaches its maximum at the time t_t.

t_{pi} is the time, where the tensile force due to the pinch occures.

Therefore it is necessary at first to estimate the maximum swing-out angle δ_m and the angle δ_k at the end of the short-circuit current flow.

4.2.3 *Maximum Swing-Out Angle and Angle at the End of the Short-Circuit Current Flow*

In the following, the shape of the conductor span is assumed to be a parabola and the shape remains in a plane during the swing out motion, Figure 4.3a. The angle between this plane and the vertical axis is the swing-out angle $\delta(t)$. Longitudinal and transversal conductor waves are excluded.

Each main conductor consists of n sub-conductors with the mass per unit length m'_s, cross section A_s, and the actual Young's modulus E_s, (see section 4.4.3). In the case of a single conductor, $n = 1$, $m'_s = m'$, $A_s = A$ hold.

a)

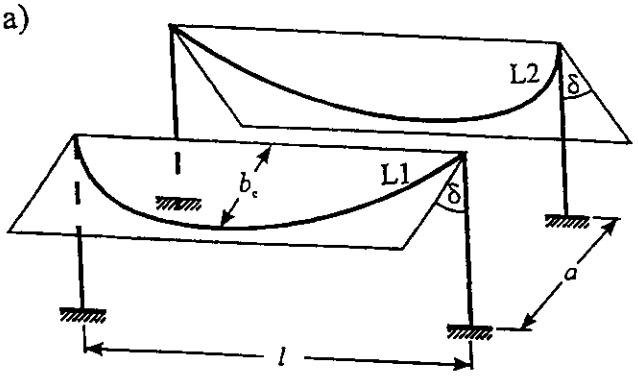

b)

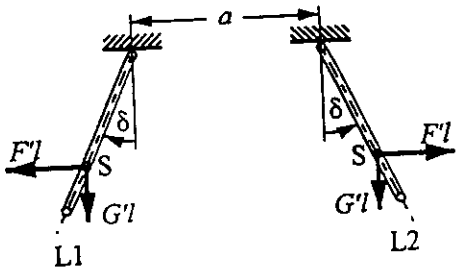

Figure 4.3: Spans L1,L2 side-by-side during a line-to-line short ciruit

For calculation of the maximum swing-out angle δ_m the movement of the span is described by the nonlinear physical pendulum Figure 4.3 b, which obeys the differential equation

$$J\ddot{\delta} + mg_n s \sin\delta = M(t) \qquad (4.1)$$

where

$m = \int dm \approx nm'_s l$ mass

$s = \dfrac{\int y(x)\,dm}{m} \approx \dfrac{2}{3} b_c$ distance to center of gravity

$J = \int y^2\,dm \approx \dfrac{8}{15} nm'_s l b_c^2$ moment of inertia

$M = \int F'(x) y(x) \cos\delta\,dx$ exciting moment

The approximations apply to typical spans where $b_C << l$ for the static sag is a valid relationship. The period of conductor oscillation for small angles δ and constant sag b_c is given by

$$T = 2\pi\sqrt{\frac{J}{mg_n s}} \approx 2\pi\sqrt{0{,}8\frac{b_c}{g_n}} \qquad (*23)$$

The double integration of (4.1) can only be done numerically. Because the period of oscillation of the span is long compared with the period of the short-circuit current, the time history of the current can be substituted by the initial short-circuit current, whereby the force becomes independent of time. If the moment is calculated by a substitute force on the center of gravity averaged over the swing-out angle:

$$M = F'(\tilde{m} + \tilde{n}) k_d l s \cos\delta, \qquad (4.2)$$

Now (4.1) can be integrated analytically twice. F' is the constant force per unit length caused by the initial short-circuit current I''_{k2}:

$$F' = \frac{\mu_0}{2\pi}\frac{(I''_{k2})^2}{a} \qquad (4.3)$$

After the breaking of the current at $\delta = \delta_k$, the moment M is zero. The factors $\tilde{m}$ and $\tilde{n}$ from [107], here marked by a tilde to distinguish them from other variables used, consider the a.c. and d.c. components of the short-circuit current. Figure 4.4 shows the factor $\tilde{m}$ and for distribution networks usually $\tilde{n} = 1$ holds. The factor k_d is the averaged influence of the angle δ, see Figure 4.5 [104].

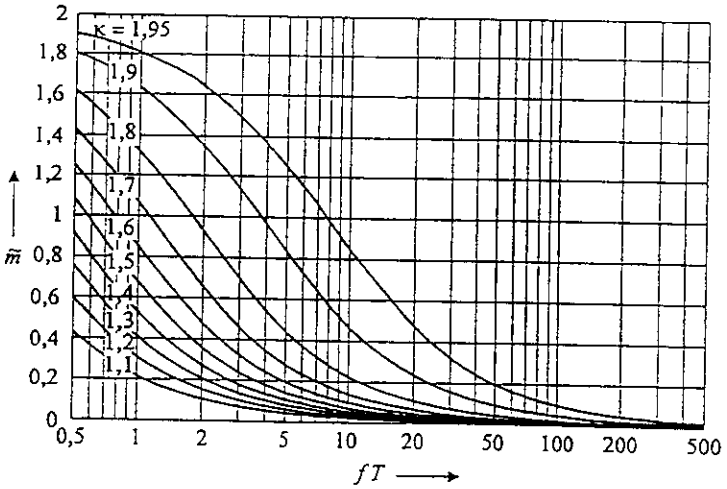

Figure 4.4: Factor $\tilde{m}$, the d.c (aperiodic) component constribution to the short-circuit loads on flexible conductors and to thermal effect [107]. κ is the factor for calculating the peak short-circuit current [40] and f the system frequency.

With these assumptions, (4.1) can be written:

$$\ddot{\delta} = \begin{cases} -\dfrac{4\pi^2}{T^2}\sqrt{1-r^2}\,\sin(\delta - \delta_1) & \text{for } 0 \le \delta \le \delta_k \\ -\dfrac{4\pi^2}{T^2}\sin\delta & \text{for } \delta > \delta_k \end{cases} \qquad (4.4)$$

where r is the ratio of electromagnetic force per unit length to gravitational force per unit length $G' = nm'_s g_n$

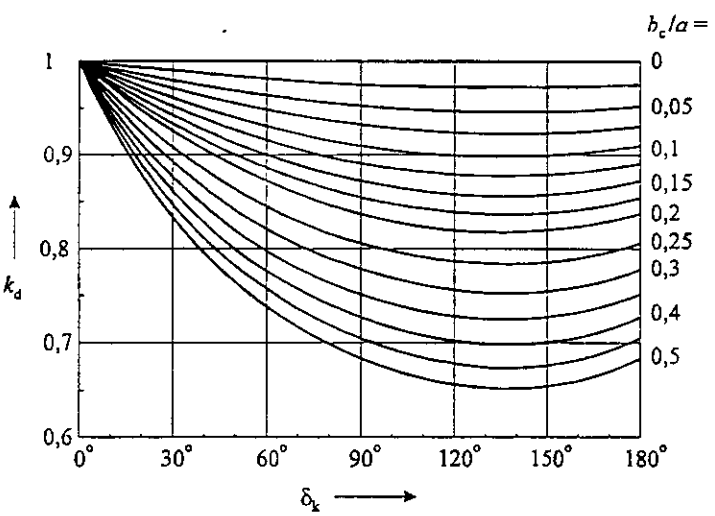

Figure 4.5: Factor k_d describing the averaged change of the moment in (4.2)

$$r = \frac{F'(\tilde{m}+\tilde{n})k_d}{G'} \tag{4.5}$$

and

$$\delta_1 = \arctan r \tag{*21}$$

Integration of (4.4) with $d\dot{\delta}^2/d\delta = 2\ddot{\delta}$ leads to:

- for $0 \le \delta \le \delta_k$ with the initial values $\delta = \dot{\delta} = 0$

$$\dot{\delta} = \sqrt{\frac{8\pi^2}{T^2}(r\sin\delta + \cos\delta - 1)} \tag{4.6}$$

- for $\delta > \delta_k$ with the initial values $\delta = \delta_k$ and $\dot{\delta} = \dot{\delta}_k$

$$\dot{\delta} = \sqrt{\frac{8\pi^2}{T^2}(\cos\delta - \cos\delta_k) + \dot{\delta}_k^2} \tag{4.7}$$

For the second integration of (4.6), the following substitutions are inserted to calculate the angle δ_k at the end of the short-circuit current:

$$\delta^* = \delta - \delta_1, \quad \xi = \frac{1}{k}\sin\frac{\delta^*}{2}, \quad k = \sin\frac{\delta_1}{2}$$

by which the span swings around the steady state position δ_1:

$$\dot{\xi} = \frac{2\pi}{T_{pend}}\sqrt{(1-k^2\xi^2)(1-\xi^2)}$$

with the amplitude dependent oscillation period

$$T_{pend} = \frac{T}{\sqrt[4]{1+r^2}}$$

Separation of variables gives an elliptic integral of the first kind; the result is the Jacobis elliptic sinus amplitudinis function sn [122]. Taking the initial value $\delta^* = -\delta_1$, one obtains after substituting back:

$$\delta(t) = \delta_1 + 2\arcsin\left[k\,sn\left(2\pi\frac{t}{T_{pend}} - \frac{\pi}{2}, k\right)\right]$$

For the usual range $0 < r < 10$, a simple approximation can be given, which is derived from the linearization of equation (4.1) for small angles and contains the amplitude-dependent periodicity of the sn-function by approximation:

$$\delta(t) = \delta_1\left[1 - \cos\left(2\pi\frac{t}{T_{res}}\right)\right]$$

The period of the sinus amplitudinis function sn is quadratically approximated which gives the resulting period during short-circuit current flow:

$$T_{res} = \frac{T_{pend}}{1 - \frac{\pi^2}{64}\left(\frac{\delta_1}{90°}\right)^2} = \frac{T}{\sqrt[4]{1+r^2}\left(1 - \frac{\pi^2}{64}\left(\frac{\delta_1}{90°}\right)^2\right)} \tag{*24}$$

Therefore, the angle at the end of the short-circuit current flow is, with $t = T_{k1}$:

$$\delta_k = \delta(t = T_{k1}) = \delta_1\left[1 - \cos\left(2\pi\frac{T_{k1}}{T_{res}}\right)\right] \tag{4.8}$$

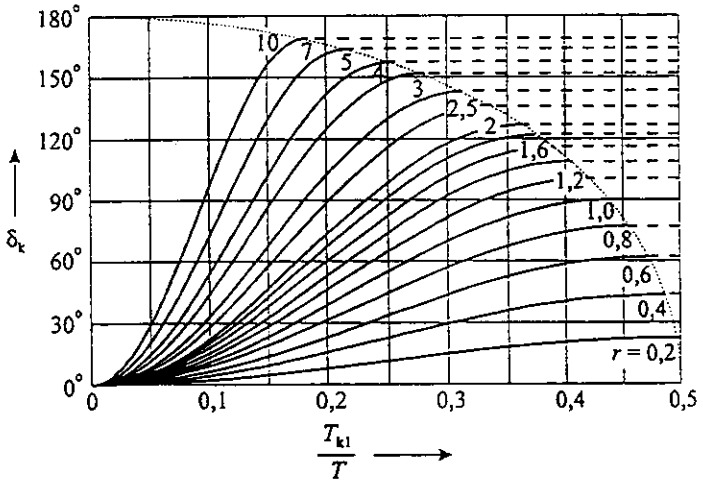

Figure 4.6: Swing-out angle δ_k at the end of the short-circuit current flow

—— δ_k for $T_{k1}/T_{res} \le 0{,}5$.

– – δ_k for $T_{k1}/T_{res} > 0{,}5$.

· · · locus of maxima for $T_{k1}/T_{res} = 0{,}5$.

Figure 4.6 shows δ_k as a function of T_{k1}/T with the parameter r. δ_k reaches its maximum at $T_{k1}/T_{res} = 0{,}5$ indicated by the dotted line and is then decreasing. When $T_{k1}/T_{res} > 0{,}5$, the maximum value of δ_k for $T_{k1}/T_{res} = 0{,}5$ shall be inserted for design purposes, because the actual short-circuit duration T_k can be lower than the short-circuit duration T_{k1} given by the protection concept, and the worst case shall be considered. Therefore (4.8) becomes:

$$\delta_k = \begin{cases} \delta_1 \left[1 - \cos\left(2\pi \frac{T_{k1}}{T_{res}} \right) \right] & \text{for } 0 \le \frac{T_{k1}}{T_{res}} \le 0{,}5 \\ 2\delta_1 & \text{for } \frac{T_{k1}}{T_{res}} > 0{,}5 \end{cases} \qquad (*29)$$

The dashed lines in Figure 4.6 are valid for $T_{k1}/T_{res} > 0{,}5$.

The maximum swing-out angle is obtained as follows: At the reversal point of the movement $\delta = \delta_m$, $\dot{\delta} = 0$ in (4.7). Inserting (4.6) with $\delta = \delta_k$

leads to the maximum swing-out angle, which is only dependent on r and δ_k:

$$\delta_m = \arccos(1 - r \sin \delta_k) = \arccos \chi \qquad (4.9)$$

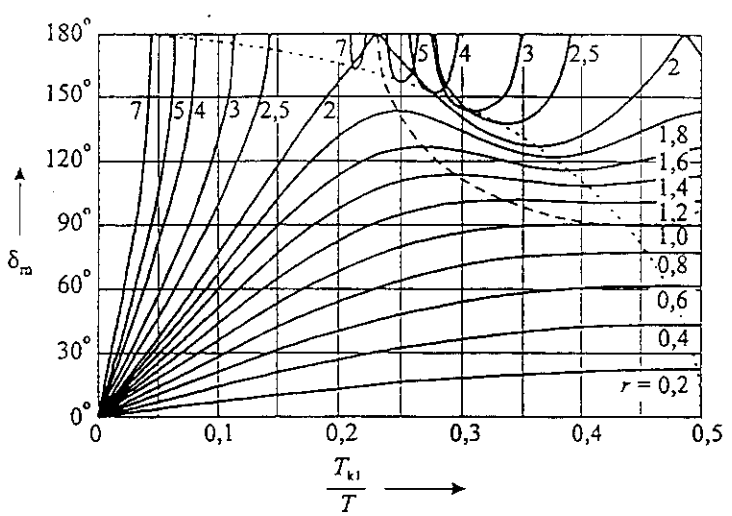

Figure 4.7: Maximum swing-out angle δ_m according to (4.9)

——— δ_m
– – locus of δ_m for δ_k =90°
· · · locus of δ_m for $\delta_m = \delta_k$

Figure 4.7 shows δ_m as a function of T_{k1}/T with the parameter r. The dashed line indicates δ_m when $\delta_k = 90°$, The dotted line shows δ_m, when δ_k is maximum, that means the short-circuit current flow stops at the highest point of the conductor movement: $\delta_m = \delta_k = 2\delta_1$. Three cases can be seen:

- $0 \le r \le 1$: The maximum of δ_m is reached at the maximum of δ_k, i. e. $\delta_m = \delta_k = 2\delta_1$.
- $1 < r \le 2$: The maximum of δ_m is reached at δ_k=90°. Then the course of δ_m decreases and has its minimum at $\delta_m = \delta_k = 2\delta_1$.
- $r > 2$: The course of δ_m increases and δ_m = 180° is obtained if χ = -1. χ < -1 results in rotating of the conductor span. Greater short-circuit durations can lead to ranges, where χ > -1 holds and the conductor stops movement before 180°; the minima of these parts are marked by the dotted line.

Because $T_k \le T_{k1}$ can occur, the worst case δ_k = 90° shall be used in this case for design. So it follows that:

$$\chi = \begin{cases} 1 - r \sin \delta_k & \text{for } 0 \le \delta_k \le 90° \\ 1 - r & \text{for } \delta_k > 90° \end{cases} \qquad (*30)$$

A comparison with test results [104, 78] shows that δ_m is too low when calculated by (4.9). This is due to the simple model of a constant force per unit length in (4.2) on the one hand, and the pendulum movement superposed by longitudinal oscillations of the conductor on the other hand. Therefore, the following corrections are made in (4.9): Small swing-out angles are adjusted by a constant factor of 1.25 and large angles with the addition of 10°, which gives continuation at δ_m=50° and 180°.

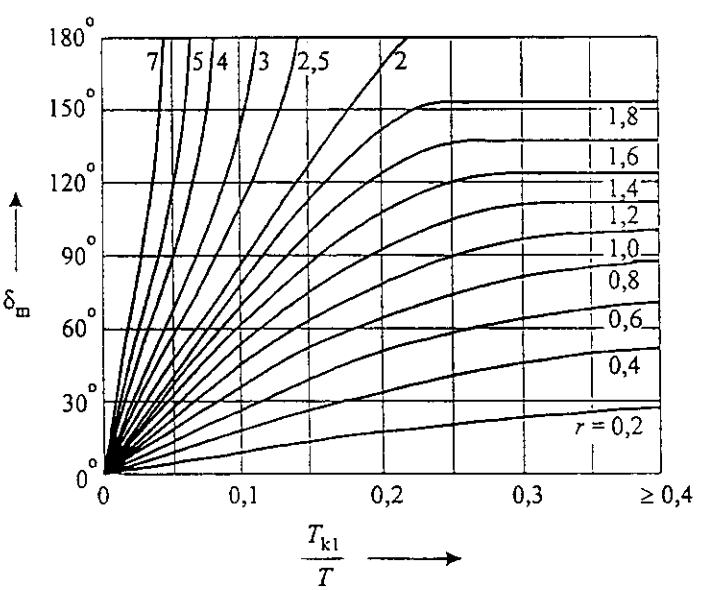

Figure 4.8: maximum swing-out angle δ_m according to (*31) for design purposes

Hence

$$\delta_m = \begin{cases} 1{,}25\arccos\chi & \text{for } 0{,}766 \le \chi \le 1 \\ 10° + \arccos\chi & \text{for } -0{,}985 \le \chi < 0{,}766 \\ 180° & \text{for } \chi < -0{,}985 \end{cases} \quad (*31)$$

which is shown in Figure 4.8 which is identical with Figure *6. If the short-circuit duration T_{k1} is greater then $0.4T$ or T_{k1} is unknown, then the value $0.4T$ shall be used for T_{k1} in (*29) and (*37).

The factor $\tilde{m}$ can be taken from Figure 4.4 with

$$T = \begin{cases} T_{res}/4 & \text{for } T_{k1} \ge T_{res}/4 \\ & \text{or } T_{k1} \text{ is unknown} \\ T_{k1} & \text{for } T_{k1} < T_{res}/4 \end{cases} \quad (4.10)$$

For short-circuit durations greater than 0.1 s the influence of the d.c. component is low and $\tilde{m}$ can be disregarded. As $0.9 < k_d < 1$ applies for usual spans, $k_d = 1$ can be used which is on the safe side as given in Figure 4.4. Accordingly, (4.5) becomes:

$$r \approx \frac{F'}{G'} = \frac{F'}{n m'_s g_n} \quad (*20)$$

4.2.4 *Short-Circuit Tensile Force F_t*

Figure 4.9 shows the sectional view of a span. The forces per unit length act on a conductor element:

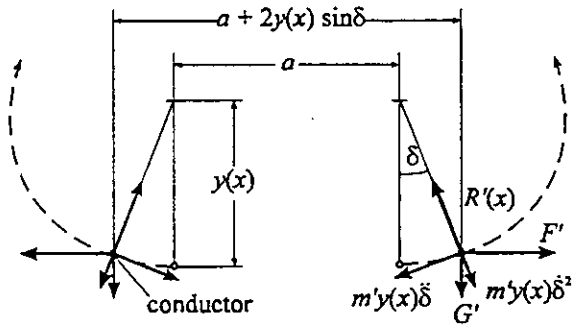

Figure 4.9: Swing-out of the conductor in midspan and forces during current flow

radial $\quad R' = F'\sin\delta + G'\cos\delta + m'y\dot{\delta}^2$

tangential $\quad nm'_s y\ddot{\delta} = F'\cos\delta - G'\sin\delta$

R' is the radial force per unit length, which changes very slowly compared with the eigenvalue of the conductor as a swinging cord. The integration of the second equation with an initial value $\dot{\delta}(t=0) = 0$ and substitution into the first equation leads to:

$$\frac{R'}{G'} = 3r\sin\delta + 3\cos\delta - 2 \quad (4.11)$$

R' reaches its maximum at

$$\delta_1 = \arctan r \quad (*21)$$

if $\delta_k \ge \delta_1$, i.e. $T_{k1} \ge T_{res}/4$, otherwise at $\delta = \delta_k$, if $T_{k1} < T_{res}/4$.

The change in conductor length by increasing the radial force from $R'_{st} = G'$ to $R'_t = G'(1+\varphi)$ becomes with the change-of-state equation for a conductor:

$$l_t - l_{st} = Nl\left(F_t - F_{st}\right) \quad (4.12)$$

The spring constant of both supports S and the Young's modulus E_s are subsumed under the flexibility norm

$$Nl = \frac{1}{S} + \frac{l}{nE_s A_s} \quad (*25)$$

The approximate lengths of the conductor

$$l_t = 2\frac{F_t}{G'}\sinh\left(\frac{R'_t}{F_t}\frac{l}{2}\right) \approx l + \frac{l^3}{24}\left(\frac{R'_t}{F_t}\right)^2$$

$$l_{st} = 2\frac{F_{st}}{G'}\sinh\left(\frac{R'_{st}}{F_{st}}\frac{l}{2}\right) \approx l + \frac{l^3}{24}\left(\frac{R'_{st}}{F_{st}}\right)^2$$

are inserted into (4.12)

$$\frac{l^3}{24}\left[\left(\frac{R'_t}{F_t}\right)^2 - \left(\frac{R'_{st}}{F_{st}}\right)^2\right] = Nl\left(F_t - F_{st}\right) \quad (4.13)$$

Hence the short-circuit tensile force F_t is estimated as:

$$F_t = \begin{cases} F_{st}(1+\varphi\psi) & \text{for } n = 1, \text{ single conductor} \\ 1{,}1\,F_{st}(1+\varphi\psi) & \text{for } n \ge 2, \text{ bundled conductor} \end{cases} \quad (*34)$$

where the factor 1.1 in the case of bundled conductors an increasing of F_t due to the pinch effect considers, see also chapter 4.4.2.1.

φ follows from (4.11)

$$\varphi = \frac{R'_{max}}{G'} + 1 = \begin{cases} 3\left(\sqrt{1+r^2} - 1\right) & \text{for } \delta_k \geq \delta_l \\ 3\left(r\sin\delta_k + \cos\delta_k - 1\right) & \text{for } \delta_k < \delta_l \end{cases} \quad (*32)$$

With the stress factor

$$\zeta = \frac{\left(n m'_s l g_n\right)^2}{24 F_{st}^3 N} \quad (*28)$$

(4.13) becomes

$$\varphi^2\psi^3 + \varphi(2+\zeta)\psi^2 + (1+2\zeta)\psi - \zeta(2+\varphi) = 0 \quad (*33)$$

with which ψ can be determined by $0 \leq \psi \leq 1$ or taken from Figure 4.10 which is identical with Figure *7.

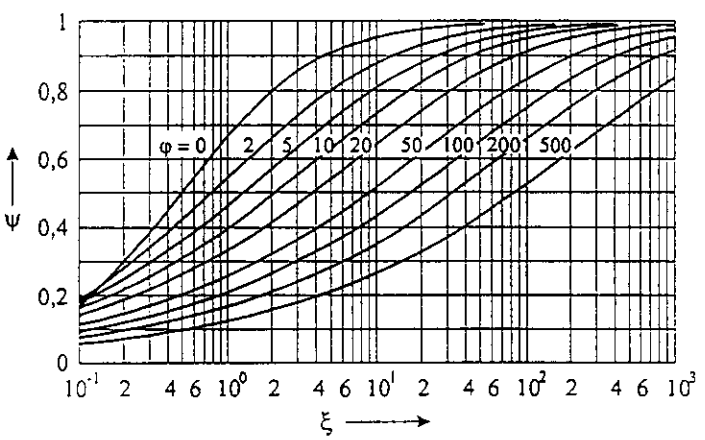

Figure 4.10: Factor ψ for tensile forces

4.2.5 *Drop Force F_f*

At the highest point of the conductor movement δ_m according to Figure 4.11, the maximum potential energy is stored:

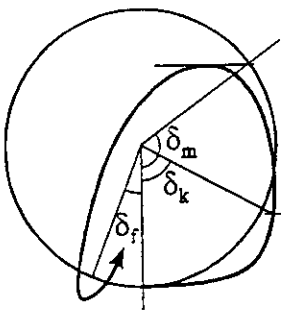

Figure 4.11: Conductor movement in midspan for calculating the tensile force F_f

$$E_{pot} = \left(1 - \cos\delta_m\right) n m'_s l g_n s$$

During the fall, the energy is partially or completely converted into elongation energy depending on height and movement of fall:

$$E_{ela} = \frac{1}{2} N l \left(F_f^2 - F_{st}^2\right)$$

From the height of fall one obtains the balance of the complete energy conversion:

$$\left(\cos\delta_f - \cos\delta_m\right) n m'_s l g_n s = \frac{1}{2} N l \left(F_f^2 - F_{st}^2\right)$$

and from this:

$$F_f = F_{st}\sqrt{1 + 4\zeta\left(\cos\delta_f - \cos\delta_m\right)}$$

The upper limit follows with $\delta_f = 0$:

$$F_f = F_{st}\sqrt{1 + 4\zeta\left(1 - \cos\delta_m\right)} \quad (4.14)$$

and with the approximation $1 - \cos\delta_m \approx (2/\pi)\,\delta_m$:

$$F_f = F_{st}\sqrt{1 + 8\zeta\frac{\delta_m}{180°}} \quad (4.15)$$

In general the velocity and hence the potential energy of the conductor are not zero and drop forces are observed in tests which are greater than those calculated with (4.13). This can be taken into consideration by a factor of 1,2:

$$F_f = 1{,}2 \cdot F_{st}\sqrt{1 + 8\zeta\frac{\delta_m}{180°}} \quad (*35)$$

The drop force only needs to be calculated if $\delta_m \geq 70°$, which occures if $r > 0{,}6$, see Figure 4.7.

In short spans the bending stiffness of the span reduces the span drop, which means that the span drop is calculated too large if the span length is less than approximately 100 times the diameter of the single conductor, i. e. $l < 100 \cdot d_s$.

4.2.6 *Horizontal Span Displacement and Minimum Air Clearance*

Into the change-of-state equation in the case of elastic and thermal elongation

$$\frac{l^2}{24}\left[\left(\frac{R_t'}{F_t}\right)^2 - \left(\frac{G'}{F_{st}}\right)^2\right] = \varepsilon_{ela} + \varepsilon_{th}$$

the sags in the midspan

$$b_c = \frac{G' l^2}{8 F_{st}}, \qquad b_{ct} = \frac{R_t' l^2}{8 F_t}$$

are inserted and solved for b_{ct}:

$$b_{ct} = b_c \sqrt{1 + \frac{3}{8}\left(\frac{l}{b_c}\right)^2 \left(\varepsilon_{ela} + \varepsilon_{th}\right)} = C_D b_c \quad (4.16)$$

The factor C_D corresponds to (*38). The elastic elongation is generated due to the change of the tensile force from F_{st} to F_t

$$\varepsilon_{ela} = N\left(F_t - F_{st}\right) \qquad (*36)$$

and the thermal elongation due to the heating by the short-circuit current

$$\varepsilon_{th} = \frac{\alpha_{th}}{\kappa c \rho}\left(\frac{I_{k2}''}{n A_s}\right)^2 T = c_{th}\left(\frac{I_{k2}''}{n A_s}\right)^2 T \qquad (*37)$$

with the temperature coefficient α_{th}, the specific conductivity κ, the specific thermal capacity c and the specific mass ρ, which all give the material constant c_{th}:

c_{th} in $m^4/(A^2s)$	type of conductor
$0{,}27 \cdot 10^{-18}$	aluminium, aluminium alloy, aluminium/steel conductors with a cross section ratio of Al/St > 6
$0{,}17 \cdot 10^{-18}$	aluminium/steel conductors with a cross section ratio of Al/St ≤ 6
$0{,}088 \cdot 10^{-18}$	copper

The maximum sag b_{ct} for $T_{k1} \geq T_{res}/4$ is reached at the angle δ_1 and for $T_{k1} < T_{res}/4$ at the end of the current flow at δ_k. Thus T is:

$$T = \begin{cases} T_{res}/4 & \text{for } T_{k1} \geq T_{res}/4 \\ T_{k1} & \text{for } T_{k1} < T_{res}/4 \end{cases} \qquad (4.10)$$

Because the shape already differs from the parabola with low values of r and approaches a triangle with high values of r, the actual sag is higher than that estimated with (4.14) [6-8, 16]. The correction is made using the form factor C_F with linear interpolation in the range $0.8 < r < 1.8$ [121, 124]:

$$C_r = \begin{cases} 1{,}05 & \text{for } r \leq 0{,}8 \\ 0{,}97 + 0{,}1r & \text{for } 0{,}8 < r < 1{,}8 \\ 1{,}15 & \text{for } r \geq 1{,}8 \end{cases} \qquad (*39)$$

C_F is derived from tests, because it is only possible numerically to get the form factor for each span.

The maximum horizontal displacement is the projection of the sag onto the horizontal axis

$$b_h = \begin{cases} C_F C_D b_c & \text{for } \delta_m \geq 90° \\ C_F C_D b_c \sin\delta_m & \text{for } \delta_m < 90° \end{cases} \qquad (*40)$$

In the worst case, the minimum air clearance a_{min} according to Figure 4.1 is given by

$$a_{min} = a - 2b_h \qquad (*42)$$

This minimum air clearance is on the safe side because the actual conductor movement towards each other depends on the short-circuit parameters and varies in a wide range due to parameter inaccuracies, which can not be distinguished.

4.2.7 *Extension on Strained Conductors*

The methods written above are only valid for slack conductors, which are connected to support insulators, and hence represent a homogenious arrangement. In long spans, the mass of the insulator strings is significant compared with the conductor mass and is essentially decisive for the sag. The period T according to (*23) contains only the sag. To take the insulator strings into account, an equivalent static conductor sag at midspan is defined:

$$b_c = \frac{G' l^2}{8 F_{st}} \qquad (*22)$$

which is
- for slack conductors, the actual static sag,
- for strained conductors, the sag, when the actual arrangement is replaced by an arrangement of conductors with the same conductor type and static tension, but without insulator strings.

As the electromagnetic force acts only on the conductor, the difference between the conductor length l_c and the span length l is to be taken into account in (4.3):

$$F' = \frac{\mu_0}{2\pi}\frac{(I''_{k2})^2}{a}\frac{l_c}{l} = \frac{\mu_0}{2\pi}\cdot 0{,}75\cdot\frac{(I''_{k3})^2}{a}\frac{l_c}{l} \qquad (*19)$$

where

$l_c = l$ for slack conductors,

$l_c = l - 2l_i$ for strained conductors, where l_i is the

length of one insulator string.

The maximum horizontal displacement is

$$b_h = \begin{cases} C_r C_D b_c \sin\delta_1 & \text{for } \delta_m \geq \delta_1 \\ C_r C_D b_c \sin\delta_m & \text{for } \delta_m < \delta_1 \end{cases} \qquad (*41)$$

because the conductors swing out almost horizontally [127], so that b_h is a maximum at about δ_1.

With both assumptions (*22) and (*41) a good concurrence is achived with test results [127, 131].

The investigations show that the dynamical behaviour of the span and therefore the forces and displacements can be described by three parameters:
- the ratio r of the electromagnetic short-circuit force to the gravitational force on the conductor according to (*20);
- the ratio T_k/T of the short-circuit duration to the period of the conductor oscillation, which is approximately a function of the static sag;
- the stress factor ζ, which subsumes the gravitational force, the static tensile force and the stiffnesses of the conductor and the supporting structures according to (*28).

For design load see chapter 4.3.3.

4.2.8 *Young's Modulus for Stranded Conductors*

Young's modulus for aluminium-steel stranded conductors ACSR is extremely non-linear in the range of relatively low stress (< 50 N/mm²). This is the situation usually found with outdoor substations, and it may even take on values far below those given by standards or furnished by manufacturers, respectively. On the one hand, Young's modulus is an important parameter for calculating the tensile forces, but on the other hand, exact establishment of the modulus by expensive tensile testing is neither possible nor desirable. Figure 4.19 shows tests with ACSR conductors of different cross section [129]. As a result of such tests, an empirical expression for the approximate calculation of the actual Young's modulus for simplified method can be given:

$$E_s = \begin{cases} E\left[0{,}3 + 0{,}7\sin\left(\dfrac{F_{st}}{nA_s\sigma_{fin}}90°\right)\right] & \text{for } \dfrac{F_{st}}{nA_s} \leq \sigma_{fin} \\ E & \text{for } \dfrac{F_{st}}{nA_s} > \sigma_{fin} \end{cases} \qquad (*26)$$

where σ_{fin} = 50 N/mm² is the lowest value of σ_{st}, when Young's modulus becomes constant. The final Young's modulus E for stranded conductors shall be used.

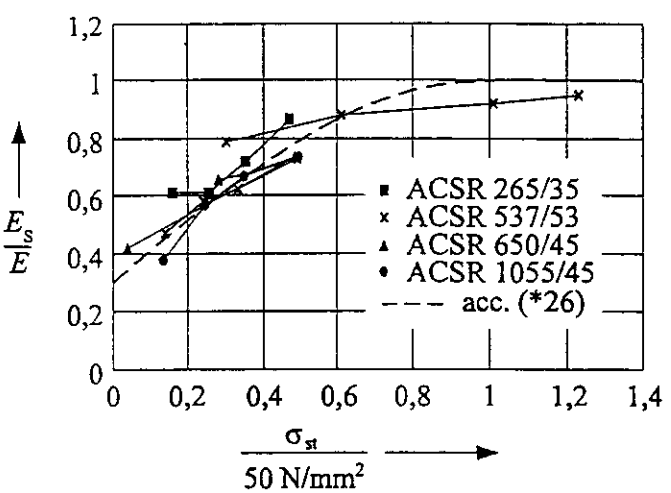

Figure 4.19: Measured actual Young's modulus E_S of different ACSR related to their final Young's modulus E, and approximation according to (*26) as a function of $\delta_{st} = F_{st} / (nA_s)$

4.3 Bundled Conductor Pinch Effect Calculation

4.3.1 Introduction

Normal or emergency ampacity, and (in HV and EHV systems) corona loss and radio noise requirements typically can only be satisfied for flexible bus systems through the use of more than one conductor per phase. Traditionally, the number of conductors per phase, conductor size and bundle spacing, for such bus systems, have been determined primarily from ampacity and radio noise specifications. Two, three and four conductor per phase designs are typical in HV and EHV systems. As is well described in Chapter 1 of this brochure, currents flowing in conductors generate forces acting between the conductors. For bundled conductor systems, the relatively close bundle spacing and typically large short-circuit currents can result in very significant conductor forces.

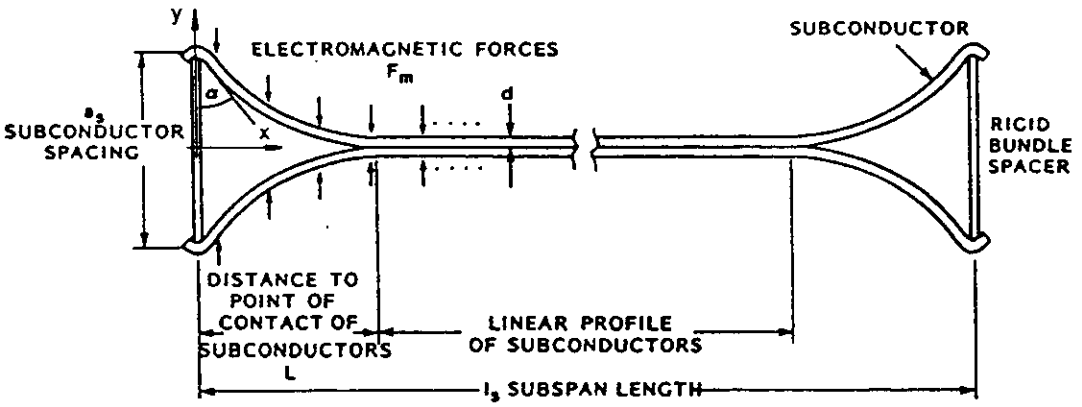

Figure 4.12: Position of sub-conductors of one subspan during bundle pinch

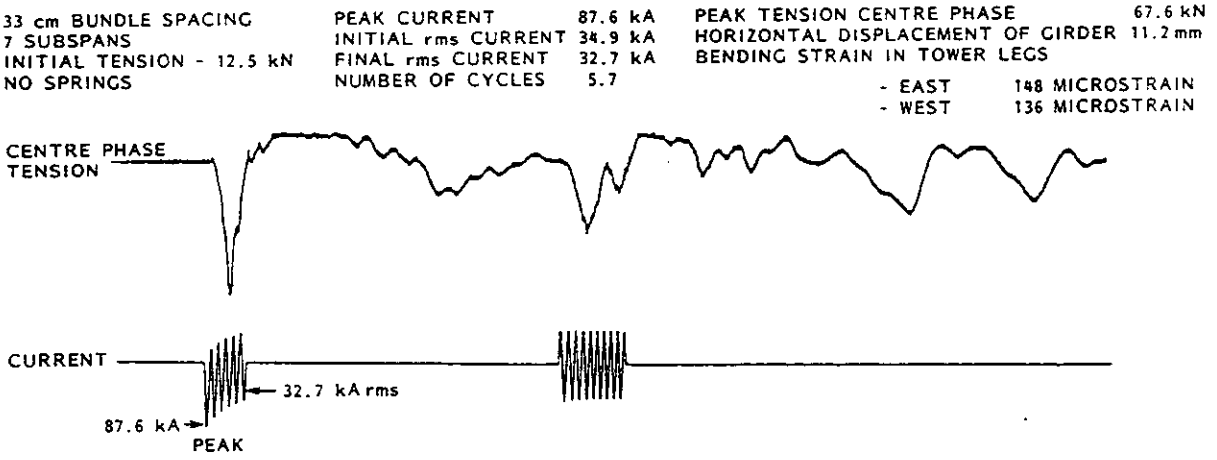

Figure 4.13: Oscillogram of a typical bundle pinch tensile force

As illustrated in Figure 4.12, the forces acting on the conductors cause a rapid acceleration of the conductors towards each other until they clash together. This rapid pinching together of the conductors causes an effective shortening of the conductor length available for the bus span which results in a rapid increase in conductor tension. This rapid increase in conductor tension, which occurs typically in the range 10-50 ms after fault initiation, is transmitted to the span support points (insulators, hardware and support structures) as an impulse loading.

Figure 4.13 shows a typical oscillogram of a short-circuit current waveform and the corresponding phase tension. The support structures respond dynamically to this rapid increase in phase tension and interact with the bus span in a complex fashion depending on their mass, stiffness and other parameters. Components of the increased tension are also applied to any bundle spacers which may be present [see the companion CIGRE brochure on data reference tests, and also 48, 106, 132, 133,]. For EHV substations, bundle and phase spacings are such that the dynamic bundle pinch tensions acting on the hardware, insulators and support structures can exceed the tensions generated by the swinging motion of the phases. But the pinch tension is not a design load in itself. In fact actual design is based on static loading and pinch effect is essentially (this is not the case for phase swing and falling down) an impulse force applied to the fittings, apparatus and supporting structures. To define the design load requires a structural dynamic evaluation, this will be detailed in a future brochure under discussion in CIGRE WG23-11.

Of concern to designers are the compressive loadings on bundle spacers, possible damage to conductors caused by clashing and the impulse loading of the bus support system. As a result of these concerns, a number of experimental and/or theoretical studies have been carried out. Because of the complexity of the dynamics of the bundle pinch effect and its interaction with the support structures, generalized analytical representation has not yet been accomplished. The most accurate method to determine bundle pinch tensions is through full scale high-current testing [see the companion CIGRE brochure on data reference tests, and also 48, 50, 65, 30]. Unfortunately, the cost to carry out such testing for the range of bus configurations encountered in practical substation designs, makes this approach impossible. As a result, designers have resorted to a number of simplified and approximate methods to estimate bundle pinch effects. Several of these methods are briefly described in the following section.

4.3.2. Pinch Force - Simplified Calculation Method

4.3.2.1. General Information

Figure 4.14 shows a contracted regular twin-bundle. Regular, here, means that the position of the cross sectional centres of the n sub-conductors of the bundle are marked by the corners of a regular polygon.

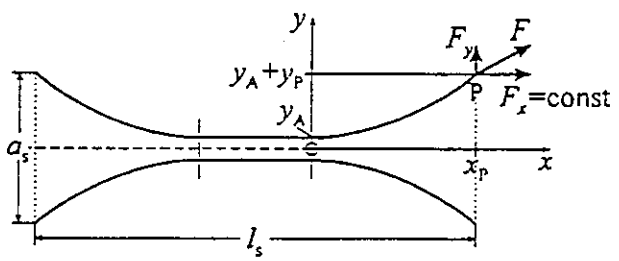

Figure 4.14: Idealized geometry of a clashed twin-bundle

Sub-conductors are considered to clash effectively if the clearance a_s between the midpoints of adjacent sub-conductors, as well as the distance l_s between two adjacent spacers fulfil either (*43) or (*44)

$$a_s/d_s \leq 2{,}0 \text{ and } l_s \leq 50\, a_s \qquad (*43)$$

$$a_s/d_s \leq 2{,}5 \text{ and } l_s \leq 70\, a_s \qquad (*44)$$

Tests show, that a calculation of the bundle force under such circumstances does not have to be done; in this case it is sufficient to add 10% to the tensile force F_t in (*34) [57].

Calculations for contraction of the bundle described in the literature to date can only be solved numerically [46, 69, 110-112, 123, 50, 128]. Hence, the parabola model is introduced below, based on equations and diagrams which can be solved analytically for the most commonly occurring cases of clashing sub-conductors and by diagrams or numerically for non-clashing sub-conductors [116,120, 126].

In most cases, the pinch effect occurs in the first period of the short-circuit current while the move-

ment of the span lasts some hundreds of milliseconds to seconds. Therefore, the pinch effect can be calculated separately from the short-circuit tensile force, the drop force and the horizontal displacement.

In contrast to the short-circuit tensile force F_t and the drop force F_f, the force F_{pi} caused by the pinch effect between bundled conductors is to be calculated in a single-phase system for the line-to-line short-circuit current I''_{k2} and in a three-phase system for the three-phase short-circuit current I''_{k3}. The line-to-earth short-circuit current I''_{k1} shall be used if it is greater than the three-phase short-circuit current I''_{k3}.

4.3.2.2. Physical model for regular n-conductor bundles

The sub-conductors touch each other in the range $2x_P - l_s < x < 0$. When considering the bundle in its static steady state of contraction and assuming the shape of the curve of the non-clashing section a parabola, the equation for the first quadrant is:

$$y(x) = y_A + y_P\left(\frac{x}{x_P}\right)^2 \qquad (4.11)$$

The flexural stiffness of the conductor which acts above all near the spacers is ignored, so that for the ratio of the transversal and the longitudinal component of the tensile force between two adjacent spacers the following holds

$$\frac{dy}{dx} = \frac{F_y(x)}{F_x} = 2\frac{y_P}{x_P}\frac{x}{x_P} \qquad (4.12)$$

The longitudinal component F_x is locally independent. On the other hand, the transversal component per unit length F'_y is locally independent with respect to (4.12)

$$F_x\frac{d^2y}{dx^2} = F'_y(x) = 2\frac{y_P}{x_P^2}F_x \qquad (4.13)$$

At the location x_P of the spacer, (4.12) becomes

$$F_y(x_P) = 2\frac{y_P}{x_P}F_x \qquad (4.14)$$

and according to (4.13) yields

$$F_y(x_P) = x_P\overline{F}'_y(x_P) \qquad (4.15)$$

$\overline{F}'_y(x_P)$ is the electromagnetic force per unit length acting on a parabolic arc caused by the other n-1 sub-conductors of the bundle.

The tensile force on the bundle clamp for n sub-conductors consists of the static tensile force F_{st} and the tensile force F_{ela} brought about by the lengthening of the span and the bending of the dead end structure

$$F_{pi} = nF_x = F_{st} + F_{ela} = F_{st}\left(1 + \frac{1}{NF_{st}}\frac{\Delta l}{l}\right) \qquad (4.16)$$

With k equidistant spacers in the span, one obtains by the approximation for the curve lengthening of the parabolic arcs

$$\Delta l = (k+1)\frac{4}{3}\frac{y_P^2}{x_P} \qquad (4.17)$$

By substituting equations (4.13) and (4.17) in equation (4.16) the equation for determining x_P or y_P is:

$$nF'_y x_P^3 - F_{st}x_P y_P - 2\frac{k+1}{Nl}\frac{4}{3}y_P^3 = 0 \qquad (4.18)$$

If x_P and y_P are related to their maximum values and abbreviated by $1/\xi$ and η

$$\frac{1}{\xi} = \frac{x_P}{x_{P,max}} \le 1 \quad \text{with} \quad x_{P,max} = \frac{l_s}{2} = \frac{l_c}{2(k+1)}$$
$$\eta = \frac{y_P}{y_{P,max}} \le 1 \quad \text{with} \quad y_{P,max} = \frac{a_s - d_s}{2\sin(180°/n)} \qquad (4.19)$$

then (4.18) becomes

$$\xi^3\eta^3 + \varepsilon_{st}\xi^2\eta - \varepsilon_{pi}f_\eta = 0 \qquad (4.20)$$

with the strain coefficients

$$\varepsilon_{st} = \frac{3}{2}\frac{F_{st}l_s^2N}{(a_s - d_s)^2}\left(\sin\frac{180°}{n}\right)^2 \qquad (*47)$$

$$\varepsilon_{pi} = \frac{3}{8}n\frac{F_v l_s^3 N}{(a_s - d_s)^3}\left(\sin\frac{180°}{n}\right)^3 \qquad (*48)$$

the electromagnetic force per unit length is also related to the maximum value

$$f_\eta = \frac{\overline{F}'_y}{\overline{F}'_{y,max}} \le 1$$

and the substitution

$$F_v = \overline{F}'_{y,max} l_s \qquad (4.21)$$

For the solution of (4.20) one must decide whether or not the sub-conductors are clashing or only reducing their distance. If the sub-conductors touch at one point, then $\xi = \eta = f_\eta$. In this case $\varepsilon_{pi} = 1 + \varepsilon_{st}$ follows from (4.20). The quantity

$$j = \sqrt{\frac{\varepsilon_{pi}}{1+\varepsilon_{st}}} \qquad (*49)$$

indicates:

$j \geq 1$ the sub-conductors are clashing,

$j < 1$ the sub-conductors have reduced their distance, but are not clashing.

4.3.2.3. Electromagnetic force

To determine $\overline{F}'_y(x_P)$, the electromagnetic force on a parabolic arc of the length x_P through the n - 1 sub-conductors of the bundle is to be calculated:

$$F_y(x_P) = (n-1)\frac{\mu_0}{2\pi}\left(\frac{I}{n}\right)^2 \frac{x_P}{a_{sw}}$$

with the effective short-circuit current I of the main conductor and the effective centre-line distance a_{sw} between sub-conductors. With (4.12) the transversal component becomes

$$F_x = (n-1)\frac{\mu_0}{2\pi}\left(\frac{I}{n}\right)^2 \frac{x_P}{a_{sw}}\frac{x_P}{2y_P} \qquad (4.22)$$

The effective distance a_{sw} between the sub-conductors depends on y_P and can be approximated by the equation of a parabola. The electromagnetic force is estimated at the location x_P with the distance $2y(x)$ of the parabolic arcs according to (4.11):

$$F_y(x_P) = (n-1)\frac{\mu_0}{2\pi}\left(\frac{I}{n}\right)^2 \int_0^{x_P} \frac{dx}{2y(x)}$$

The integration and the comparison with (4.22) leads to:

$$a_{sw} = \frac{2y_A\sqrt{y_P/y_A}}{\arctan\sqrt{y_P/y_A}} \qquad (4.23)$$

According to (4.15) and (4.22), the local independent transversal force per unit length $\overline{F}'_y(x_P)$ is a maximum, if the sub-conductors clash in one point, i.e. if

$$y_P = y_{Pmax} = \frac{a_s - d_s}{2\sin(180°/n)}$$

Then

$$y_A = \frac{d_s}{2\sin(180°/n)}$$

and a_{sw} becomes its maximum:

$$a_{sw,max} = \frac{d_s}{\sin(180°/n)}\frac{\sqrt{a_s/d_s - 1}}{\arctan\sqrt{a_s/d_s - 1}} = a_s v_3 \qquad (*A.7)$$

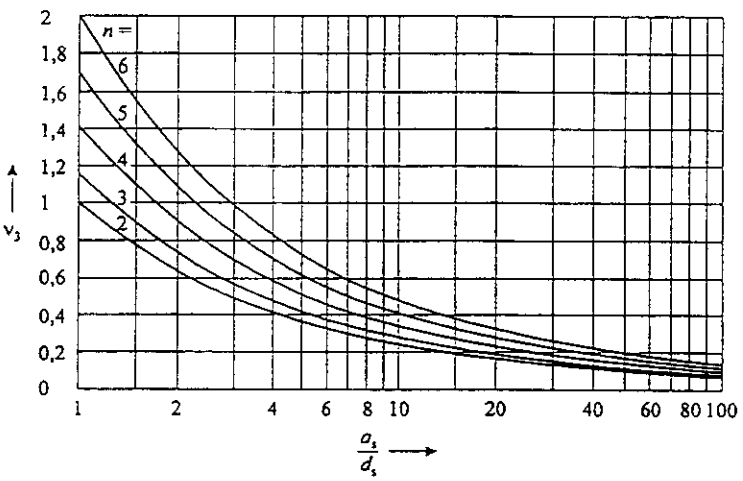

Figure 4.15: Factor v_3 for calculation of the effective distance between the sub-conductors

with the related effective centre-line distance v_3. Figure 4.15 gives v_3 as a function of a_s/d_s with the parameter n. The product $v_3 \cdot \sin(180°/n)$ is independent of n and leads to one curve equal $n = 2$, Figure *9.

This gives the electromagnetic force according to (4.21)

$$F_v = (n-1)\frac{\mu_0}{2\pi}\left(\frac{I}{n}\right)^2 \frac{l_s}{a_s v_3} \qquad (4.24)$$

In any case, f_η is thus equal to the quotient of the effective distances and depends on the conductor geometry:

$$f_\eta = \frac{\overline{F}'_y}{\overline{F}'_{y,max}} = \frac{a_{sw}(y_{P,max})}{a_{sw}(y_P)} \leq 1$$

$a_{sw}(y_P)$ and $a_{sw}(y_{P,max})$ are determined with (4.23) and (*A7).

The effective short-circuit current has been inserted in (4.22) without stating the functional connection between I and the initial short-circuit current I_k''. The time elapsed until the contraction of the bundle is complete, T_{pi} may be assessed from the boundary value problem for the middle of the bundled conductor. It is far easier to establish analytically, assuming a close bundle and the usual short-circuit currents, by stating a constant force. The results are in good accordance as long as the assumptions are observed. The differential equation for a mass element m_s' accelerated by a constant electromagnetic force per unit length

$$m_s'\ddot{y} = -F_y'(t) = \text{const} = -(n-1)\frac{\mu_0}{2\pi}\left(\frac{I}{n}\right)^2 \frac{\sin(180°/n)}{a_s}$$

is integrated with the initial values $\dot{y}(t=0) = 0$ and $y(t=0) = a_s/(2\sin(180^\circ/n))$:

$$m_s' y = \frac{a_s}{(2\sin(180^\circ/n))} m_s' - \frac{n-1}{2}\frac{\mu_0}{2\pi}\left(\frac{I}{n}\right)^2 \frac{\sin(180°/n)}{a_s} t^2$$

For $y = d_s/(2\sin(180^\circ/n))$, t becomes T_{pi}:

$$T_{pi} = \frac{1}{\sin\frac{180°}{n}} \sqrt{\frac{(a_s - d_s)m_s'}{\frac{\mu_0}{2\pi}\left(\frac{I}{n}\right)^2 \frac{n-1}{a_s}}} \qquad (4.25)$$

With the abbreviation

$$\nu_1 = f\frac{1}{\sin\frac{180°}{n}} \sqrt{\frac{(a_s - d_s)m_s'}{\frac{\mu_0}{2\pi}\left(\frac{I_k''}{n}\right)^2 \frac{n-1}{a_s}}} \qquad (*46)$$

it follows:

$$T_{pi} = \frac{\nu_1}{f}\frac{I_k''}{I} \qquad (4.26)$$

f means the frequency of the power system. The natural frequency of the bundled conductors as oscillating strings is in the range of a few Hz and therefore well below the excitation frequency of 50 Hz and 100 Hz, respectively. Thus, the time-averaged values of the force per unit length as well as of the short-circuit current are relevant for the pinch force. Therefore:

$$I^2 = \frac{1}{T_{pi}}\int_0^{T_{pi}} i^2(t)\,dt \qquad (4.27)$$

For long contraction periods, like those occurring with wide bundles, the squared current may be approximated by using the factors $\tilde{m}$ and $\tilde{n}$ taken from [107], see also chapter 1.3. However, for short contraction periods, it is absolutely necessary to resolve (4.27) exactly with

$$i(t) = I_k''\sqrt{2}\left[\sin(\omega t - \gamma) + e^{-t/\tau}\sin\gamma\right]$$

for short circuits far from generation sources, where τ is the time constant of the network and $\gamma = \arctan(2\pi f\tau)$ the impedance angle [40, 118]:

$$\left(\frac{I}{I_k''}\right)^2 = 1 - \frac{\sin\left(4\pi f T_{pi} - 2\gamma\right) + \sin 2\gamma}{4\pi f T_{pi}} + \frac{f\tau}{f T_{pi}}\left(1 - e^{-\frac{2fT_{pi}}{f\tau}}\right)\sin^2\gamma - \frac{8\pi f\tau\sin\gamma}{1+(2\pi f\tau)^2}$$

$$\left\{\left(2\pi f\tau\,\frac{\cos\left(2\pi f T_{pi} - \gamma\right)}{2\pi f T_{pi}} + \frac{\sin\left(2\pi f T_{pi} - \gamma\right)}{2\pi f T_{pi}}\right)e^{-\frac{fT_{pi}}{f\tau}} + \frac{\sin\gamma - 2\pi f\tau\cos\gamma}{2\pi f T_{pi}}\right\}$$

fT_{pi} is the solution of (4.26), here abbreviated by:

$$fT_{pi}\sqrt{\nu_2} = \nu_1 \qquad (*A.5)$$

with

$$\nu_2 = \left(\frac{I}{I_k''}\right)^2$$

where T_{pi} is dependent on I. Figure 4.16 shows ν_2 as a function of ν_1, which converges more and more to $1+\tilde{m}$ according to Figure 4.3 for increasing ν_1.

Substituting (4.25) in (4.24) gives the electromagnetic force which is to be inserted into (*48):

$$F_v = (n-1)\frac{\mu_0}{2\pi}\left(\frac{I_k''}{n}\right)^2 \frac{l_s}{a_s}\frac{\nu_2}{\nu_3} \qquad (*45)$$

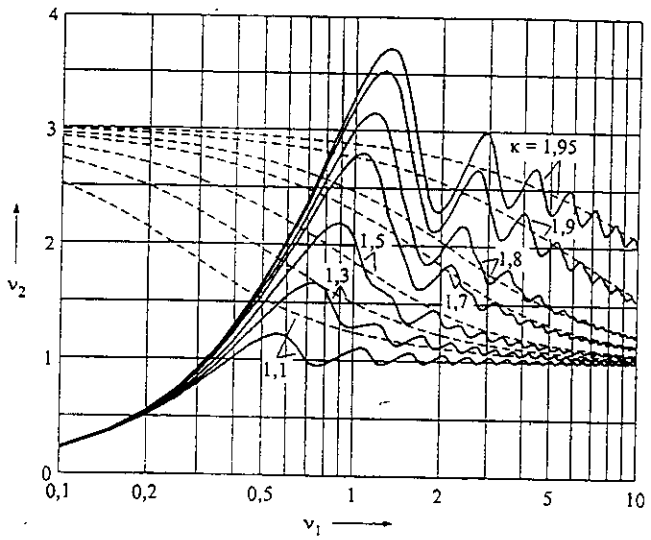

Figure 4.16: Factor ν_2 for the influence of the time history of the short-circuit current on the electromagnetic force

—— exact solution according to (*A5)

– – factor $1+\tilde{m}$

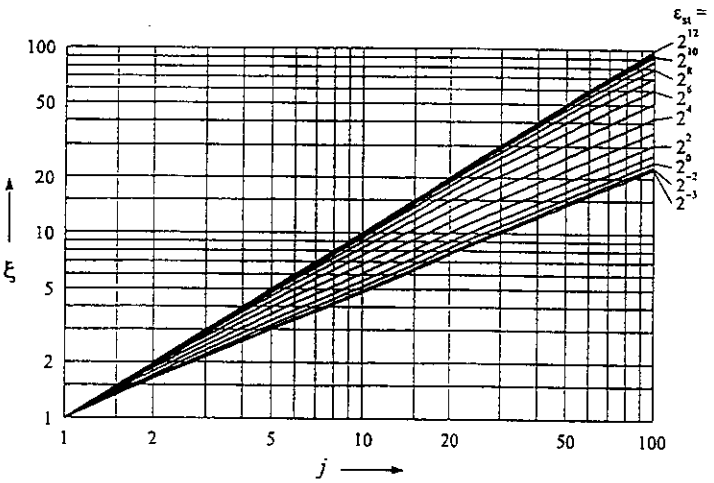

Figure: 4.17: Factor ξ for the calculation of the pinch forces in the case of clashing sub-conductors

The pinch Force F_{pi} will be dependent on three parameters:

- the ratio

$$\frac{l_s}{a_s - d_s} \tag{4.28}$$

- the time constant τ of the network

- the stiffness norm N according to (*25) which subsumes the stiffnesses of the conductors and the supporting structures.

4.3.2.4. *Clashing of sub-conductors*

If the sub-conductors are clashing, then $f_\eta = 1$ and (4.20) becomes with $\eta = 1$:

$$\xi^3 + \varepsilon_{st}\xi^2 - \varepsilon_{pi} = 0 \tag{*51}$$

This expression contains constant coefficients. ξ is analytically calculable, dependent on j with the parameter ε_{st}, Figure 4.17. For $\varepsilon_{st} = 0$ follows $\xi^3 = j^2$ from (*49) and (*51) and therefore a lower limit $\xi = j^{2/3}$. For $\varepsilon_{st}\xi^2 - \varepsilon_{pi} >> \xi^3$, an upper limit $\xi = j$ can be derived.

From (4.16) the tensile force in the bundle clamp can be given

$$F_{pi} = F_{st}\left(1 + \frac{\nu_e}{\varepsilon_{st}}\xi\right) \tag{*50}$$

Here, an overswing factor ν_e is introduced, which accounts for the dynamic process in the clashing of bundled conductors and has still to be determined more exactly in chapter 4.3.2.6.

4.3.2.5. *Non-clashing of sub-conductors*

If the sub-conductors reduce their distance without clashing, then $x_P = l_s/2$ and $y_A = a_s/(2\sin 180°/n) - y_P$ according to Figure 4.14. (4.20) becomes with $\xi = 1$:

$$\eta^3 + \varepsilon_{st}\eta - \varepsilon_{pi} f_\eta = 0 \tag{*62}$$

Here, the non-linear factor f_η must be considered, too, which is a function of a_s/d_s and η.

Therefore, the quantity η can only be numerically determined dependent on j and the parameters ε_{st} and a_s/d_s, whereby $0 < \eta < 1$.

Instead of determining $\eta(j)$ by (*62), an analytical solution $j(\eta)$ can be obtained from (*49) with the inverse function:

$$j = \sqrt{\frac{\eta^3 + \varepsilon_{st}\,\eta}{(1+\varepsilon_{st})\,f_\eta}} \qquad (*61)$$

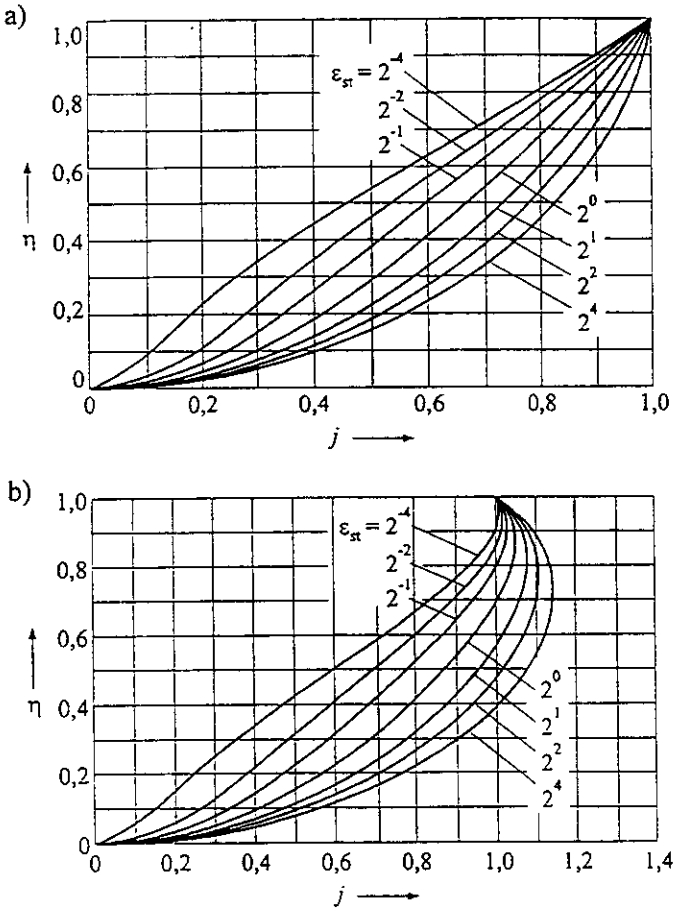

Figure 4.18: Factor η for calculation of the pinch force in the case of non clashing sub-conductors

a) $\frac{a_s}{d_s} = 2.5$ b) $\frac{a_s}{d_s} = 7.5$

Figure 4.18 a shows the factor η as a function of j with ε_{st} as parameter for close bundling $a_s/d_s = 2{,}5$ and Figure 4.18 b for wide bundling $a_s/d_s = 7{,}5$. All curves start at the origin with $dj/d\eta > 0$ and end at the point $j = 1$, $\eta = 1$. In Figure 4.18 b, all curves have horizontal tangents for $j > 1$. This is the stability limit: The following part of the curves describes (with $dj/d\eta < 0$) an unstable state. If a vertical tangent exists, there is a range $1 \le j \le j_{max}$ in which (4.20) has a stable solution η as well as a solution ξ for clashing bundles. The final static state of the sub-conductors depends on the initial state. In this case the worst has to be taken into account for design purposes: The assumption of clashing sub-conductors according to chapter 4.3.2. The difference between η and ξ near $j = 1$ is caused by the physical model of the bundle and the quasi static calculation.

From (4.16) the tensile force in the clamp can be given with the overswing factor v_e:

$$F_{pi} = F_{st}\left(1 + \frac{v_e}{\varepsilon_{st}}\eta^2\right) \qquad (*54)$$

4.3.2.6. *Dynamic overswing factor*

The calculation of the pinch force F_{pi} has been based on quasi-static considerations of the geometry and forces observed with the final state of the contracted bundle. However, in practice the sub-conductors are accelerated by the electromagnetic force acting upon them. The kinetic energy thereby absorbed is converted into elongation work in the system. However, the elongation work required to reach the final state of contraction, is lower than the kinetic energy absorbed until the final static position has been reached for the first time. The balance is converted into collision, deformation, and frictional energy, as the sub-conductors oscillate around their final position. Thereby, the first overswing movement leads to the actual maximum of the pinch force. So far, the above situation has been accounted for by a constant factor, which in practice, will be dependent upon the geometry of the bundle and the boundary conditions of the contraction.

On a differential portion of a sub-conductor, the electromagnetic force performs a differential work dW_m. Taking into account the number of sub-conductors and spacers, and assuming the shape of the curve of the clashed conductors to be a parabola, the summation of these differential works along the non-clashing section gives the work performed on the whole bundle, as:

$$W_m = n2(k+1)\int_0^{x_P}\int_{y_{P,max}}^{y(x)} \frac{\mu_0}{2\pi}\left[\frac{I}{n}\right]^2 (n-1)\frac{dy}{2y(x)}dx$$

$$= n2(k+1)\frac{\mu_0}{2\pi}\left[\frac{I}{n}\right]^2 (n-1)x_p\left\{\sqrt{\frac{y_A}{y_P}}\arctan\sqrt{\frac{y_A}{y_P}} - 1\right\}$$

(4.29)

with $y(x)$ according (4.11). With the energy conservation law and neglecting the bending stiffness of the conductor as well as the friction between the individual conductors it is:

$$W_m + W_{kin} + W_{spring} = 0 \qquad (4.30)$$

This means that the electromagnetic work performed has been converted into elongation work and kinetic energy at that point in time when the final static position has been reached for the first time. The elongation work of the spring is:

$$W_{spring} = \frac{1}{2}\frac{1}{N}\frac{\Delta l}{l}\Delta l \qquad (4.31)$$

Subsequently, the kinetic energy causes a further elongation of the equivalent spring of the overall system and thus an additional variation in length of the sub-conductors, Δl_+:

$$W_{kin} = \frac{1}{2}\frac{1}{N}\frac{\Delta l_+}{l}\Delta l_+ \qquad (4.32)$$

At the time of maximum contraction of the bundle and in analogy to (4.16), the tensile force becomes:

$$F_{pi} = nF_x = F_{st}\left[1 + \frac{1}{NF_{st}}\frac{\Delta l}{l}\left(1 + \frac{\Delta l_+}{\Delta l}\right)\right]$$

and comparison with (*50) and (*54), respectively, results in the overswing factor v_e, which is weighted by a factor of 1/2 in order to account for energy dissipation due to deformation, friction, emission of sound, etc.:

$$v_e = \frac{1}{2}\left(1 + \frac{\Delta l_+}{l}\right)$$

From (4.30) with (4.29), (4.31) and (4.32) it is found

$$\frac{\Delta l_+}{\Delta l} =$$

$$\sqrt{\frac{9n(n-1)Nl}{4(k+1)}\frac{\mu_0}{2\pi}\left(\frac{I}{n}\right)^2\frac{x_P^3}{y_P^4}\left\{1 - \sqrt{\frac{y_A}{y_P}}\arctan\sqrt{\frac{y_A}{y_P}}\right\}} - 1$$

Hence the different overswing factors v_e for the cases of clashing and non-clashing sub-conductors can be calculated

- for clashing sub-conductors

$$v_e = \frac{1}{2} + \left[\frac{9}{8}n(n-1)\frac{\mu_0}{2\pi}\left(\frac{I_k''}{n}\right)^2 N v_2\left(\frac{l_s}{a_s - d_s}\right)^4 \cdot \frac{\left(\sin\frac{180°}{n}\right)^4}{\xi^3}\left\{1 - \frac{\arctan\sqrt{v_4}}{\sqrt{v_4}}\right\} - \frac{1}{4}\right]^{1/2} \qquad (*52)$$

with

$$v_4 = \frac{a_s - d_s}{d_s} \qquad (*53)$$

- for non-clashing sub-conductors

$$v_e = \frac{1}{2} + \left[\frac{9}{8}n(n-1)\frac{\mu_0}{2\pi}\left(\frac{I_k''}{n}\right)^2 N v_2\left(\frac{l_s}{a_s - d_s}\right)^4 \cdot \frac{\left(\sin\frac{180°}{n}\right)^4}{\eta^4}\left\{1 - \frac{\arctan\sqrt{v_4}}{\sqrt{v_4}}\right\} - \frac{1}{4}\right]^{1/2} \qquad (*55)$$

with

$$v_4 = \eta\frac{a_s - d_s}{a_s - \eta(a_s - d_s)} \qquad (*56)$$

4.3.3 *Design load*

For the design of substations, the following should particularly be noted:

- In most cases, the tensile forces F_t during a short-circuit are maximum for the coldest conductor.
- The higher the span temperature the higher the span displacements and the tensile forces F_f after a short circuit. Therefore, in most cases, the tensile forces F_f after a short circuit are maximum for high temperatures.
- The tensile forces F_{pi} caused by the pinch effect are also maximum for the coldest conductor.

To be sure to get the worst case, it is necessary to do the calculations of F_t, F_f and F_{pi} on the basis of the static tensile force F_{st}

- at the local minimum winter temperature, e.g. -20°C,

– at the maximum operating temperature, e.g. 60°C.

For each tensile force, the highest value shall be taken into account.

The maximum value of F_t, F_f or F_{pi} shall not be greater than the rated withstand value given by the manufacturer of supports and insulators. The connectors for the conductors shall be rated on the basis of

– the maximum value of $1.5F_t$, $1.0F_f$ or $1.0F_{pi}$ in the case of slack conductors on post insulators,
– the maximum value of $1.0F_t$, $1.0F_f$ or $1.0F_{pi}$ in the case of strained conductors with insulator chains.

The design load may be treated as an exceptional load case, e. g. as for earthquakes, according to design standards, because high value short-circuits are rare events.

For three-phase short-circuits in structures with strained conductors, it should be remembered, that the maximum value of F_t or F_f will appear in outer two phases, and the third phase will be subjected only to the static tensile force, see Figure 1.1. Different values of F_{pi} at different times may occur in the three phases; this effect will be met approximately by applying the calculated F_{pi} in two phases of the structure.

More complex dynamic structural analysis will be investigated in the next brochure to better fit F_{pi} with actual design load.

4.4 ADVANCED CALCULATION METHODS

The use of modern finite element analysis is particularly suited for detailed dynamic analysis of substation bus systems under short-circuit conditions. The use of such methods can be very cumbersome; but recently the development of "conviviality" tools has been of significant help for some users. They are needed if the complexity of the phenomenon is to be adequately represented. The use of such methods will allow, for example, the accurate and detailed modelling of the conductors, the connecting hardware, the droppers to lower apparatus and to the support structures. Interactions between conductors, hardware and support structures can be easily taken into account, even with a simplified model for the supporting structure. Work on the development of such models for short-circuit structural analysis has been and is being carried out in several countries (mainly France, Belgium and Germany). Nowadays advanced methods can be used by designers for single conductor arrangement, sometimes with advanced user-friendly tools (using a conductor data base, user-friendly interface, automatic report generation, etc...). Of course dynamic analysis is also available for other kinds of loads (wind, ice) and sagging conditions. This has been made possible as a result of the impressive gains in computer hardware and software tools (computation times are nowadays only a few minutes on classical up-to-date workstations), especially on workstation on which these kinds of tools are available. But as indicated earlier, bundle pinch effects models, even if available, still remain tools for specialists.

In brief, modern design engineering offices now have the possibility to apply directly advanced methods on single conductor bus-bars (a bundle can also be studied by single conductor),to calculate both swing-out and falling down maxima. But the pinch effect is still in the domain of research and can only be applied by specialists.

Uprating of existing structure

In this case, the use of advanced methods to get less conservative and more accurate results may be justified in comparison with the costs of possible structural modifications.

In some cases, depending on technical requirements and cost/benefit considerations, uprating may be limited to avoid any modification, by accepting the evaluation of the existing structure and fully utilizing the revised rating.

Generalities

The occurrence of short-circuit currents in substations with flexible conductors leads to large transverse conductor motions. These motions cause an increase in conductor tension, resulting in dynamic loadings on several components of the bus structure. For severe short-circuit conditions, extreme conductor motions result, which lead to highly non-linear dynamic behaviour. As described in the previous sections, designers have the option of considering testing or simple calculation methods. However, in some cases there is a need for more detailed results covering a range of design parameters, which leads to the possibility of using advanced dynamic non-linear simulation

analyses. These analyses can be used for all cases A, A+B, C, D , etc... (as illustrated in Fig. 1.8) and can provide the designer the possibility to evaluate relatively easily, stresses and strains anywhere in a substation and for a range of substation parameters and configurations. This capability contrasts with simplified methods which may not provide good representation for some of the design parameters and experimental testing, where detailed studies are restricted to a limited number of locations and configurations.

General Features of Mechanical Model

A reasonable electromechanical model of a substation should represent not only large displacements of cables (non-linear theory) but also temperature and damping effects, various boundary conditions (for example, clamped and free-supported joints), the type of foundation for the supporting structures, service conditions such as the type of short circuit, duration of short-circuit current, multiple reclosure, actual short-circuit electromagnetic forces and so on.

A very important problem is the exact system loading caused by electromagnetic short-circuit current forces, including conductor to conductor interactions. These electrodynamic interactions essentially depend on the actual configuration of conductors. In this way electromagnetic and mechanical effects are combined. Portal structures can be modelled with finite elements. However, these can be replaced for analysis purposes by simpler equivalent substructure representations.

A detailed presentation of advanced computation methods will be found in the next brochure, including experimental validations which are impressive.

Further information on the current state-of-the-art for advanced analysis techniques can be obtained through any members of the ESCC task force, especially from those from Belgium, France and Germany.

4.5 PARAMETER ANALYSIS

4.5.1 Introduction and General Parameters

The aim of this parameter study is to give design engineers a good qualitative and hopefully intuitive understanding of how short-circuit phenomena are influenced by the respective physical and electrical parameters. Readers new to this field, may be able to obtain a better understanding of the phenomenon by not focusing on a specific case with specific data; but attempt to get an overall view of the influences of various parameters by understanding what happens when they are varied. For example, a parametric study on the choice of subspan length can be very instructive. The analysis described in this section is the result of numerous calculations based on IEC method according to sections 4.2 and 4.3.2.

The parameter analyses have been limited to the following two items (Case A, C, D according to Fig. 1.8):

- phase-to-phase interactions (cases A and C, excluding pinch effect), effects on tensile forces (section 4.5.2) and deflections (section 4.5.3)
- bundle pinch effect (section 4.5.4)

Note that for Case D (jumper) clearance is developed in section 4.5.3 and bundle jumper in section 4.5.4.

The approach is more qualitative than quantitative; nevertheless, it provides useful guidance to the design engineer. The parameters that have been considered are listed in Table 4.1.

Table 4.1: Parameters included

Current parameters: - r.m.s. short-circuit current magnitude - network time constant - duration of short-circuit - automatic reclosing
Conductor parameters: - initial static tensile force - (sub)span length - distance between main conductors - distance between sub-conductors - number of sub-conductors - cross section - mass - Young's modulus - spacer stiffness
Supporting structure parameters: - anchoring structure stiffness (spring constant) - dynamic spring constant (bundle only)

As conductor heating is always associated with short-circuit current flow, this effect has been included in the analysis.

Results of importance for the designer are:

- In cases A and C: short-circuit tensile force F_t, drop force F_f, and deflections;
- For bundled conductor configurations, only the pinch force F_{pi} is discussed.

For the general purposes of parameter analysis, independent consideration of each of the parameters in Table 4.1 is awkward because of the compensating interactions between the parameters. Therefore, more general undimensional parameters have been introduced by selectively grouping related parameters from Table 4.1. A very limited number of dimensionless parameters gives a better understanding of the interactions between the parameters. As a result of numerous discussions, four parameters were identified for main conductor effects; and three for pinch effect. They are described in the following paragraphs.

The Force Factor

Short-circuit forces can cause relatively high acceleration in comparison with the forces of gravity depending on the magnitude of short-circuit current. The ratio between the forces per unit length (short-circuit and gravitational forces) which is equal to the corresponding acceleration ratio, is defined as the first parameter (the force factor):

$$r = \frac{F'}{G'} = \frac{F'}{n m'_s g_n} \qquad (*20)$$

where

$$F' = \frac{\mu_0}{2\pi} \frac{(I''_{k2})^2}{a} \frac{l_c}{l} \qquad (4.3)$$

see section 4.2.7. The factor r is only valid for main conductor effects.

For bundle configurations, the effects between the sub-conductors of one main conductor are given by a specific case of r indicated by r_S:

$$r_s = \frac{F'_s}{G'_s} = \frac{F'_s}{m'_s g_n} \qquad (4.33)$$

where

$$F'_s = (n-1)\frac{\mu_0}{2\pi}\left(\frac{I''_k}{n}\right)^2 \frac{\sin(\pi/n)}{a_s} \qquad (4.34)$$

$a_s/\sin(\pi/n)$ is the diameter of the bundle.

In practice, r values are in the range 0 to 6 and r_s values are in the range 0 to 100.

The Network Factor

As discussed in section 1.1, the waveform of the short-circuit current can be approximated by a mathematical formula which includes only one time constant τ. This value is fixed by the network. Obviously, τ is an independent parameter. The dimensionless time parameter $\omega\tau$ is obtained using the frequency of the current.

Although $\omega\tau$ is independent of the asymmetry level of the current, the current waveform asymmetry is an important parameter. The current waveform asymmetry is dependant on the angle of fault initiation which, in practice, is an independent, statistical parameter. For practical design purposes, the conservative assumption of maximum asymmetry is usually made.

Values of $\omega\tau$ are typically in the range of 5 and 50 (τ from 15 to 160 ms).

Short-Circuit Duration Factor

For main conductor effects, the short-circuit duration is an important parameter. As described in earlier sections, line-to-line short-circuits (worst case) can induce significant low frequency displacements. The frequency is related to the oscillation period of the pendulum model of the span. In situations like case A or C, this oscillation period is given by the simple pendulum formula:

$$T = 2\pi\sqrt{0{,}8\frac{b_c}{g_n}} \qquad (*23)$$

The maximum swing out of the cable is a function of the duration of the short-circuit and the period of oscillation of the busbar. This leads the next parameter given by:

$$\frac{T_{k1}}{T} \qquad (4.35)$$

For sags between 0,5 and 2 meters, T ranges from 1,25 to 2,5 s. Values of T_{k1}/T typically range between 0,015 and 0,3, sometimes higher; but the maximum stress increases until T_{k1}/T_{res} reaches a maximum of 0,25, T_{res} according to (*24).

The Structural Factor

The response of the structure to the applied force is not obvious. There is a complex relationship between sag, tensile force, span length, mass and stiffness of conductors and the stiffness of the anchoring structure. In order to determine the structural behaviour of the complete bus the stress factor

$$\zeta = \frac{(n m'_s l g_n)^2}{24 F_{st}^3 N} \qquad (*28)$$

is used as a parameter.

In a physical sense, ζ is a ratio between two flexibilities, namely:

- the intrinsic stiffness of the cable in series with the anchors:

$$Nl = \frac{1}{S} + \frac{l}{nE_s A_s} \qquad (*25)$$

- the extrinsic stiffness resulting from the initial conditions, mainly the ratio sag to span length:

$$\frac{64}{3}\frac{1}{n m'_s g_n}\left(\frac{b_c}{l}\right)^3 \qquad (4.35)$$

In practice, anchoring stiffnesses range between 10^5 and $5{\cdot}10^6$ N/m, and values of parameter ζ are between 15 and 300.

For bundle pinch effect

$$\frac{l_s}{a_s - d_s}\sin\frac{180°}{n} \qquad (4.28)$$

is the subspan parameter. In the flexibility norm Nl the stiffness S_z of the spacers can be included:

$$Nl = \frac{1}{S_d} + \frac{1}{S_z} + \frac{l}{nE_s A_s} \qquad (4.36)$$

S_d is the equivalent dynamic stiffness, which can include dynamic behaviour of supporting structure and S_z is the spacer stiffness.

In practice, values are between:

$$3 \le \frac{l_s}{a_s} \le 500, \quad 1 \le \frac{a_s}{d_s} \le 40$$

and therefore

$$3 < \frac{l_s}{a_s - d_s} \sin\frac{180°}{n} < 1700$$

Normalised tension and deflection

The increase of tension is the main concern for the design of the structure. For main conductor interactions, F/F_{st}, with $F = F_t$ or F_f or F_{pi} has been selected as the basis for normalisation.

Another design value for the substations is the clearance. It can be easily deduced from the normalised deflection b_h/b_c.

Example of calculation

In the following paragraphs, the parameter values for a typical example bus configuration are calculated. In later parts of this section, the example is continued to illustrate specific aspects of the variation of parameters.

Data of a 380-kV-span with strained conductors:

Three-phase initial symmetrical short-circuit current (r.m.s.) I''_{k3} = 63 kA
Factor for calculation of peak short-circuit current κ = 1,81
Duration of the first short-circuit current flow T_{k1} = 0,5 s
Distance between supports l = 48 m
Length of the conductor carrying short-circuit current ($l_c = l - 2l_i$, where l_i is the length of one insulator chain l_i = 5,3 m)
Centre line distance between main conductors a = 5 m
Twin conductor 2 ACSR 1045/45
- Number of sub-conductors n = 2
- Sub-conductor cross section A_s = 1090 mm²
- Sub-conductor mass per unit length m'_s = 3,25 kg/m
- Young's modulus E = 60000 N/mm²
- Sub-conductor diameter d_s = 43 mm

Distance between sub-conductors a_s = 400 mm
Distance between to adjacent spacers l_s = 9,4 m
Mass of one insulator chain m_I = 250 kg
Resulting spring constant of both supports of one span S = 500 N/mm
Static sag at midspan at a temperature of 60 °C, that gives $b_{c,st}$ = 1,7 m
- Static conductor tensile force at local minimum winter temperature -20 °C F_{st} = 17 kN
- Static conductor tensile force at maximum operating temperature 60 °C F_{st} = 14 kN

Table 4.2: Parameter values for the effects

Temperature	°C	-20	60
E_s	N/mm²	28280	26410
N	10^{-8}/N	5,79	5,9
$b_{c,st}$	m	1,4	1,7
$b_{c,st}/l$	%	2,9	3,5
b_c	m	1,08	1,31
b_c/l	%	2,3	2,7
F'	N/m	92,78	92,78
r	1	1,455	1,455
ζ	1	1,371	2,409
τ	ms	45,5	45,5
T	s	1,865	2,055
T_{k1}/T	1	0,268	0,243
T_{k1}/T_{res}	1	0,335	0,304
r_s	1	15,6	15,6
a_s/d_s	1	9,3	9,3
l_s/a_s	1	23,5	23,5
$\frac{l_s}{a_s - d_s}\sin\frac{180°}{n}$	1	26,3	26,3

4.5.2 Effects on Tensile Forces F_t and F_f

A qualitative approach can be used to determine the effects on the conductor tension caused by variations in electrical and physical parameters. These effects are illustrated by families of curves given in Figures 4.20 and 4.21 at local minimum winter temperature of -20 °C.

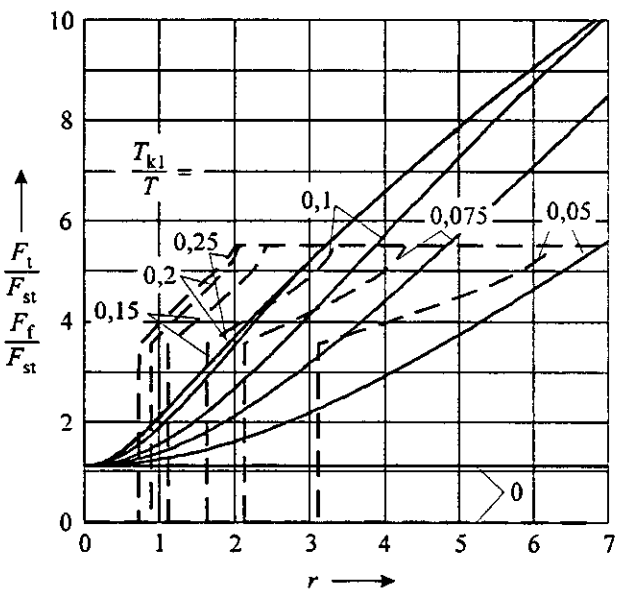

Fig. 4.20: Effect of force factor r on normalised conductor tensile force for several short-circuit duration ratios T_{kl}/T

sress factor $\zeta = 2,5$

—— short-circuit tensile force F_t

– – – drop force F_f

Parameters : I_k, a, m', Heating, T_{kl}

The combined interaction of the first four parameters (I_k, a, m', heating) are included in r, the most important parameter. As a result, all of the curves in Figures 4.20 and 4.21 describe the effect on r (abscissa) caused by all of the other parameters.

The short-circuit tensile force F_t is increasing monotonously with r whereas the drop force F_f is zero for $\delta_m < 70°$ (no fall down occurs) and becomes constant for $\delta_m > 180°$ (maximum at $\delta_m = 180°$ is decisive), see clauses 4.2.2 and 4.2.5.

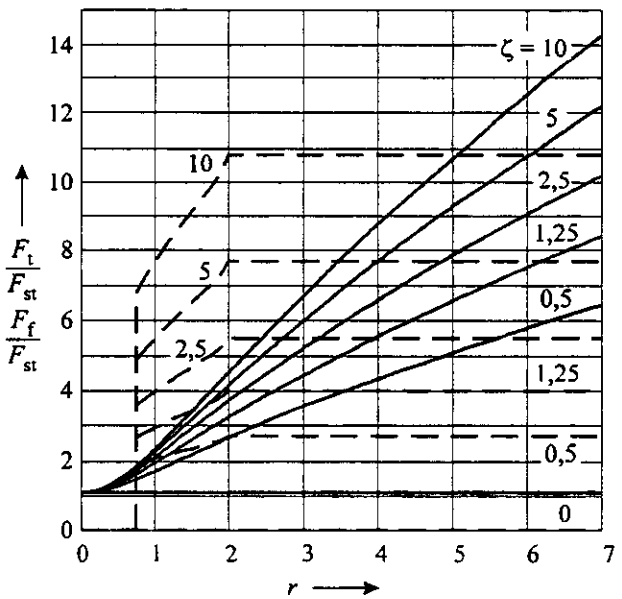

Fig. 4.21: Effect of force factor r on normalised conductor tensile force for several stress factors ζ short-circuit duration $T_{kl}/T = 0,25$

Obviously, r should be as low as possible (because a lower r implies a lower normalised tension). From the definition of r, an increase of fault current level of a factor 1,25 (for example from 63 to 80 kA) can be fully compensated by an increase in the distance between main conductors or main conductor weight by a factor of 1,56.

If the product $r\ T_{kl}/T$ (input energy) is lower than approximately 0,25 (this value can be found in Figure 4.20), the drop force is higher than the short-circuit tensile force. Both maximum forces are of the same order of magnitude for a very limited range of r.

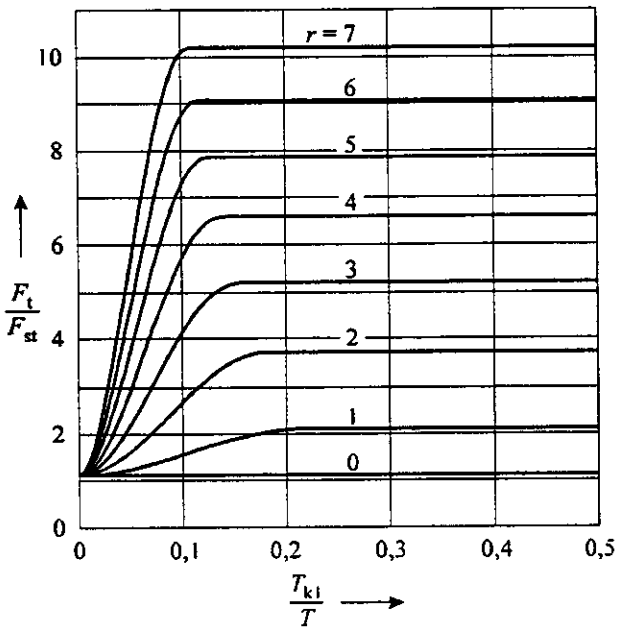

Fig. 4.22: Effect of several short-circuit duration ratio T_{kl}/T on normalised conductor tensile force for force factors r sress factor $\zeta = 2,5$

Figure 4.22 illustrates the effect of T_{kl}/T_{res} (relative time duration of the fault). Swing out maximum F_t for a given r (relative short-circuit force), increases with the time duration of the fault until this time is equal to a quarter of the period of the pendulum oscillation of the cable busbar T_{kl}/T_{res}. Beyond this value T_{kl}/T_{res} = 0,25, a saturation effect is apparent. This is logical because at this moment, the cable has just reached its maximum horizontal displacement limited by elasticity. If the short-circuit duration is greater than $T_{res}/4$, natural movement of the cable is disturbed by the electromagnetic force action. Generally, this case will cause lower stresses because swing out is not amplified and falling down pattern is disturbed. This is fully compatible with the worst case of the simple method developed in section 4.2.

Parameter: τ

For a given short-circuit force (r fixed) there is an increase of the swing out stresses when the power system time constant increases. The increase is the result of increased input energy. In addition, as indicated previously, short-circuit tensile force is significantly affected by the extent of the current waveform asymmetry. The network time constant varies at different locations in the power system. At a given location in the network, network time constant and $\omega\tau$ are fixed; but the level of asymmetry depends on the time of initiation of the fault. As stated earlier, the time of short-circuit initiation is an uncontrolled statistical parameter for which designers typically make the conservative assumption that in all cases maximum current offset occurs.

Parameters: S, S_d, b_c, F_{st} and l

The structural parameter ζ, has a fundamental relationship with the fall of span maximum tension Figure 4.21. The ratio between the drop force and the short-circuit tensile force F_f/F_t decreases very quickly with ζ. High anchoring stiffness is generally not recommended. If necessary for other purposes, anchoring stiffness can be balanced by high initial tensile force. Increasing ζ for example by using a higher anchoring stiffness also has a sensitive effect on the swing out maximum tension. An increase in anchoring stiffness of 100 % can result in an increase in the short-circuit tensile force of about 25 %.

The ratio of sag to span also has a significant influence on ζ. If this ratio is held constant, ζ remains quasi-constant independent of the span length. In such cases, span length has no influence on the normalised forces.

Automatic reclosing

The problems associated with unsuccessful automatic reclosing cannot be studied in detail by simple method given in clause 4.2 because the response varies depending on the new initial conditions at the instant of automatic reclosing. The span movements can be amplified if automatic reclosing occurs during the swing out or limited if it appears after the swing out maximum. The worst case occurs when automatic reclosing coincides with the maximum separation speed. Critical cases are then:

$$T_{kl} + T_u < 0,25\ T_{res} \quad \text{and}$$

$$0,75\ T_{res} < T_{kl} + T_u < 1,25\ T_{res}$$

where T_u is the dead time(time without current).

In general, the effects of automatic reclosing are smaller for flexible bus than for rigid bus; tension

and deflections are not usually amplified by a factor of 2.

4.5.3 Effects on Deflections

These effects are illustrated qualitatively in the curves given in Figs. 4.23 to 4.24 at 60 °C which gives the greatest deflections.

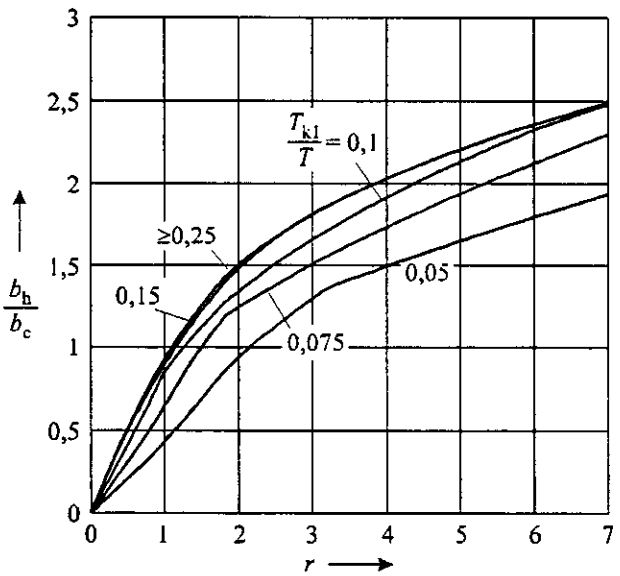

Fig. 4.23: Sensitivity of relative displacement to force factor r for several short-circuit duration ratios T_{k1}/Tsress factor $\zeta = 2,5$

Increases in effective sag are the result of conductor heating, elasticity of the conductors and anchoring structure and changes in the span geometry. For case A, movement of the bus is strongly influenced by the presence of droppers (connections to apparatus). For case D, the initial static tension may be very low, and thus ζ may be considered at the highest value. Clearance is simply given by:

$a - 2b_h$

where b_h is the inwards deflection of the span at midpoint. Recalling that b_c is the sag of the cable only excluding the insulator string, real clearance will also be reduced by the movement of insulator strings.

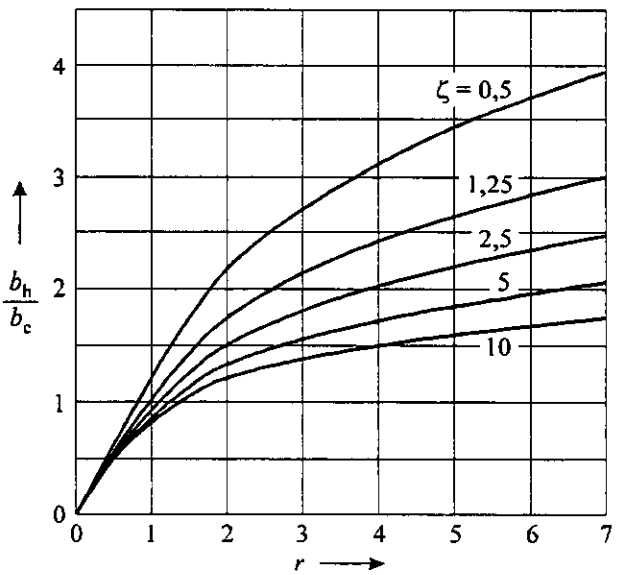

Fig. 4.24: Sensitivity of relative displacement to force factor r for stress factors ζ short-circuit duration $T_{k1}/T = 0,25$

In general the influence of ζ, $\omega\tau$, T_{k1}/T on deflections is similar to that for the short-circuit tensile force F_t. Figure 4.23 illustrates the significant influence that the duration of the short-circuit has on deflections; deflections can be amplified by a factor of 2 between a very short and a very long fault. A very long fault time could, for the purposes of parameter analysis, be equivalent to a normally cleared fault followed quickly by unsuccessful automatic reclosing.

The hypothesis that maximum inward movement is limited to the initial sag ($b_h/b_c < 1$) is not correct. As with mechanical tension, the structural factor ζ relates to clearance effects; an increase of ζ, i. e. a more rigid structure, will limit the displacement and increase the stress. But the benefit in clearance caused by an increase of ζ is much lower than the increase in stress (fall of span) for the same modification of structural stiffnesses.

Automatic reclosing effects can clearly amplify the displacement and critical cases are the same as for tensile forces.

4.5.4 Pinch Effects

Bundle pinch tension is clearly a separate problem from that of interphase effects. This fact is a result of the completely different mechanical time constants for the two phenomena. A simplified method for the bundle pinch phenomenon has been described in section 4.3. This section discusses the parameter sensitivity aspects of bundle pinch.

Parameter sensitivity

This study is based on the sensitivity of the peak value of the pinch force F_{pi}, as a function of the parameters which influence it, see Table 4.5.1. As discussed earlier, dimensionless parameters for bundle pinch effect are reduced to only three values: short-circuit force factor r_s, time constant $\omega\tau$ and geometry of the bundle $l_s/(a_s - d_s)\cdot\sin(\pi/n)$. As far as a qualitative approach is concerned, $\omega\tau$ is not varied but included in m, as in section 4.2 by the factor ν_2.

Figures 4.25 to 4.29 illustrate influences on the design F_{pi}. On the abscissa, there is always $l_s/a_s\cdot\sin(\pi/n)$ and the pinch force is related to the static tensile force F_{st}. Due to the complexity of the dependence of the parameters on F_{pi}, the change is shown by variation of r_s, a_s/d_s, F_{st}, S and n to give a physical feeling on the phenomena. Based on the data given in section 4.5.1, one of the values is varied. In all diagrams, in the left part of the curves for low $l_s/a_s\cdot\sin(\pi/n)$ the conductors reduce their distance without clashing, in the right part they are clashing.

Figure 4.25 shows the influence of r_s. In Figure 4.25a the mass per unit length of the sub-conductors is the parameter. The diameter is adopted to the mass so that the mass density remains equal. The sag b_c and the short-circuit current I''_k are constant. In Figure 4.25b the short-circuit current I''_k is parameter, 20 kA ≤ I''_k ≤ 80 kA and the mass per unit length of the sub-conductors is constant. In both cases, F_{pi} decreases with decreasing r_s: Higher conductor mass or lower current give lower forces.

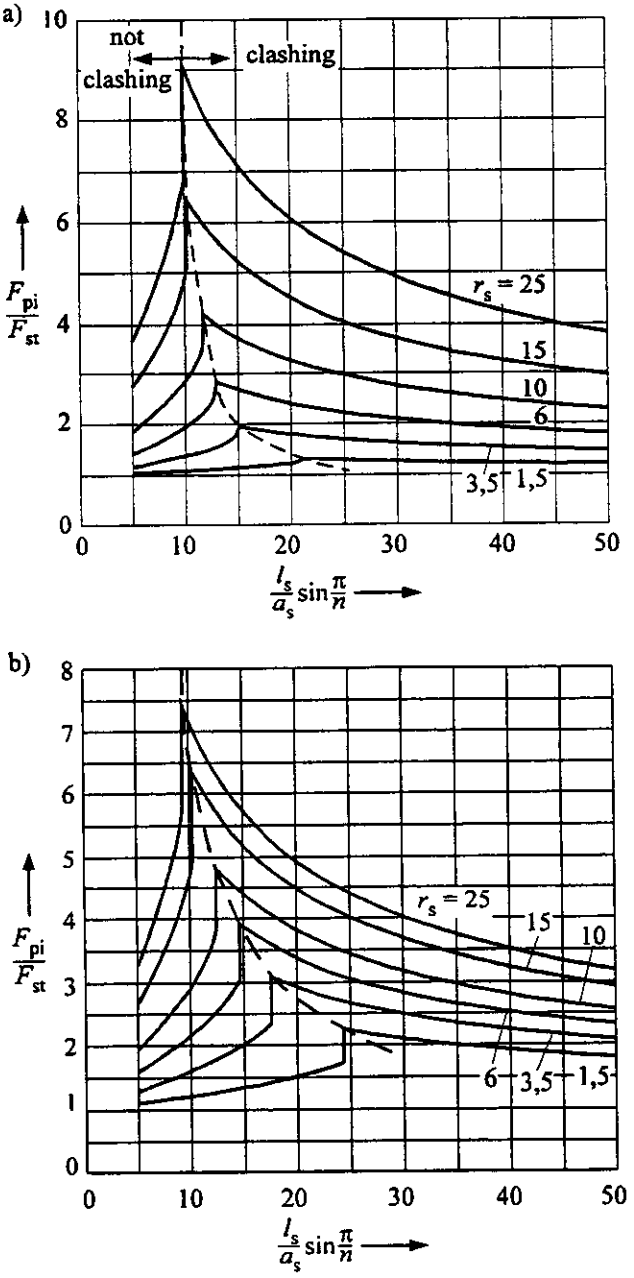

Fig. 4.25: Effect of bundle diameter $l_s/a_s\cdot\sin(\pi/n)$ on normalised pinch force F_{pi} for several force factor r_s

a) variation of conductor mass; short-circuit current I''_{k3} and equivalent static sag b_c are constant
b) variation of short-circuit current I''_{k3}; conductor mass is constant

The dotted line is the border between sub-conductor contact and non-contact. For low r_s

(low short-circuit force) contact between sub-conductors does not occur. But this current level is more an overload than a short-circuit and for these cases designers should refer to [22]. For a given short-circuit force, the maximum peak will occur at the border line. This is logical because the border line corresponds to conditions for maximum force action (shortest contact length). On crossing the border into the contact zone, there is a rapid decrease of the peak force because the contact length increases very quickly and the effective length contributing electromagnetic force decreases proportionately.

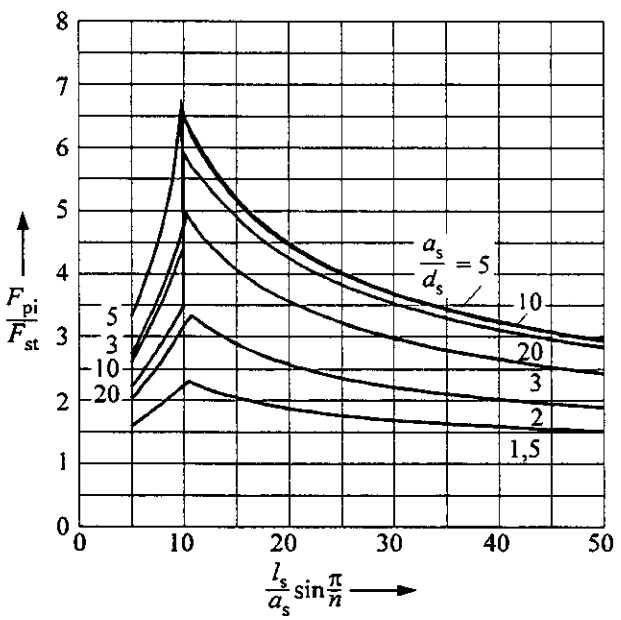

Fig. 4.26: Effect of bundle diameter $l_s/a_s \cdot \sin(\pi/n)$ on normalised pinch force F_{pi} for several ratios a_s/d_s

Figure 4.26 demonstrates the change in spacing related to the conductor diameter a_s/d_s, where 65 mm $\leq a_s \leq$ 860 mm. As the abscissa is also related to a_s, all maxima occur near $l_s/a_s \cdot \sin(\pi/n) \approx 10$ and the highest forces are got near $a_s/d_s \approx 5$ for the same value of l_s/a_s. For equal values of l_s, they decrease with the space between the sub-conductors. Therefore the distance between the conductors should be as low as possible.

The related pinch force decreases with increasing static tensile force, Figure 4.27, whereas the actual value of the pinch force increases little.

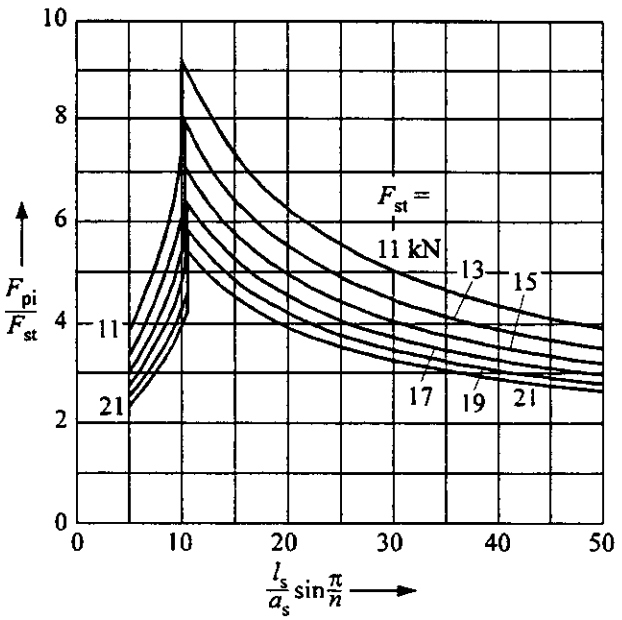

Fig. 4.27: Effect of bundle diameter $l_s/a_s \cdot \sin(\pi/n)$ on normalised pinch force F_{pi} for several static tensile forces F_{st}

The higher the spring rate of the substructure, the higher the pinch force, Figure 4.28.

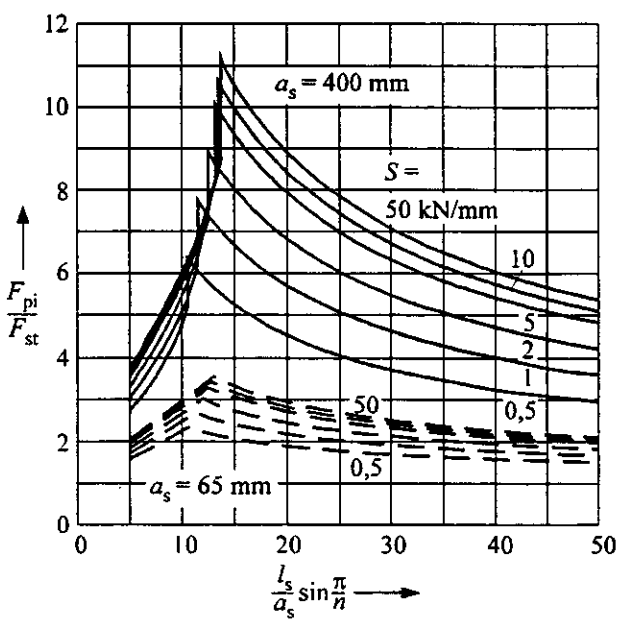

Fig. 4.28: Effect of bundle diameter $l_s/a_s \cdot \sin(\pi/n)$ on normalised pinch force F_{pi} for several spring rates of the substructure S and spacings a_s = 400 mm and 65 mm

For design, the substructure should be as flexible as possible. Close bundling results in lower forces, but the effect of the spring rate is the same.

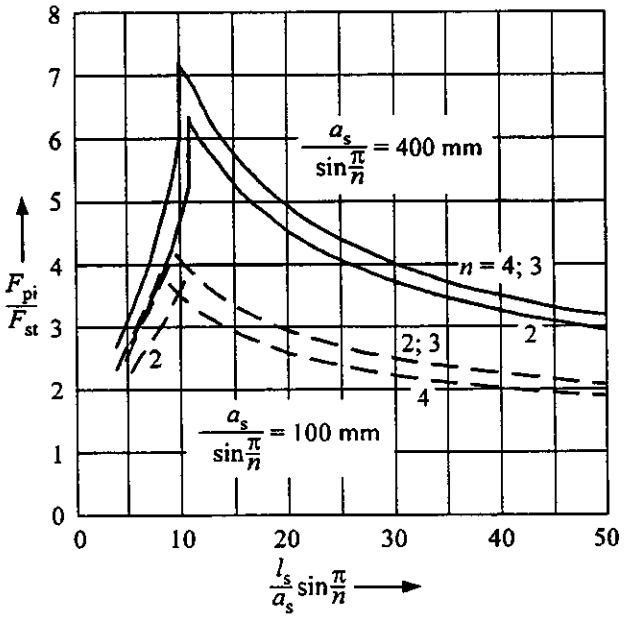

Fig. 4.29 Effect of bundle diameter $l_s/a_s \cdot \sin(\pi/n)$ on normalised pinch force F_{pi} for several number n of sub-conductors and bundle diameters $a_s/\sin(\pi/n)$ = 400 mm and 100 mm

In Figure 4.29, the number of sub-conductors is varied. For the diameter of the bundle $a_s/\sin(\pi/n)$ two different values are chosen: 400 mm and 100 mm. a_s becomes lower with increasing number n because $a_s/\sin(\pi/n)$ is constant. As the abscissa does not depend on n, it shows, that more sub-conductors cause higher forces in the case of wide bundling, whereas lower forces can be possible with close bundling.

Configurations in substations can typically fall in the dangerous zone of high peak tension. Jumpers, because of the very short subspan length, are generally designed in the non-contact zone. Overhead lines are typically designed with a very large l_s/a_s and contact will always occur. Sub-station busbars (case A) or connections between apparatus (case C) are in between. Hence, this problem should be given careful consideration in design.

Heating of the conductors resulting from the short-circuit current does not influence F_{pi} because the temperature increase is usually negligible before the time of peak tension. Short-circuit time duration T_{k1} generally has no influence on bundle pinch because peak tension usually occurs before T_{k1}. Automatic reclosing causes the same effects as the first fault, but the automatic reclosing pinch effect must be superimposed on the interphase effect to obtain the total phase tension. Thus, coincidence of unsuccessful automatic reclosing with maximum swing out or fall of span time will cause a very significant increase of the stress as shown in Figure 4.30.

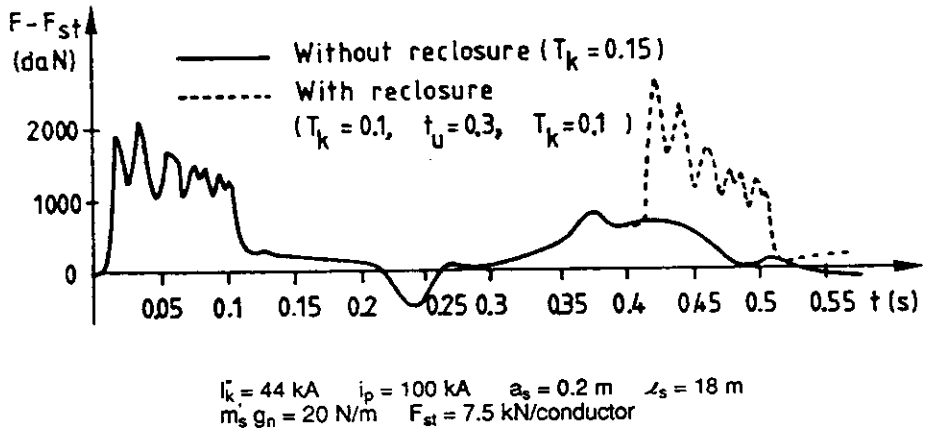

Fig. 4.30: Tensile force in a twin bundle ACSR 2×587 mm² (d_s = 31,5 mm) according to the calculations by Mlodzianowski

Generally the analysis of one subspan will give the same results as for the complete span. Also as indicated above, this effect can be superimposed on the interphase effects. However, in some cases, unsymmetrical subspan lengths can cause additional effects. This is represented in ε_{st} by S_d the equivalent dynamic spring rate of end point of the subspan. Because of the high frequency of the phenomenon, this value is not the same as the static spring rate. It is always a larger value than the static spring rate and it is also indirectly a function of the current. S_d is also dependant on the inertial behaviour of end points of the subspan. For case C, it can be considered to be infinite; but for case A, S_d is a function of the inertial behaviour of the connecting hardware and insulator string. An estimate of the order of magnitude of S_d is 10^7 N/m.

4.5.5 Applications

The qualitative effects of variations of parameter values can be easily deduced from the grouped parameters described in the previous sections. Thus a good appreciation for the design sensitivity can be obtained. The following examples are based on the data given in section 4.5.1.

Main conductor effects

Figures 4.20 to 4.24 can be used as correcting factors. Referring to section 4.5.1 (example of calculation), the 380-kV-substation busbar is characterised by r, T_{kl}/T and ζ according to Table 4.2. This gives with Figures 4.21 and 4.24:

Temperature	-20 °C	60 °C
F_t/F_{st}	2,6	2,8
F_t	44,2 kN	39,2 kN
F_f/F_{st}	3,5	4,5
F_f	59,9 kN	63,0 kN
b_h/b_c	1,32	1,22
b_h	1,42 m	1,60 m

This shows, that in the example

- the short-circuit tensile force F_t has its maximum at the lowest winter temperature;
- the drop force F_f has its maximum at the highest operating temperature;
- the drop force F_f at the highest operation temperature is decisive for the short-circuit strength due to main conductor effects;
- the horizontal deflection b_h has its maximum at the highest operating temperature.

Therefore only the influences on the drop force F_f and the horizontal displacement at the highest operation temperature are investigated in the following.

Qualitative influences can then be deduced:

- The influence of a decrease of the mass by 20 %, which means for example a conductor ACSR 680/85, keeping the equivalent static sag according (*22) constant, resulting in $m'_s = 0{,}8 \cdot 3{,}25$ kg/m = 2,6 kg/m. This leads to following correction factors

$$F_{st} = 0{,}8 \cdot 14\text{kN} = 11{,}2\text{kN}$$

$$r = \frac{1}{0{,}8} \cdot 1{,}455 = 1{,}82$$

$$\zeta = \frac{0{,}8^2}{0{,}8^3} \cdot 2{,}409 = 3{,}01$$

with Figure 4.21:

$$\frac{F_f}{F_{st}} = 5{,}5$$

which gives

$$F_f = 5{,}5 \cdot 0{,}8 \cdot 14\text{kN} = 61{,}6\text{kN}$$

Thus, the decrease and also the increase of mass, keeping the equivalent sag constant, makes no modification of the tensile forces which has to be supported by the anchoring structure. Keeping the actual sag constant gives the same result.

Figure 4.24 gives for the relative horizontal displacement

$$\frac{b_h}{b_c} = 1{,}4$$

$$b_h = 1{,}4 \cdot 1{,}31\text{m} = 1{,}82\text{m}$$

On the other side the decrease of mass leaving the static sag constant increases the horizontal displacement by about 14 % and decreases the air clearance accordingly.

- The influence of an increase of the span length, by 20 %, keeping the ration of equivalent sag to span length b_c/l constant, leads to:

$$\frac{b_c}{l} = \frac{G'l}{8F_{st}} = \text{constant}$$

$$F_{st} = 1{,}2 \cdot 14\text{kN} = 16{,}8\text{kN}$$

$$N = 50 \cdot 10^{-6} \frac{1}{N}$$

N decreases about 15 %. This gives

$$\zeta = \frac{1{,}2^2}{1{,}2^3 \cdot 0{,}85} \cdot 2{,}409 = 2{,}362$$

which is nearly constant. With Figure 4.21 and $r = 1{,}455$ it follows that F_f / F_{st} is not affected. Because F_{st} had to be increased by 1,2 to keep the ratio b_c/l constant, *the final absolute tensile force is increased by 20 % in comparison with that of the initial structure.*

Figure 4.24 gives for the relative displacement

$$\frac{b_h}{b_c} = 1{,}35$$

$$b_h = 1{,}35 \cdot 1{,}31\text{m} = 1{,}77\text{m}$$

The displacement increases about 11 %.

- The influence of an increase in initial static tensile force by 20 % leads to:

$$F_{st} = 1{,}2 \cdot 14\text{kN} = 16{,}8\text{kN}$$

With

$$b_c = \frac{G'l^2}{8F_{st}} = \frac{1}{1{,}2} \cdot 1{,}31 = 1{,}09$$

$$T \approx 2\pi\sqrt{0{,}8 \cdot \frac{b_c}{g_n}}$$

it follows

$$\frac{T_{k1}}{T} = \sqrt{1{,}2} \cdot 0{,}243\text{ s}$$

$$\zeta = \frac{1}{1{,}2^3} \cdot 2{,}409 = 1{,}394$$

The correcting factor resulting from T_{k1}/T is negligible. The correcting factor resulting from ζ (Figure 4.20) which means a decrease by about 20 % in the relative stress F_f/F_{st}, but the increase, by the same 20 %, in initial static tension *gives no change in the final absolute drop force* F_f.

Figure 4.24 gives for the relative displacement

$$\frac{b_h}{b_c} = 1{,}4$$

$$b_h = 1{,}4 \cdot 1{,}09\text{m} = 1{,}53\text{m}$$

The displacement decreases about 4 %.

- The increase of anchoring stiffness about 100 % from S = 500 kN/m to S = 1000 kN/m. N = $31 \cdot 10^{-6}$ 1/N which is about 62 % of the initial stiffness gives

$$\zeta = \frac{1}{0{,}62} \cdot 2{,}409 = 3{,}89$$

with Figure 5.31:

$$\frac{F_f}{F_{st}} = 5{,}5$$

and

$$F_f = 5{,}5 \cdot 14\text{kN} = 77\text{kN}$$

Thus a increase of 100 % in anchoring stiffness gives about a 25 % increase in maximum stress due to drop force. Figure 4.21 also shows that the fall of span maximum tension increases very quickly with ζ, thus a flexible structure is favoured.

Figure 4.24 gives for the relative displacement

$$\frac{b_h}{b_c} = 1{,}1$$

$$b_h = 1{,}1 \cdot 1{,}31\text{m} = 1{,}44\text{m}$$

The displacement decreases about 10 %.

- The reduction of the short-circuit duration T_{k1} from 0,5 s to 0,3 s does only change

$$\frac{T_{k1}}{T} = \frac{0{,}3\text{ s}}{0{,}5\text{ s}} \cdot 0{,}243 = 0{,}146$$

Figure 4.20 gives

$$\frac{F_f}{F_{st}} = 4$$

and

$$F_f = 4 \cdot 14\text{kN} = 56\text{kN}$$

A reduction of the short-circuit duration reduces also the forces on the sub-structure, in this case about 13 %.

Figure 4.23 shows that this reduction of the short-circuit duration is too low and does not change the deflection.

Bundle pinch effect

Figures 4.25 to 4.29 can be used as correcting factors. Referring to section 4.5.1 (example of calculation), the 380-kV-substation busbar is characterised by: This gives with Figure 4.27:

Temperature	-20 °C	60 °C
F_{pi}/F_{st}	4,1	4,8
F_{pi}	69,7	67,2

Modification of the structural data gives the following effects:

- The influence of a decrease of the mass by 20 %, keeping the equivalent static sag according to (*22) constant, resulting in m'_s = 0,8 · 3,25 kg/m = 2,6 kg/m. This leads to following correction factors

$$F_{st} = 0{,}8 \cdot 17\text{kN} = 14{,}5\text{kN}$$

$$r_s = \frac{1}{0{,}8} \cdot 15{,}6 = 19{,}5$$

with Figure 4.25a:

$$\frac{F_{pi}}{F_{st}} = 4{,}7$$

which gives

$$F_{pi} = 4{,}7 \cdot 14{,}5\text{kN} = 68{,}2\text{kN}$$

Thus, the decrease and also the increase of mass, keeping the equivalent sag constant, makes less modification of the pinch force.

- The influence of a decrease of the short-circuit current by 20 %, resulting in I''_{k3} = 0,8 · 63 kA = 50 kA. This leads to following correction factors

$$r_s = (0{,}8) \cdot 15{,}6 = 10$$

with Figure 4.25b:

$$\frac{F_{pi}}{F_{st}} = 3{,}6$$

which gives

$$F_{pi} = 2{,}6 \cdot 17\text{kN} = 61{,}2\text{kN}$$

The decrease of the short-circuit current reduces also the pinch force, in this case about 12 %.

- The reduction of the distance between the sub-conductors on 50 % means a_s = 200 mm. Therefore

$$\frac{l_s}{a_s} = \frac{9{,}4\text{ m}}{0{,}2\text{ m}} = 47$$

with Figure 4.26:

$$\frac{F_{pi}}{F_{st}} = 3$$

which gives

$$F_{pi} = 3 \cdot 17\text{kN} = 51\text{kN}$$

The decrease of the spacing reduces the pinch force, in this case about 17 %.

- The increase of the distance between two spacers about 50 %, that is two spacers instead of three, resulting in l_s = 1,5 · 9,4 m = 14,1 m:

$$\frac{l_s}{a_s} = 1{,}5 \cdot 23{,}5 = 35{,}3$$

with Figure 4.27:

$$\frac{F_{pi}}{F_{st}} = 3{,}4$$

which gives

$$F_{pi} = 3{,}4 \cdot 17\text{kN} = 57{,}8\text{kN}$$

The increase of subspan length decreases the pinch force, in this case about 17 %.

- The influence of an increase in initial static tensile force by 20 % leads to:

$$F_{pi} = 1{,}2 \cdot 17\text{kN} = 20{,}4\text{kN}$$

With Figure 4.27

$$\frac{F_{pi}}{F_{st}} = 3{,}7$$

which gives

$$F_{pi} = 3{,}7 \cdot 20{,}4\text{kN} = 75{,}5\text{kN}$$

An increase of the initial static tensile force increases also the pinch force, in this case about 8 %.

The increase of anchoring stiffness about 100 % from S = 500 kN/m to S = 1000 kN/m. With Figure 4.28:

$$\frac{F_{pi}}{F_{st}} = 5{,}3$$

which gives

$$F_{pi} = 5{,}3 \cdot 17\text{kN} = 90\text{kN}$$

Thus a increase of 100 % in anchoring stiffness gives about a 30 % increase in maximum stress due to pinch force.

- Three sub-conductors instead of two by no change of bundle diameter gives

$$a_s = 400\text{ mm} \cdot \sin\frac{\pi}{3} = 346\text{ mm}$$

$$\frac{l_s}{a_s} \cdot \sin\frac{\pi}{3} = 23{,}5$$

with Figure 4.28:

$$\frac{F_{pi}}{F_{st}} = 4{,}5$$

which gives

$$F_{pi} = 4{,}5 \cdot 17\text{kN} = 76{,}5\text{kN}$$

The choose of more sub-conductors increases the pinch force, in this case about 10 %.

These examples illustrate that a decrease in subconductor separation is compensated by an increase of r_s and $l_s/a_s \cdot \sin(\pi/n)$. The overall effect is a limited reduction in bundle pinch tension. Nevertheless, sub-conductor separation should be chosen as small as possible to maintain separation for ampacity considerations (minimisation of mutual heating) and the subspan length should be chosen as long as possible. The combined selection of a_s and l_s must ensure bundle separation under normal maximum load conditions. In the example, the ratio l_s/a_s must be greater than 10 to avoid the critical range, Figure 4.26. For example, a_s < 400 mm and l_s < 4 m. Figure 4.26 shows also the validity of (*43) and (*44) in section 4.3.1. In practice l_s is sometimes constrained by dropper connections and a_s must be co-ordinated.

Case D corresponds with very short spans having very low static tensile force F_{st} and very high supporting stiffness $S \rightarrow \infty$. In these cases (very low l_s/a_s), there is generally no contact. Thus l_s/a_s must be adjusted to as low a value as possible by the correct choice of a_s and l_s. Figures 4.27 and 4.28 give an increase of F_{pi}/F_{st}. For the same example with jumper length l = 11 m, static sag b_c = 2,5 m, l_s = 0,8 m and a_s = 0,4 m, the calculation gives F_{st} = 400 N and F_{pi} = 24 kN is obtained. The jumpers are fastened to the span on both sides of the towers where high static tensile forces and pinch forces occur, therefore the pinch force in the jumper is not decisive. Only the deflection of the bundle is to be noticed. A considerable decrease of the pinch force is reached only if $a_s \approx d_s$.

Cases A and C must be considered differently from that of jumpers (case D). For cases A and C, contact is advantageous because it results in lower stresses. *Thus* $l_s/a_s \cdot \sin(\pi/n)$ *must be chosen as high as possible,* in the example greater than 10. For other configurations, the factor j according to (*49) is to be calculated and $j > 1$ is recommended.

5 GUIDELINES FOR DESIGN

5.1 Introduction

The mechanical phenomena, which are a consequence of short-circuit currents in substations, as presented in Chapter 3 (for rigid conductors) and in Chapter 4 (for flexible conductors), must be considered in design. These phenomena influence the design arrangements and mechanical strength requirements of substation components. In particular, the mechanical strength of apparatus, insulators and conductors and the supporting structures have to be considered. In addition, in substations with flexible conductors, conductor displacements and the resulting reductions in electrical clearances can be significant. This chapter of the Brochure provides guidelines for design with respect to arrangements, mechanical loads and electrical clearances.

5.2 Arrangements

Typical arrangements used for the physical design of outdoor substations are described in section 1.4. The design of open outdoor substations to withstand mechanical short-circuit effects, indicate the following general considerations.

Rigid bus arrangements:

- In the case of high short-circuit currents, rigid bus systems have relatively straightforward designs and result in effective substation con_figurations including apparatus connections with lengths exceeding a few meters.

- All possible mechanisms for the initiation of secondary faults should be limited. Therefore, insulator-tube-clamp arrangements for busbars and rigid connections must be designed such that a "domino-effect" will be avoided in the case of a post insulator failure.

- As far as possible, designs should be flexible, that is, some changes must be possible without greatly influencing the short-circuit design concept (e.g. avoiding resonance).

- When designing equipment surrounding isolators (for example supporting structures and in the case of pantograph isolators) it is necessary to check particularly that too much flexibility does not jeopardise the function of the apparatus. Equivalent checks are essential for earthing switches.

Flexible bus arrangements:

- When the current carrying conductors are made of strained conductors, the physical conditions for design are significantly different compared to rigid bus systems. The electromagnetic transversal force give rise to tensile stresses in the supporting structures, clamping devices, insulator strings and apparatus terminals.

- Installations with flexible conductors give rise to conductor swing-out which typically results in decreasing minimum clearance.

- The representation of the problems are distinct if the conductors consists of single as opposed to bundle conductors.

- Short circuit design with regard to conductor displacement aims principally to prevent that a near-by fault on a power line will cause conductor deflections in a feeding substation such that a secondary fault might appear there. However, conductor movement must never be of such nature that there is a risk that faults could spread to other branches or substation elements.

For both rigid and flexible bus arrangements it is necessary also to check that the temperature rise due to short-circuit currents does not exceed the highest permitted temperatures for supporting devices or connected apparatus.

In the following sections describe aspects of the most common arrangements.

5.2.1 *Special Aspects of Strain Bus Arrangements*

In this section, aspects related to increased tension in a bus configuration of type Case A (Fig 1.8) resulting from a short-circuit are discussed. However, for practical design, the final solution must also satisfy other requirements such as limitations caused by conductor displacements (section 5.4) and sag variations, corona and radio noise (RIV) requirements, component standards, requirements associated with other load combinations, control equipment principles and so

on. Questions of special interest centre on swing-out tensions and bundle pinch forces.

Swing-out Tensions

Concerning swing-out tensions (F_t and F_f), the reader should note that in certain cases savings may be possible if the maximum short-circuit duration for design purposes is low (for example, 0.3 s). Such a value could be accepted if the appropriate local back-up and breaker failure protection exist. In addition, the static tension and the resulting sag are important design variables. If, for example, the sag is 3.5 m, then the period of the equivalent pendulum oscillation will be:

$$T = 1{,}79\sqrt{3{,}5s} = 3{,}35 \text{ s} \quad \text{(eq. *23 of section 4.5.1)}$$

and from the same section:

$$\frac{T_{k1}}{T} = \frac{0{,}3}{3{,}35} = 0{,}09$$

From Fig. 4.32 the effect of these key design parameters on F_t is apparent. Also as a result of the specified conditions F_f is not expected to be a limiting consideration in this example. The use of heavy conductor spans, by decreasing the relation $\frac{F}{n' m_s g_n}$ always results in a decrease of short-circuit loads and cause less problem for clearance.

Bundle Pinch Forces

Suitable spacing, between conductors and between bundle spacers, are important factors for the limitation of pinch tensions (Chapter 4.5). Generally the distance between spacers should be as large as possible, while maintaining conductor separation under maximum operating current conditions [22, 34, 67]. The other possible solution for minimising bundle pinch tensions, involves the use of a very large number of spacers to ensure that the design is not in the dangerous zone. This solution might be used in special cases for jumpers, connections between apparatus and loops; but is generally not recommended for the majority of applications. This is because of very large rate of increased pinch effect with subspan length in such case.
The spacing between subconductors may be wide (for example, 450 mm at 420 kV) for short-circuit levels up to 40-50 kA rms as the resulting low number of spacers reduces costs and corona and RIV problems. However, for higher short-circuit currents, reduced spacing (with the centre-to-centre spacing between conductors $\geq$ twice the conductor diameter) is preferred.
The use of relatively heavy conductors in a bundle results in several advantages:

- Designs with reduced spacing are facilitated without corona or RIV problems.
- Heavy conductors result in lower pinch forces than a lighter conductors [12].
- Ampacity requirements can be satisfied with fewer sub conductors of heavy size which is consistent with reducing pinch tension.
- Static load combinations, including wind, ice and so on, result in lower static tensions if fewer and heavier conductors are used compared with more numerous and weaker conductors.
- Labour costs are reduced and arrangements for terminations, T-connections, and so on, are simpler.

The static tension has very little influence on the pinch tension as indicated in reference [12]. Furthermore, increased static tension allows distances between bundle spacers to be increased, which reduces pinch tension. As a result, the relative increase of pinch tension becomes more significant as static tension is decreased.

In the normal design procedure, preliminary values for static tension are based on static load combinations and clearance requirements resulting from conductor swings. For example, the procedure outlined in [12] is to choose the initial tension such that the sag is in the range of 3% of the span length. Otherwise, if no other requirements exist, a static tension of 5-10 N/mm^2 is recommended as a first design value. The final and optimal sag is based on further calculations (according to Chapter 4 for the short-circuit load case).

5.2.2 *Connections to Apparatus*

The following aspects refer to both rigid and flexible connections. In switchgear bays a simple and inexpensive solution is to use the terminals of

apparatus as supports. The problem with this is that acceptable dynamic loading limits on these terminals are not very well known. The allowable loading depends on terminal strength, clamp strength, the terminal-connection-clamp arrangement, the strength of supporting insulators, the design of isolator bearings, current paths in the apparatus, dynamic characteristics and so on. In most cases, often as a result of standards, the static withstand strength or the highest static loading, which will not cause maloperation, is given by the manufacturer as well as the safety factor. Higher acceptable loadings in the case of short-circuits can be estimated based on reduced safety factors. If no information is available concerning an acceptable dynamic peak loading, up to 3 kN at the outermost end of the apparatus terminal could be expected and accepted at the risk of the user for circuit-breakers, isolators and current transformer when $I_n > 1250$ A.

A safer way to design connections to apparatus for mechanical effects of short-circuits is to use information from tests on realistic apparatus-conductor configurations (for example, according to [38] for isolators). In this way, very difficult configurations, such as pantograph isolators connected to busbars, can also be carefully designed.

Some additional effects to be taken into account include:

- When slack bundled conductors are used as connections (case C, Fig. 1.8), it is very important that the sub conductors be spaced closely in order that they can touch each other effectively in the case of a short-circuit [57, 65].

- For case C arrangements, a sag of about 8% of the span length will usually lead to acceptable results [12].

- In the case of rigid conductors connected to apparatus with fast operating mechanisms the influence of dynamic switching forces (for example caused by vibrations from the drive mechanism of a circuit breaker when it is opening or reclosing) should also be considered because the short-circuit forces and switching forces might appear simultaneously.

- Depending on the apparatus-conductor configuration and phase-to-phase distances, the relative influence of angle forces may require consideration in calculating terminal loadings.

5.2.3 *Droppers to Apparatus*

Droppers connecting a span to apparatus below (Case A + B illustrated in Fig. 1.8) is an important but difficult arrangement from the design point of view. Forces on the terminals of the connected apparatus, as well as the displacements of droppers must be considered for the range of temperatures appropriate for the span. The required position and length of the droppers to satisfy static and dynamic demands must be determined. As well, designers must recognise the increased tendency of droppers to swing if the droppers are connected to isolators having terminals which are journaled in bearings. Calculations for specific dropper connections are presently possible using advanced methods. Therefore, no parametric studies for the purpose of finding general or optimal solutions have been done.

One possible design concept is to limit the motions of the span by the use of V-string insulators and by choosing a suitable static tension. The droppers in such arrangements can be designed so that the risk of flashover, as well as of violent dropper stretching due to span motions, can be avoided [66]. In some countries, a minimum bending radius at the bottom of the dropper is recommended (10-50 cm, depending on the conductor). In other cases, the use of common sense or engineering judgement is the preferred approach (Fig. 5.2.1). When mutual influences of droppers may be significant, a specific check is necessary (Fig. 5.2.2). Figure 5.2.3 shows how a dropper connection to a span can function as a flexible spacer in the span.

5.2.4 *Design of Jumpers*

The relatively large sag of jumpers (Case D Fig. 1.8) and the proximity of earthed structures frequently necessitates the use of means for restricting jumper displacement to avoid secondary faults and conductor damage. Suitable means include additional weights, V-string insulators for the span, vertical insulators, pinch-limiting spacers or combinations of these solutions. Vertical insulators are effective, especially vertical V-string or post insulators. The disadvantage is that more insulators and their associated leakage paths are introduced, which increases the risk of

insulator flashover especially in contaminated areas.

By using V-string insulators to support the span, the jumper terminations are nearly fixed and jumper movements can be easily calculated using a simple pendulum model.

Single insulator strings and additional jumper weights provide an effective and cheap design, which also minimises the number of insulators (Fig. 5.2.4). The swing of the span insulator strings during short-circuits is an additional complicating influence which makes jumper movement difficult to predict.

5.3 Loads and load combinations

Conductors in outdoor switchyards are not only influenced by short-circuit forces, they may also be affected by other external forces such as wind, ice and earthquakes. Mechanical design must be based on several load cases which include the relevant load combinations. Some of these exclude short-circuit forces, and they must be based on local conditions, which will not be discussed here.

Regarding the combination of short-circuit forces with the environmental forces, there are differing opinions [18, 21, 28]. However, there are several indications that short-circuit forces need not be combined with wind and ice:

- The probability that ice and snow coatings can withstand vibrations due to a short-circuit is very low. Furthermore, experience indicates that ice and heavy snow loads are much less frequent on substation conductors than in other applications.

- Wind load and short-circuit load both vary in time, independently of each other. As well, the direction of wind varies. There are no mathematical procedures available or standards for a true or reasonable combination of short-circuit and wind loads. (Although probabilistic methods may be possible.) Therefore, no equivalent static load-case can be formulated and short-circuit test results cannot be transferred to any other loading condition.

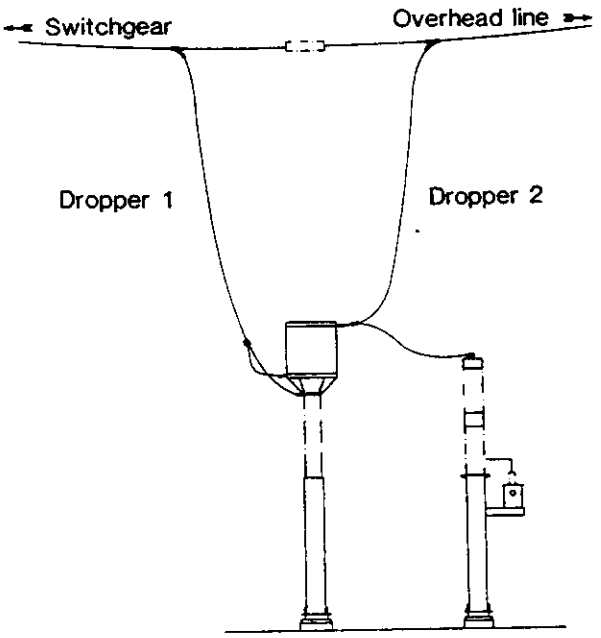

Fig. 5.2.1 Dropper 1 has the highest tension and is connected to the top of the post insulator supporting the line trap. In this way no terminals of the apparatus will be over stressed.

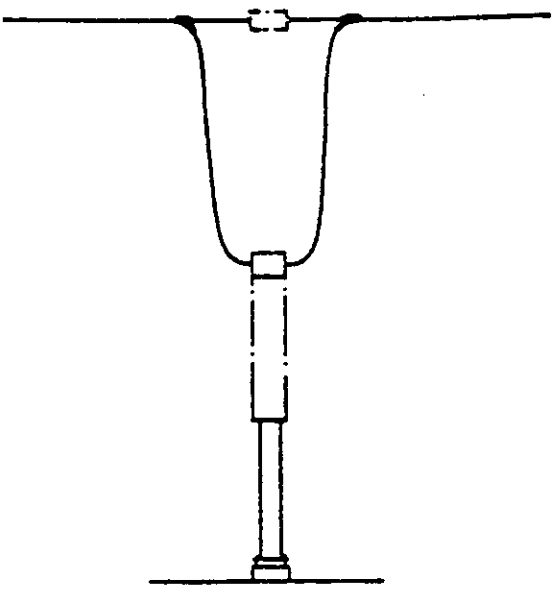

Fig. 5.2.2 Two parallel droppers with narrow spacing cause short-circuit load components which must be considered. This example refers to the connection of a current transformer.

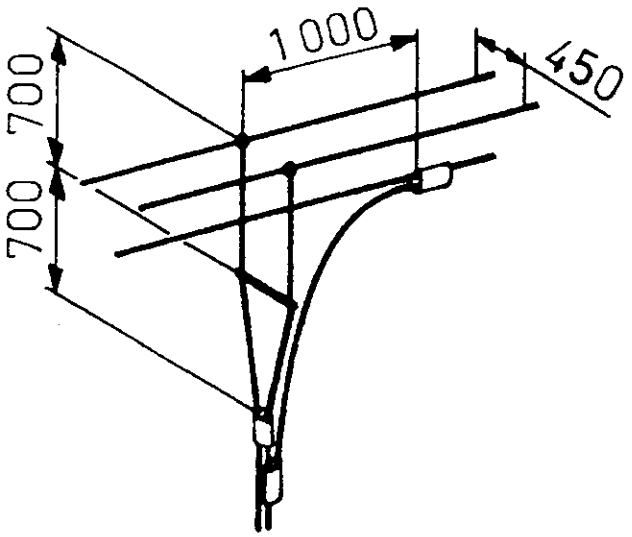

Fig. 5.2.3 The connection of a dropper to a span can be arranged such that it has the effect of a flexible spacer in the span.

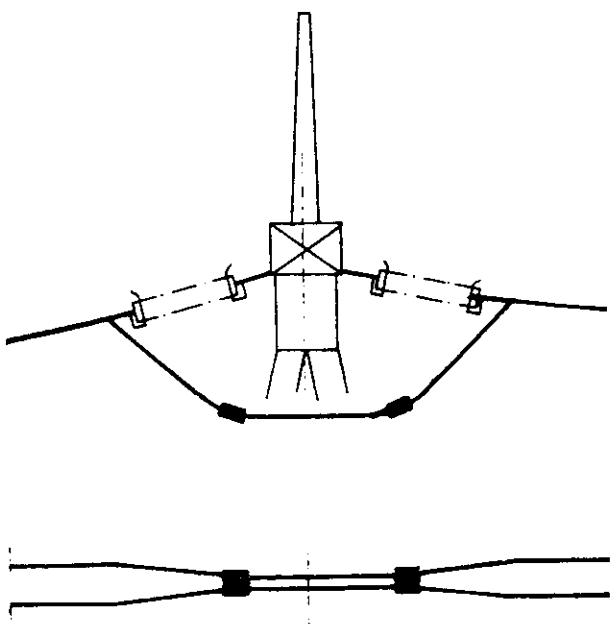

Fig. 5.2.4 Additional jumper weights introduced to limit conductor swing. The weights are so arranged that the pinch lifting effect can be reduced and some extra clearance obtained thanks to the reduced sub conductor distance. As an example, masses of 2 x 40 kg placed at the 3rd of the length has been used rather frequent spacing conditions.

- The short-circuit loading may depend on very special effects which cannot easily be combined with other loads. Examples include the consequences of unsuccessful autoreclosure which may be of considerable importance in the case of rigid conductors or in relation to pinch- and conductor-fall sequences in the case of flexible conductors.

- The magnitudes of the conductor weight and wind load depend on rigid or flexible conductor characteristics but are roughly of the same order.

Based on these reasons, it seems credible to consider short-circuit as a separate load case (particularly if the short-circuit calculation gives results on the safe side) for the mechanical dimensioning of flexible as well as rigid busbars and connections.

5.3.1 *Conductors and Insulators*

Loads on Insulators

The calculated dynamic force acting perpendicular to the top of a post insulator, F_d for rigid conductors and F_t, F_f or F_{pi} for flexible conductors, must not exceed the minimum failing load. Limits on acceptable loading as low as 70% of the minimum failing load, (that is the loading used for routine tests of post insulators) are preferred by some users. If the force is acting at a point higher than at the top of the post insulator, (this is the situation for rigid buses and in some special applications) a force which gives an equivalent moment must be considered. The critical point is not necessarily the insulator base.

For insulator strings of the cap and pin type, allowance for 65% of the electromechanical failing load (porcelain) or mechanical failing load (glass) is reasonable. The basis for this is that insulator units are type tested with that load to verify the withstand mechanical strength in case of a disk crack.

Conductor Stress

As a consequence of the theory of plastic deformation, the calculated tubular-conductor stress must not exceed 1.35 - 1.50 times the yield point ($R_{p0,2}$) for bending depending on the ratio between conductor wall thickness and diameter [39].

Flexible conductors in strain bus systems are not expected to be significantly over stressed in the case of a short-circuit. However, in exceptional cases, a check to ensure that 70% of the breaking load will not be exceeded, is recommended. The reason for this recommendation is that some margin is necessary to take into account reduced conductor strength in the anchoring points. Some users prefer a lower allowable stress (55% instead of 70%). Subconductors in slack bundle connections may be permanently deformed at the spacers in the case of a short-circuit if the design is unsuitable.

Loads on Conductor Hardware

Connectors, clamps, spacers and other arrangements for terminating conductors are directly exposed to the full force amplitudes generated by short-circuits. Therefore, their dynamic loading will not be reduced by the filtering effects which reduce the effective loadings for supporting structures, rigid bus post insulators and so on (Fig. 5.3.1). For this reason, a factor of 1.5 is taken into account in the calculations, if the maximum tension in the conductor is determined according to formula 4.2.6. Also, the use of conductor hardware with a sufficient degree of toughness is recommended. For connection clamps manufactured from aluminium alloy, type test specification of the percentage elongation after fracture according to [44] is recommended, (for example, A_5 = min 2% for a separate cast-to-size piece). For a machined test piece manufactured from connector parts, a minimum of 1% seems reasonable for a cast piece and a minimum of 5% for a wrought piece. Other components such as tension clamps, spacers, and so on, should have a good toughness value down to the lowest temperature which may be expected.

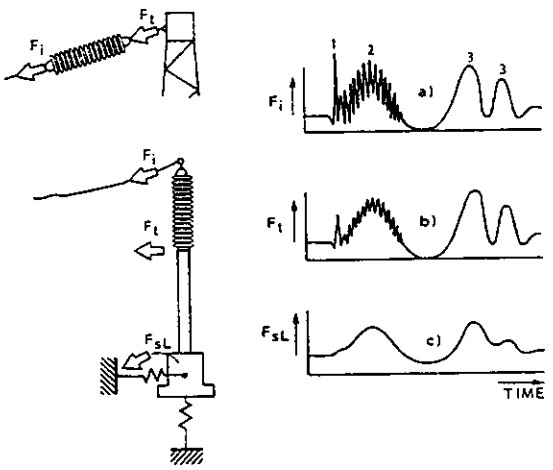

Fig. 5.3.1 Typical time histories of tensile forces caused by short-circuit loads on flexible conductors.
a) Tensile forces in the flexible conductors and insulator string.
Peak 1 - bundle pinch effect
Peak 2 - span motions within the short-circuit duration.
Peak 3 - span motions subsequent to the short-circuit.
b) Smoothed tensile force applied to the structures.
c) Soil loading further reduced by foundation inertia.

Short-Circuit design recommendations for connection clamps include:

- The connectors must not apply excessive forces to apparatus terminals.
- Connection tongues of connectors should be so arranged that the effective section modulus for the case of a short-circuit loading is as large as possible.
- Short-Circuit stresses must not give rise to permanent deformation, cracks or failure of the connectors. However, permanent deformation of flexible parts can be accepted if such deformation does not affect the function of the connectors.
- Permanent deformation, cracks or failures must not occur in connectors for bundled

stranded conductors as the result of conductor clash in the event of a short-circuit.

- Electric current must not be carried by the mechanical bearing parts of tube connectors, whether during normal operation or during short-circuits. Arcs must not be established during short-circuits.

- Tubes should be so supported that it is not possible for a direct impact to arise between a tube and terminal in the event of a short-circuit.

- Connectors should be so designed that tubes cannot fall out of them in case of a short-circuit.

The short-circuit withstand capability of conductor hardware, and especially of spacers and connection clamps, should be verified by tests under relevant conditions. After the short-circuit duration the conductor may be wrenched out of the clamp. This must be taken into account in the design of the spacer clamps.

5.3.2 *Supporting Structures*

Introduction

There exist two main kinds of supporting structures in outdoor substations:

1. Portal structures for strained conductors, typically consisting of two vertical towers and a horizontal beam, and

2. Pillars supporting the post insulators for rigid bus or apparatus.

These structures are made typically from steel, latticed, bolted or welded or solid webbed, and erected on concrete foundations [15]. Their design is typically carried out by civil engineers.

Based on national or company standards, all substation supporting structures are designed for existing and/or probabilistic combinations of different loads: dead loads, conductor tensile loads, thermal loads, ice, wind, reaction forces from circuit breakers [28]. These loads appear during normal substation operation and therefore adequate factors of safety are usually available. However, the structures may also be subjected to the exceptional load caused by short-circuit current.

With regard to this relatively rare phenomenon, the dimensioning of pillar type structures for post insulators is usually based on the guaranteed breaking strength of the insulators, which is needed to meet the short-circuit current load. Reduced safety factors approximately 1.0 are considered for supporting structures.

On the other hand, portal structures have generally not been designed to withstand the full dynamic forces caused by short-circuit currents. For example, the current German Standard [41] states that according to their experience, strength calculation of portal structure subjected to short-circuit forces is not necessary. This recommendation for design was justified by the following:

- there have been no recorded destructions of structures,

- short-circuit current levels have been moderate in the past,

- there was a lack of verified calculation methods.

However at the present time, the majority of companies which responded to the CIGRE SC23 inquiry [28] take into account short-circuit forces in structure design. This is justified by the increasing levels of short-circuit currents, substation security requirements and economic pressures. Thus, the following basic strategy seems to be reasonable at the present state-of-the-art:

> "First design structures for standard loads, later verify the structures for short-circuit current loads."

In the calculation procedures described in Chapter 4, the problems of analysis of supporting structures are associated with:

- the selection of a general mechanical model for calculation of mechanical effects of short-circuit currents in the substation, and in

- the stress analysis which concludes all calculations.

The problem of stress analysis of foundations for substation supporting structures working under short-circuit conditions has not been considered by WG 23.02 to date. However, adequate engineering precision can be obtained using the general routine approach. That is, the foundations are subjected to loads transmitted through the supporting structure. These loads, which have been deprived of high frequency oscillations (Fig. 5.3.1c) due to the filtering influence of the insulators and supporting structures, are known from the global dynamic analysis described in Chapter 4.

Short-Circuit loading

The well known typical time history of the tensile forces in flexible conductors, caused by short-circuit loads is presented in Fig. 5.3.1a [70]. From the point of view of the civil design engineer, two characteristic types of forces are noted (Fig. 5.3.1):

- the bundle pinch maximum (1), acting as a short but high impulse force (representative frequency: 100 Hz)

- the motion maxima during (2) and subsequently (3) to the short-circuit duration with relatively slow variation in time (representative frequencies from about 0.5 to 3 Hz).

The force acting on the structure is presented in Fig. 5.3.1b and on the foundation in Fig. 5.3.1c. The filtering effect of insulators and of the supporting structure is indicated. The bundle pinch forces appear during all types of short-circuits (one, two- or three-phase) at almost the same time. For practical calculations, a simultaneous and equal pinch force in all phases can be assumed for three-phase faults which is usually the worst case.

The swing and fall forces are different in the case of two- or three-phase faults. In the first case, large forces appear only in the two faulted phases. The force in the third unfaulted phase, caused by structure deflection, is of a much lower value. In the case of a three-phase fault, the large forces appear in the outer phases, which experience significant displacement; the middle phase experiences only restricted movement and therefore the force in this phase is much smaller. Thus, considering the stress in the beam of the portal, the case of a two-phase short-circuit (one outer phase and the middle phase) is taken as the worst case, (that is, the largest bending moments will be produced).
The short-circuit current forces always act together with the dead loads. However, in some countries additional preliminary loads are added, (for example, wind load or ice load (section 5.3)). The selection of load combinations depends on the local climate conditions [28].

As presented in Chapter 4, short-circuit current forces may be calculated using a range of different methods (simple or advanced) and also some combinations of these methods, if their accuracy is reasonable. In the most advanced methods a whole system is analysed at the same time. Thus short-circuit current forces and stress analysis in a structure are obtained together. However, in other cases the output of short-circuit current force calculations for insulators serves as an input to the stress analysis of a supporting structure. The following forms for that input may be used:

- the complete time history of a variable force

- the peak value and the duration of a representative impulse

- a single value force, (usually the maximum force)

With the simple method no time characteristic of forces acting on the structure is available, so dynamic analysis is not possible and static analysis should be used as an approximation.

As discussed in earlier sections, there exists the danger of resonance between the supporting structure vibrations and the excitation force originating from the conductors. Therefore, the frequency of conductor movement should be checked to ensure that it is sufficiently different from the eigenfrequency of the structure. Thus, a detailed or simplified analysis of the modes of vibration of the supporting structure (portal) is suggested. Usually only the structural vibrations of the first mode need to be considered. In Table 1.3 in section 1.4 some typical Eigen frequencies for supporting structures are given .

Stress evaluation

Stress analysis is performed using routine methods for the full representative structure. In the case of the most advanced methods of analysis, the steel structure is fully represented

(see Chapter 4). As a result, the full time history of stresses, s = s(t), in the required elements of the structure is obtained. However, such direct dynamic analysis is relatively time consuming, expensive and usually not necessary.

Alternatively, stress analysis is obtained indirectly if the structure is considered to be loaded by short-circuit forces obtained from a preliminary conductor, insulator, structure model. For advanced methods the results may be almost as good as those obtained from the direct approach.

Stresses s_i in an element i of cross-sectional area A_i are evaluated according to

$$A_i s_i = K_i u_i + M_i \ddot{u}_i \qquad (5.3.1)$$

where i numerates stress components.

The first term represents the "static" and the second, the "dynamic" components of s_i. Except for the very rapidly changing loads (for example, large pinch forces), the last term is much smaller than the first one and is often neglected.

The common design practice in the case of phase-to-phase forces is to assume that they are static forces and consequently to consider portal structures to be subjected to two equal static forces (corresponding to the two phases having significant displacement) applied on the crossarm.

The dynamic character of pinch forces is taken into account in particular countries using various approaches. In principle it may be done by addition of appropriate inertia forces. In the Canadian design practice, the pinch forces are treated as impulsive load represented by an equivalent static load [69].

The admissible stress for short-circuit load must satisfy general regulations and usually is assumed to be higher than ordinary loads. Therefore, the effective safety factor is lower. In common engineering practice for short-circuit loading (in exceptional cases), the safety factor is typically about 1.3, while for normal loads, the safety factor is about 1.5.

In the case of short impulsive loads, for which large stress rates occur, structural steels experience a delayed plastic flow phenomenon which results in a temporary increase of strength (yield point) [87]. For example, in the case of load changing with a frequency of 100 Hz, steel strength increases by about twice. This phenomenon provides an additional justification for assuming allowable stresses higher than for static loads.

Recommendations

Obviously the more advanced methods of analysis have the potential to produce the most detailed and accurate results; but the results obtained are more expensive. The basic practical question for the design engineer is, "Is it necessary to apply advanced methods or are the simple methods adequate?".

The answer depends on many factors, such as designer experience, access to appropriate computer software and hardware, availability of detailed structural data and so on. Overall experience with stress analysis of supporting structures working under short-circuit current conditions is relatively limited. Consequently, no detailed recommendations can be given here. However, the following general pattern may be suggested:

- Simple methods may be applied either for structures and current levels for which design practice and service conditions and experience have proven to be sufficient or for those cases that have been verified against confirmed advanced methods and models.

- In the case of significant change in the type of structures, their parameters or short-circuit current level, and where the cost of failures or overly conservative design is significantly greater than the cost of detailed design methods, the advanced methods are strongly recommended.

5.4 Conductor Displacement and Temporary Air Clearances

5.4.1 *Introduction*

Multiphase short-circuit currents generate interphase forces which result in phase conductor displacements. In rigid bus systems, the resulting displacements are relatively minor and do not significantly reduce the phase-to-phase clearance. However, for flexible bus systems the phase displacements can be very significant depending on

the bus configuration, the short-circuit current magnitude and duration. The mechanics of the phenomenon are described in Chapter 4 of this brochure. This section is concerned primarily with means to design for temporarily reduced clearances and with the consequences of the temporarily reduced clearances in terms of the capability of buses to withstand the applied voltage stresses following short-circuits. The ability of buses to operate successfully following short-circuits is an important factor for substation and system reliability. Secondary bus faults can also have a severe effect on power system operations and stability. For line entrance buses the impact of secondary faults may be relatively small; however, for main bus sections the impact would likely be severe.

5.4.2 *Conductor Displacement*

In substations with low tensioned spans without droppers or other restricting arrangements, conductor displacements are usually a more serious problem than other short-circuit effects, especially if the short-circuit power is not high. Figure 5.4.1 illustrates the movements of a typical 130 kV, 36 m strain bus in the cases of normal fault tripping (duration 0.1 s) and back-up tripping (duration 0.5 s). The conductor movements are complicated in general, but they are particularly complicated for the case of back-up clearing. Conductor behaviour varies significantly depending on physical and short-circuit parameters. Representation of the more violent motions obtained for back-up clearing or in situations involving relatively light conductors and high fault currents, more elaborate modelling is required. Figure 5.4.2 presents, in a simplified way, the conductor movements in two typical cases: namely two and three-phase faults.

The three-phase fault causes the outer phase conductors (phases L1 and L3) to swing outwards from their normal position, whereas the middle phase (phase L2) experiences a very restricted motion. After interruption of the fault, phases L1 and L3 swing back. During the two phase fault, for example between phases L1 and L2, both conductors swing initially outwards then inwards in synchronism. For relatively short duration faults, the maximum swing out angle for the outer phases is nearly the same for two or three-phase faults, as the forces at the rest position are nearly the same.

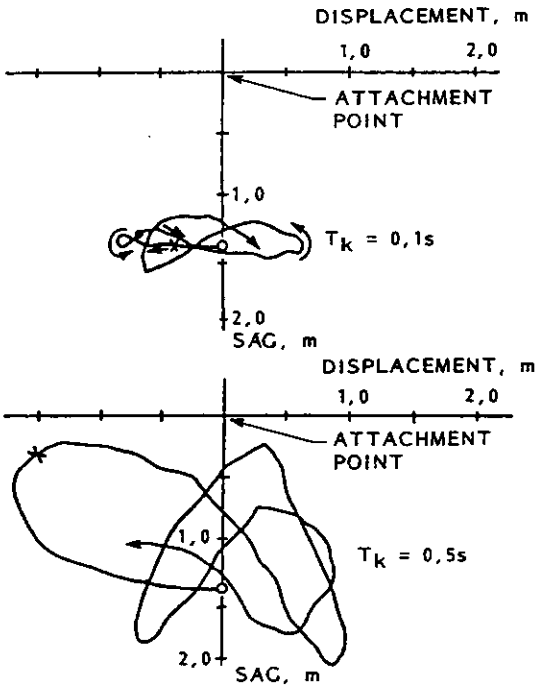

Fig. 5.4.1 Movements of the mid-point of a span resulting from a two-phase short-circuit test (36 m span, 130 kV, single insulator string, phase separation 4,0 m, sag of insulators and conductor 1,45 m, conductor 2 x 910 mm^2 Al, I_k'' = 40 kA, X = short-circuit interruption).

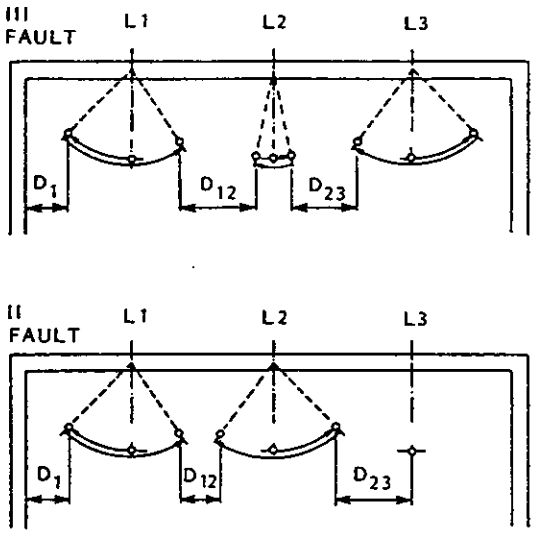

Fig.5.4.2 Simplified phase conductor motions caused by multiphase faults.
III: Three-phase fault.
II: Two-phase fault in outermost conductors.

Therefore, the affected phase conductors approach one another more closely in the case of the two phase fault. Hence, designers should consider the two phase fault as the decisive case for clearance calculations.

Referring to Fig. 1.8, the displacements of span A and also of jumper (Fig. 5.2.4) are of interest. Concerning jumper, the approach of the outer conductor (phase L1) to the structure is also important. In the case of bundled conductors, the effective swing out angles may also be affected by subconductor swings within the bundle configuration. Also, under certain circumstances, jumpers consisting of multiple conductors can be thrown vertically against the girder due to pinch forces. Although clearance problems for jumpers are potentially more severe than span clearance because of the proximity of the jumpers to the grounded structures, the presence of the support structures provides relatively straightforward means to limit jumper displacement. In this regard, the use of rigid post insulators and jumper connections, the provision of stabilising weights, the use of V-string insulator arrangements and the application of inter-phase insulating links provide effective means for limiting jumper displacement and thereby circumventing clearance problems.

Three minimum distances D_1, D_{12} and D_{23} are important for air insulation considerations as illustrated in Fig. 5.4.2. If a typical swing frequency of approximately 0.5 Hz. is assumed, it is clear that the air distances D_1 and D_{23} appear in the first second of conductor swing and the distance D_{12} usually not earlier than one second after fault initiation. The minimum distance D_{23} for two-phase faults (mutual deflection of only one phase conductor), which appears also in the first half of the conductors swing cycle, is considerably greater than the distance D_{12} and is not decisive.

The philosophy of avoiding secondary faults must be based on control equipment principles and substation design. For example, consider the one line diagrams shown in Fig. 5.4.3 and assume an overhead line fault at L just outside the substation. The overhead line circuit breaker CBL has high speed autoreclosure capability as presented in Fig. 5.4.4 (discussions concerning autoreclosure are valid only as far as three-phase, high-speed autoreclosure is concerned). Also assume that there is no delay between the two relay systems in the case of local back-up and that the high speed autoreclosure is blocked if normal fault clearing does not occur.

Possible sequences regarding the affected conductor movements are shown in Fig. 5.4.5. Figure 5.4.5 I, illustrates the behaviour of the conductors outside CBL for normal fault clearing. Figure 5.4.5 II, illustrates the motion of bus spans for normal clearing and Fig. 5.4.5 III, illustrates the conductor motion when the failure is cleared by breaker failure protection or by remote back-up protection. In this example, unsuccessful high-speed autoreclosure is not expected to be the decisive dimensioning factor for the displacement of energised bus spans because of the common relations between swing frequency and dead time interval. Of greatest interest are movements of the spans affected by the short-circuit current when the circuit breaker operates normally (Fig. 5.4.5 I and II). The primary fault just outside the substation, might cause a secondary fault after the reclosure at point 1 (Fig. 5.4.3) at the bus (point 2b) as well, if the conductor swing out at these locations is high enough. A secondary fault could also appear at point 3 resulting in the loss of a main feeding transformer.

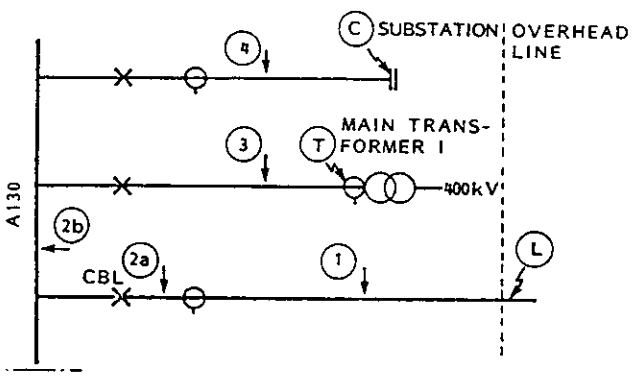

Fig. 5.4.3 Possible secondary fault locations (1, 2a, 2b and 3) in a substation in the case of a primary overhead line fault at L. Primary faults at C and T are also discussed.

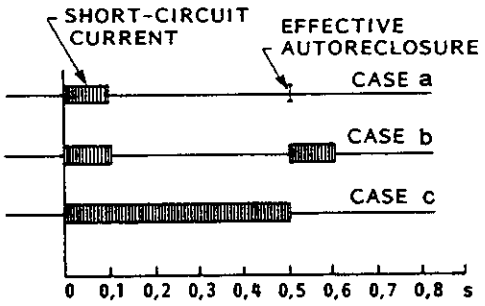

Fig. 5.4.4 Examples of time sequence of fault current for line faults.
- a: fast clearing and subsequent successful reclosure.
- b: fast clearing, unsuccessful reclosure and ultimate clearing.
- c: failure to clear by relevant circuit breaker or protection and subsequent clearing by relay or breaker back-up protection.

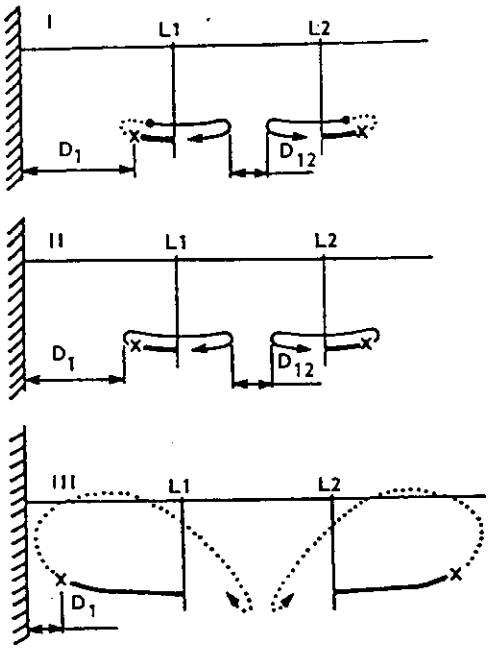

Fig. 5.4.5 Movements of conductor at possible secondary fault locations in the case of a primary line fault at L (Fig. 5.4.3).

- I: refers to locations 1 and 2a (Fig. 5.4.3) and to Fig. 5.4.4 case a.
- II: refers to locations 2b and 3 and to case a.
- III: refers to case c and to locations 1, 2a and 2b.

A secondary fault in a substation constitutes a very serious disturbance from the operational point of view because it causes an enlargement of the de-energised network area. In particular, it is very disturbing for the operation of the network if a secondary flashover results in a main bus fault. A secondary fault (unsuccessful auto-reclosure) outside the current transformer (for example point 1) is not particularly disturbing because it will affect only one outgoing overhead line. From an operational point of view, the case of fault tripping via breaker failure or remote backup protection (Fig. 5.4.5 III) is equivalent to a bus fault, as the fault is connected to the bus via the non operative circuit-breaker until the bus is disconnected from the network. Following clearing, clashing of non-energised conductors or contact between a jumper and a steel structure is harmless. However, risk of flashover between affected conductors and any other circuit (for example, conductors in a neighbouring bay or at another level) cannot be accepted. In the case of faults initiated at C or T in Fig. 5.4.3, the situation will not be significantly worse as a result of excessive displacements of connecting spans (possible secondary fault locations 3 and 4). In considering secondary fault risk as a whole, knowledge of deflections, possible overvoltages and consequences of flashovers is necessary. The overvoltages which might appear must be considered consistent with the autoreclosure sequence (high speed as described above or delayed as is also common). Concerning the possible consequences of flashovers, conductor damage should be considered. Under many situations, the electromagnetic and thermal forces acting on flashover arcs cause the arc to move rapidly along the bus resulting in relatively minor damage. However, in some configurations and particularly for high current arcs, it is possible that an arc will establish a stable root point, in which case, significant conductor damage can result. To avoid fully the risk of flashover and subsequent conductor damage in all situations may not be possible.

Several approaches have been established to calculate clearances between phases of bus systems under short-circuit conditions. These

include several models, of varying sophistication, based on the pendulum and finite element analysis. All of these techniques are similar or identical to the methods used to calculate swing tensions, with the provision built into the programs to calculate the bus clearances from the geometrical relationships between adjacent phases under multiphase fault conditions.

6 GENERAL CONCLUSION

Based on international experience, failures of substations, caused by the mechanical effects of short-circuit currents, have been extremely rare. However, design engineers must ensure that substation designs meet the extreme requirements associated with short-circuit conditions. This can be achieved through the use of the calculation methods and criteria provided in the previous sections, and in exceptionally complicated cases through laboratory testing.

The authors hope that this brochure will help engineers ensure safe and economical design, uprating or refurbishment.

This brochure is a revision of former CIGRE brochure published in 1987 on the same subject. It can be used as an aid for designers to get a general overview of short-circuit phenomena and methods which can be applied to evaluate the consequences. The background of IEC 865 (TC73) is detailed in this document. The main changes which occured in the last ten years concern the wider range of application of simplified methods and the impressive increase of computer hardware capability which make possible the use of advanced methods in up-to-date workstations in relatively short times. Also user-friendly interfaces help designers in using such methods. Nevertheless the computation of bundle conductors arrangements, even if possible by advanced users, cannot be used in routine engineering calculations today. Other main topics, like spacer compression, probabilistic approach and temporary air clearance will be more detailed in the next brochure.

The actual state of knowledge has taken a big step forward by using structural dynamic approachs to better define design loads. This will be the subject of another CIGRE brochure intended to be published after 1998.
Together with this brochure a data reference book is also being published which gives access to data and results of more than 40 experimental short-circuit tests, on rigid and flexible bus, two and three-phase short-circuits, with and without autoreclosure, with single and bundled configurations (including tests with dropper connections). This is an impressive collection of tests data from all around the world which will help designers to better appreciate the phenomenon, and to evaluate the efficiency of simplified and advanced methods of calculation.

7 REFERENCES

1. Palante, G. "*Study and Conclusions from the Results of the Enquiry on the Thermal and Dynamic Effects of Heavy Short-circuit Currents in High Voltage Substations. Appendix III: Cakebread, R.J. Electrodynamic stress in the design of rigid conductor arrangements. Appendix IV: Hosemann, G., Deter, O. Methods of calculating the forces to which support insulators are subjected during short-circuits.*" Electra, No. 12, 1970, pp 51-89.

2. Deter, O., Gibbon, R.R., Hosemann, G., Stein, N. "*Measurement of Short-circuit Stresses on Rigid Conductor Busbar Systems and Comparison of Test Results.*" Electra, No. 30, 1973, pp 35-54.

3. Palante, G. "*Behaviour of Rigid Conductors and Their Supports Under Short-circuit Conditions. Comparison of Calculated and Measured Values.*" CIGRE 1976, Report 23-10.

4. Hosemann, G., Tsanakas, D. "*Calculated and Measured Values of Dynamic Short-circuit Stresses in a High-Voltage Test Structure with and without Reclosure.*" Electra, No. 63, March 1979, pp. 147-161.

5. Hosemann, G., Tsanakas, D. "*Dynamic Short-circuit Stress of Busbar Structures with Stiff Conductors. Parameter Studies and Conclusions for Simplified Calculation Methods.*" Electra, No. 68, January 1980, pp. 34-64.

6. Adami, H., Batch, B.A. "*Aeolian Vibrations of Tubular Busbars in Outdoor Substations.*" Electra, No. 75, 1981, pp. 99-120.

7. Lehmann, W., Lilien, J.L., Orkisz, J. "*The Mechanical Effects of Short-circuit Currents in Substations with Flexible Conductors. Numerical Methods - Computer Approach.*" CIGRE 1982, Report 23-08.

8. Matagne, E., Orkisz, J. "*Computer Aided Approaches to Evaluate the Mechanical Effects of Short-circuit Currents in Substations with Stiff Busbars.*" Electra, No. 88, 1983, pp. 115-130.

9. Gauffin, L., Lilien, J.L. "*Mechanical Effects of Short-circuits in Substations with Strain Bus Systems - Medium Complexity Calculation Methods.*" CIGRE Symposium Brussels, 1985, Report 330-01.

10. Fraikin, R. "*Mechanical Effects of Short-circuit Currents in Substations with Strain Bus Systems - Comparison Between Calculation Results.*" CIGRE Symposium Brussels, 1985, Report 330-05.

11. Landin, I., Gauffin, L., Fraikin, R., Ford, G.L. "*Mechanical Effects of Short-circuit Currents in Substations with Strain Bus Systems - A General Description.*" CIGRE Symposium Brussels, 1985, Report 330-06.

12. Dalle, B., Ford, G.L. "*Behaviour of Bundled Conductors in Substations Under High Short-circuit Currents.*" CIGRE Symposium Brussels, 1985, Report 330-08.

13. Lilien, J.L., Brokamp, L. "*Mechanical Effects of Short-circuit Currents in Substations with a Strain Bus System - Parameter Analysis and Simple Method of Calculation.*" CIGRE Symposium Brussels, 1985, Report 330-07.

14. Buter, J., Markworth, E., Richter, F. "*Field Tests in a 220 kV Network of High Short-circuit Power.*" CIGRE 1968, Report 13-09.

15. Nartowski, Z. "*Foundations, Supporting Structures of Steel and Prefabricated Concrete.*" Electra, No. 34, 1974, pp. 75-100.

16. Parizy, M.J., Muller, M.H.G., "*Insulation Characteristics of Substations with a Nominal Voltage up to 765 kV.*" Electra, No. 39, March 1975, pp. 31-46.

17. Ford, G.L., Cenanovic, M., Craig, D.B., Huestis, H.W., Short, T.A. "*Studies Leading to Increased Current Ratings for Substation Buses.*" CIGRE 1976, Report 23-04.

18. Deter, O., Lehmann, W., Rameil, W., Stein, N., Terhorst, A. "*Influence of the Very High Load and Short-circuit Currents on Outdoor Substation Design for the Highest system Voltages of the German Interconnected Grid.*" CIGRE 1976, Report 23-05.

19. Thomas, Y., Pigoet, P., Benistan, G., Kupiec, M. Casale, J.P., Roussel, P., Coullot, J. "*Influence of an Increase in Short-circuit Currents on the Design of 400 kV Installations of the Electricite de France.*" CIGRE 1976, Report 23-06.

20. Hosemann, G., Tsanakas, D. "*Dynamic Stress in Substations Taking into Account the Short-circuit Currents and Electromagnetic Forces due to Non-simultaneous Faults.*" CIGRE 1978, Report 23-04.

21. Cakebread, R.J., Brown, H.J. "*Integrated Mechanical Design Loading for Open Type EHV Substation Structures and Equipment.*" Electra, No. 60, October 1978, pp. 31-55.

22. Adami, H., Leppers, P.H., Lilien, J.L. "*The Behaviour of Spacerless Bundles due to High Load Current. Experimental Results and Theoretical Calculations.*" Electra, No. 90, 1983, pp. 23-43.

23. Thione L. "*Evaluation of the Switching Impulse Strength of External Insulation*" Electra No. 94 May 1984 pp77-95.

24. Ketola, A., Maaskola, J., Hiironniemi, E., Komulainen, R., Uusipaikka, U. "*Disconnector Dimensioning and Comprehension of Tests.*" CIGRE 1984, Report 13-05.

25. Neumann, C., Suiter, H., Kugler, R., Rees, V., Voss, V. "*Design and Testing of 420 kV Pantograph Disconnector for Rated Withstand Current of 80 kA/200 kA.*" CIGRE 1984, Report 13-11.

26. Stein, N., Bauer, E., Brandt, E., Dannheim, H., Lehmann, W., Meyer, W., Pietsch, K. "*Dynamic Behaviour and Strength of High Voltage Substation Post Insulators Under Short-circuit Loads.*" CIGRE 1984, Report 23-12.

27. Stein, N. "*Strain/Stress Concentrations in Insulators due to Sheds.*" CIGRE Proceedings 1984, Vol. 1, Group 23, pp. 45-46.

28. Arhomaa, A. "*Mechanical Design Criteria of Outdoor Substations.*" CIGRE Symposium Brussels, 1985, Report 310-01.

29. Stegemann G. and F. Berger "*Stochastic Determination and Evaluation Concerning Loads of Short-Circuit Current in Electric Energy Transmission Installations.*" CIGRE Symposium Brussels 1985, paper No. 310-02

30. Adami, H., Vos, C.W.M., KEMA N.V. "*Short-circuit Tests and Measurements of Mechanical Stresses on Full-scale Sections of 420 kV Outdoor Substations.*" CIGRE Symposium Brussels, 1985, Report 330-03.

31. Kind, R., Neumann, C. "*Dynamic Short-circuit Stress of 380 kV Busbar Arrangement with Flexible and Stiff Conductors.*" CIGRE Symposium Brussels, 1985, Report 330-09.

32. Tsanakas, D. "*Dynamic Stress in High-Voltage Structures by Short-circuits of Short Duration.*" CIGRE Symposium Brussels, 1985, Report 500-01.

33. Hosemann, G., Lehmann, W., Landin, I. "*Calculation of Short-circuit Currents and Their Mechanical and Thermal Effects - State of International Standardization.*" CIGRE Symposium Brussels, 1985, Report 500-02.

34. Leppers, P.H., Lilien, J.L. "*The Behaviour of Spacerless Bundles. Attraction and Release Values Arising from High Load Currents.*" Electra, No. 81, 1982, pp. 91-116.

35. IEC Publication 168. Tests on Indoor and Outdoor Post Insulators of Ceramic Material or Glass for Systems with Nominal Voltages Greater than 1000 V. Genève: IEC, 1994.

36. IEC Publication 38. IEC Standard Voltages. Genève: IEC, 1983.

37. IEC Publication 71 Insulation Co-ordination. Part 1 (1993): Terms, Definitions, Principles and Rules. Part 2 (1976): Application Guide. Part 3 (1983): Phase-to Phase insulation Co-ordination Principles, Rules and Application Guide. Genève: IEC.

38. IEC Publication 129: A.c. Switchgear and Controlgear for Voltages above 1 kV. Alternating Current Disconnectors and Earthing Switches. Genève: IEC, 1984.

39. IEC Publication 865. Calculation of the Effects of Short-Circuit Currents. Genève: IEC, 1986.

40. IEC Publication 909. Short-circuit Current Calculation in Three-Phase A.C.-systems. Genève: IEC, 1988.

41. DIN EN 60865-1 (VDE 0103): 1994-11: Short-circuit currents - Calculation of effects. Part 1: Definitions and calculation methods. German Standard. Berlin: Beuth, VDE, 1994.

42. Canadian Standards Association "Electric Strength of Insulation" CSA Standard CAN3-C308-M80 Section 4.4.2, 1980.

43. DIN VDE 0141/7.89. Earthing in installations for rated voltages above 1 kV ac. German Standard. Berlin: Beuth, VDE, 1989.

44. ISO-6892: Metallic Materials Tensile Testing, 1984.

45. Lehmann, W. "*Elektrodynamische Beanspruchung Paralleler Leiter.*" ETZ-A, 1955, Vol. 76, pp. 481-488.

46. Atwood, A.W. et al "*Dynamic Behaviour of a 220 kV Dead-end Suspension Bus During Short-circuit.*" Transactions of AIEE, Vol. 81, Pt III, June 1962, pp. 153-169.

47. Lehmann, W., Sieber, D. "*Mechanische Kurzschlussbeanspruchungen durch Leitungsseile in Schaltanlagen.*" VDE-Fachberichte 24, 1966, VDE-Verlag Berlin, pp. 149-153.

48. Manuzio, C. "*An Investigation of Forces on Bundle Conductor Spacers under Fault Conditions.*" IEEE Transactions on PAS, Vol. 86, No. 2, 1967, pp. 166-184.

49. Attri, N.S., Edgar, J.N. "*Response of Busbars on Elastic Supports Subjected to a Suddenly Applied Force.*" IEEE Transactions on Power Apparatus and Systems, PAS-86, 1967, pp. 636-650.

50. Serizawa, Y. "*Behaviour of Dead-end Suspension Double-conductor Bus During Short-Circuit.*" The Journal of the Institute of Electrical Engineers of Japan, Vol. 87, No. 11, November 1967, pp. 100-111.

51. Schaffer G. "*Kurzschlusskräfte von Zweierbündelleitern in Schaltanlagen.*" Elektrotechnik und Maschinenbau Vol. 86 1969, pp. 357-361

52. Borhaug, J.E., Cambias, S.M., Devey, J., Thompson, H.A. "*The Response of Substation Bus Systems to Short-circuit Condition. Part I: A comparison of design methods. Part II: Measurements on the transverse vibration of selected station post and pin-cap insulators.*" IEEE Transactions on Power Apparatus and Systems, PAS-90, 1971, pp. 1698-1718.

53. Logunov, L.P. "*On the Impact Strength of Porcelain Support Pin Insulators.*" Soviet Power Engineering, No. 12, 1974, pp. 729-734.

54. Deter, O. "*Calculation of the Dynamic Short-circuit Stress in Substations with Stiff Conductors and Elastic Supports.*" Brown Boveri Review, 62, 1975, pp. 99-104.

55. Adami, H., Ykema, Th. "*Aeolian Vibration of Tubular Busbars in Outdoor Substations and Its Damping.*" Journal of Applied Science and Engineering, A,1 (1975/76), pp. 259-280.

56. Hosemann, G., Tsanakas, D. "*Beitrag zur analytischen Berechnung der dynamischen Kurzschlussbeanspruchung von Schaltanlagen.*" ETZ-A, 97, 1976, pp. 493-498.

57. Mathejczyk, M. and Stein, N. "*Kurzschlusseilzuge enggebündelter Doppelseile in Schaltanlagen.*" ETZ-A, Bd 97, 1976, pp. 323-328.

58. Grober, R. and Stein, N. "*Beitrag zur dynamischen Kurzschlussbeanspruchung in Schaltanlagen.*" ETZ-A, 1976, Vol. 97, pp. 293-298.

59. Landin, J.I., Lindquvist, C.J., Bergstrom, L.R., Cullen, G.R. "*Mechanical Effects of Short-Circuit Currents in Substations.*" IEEE Transactions on Power Apparatus and Systems, Vol. PAS-94, No. 5, September/October 1975, pp. 1657-1665.

60. Olszowski, B., Orkisz, J., Waszczyszyn, Z. "*Calculation of Mechanical Effects in EHV Outdoor Substations at Short-circuit Currents.*" Revue Electrotechnique, 12, 1977, pp. 275-285.

61. Tsanakas, D. "*Dynamische Kurzschlussbeanspruchung von Hochspannungsschaltanlagen mit biegesteifen Leitern.*" ETZ-A, Bd. 98, 1977, pp. 399-403.

62. Stefanik, W., Votta, G.A., Stipcevich, J.M. "*Short-circuit Tests on a 3-Phase, 230 kV Rigid Bus Assembly.*" IEEE Summer Meeting, Mexico, July 1977.

63. Tsanakas D. "*Erhöhung der dynamischen Kurzschlussbeanspruchung infolge erfolgloser Kurzunterbrechung.*" ETZ-A, 99, 1978, pp. 86-88.

64. Ford G.L. and Srivastava K.D. "*Probabilistic Short-Circuit Design of Substation Bus Systems.*" IEEE Winter Power meeting New York 1978 Paper No. A 78 211-5.

65. Stein, N., Hermann, B. "*Kurzschluss-Seilzuge in Schaltanlagen.*" Elektrizitatswirtschaft, 78, 1979, pp. 179-186.

66. Engel, B. "*Mechanische Beanspruchung von Teilleiterseilen in Anlagen nach einem Kurzschluss.*" Elektrizitatswirtschaft 78, 1979, pp. 186-189.

67. Awad, M.B., Huestis, H.W. "*Influence of Short-circuit Currents on HV and EHV Strain Bus Design.*" IEEE Transactions on Power Apparatus and Systems, PAS-99, 1980, pp. 480-487.

68. Hosemann, G. "*Stand der Ermittlung von Kurzschlussbeanspruchungen elektrischer Anlagen mit baudynamischen Methoden.*" Elektrotechnik und Maschinenbau Vol. 97, 1980, pp. 248-252.

69. Craig, D.B., Ford, G.L. "*The Response of Strain Bus to Short-circuit Currents.*" IEEE Transactions on Power Apparatus and Systems, Vol. PAS-99, 1980, pp. 422-434.

70. Lehmann, W. "*Kurzchlussbeanspruchungen in Anlagen mit Leiterseilen.*" Symposium der Forschungsgemeinschaft für Hochspannungs- und Hochstromtechnik e.V., Report 1-248/12, 1981, pp. 347-356.

71. Oeding, D., Scheifele, J., Komurka, J. "*Calculation of Short-circuit Currents in High Voltage System.*" 7th Power Systems Computation Conference, Lausanne, 1981.

72. Tavano, F., Tomassi, A. "*Sbarre di Stazione a 420 kV: Comportamento Meccanico in Corto Circuito. Analisi Teorica e Risultati Sperimentali.*" L'Energia Elettrica, No. 10, 1981, pp. 421-432.

73. Ford G.L. and S. Sengupta "*Analytical Methods For Probabilistic Short-Circuit Studies.*" Electric Power Systems Research, Vol. 5, 1982, pp13-20.

74. Tsanakas, D. "*Einfluss der Zeitverlaufe der elektromagnetischen Kurzschlusskräfte auf die dynamische Beanspruchung.*" ETZ-A, Bd. 4, 1982, pp. 365-368.

75. Stauch, G., Böhme, H. "*Schwingungsverhalten von Stromleiteranordnungen in Mittelspannungsanlagen bei Kurzschluss. Beeinflussung der Grundfrequenz.*" Elektrie Berlin 37, 1983, 12, pp. 651-655.

76. El-Kady M.A. and G.L. Ford "*An Advanced Probabilistic Short-Circuit Program.*" IEEE Transactions on Power Apparatus and Systems Vol. PAS-102 1983, pp. 1240-1248.

77. Tsanakas, D., Papadias, B. "*Influence of Short-circuit Duration on Dynamic Stresses in Substations.*" IEEE Transactions on Power Apparatus and Systems, PAS-102, 1983, pp. 492-501.

78. Waeber, M. "*Bestimmung der Ausschwingbewegung von schwach gespannten Leiterseilen und des Fallseilzugs in Schaltanlagen bei Kurzschlüssen.*" ETZ-A, 5, 1983, pp. 103-107.

79. Lilien, J.L. "*Contraintes et Consequences Electromecaniques liees au passage d'une intensite de courant dans les structures en cables.*" Universite de Liege, Collection des Publications de la Faculte des Sciences Appliquees, No. 87, April 1983.

80. Miri A.M. and Heinrich C. "*Berechnung des Bewegungsablaufs und des dynamischen Zugkraftverlaufs von gebündelten Seilsammelschienen im Kurzschlussfall*" Elektrizitatswirtschaft Vol. 82, No. 9, 1983, pp. 318-325.

81. Brandt, E., Kuhnel, G., Terhorst, A., DeWendt, G. "*Dynamisches Verhalten von Abspanngeruesten in Hochspannungsanlagen bei Kurzschluss.*" Elektrizitätswirtschaft, Jg 83, 1984, Heft 16, pp. 711-716

82. Tsanakas, D.: "*Dynamische Beanspruchung von Hochspannungsschaltanlagen bei kleiner Kurzschlußdauer*". *ETZ-A* 6 (1984), pp. 387-392.

83. Kugler, R. "*Thermische und dynamische Kurzschlussbeanspruchung bei Hochspanungsleistungsschaltern.*" Elektrotechnik und Maschinenbau, Jg 102, 1985, Heft 7/8, pp. 298-304

84. This reference intentionaly free

85. Orkisz, J. and Tomana, A. "*A Discrete Dynamical Model of Duplex Conductors at Short-circuit Currents.*" Polish Academy of Science, Cracow, Mechanics 10, 1979, pp. 53-78.

86. Havard D.G. et al. "*Probabilistic Short-circuit Uprating of Strain Bus System - Mechanical Aspects.*" IEEE Transactions on Power Delivery, Vol.PWRD1 July 1986, pp. 104-110.

87. Campbell, J.D. "*Dynamic Yielding of Mild Steel.*" Acta Mat. 6, 1, 1953, pp.706.

88. Newmark, N.M. "*A Method of Computation for Structural Dynamics.*" ASCE Journal, Eng. Mech. Division, 85, 1959, pp. 65-94

89. IEEE Working Group 59.1, "*Minimum Line-to-Ground Electrical Clearances for EHV Substations Based on Switching Surge Requirements.*" IEEE Transactions on Power Apparatus and Systems Vol PAS 91 No. 5 Sept/Oct 1972, pp. 1294-1930.

90. Bathe, K.J., Wilson, E., Peterson, E. "*SAP IV: A Structural Analysis Program for Static and Dynamic Response of Linear Systems.*" University of California, College of Engineering, Report No. EERC 73-11, June 1973.

91. IEEE Surge Protective Devices Committee "*Sparkover Characteristics of High Voltage Protective Gaps.*" IEEE Transactions on Power Apparatus and Systems Vol PAS 93 No. 1 Jan/Feb 1974, pp. 196-205.

92. Diesendorf, W. "*Insulation Co-ordination in High Voltage Electric Power Systems.*" Butterworths & Co. 1974.

93. Bathe, K.J., Wilson, E., Iding, R.M. "*NONSAP: A Structural Analysis Program for Static and Dynamic Response of Nonlinear Analysis.*" University of California, Engineering Laboratory, Report No. US-CESM 743.

94. Gallet, G. et al "*General Expresssion for Positive Swithing Impulse Strenth Valid up to Extra Long Air Gaps.v.*" IEEE Transactions on Power Apparatus and Systems Vol PAS 94 No. 6 Nov/Dec 1975, pp. 1989-1993.

95. Bathe, K.J., Wilson, E.L. "*Numerical Methods in Finite Element Analysis.*" Prentice-Hall Inc., 1976.

96. Roussel, P. "*Numerical Solution of Static and Dynamic Equations of Cables.*" Comp. Meths. in Appl. Mech. and Engng., 9, 1976, pp. 65-74.

97. Bathe, K.J. "*ADINA: A Finite Element Program for Automatic Dynamic Incremental Nonlinear Analysis.*" Massachusetts Institute of Technology, 1978, Report 82448-1.

98. Sander, G., Gerardin, M., Nyssen, G., Hogge, M. "*Accuracy versus Computational Efficiency in Nonlinear Dynamics.*" Congress FENOMECH 78, North-Holland Publication, II, 1979, pp. 315-340.

99. Dannheim, H., Oel, H.J. "*Einfluss von Oberflächendefekten auf die mechanische Festigkeit bei keramischen Werkstoffen für Hochspannungsisolatoren.*" Berichte der Deutschen Keramischen Gesellschaft, 56, 1979, pp. 323-327.

100. Université de Liège. SAMCEF Manuels theorique et d'utilisation." Laboratoire de technique aerospatiale.

101. Dannheim, H., Oel, H.J. "*Festigkeit von keramischem Porzellan für Hochspannungsisolatoren bei dynamischer und zyklischer Belastung.*" Ceramic Forum International, 61, 1984.

102. Ballus, H. "*Ein Beitrag zur Berechnung elektromagnetischer Kräfte zwischen stromführenden Leitern.*" ETZ-A, 90, 1969, pp. 539-544.

103. Schwab, A.J. "*High-voltage Measuring Techniques.*" The M.I.T. Press, Cambridge, Mass, 1972.

104. Kiessling, G. "*Das Seilspannfeld als physikalisches Pendel, eine analytische Lösung der Kurzschlussvorgänge.*" A für Elektrotechnik 70 (1987), pp 273-281.

105. Lilien, J.L., Pirotte, P. "*The Behaviour of H.V. Strained Cables due to Short-Circuit Currents.*" First Symposium on Electric Power Systems in Fast Developing Countries, Riyadh, March 1987, pp. 577-583.

106. Lilien, J.L., El Adnani, M. "*Faisceaux de conducteurs et efforts electrodynamiques. Vers une approche numerique fiable.*" IEEE - Montech 86, Conference on AC Power Systems, Montreal, October 1986, pp. 79-84.

107. IEC Publication 865-1, Short-circuit currents - Calculation of effects. Part 1: Definitions and calculation methods, Genève: IEC, 1993.Identical with: EN 60865-1, Short-circuit currents - Calculation of effects. Part 1: Definitions and calculation methods, Bruxelles: CENELEC, 1993.

108. IEC Publication 865-2, Short-circuit currents-calculation of effects. Part 2 : examples of calculation. Genève: IEC, 1994.

109. Mavromaras, D.; Sieber, P.: "*Beitrag zur Ermittlung der bei Kurzschlüssen für Stromleiter zulässigen mechanischen Beanspruchungen.*" *ETZ-A* 89 (1968), pp. 34-38.

110. Dalle, B.: "*Étude de pincement d'un faisceau de sousconducteurs d'une portée de ligne lors d'un courtcircuit.*" *CIGRÉ SC 22 Colloquium*, Siena, 15.-22. September 1979.

111. Dalle, B.; Ford, G.L.: "*Behaviour of bundled conductors under high short-circuit currents.*" *CIGRÉ Symposium 06-85*, Buxelles, Report 330-08, pp. 1-6, 1985.

112. El Adnani, M.; Lilien, J.-L.: "*Dynamic behaviour of bundel conductors under short-circuit current - Simplified Model.*" *CIGRÉ SC 23-85 (WG 02) IWD*, 1985.

113. Engel, B.: "*Vereinfachte Berechnung der Seilauslenkungen durch Kurzschlußkräfte bei Geräteverbindungen in Schaltanlagen.*" Archiv für Elektrotechnik, vol. 61, no. 6, pp. 287-292, 1979.

114. Engel, B.: "*Berechnung der Kurzschlußbeanspruchung in Starkstromanlagen mit ungebündelten Leiterseilen.*" Thesis University of Erlangen, 1979.

115. Herrmann, B.; Stein, N.; Kießling, G.: "*Short-circuit effects in substations with strained conductors -Systematic full scale tests and a simple calculation method.*" IEEE Trans. Power Delivery, vol. 4, pp. 1021-1028, 1989.

116. Hosemann, G.; Landin, I.; Meyer, W.: "*Progress in international standardization: mechanical effects of short-circuit currents in substations with flexible conductors.*" 4th International Symposium on Short-Circuits in Power Systems, Liège 3-4 September 1990, Report 3.3, pp. 3.3.1-3.3.8.

117. Kießling, G.: "*Das Seilspannfeld als physikalisches Pendel - Eine analytische Lösung der Kurzschlußvorgänge.*" Archiv für Elektrotechnik, vol. 70, pp. 273-281, 1987.

118. IEC Publication 909: Short-circuit current calculation in three-phase a.c. systems, Part 1: Factors for the calculation of short-circuit currents in three-phase a. c. systems according to IEC 909, Genève: IEC, 1991.

119. IEC TC 73/Cigé SC 23: The mechanical effects of short-circuit currents in open air substations. Genève, IEC and Paris, Cigré, 1985.

120. Kießling, G.: "*Kurzschlußkräfte bei Zweierbündeln - Messungen und analytische Lösung mit dem Parabelmodell.*" etzArchiv, vol. 10, pp. 53-60, 1988.

121. Kießling, G.: "*Die mechanische Kurzschlußbeanspruchung von Seilanlagen - Analytische und numerische Berechnungsverfahren.*" Thesis University of Erlangen, 1988.

122. Korn, G.A.; Korn, T.M.: *Mathematical handbook for scientists and engineers.* New York; McGraw-Hill, 1968.

123. Möcks, L.: "*Die Teilfeldlänge in Bündelleitern.*" Bull. *SEV*, vol. 59, pp. 726-723, 1968.

124. Waeber, M.: "*Dynamische Vorgänge bei der mechanischen und thermischen Kurzschlußbeanspruchung von Starkstromanlagen mit Leitungsseilen.*" Thesis University of Erlangen, 1985.

125. Zarebski, W.: "*Approximate method on calculation of pinch effect of bundles.*" CIGRÉ SC 23-86 (WG 02) 24-IWD, 1986.

126. Zeitler, E.: "*Contraction of bundled conductors in outdoor substations determined by the parabola model.*" ETEP, vol. 3, pp. 285-291, 1993.

127. Zeitler, E.: "*Berechnung der Seilbewegungen und Kräfte bei vorwiegend vertikalen Verbindungen in Schaltanlagen.*" Thesis University of Erlangen, 1993.

128. Zurbriggen, R.: "*Kurzschlußbeanspruchung von Bündelleitern in Hochspannungsanlagen.*" Bulletin SEV 61 (1970), pp. 261-265.

129. *Mechanische Kurzschlußbeanspruchung durch vertikale Seilverbindungen in Hochspannungsschaltanlagen.* Forschungsgemeinschaft für Hochspannungs- und Hochstromtechnik e.V. Mannheim. Report 8001, 1990.

130. Declercq, G.: "*Influence of the reclosure on felxible conductor arrangements evaluation of the risk to increase the stresses in comparision with first short circuit stresses.*" 6th International Symposium on Short-Circuits in Power Systems, Liège 6-8 September 1994, Report 2.4, pp. 2.4.1-2.4.8.

131. Meyer, W.; Herold, G.;Zeitler, E. : "*Short-circuit currents-calculation of effects.*" The second edition of IEC Publication 865. 6th International Symposium on Short-Circuits in Power Systems, Liège 6-8 September 1994, Report 2.1, pp. 2.1.1-2.1.9

132. J.L. Lilien, M. El Adnani. "*Bundle behaviour during short-circuit fault. Influence of insulating hardware on snatch effect.*" IIIthSymposium on fault current in power systems, Lodz (Pologne), octobre 1988 (5 pages)

133. J.L. Lilien, M. Tahar Lamchich, J. Rucinski, M. El Adnani. "*Short-circuit on overhead lines with bundle conductors.*" Vth symposium on short-circuit current in power systems, Varsovie, sept. 1992(5 pages)

134. J.L. Lilien, U. Schön. "*Mechanical loads on substation apparatuses- Equivalent static load.*" présenté au "VIth Symposium on short-circuit in Power Systems" , proceedings, session 2. report 2.6. Liège, sept 1994

135. M.T. Lamchich, M. El Adnani,J.L. Lilien "*Mechanical loads on overhead lines bundle conductors.*" VIth Symposium on short-circuit in Power Systems, proceedings, session 2. report 2.5. Liège, sept 1994

136. M. El Adnani, J.L. Lilien, M.T. Lamchich "*Short-circuit mechanical effect on bundled conductors- IEC recommendations: confrontations with tests and numerical computations.*" VIth Symposium on short-circuit in Power Systems, proceedings, session 2. report 2.2. Liège, sept 1994

137. J.L. Lilien, E. Hansenne. "*Short-Circuit mechanical effect on substation apparatuses. The equivalent static load during dropper stretch.*" VIIth Symposium on Short-Circuit Current, Warsaw, Sept. 1996

138. A.M. Miri, A. Kühner, J.L. Lilien, N. Stein. "*An analytical-Numerical method based on static equivalent load for the evaluation of maximum dynamic stresses in HV substation.*" VIIth Symposium on Short-Circuit Current, Warsaw, Sept. 1996

139. A. M. Miri, A. J. Schwab, M. Kopatz "*Kurzschlußkräfte und Leiterbewegungen in Hochspannungs-Schaltanlagen in Seilbauweise.*" Elektrizitätswirtschaft, Jg.87 (1988), S.429-436

140. G. de Wendt, T. Tietz, A. M. Miri, R. Ahlers, N. Stein: "*Dynamic and Static Case Stress Analysis of a HV Substation with Stranded Conductors (Test-results-Calculation)*" VIIth Symposium on Short-Circuit Current, Warsaw, Sept. 1996

141. A. M. Miri, N. Stein: "*Kurzschlußbeanspruchung und -festigkeit von Hochspannungs-Stützisolatoren.*"etzArchiv, Bd. 10 (1988),H.3, S.89-96

142. A. M. Miri, N. Stein:"*Short-Circuit Constraints and Strength of HV Substation Post-Insulators.*" Vth Symposium on Short-Circuit Current, Warsaw, Sept. 1992

APPENDIX
CALCULATION OF FORCES IN A RIGHT ANGLE BEND
(Special Application to Terminals of Apparatus)

The conductors are assumed to be in the same plane and forming a right angle. The influences of the neighbouring main conductors are also neglected.

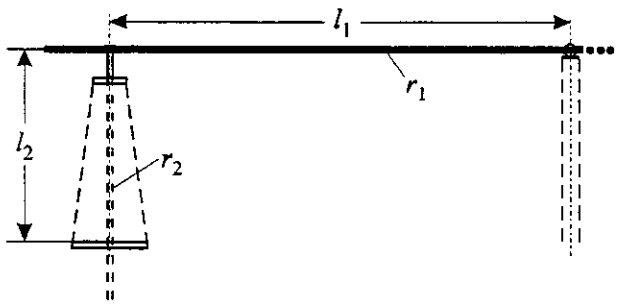

Figure A1: Connection of a rigid or flexible conductor to a cable box or bushing in a right angle
l_1, l_2 length of conductor 1, 2
r_1, r_2 radius of conductor 1, 2

The method is described with reference to a practical example, Figure A1, which could be a rigid or a flexible conductor at a right angle to a cable box or a transformer bushing. Another practical application would be a horizontal connection to a panthograph isolator.

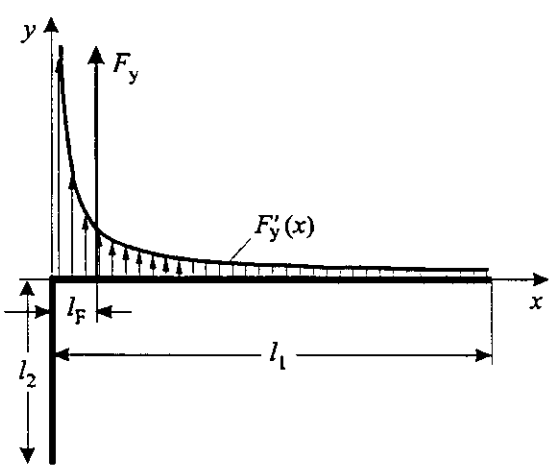

Fig. A2: Distributed force on the conductor according to Figure A1

In Figure A2, the distributed force on such a conductor with the length l_1 between supports is illustrated. To simplify the procedure, the distributed force is replaced by an equivalent concentrated force F_y acting at the distance l_F from the terminal or apparatus. Introduced symbols are explained in the figures and diagrams.

Basis for the calculation

The equivalent concentrated force F_y follows from the integration of the distributed force per unit length

$$F_y = \int_0^{l_1} F'_y(x)\ \mathrm{d}x \qquad \text{(A1)}$$

and the distance l_F results from the moment with respect to $x = 0$

$$F_y\, l_F = \int_0^{l_1} F'_y(x) \cdot x\, \mathrm{d}x \qquad \text{(A2)}$$

with the distributed force per unit length

$$F'_y(x) = \frac{\mu_0}{2\pi}\, i^2\, \frac{l_2}{x\sqrt{x^2 + l_2^2}} \qquad \text{(A3)}$$

The integral in (A1) can not be evaluated, because the denominator in (A3) becomes zero at $x = 0$. In [102] the current paths in a corner for all bending angles are carefully studied and a method which shortens the conductors in the corner is presented; the force is then calculated using the law of Biot-Savart. [A1] and [A2] use the Principle of D'Alembert of energy change in a closed current loop caused by a virtual displacement; [A1] for a right angle, [A2] for all angles. This gives an analytical expression for the bending force which needs no shortening of the conductor. Both methods are in good accordance. For right angle bends, from [A1, A2] a simple formula can be found:

$$F_y = \frac{\mu_0}{2\pi} i^2 \left[\ln\left(\frac{l_2}{r_2} + \sqrt{\left(\frac{l_2}{r_2}\right)^2 + 1} \right) - \ln\left(\frac{l_2}{l_1} + \sqrt{\left(\frac{l_2}{l_1}\right)^2 + 1} \right) \right] \quad \text{(A4)}$$

The force only depends on the ratio of the length and the radius of the field inducing conductor 2 and the ratio of the conductor lengths.

The integral in (A2) is soluble and the result is:

$$F_y \cdot l_F = \frac{\mu_0}{2\pi} i^2 l_2 \left[\ln\left(1 + \sqrt{1 + \left(\frac{l_2}{l_1}\right)^2} \right) - \ln\left(\frac{l_2}{l_1}\right) \right] \quad \text{(A5)}$$

so that l_F becomes:

$$\frac{l_F}{l_1} = \frac{l_2}{l_1} \frac{\left[\ln\left(1 + \sqrt{1 + \left(\frac{l_2}{l_1}\right)^2} \right) - \ln\left(\frac{l_2}{l_1}\right) \right]}{\frac{F_y}{\frac{\mu_0}{2\pi} i^2}} \quad \text{(A6)}$$

[102] gives a condition which should be observed:

$$\text{Max}\left\{ \frac{r_1}{l_1}; \frac{r_2}{l_2} \right\} \leq 0{,}25 \quad \text{(A7)}$$

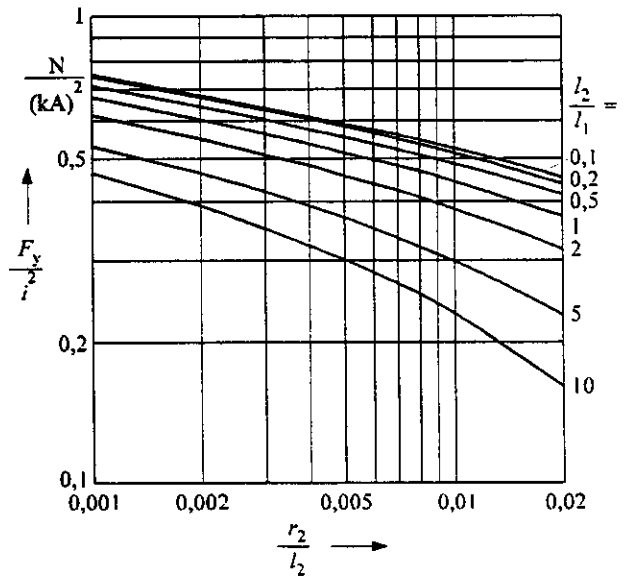

Fig. A3: Equivalent concentrated force F_y/i^2 in relation to r_2/l_2 and l_2/l_1.

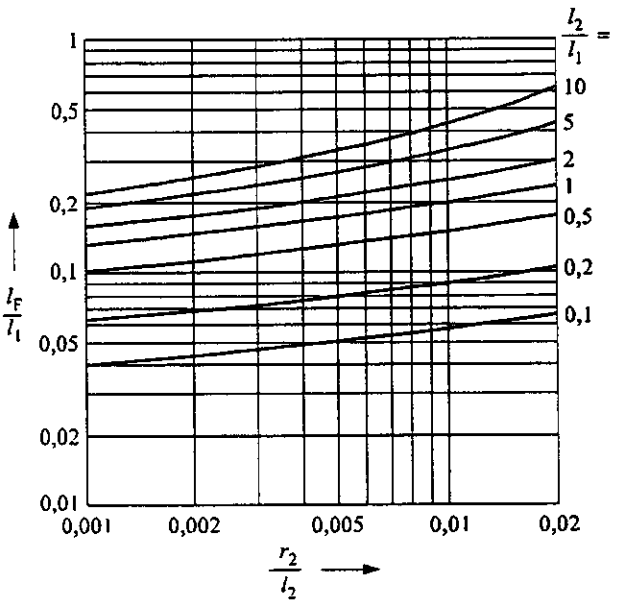

Fig. A4: Distance l_F/l_1 in relation to r_2/l_2 and l_2/l_1.

Figures A3 and A4 show the related equivalent concentrated force and the related distance.

For the design in open air substations, use of such a simplified procedure for the estimation of angle forces is reasonable because

- the ratio of conductor diameter to conductor length of interest is small,
- variability in design and influence of connectors makes it difficult and uncertain to foresee and to analyse the real current paths near the corner,
- a concentrated force is easier to analyse than varying distributed forces, especially in combination with simplified calculation methods.

Calculation procedure

Form the ratios

$$\frac{l_2}{l_1}; \quad \frac{r_2}{l_2} \quad \text{(A7)}$$

Calculate F_y according to (A4) or Figure A3 and l_F according to (A6) or Figure A4.

Superimpose angle forces with other short-circuit forces and stresses.

Example

$l_1 = 10$ m; $r_1 = 0{,}03$ m; $l_2 = 5$ m; $r_2 = 0{,}04$ m
then

$$\frac{l_2}{l_1} = 0{,}5 \qquad \frac{r_2}{l_2} = 0{,}008$$

From (A4) or Figure A3:

$$\frac{F_y}{i^2} = 0{,}5 \frac{\mathrm{N}}{(\mathrm{kA})^2}$$

From (A6) or Figure A4:

$$l_F = 0{,}14 \cdot 10 \text{ m} = 1{,}4 \text{ m}$$

Of course, advanced calculation methods can easily be used for such application and actual time response will be obtained.

References

[A1] Hak, J.: *Einige Bemerkungen zur Berechnung der auf bewegliche Leiterteile wirkenden Kräfte.* E und M 47 (1929), pp 149-154

[A2] Meyer, W.: *Eine Methode zur Berechnung von Stroemen und Kraeften in gekapselten Betriebsmitteln.* Thesis University of Erlangen-Nürnberg, 1983

CIGRE Study Committee 23 (Substations)
Working Group 23-11 (Substations and Environment)
ESCC Task Force (Effects of Short-Circuit currents)

The Mechanical Effects of Short-Circuit Currents in Open Air Substations (Rigid and Flexible Bus-Bars)

Volume 2 :

Data Base of Reference Tests

April 1996

TABLE OF CONTENT

PREFACE 3

I) RIGID BUS CONFIGURATIONS 5

CASE 1 5
Test performed at FGH (Germany) in 1976 5
A parallel rigid bus 5
(CIGRE structure D) 5
short-circuit current : 16 kA (40 kA peak) 5
with autoreclosure 5

CASE 2 8
Test performed at FGH (Germany) in 1976 8
A parallel rigid bus with inclined parts 8
short-circuit current : 9,4 kA (25 kA peak) 8
without autoreclosure 8
inclined span length tested between two supports: 3,5 to 5 m 8

CASE 3 18
Test performed at Ontario Hydro (Canada) in 1976 18
A non- parallel rigid bus including A frame 18
short-circuit current : 36 kA (90 kA peak) 18
with autoreclosure 18

II) FLEXIBLE BUS CONFIGURATIONS 22

PART 1 :

SINGLE CONDUCTOR PER PHASE

CASE 4 24
Test performed at Laborelec (Belgium) in 1980 24
cross section : 324 mm^2 24
short-circuit current : 30 kA (73 kA peak) 24
span length : 40 m 24

CASE 5 28
Test performed at Laborelec (Belgium) in 1980 28
cross section : 105 mm^2 28
short-circuit current : 30 kA (65 kA peak) 28
span length : 40 m 28

CASE 6 32
Test performed at Laborelec (Belgium) in 1980 32
cross section : 324 mm^2 32
short-circuit current : 30 kA (73 kA peak) 32
span length : 40 m 32
with added dropper (on east phase) 32

CASE 7 ..... **36**
Test performed at Laborelec (Belgium) in 1980 36
cross section : 105 mm^2 36
short-circuit current : 30 kA (73 kA peak) 36
span length : 40 m 36
with added dropper (on east phase) 36

CASE 8 ..... **40**
Test performed at FGH (Germany) in 1985 40
cross section : 590 mm^2 40
short-circuit current : 25 kA (64 kA peak) 40
span length : 40 m 40

CASE 9 ..... **45**
Test performed at EDF- Les Renardières (France) in 1990 45
cross section : 570 mm^2 ASTER 45
short-circuit current : 30 kA(80kA peak) 0,085 s, ... 45
with auto reclosure 45
span length : 68 and 34 m (test 1101) 45

CASE 10 ..... **49**
Test performed at EDF- Les Renardières (France) in 1990 49
cross section : 570 mm^2 ASTER 49
short-circuit current : 30 kA, 0,255 s 49
span length : 102 (test 1102)- 68 and 34 m (test 1003) 49

CASE 11 ..... **56**
Test performed at EDF- Les Renardières (France) in 1990 56
cross section : 570 mm^2 ASTER 56
short-circuit current : three-phase, 35 kA; 0,245s 56
span length : 68 and 34 m (test 1202) - 102 m (test 1002) 56

PART 2 : **63**

BUNDLE CONDUCTOR

CASE 12 ..... **63**
Test performed at ASEA- Ludvika (Sweden) in 1976 63
Case with bundle pinch (triple horizontal) 63
cross section : 3x772 mm^2 ACSR 63
short-circuit current : 30; 40 and 50 kA 63
span length : 70 m,subspan 12 m 63

CASE 13 ..... **66**
Test performed at ASEA- Ludvika (Sweden) in 1976 66
Case with bundle pinch (triple triangle) 66
cross section : 3x772 mm^2 ACSR 66
short-circuit current : 30; 40 and 50 kA 66
span length : 70 m,subspan 30 m 66

CASE 14 ..... **68**
Test performed at ASEA- Ludvika (Sweden) in 1976 68
Case with bundle pinch (quad) 68
cross section : 3x772 mm^2 ACSR 68
short-circuit current : 30; 40 and 50 kA 68
span length : 70 m,subspan 30 m 68

CASE 15 ..... **70**
Test performed at KEMA- Arnhem(The Netherlands) 70
in 1980 70
Case with bundle pinch (twin horizontal) 70
cross section : 2x1100 mm^2 ACSR 70
short-circuit current : 50 kA (137 kA peak) 70
span length : 30 m,subspan 6 m 70

CASE 16 ..... **73**
Test performed at Furukawa (Japan) in 1966 under supervision of 73
Prof. Serisawa (Yokohama National University) 73
Case with tripple bundle pinch without contact 73
cross section : 3x1600 mm^2 73
short-circuit current : 63 kA (164 kA peak) 73
span length : 35 m (subspan length : 2m) 73

PART 3 : **77**

DROPPER CONFIGURATION

CASE 17 ..... **77**
Test performed at FGH (Germany) in 1990 77
Case with end-dropper (single conductor) 77
cross section : ACSR 590 mm^2 77
short-circuit current : 20 ; 30 , 40 kA; 0,104 and 0,304 s 77
span length : 4 x 1,6 m (dropper length 4.9 m) 77

CASE 18 ..... **83**
Test performed at FGH (Germany) in 1990 83
Case with end-dropper (twin bundle) 83
cross section : ACSR 2x590 mm^2 83
short-circuit current : 20 ; 30 and 40 kA ; 0,104 and 0,304 s 83
span length : 7 x 3,2 m (dropper length 9 m) 83

ANNEX : TYPICAL DATA (CU, AL, ASTER, ACSR) **89**

PREFACE

During the CIGRE conference of 1992 the Study Committee 23 decided to create a new task force attached to working group 23-11 (substation and environment). The aim of the task force has been designated as followed :

- to define the short-circuit mechanical effects in substations in relation with IEC TC73.
- to revise the 1987 brochure published by the former WG 23-02
- to give updated recommendations for design, uprating of open-air substations in relation to short-circuit mechanical effects.

This brochure is a first step in presenting a detailed data-base of short-circuit tests which have been performed in recent decades. The aim is to capture the corresponding knowledge in an international document to facilitate physical understanding, and as an aid in verifying modeling and simulation case studies.

The task force would like to thank all of the utilities, research centers and universities for providing information and data and for permission to publish these data and oscillograms. Of course we could not have been exhaustive and numerous tested structures have not been reported in this compilation. We have choosen the cases for which more or less all data were available and for which oscillograms were also available. We hope that readers and users of this report will appreciate the complexity of assembling such data and understand the deliberate but difficult choice that we have made.

The members of ESCC task force :
G. Declerq (France), O. Deter (Germany), M. El Adnani (Morocco), G. Ford (Canada), J.L. Lilien, Convener (Belgium), W. Meyer (Germany), A.M. Miri (Germany), R. Nordin (Sweden), A. Polevoy (Israël), N. Stein , Secretary (Germany), D. Tsanakas (Greece)

Internet contact via e-mail :
J.L. Lilien at lilien@montefiore.ulg.ac.be
G. Ford at FordG@ice6.kcps.rd.hydro.on.ca
W. Meyer at meyer@eev.e-technik.uni-erlangen.de
A.M. Miri at miri@ieh.etec.uni-karlsruhe.de

Why do tests ?

At the current stage of studies, the main efforts of researchers are focused on evaluation of dynamic loading, caused by short-circuit effects. Tests results are the only reliable basis for proving the use of both simple and advanced calculation approaches. On the other hand, calculation approaches identify the effects and relations between different causes, and define new test directions that need to be carried out. The importance of tests has more weight due to the nonlinear character of short-circuit phenomena. Any extrapolation or generalisation of previously obtained results requires further checking .

Evaluation of the structural response to the short-circuit dynamic loading is the aim of the next stage of studies. In the case of advanced methods there is no particular problem but for simple method, due to the multifrequency character of the load, spectrum density techniques are the most suitable for describing loadings, and a transfer function is the most compatible description for structure response. Tests results are the only option to obtain practical data to built up suitable models of transfer functions for calculation approaches.

To perform tests is time consuming and expensive. Caution must be taken to avoid being biaised by some particular cases or phenomena more related to the tests themselves than the underlying phenomenon which is the purpose of such tests.

Readers are strongly adviced to understand the physics of the phenomenon, and to avoid accepting with full confidence either test or calculation results. It is always preferable to try to understand why phenomena happen as observed in tests or computations.

Typical configurations

Rigid bus-bar are generally parallel conductors on supporting insulators; but sometimes the bus cannot be the straight and parallel ideal, due to angles necessary for substation layout or orientation change. These different kinds of arrangement will be tested in several cases.

Flexible bus is typically similar to fig. 0. All cable connections can be single conductor or bundle arrangements. Tests have been performed with configurations B, B+C, D or E.

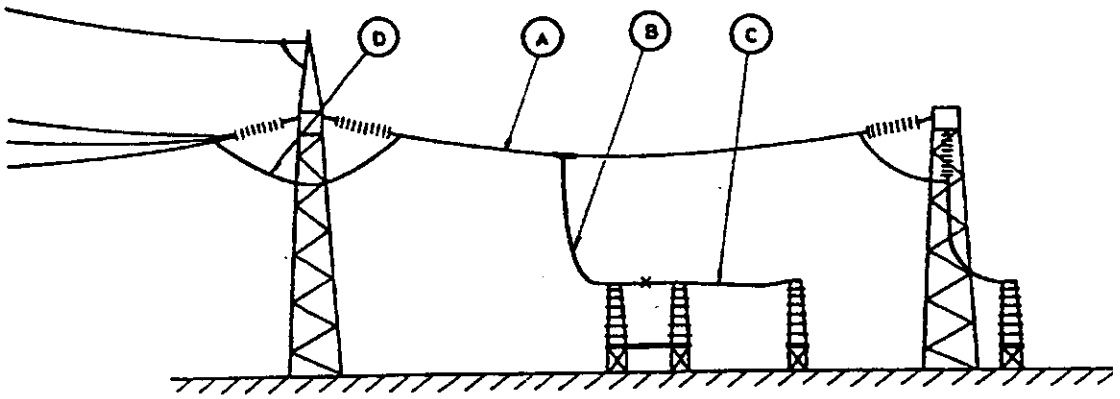

Fig. 0. Typical configurations for flexible bus-bar structure. A :horizontal strain bus connected by insulator strings to steel structures, B : vertical dropper between strain bus and apparatus, C : horizontal connection between components, D : jumpers connecting two strained conductor sections, E : end span dropper, F : first span to overhead line.

Case study

We have selected the most detailed cases with span length between 34 and 102 meters and short-circuit current between 10 kA and 40 kA (peak up to 90 kA). Classical parallel buses are treated and also more complicated ones including droppers and non-parallel bus, both in flexible and rigid bus. Tests have been performed in short-circuit laboratories in Belgium (Laborelec, Bruxelles), France (EDF, les Renardières), Canada (Ontario Hydro, Toronto), Sweden (ASEA, Ludvika) and Germany (FGH, Mannheim).

all reference cases are divided in three sub-parts :

1) bus-bar geometry

2) basic data for
- all connections
- initial conditions before testing
- short-circuit characteristics

3) results

some cases are complete, including all data and many results, data for others are only partially available.

I) RIGID BUS CONFIGURATIONS

CASE 1

Test performed at FGH (Germany) in 1976
A parallel rigid bus
(CIGRE structure D)
short-circuit current : 16 kA (40 kA peak)
with autoreclosure

Bus-bar geometry

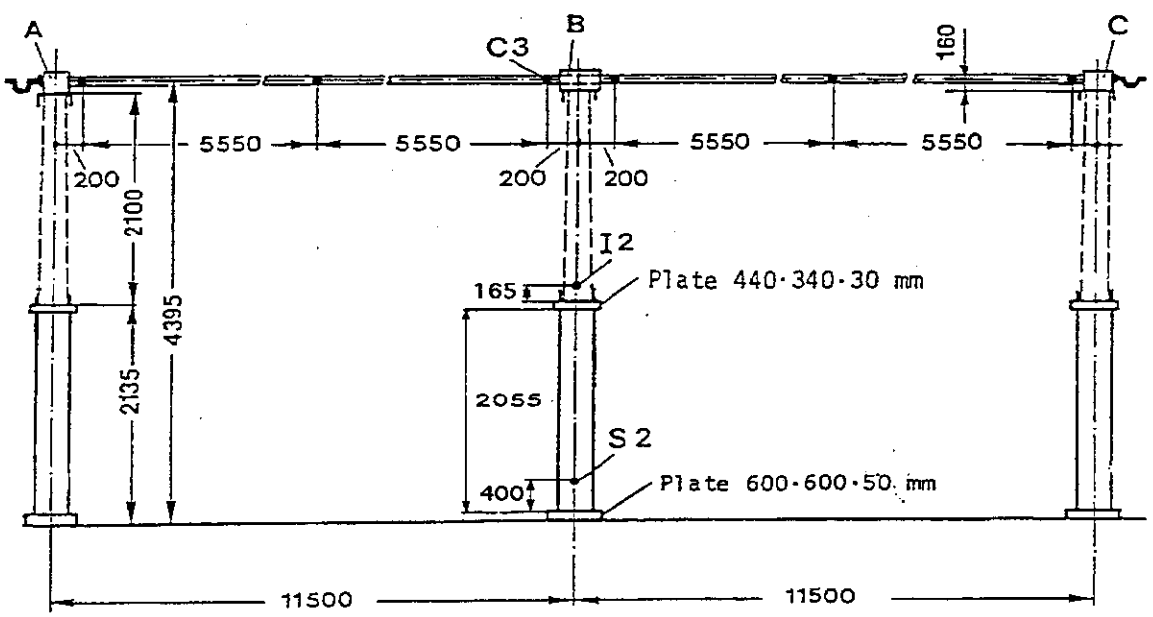

Fig. 1.1 Geometry of the rigid bus-bar tested in FGH

Test structure :
I_2, S_2 : measuring points for the bending moment in the insulators and steel pillars.
C_3 : measuring point for the bending stress in the conductor.

Other references :
G. Palante*Behaviour of Rigid conductors and their supports under short-circuit conditions. Comparison of calculated and measured values.*. Report 23-10 of the CIGRE session 1976.
G. Hosemann, D. Tsanakas. *Calculated and Measured Values of Dynamic Short-circuit Stresses in a High Voltage Test structure with and without Reclosure.* Electra N° 63 (1979), pp 147-161.

Basic data

1) bus-bar

	section (mm^2)	mass (kg/m)	Elasticity modulus	moment of inertia (cm^4)	wall thickness (mm)	outside diameter (mm)
upper bus-bar	2238,0	6,04	$7\ 10^{10}$	370,4	6,2	121,1

logarithmic decrement : 0,05
Centre line distance between phases : 1 m

2) Support

	length (m)	frequency (Hz)	stiffness (kN/mm)	mass (kg/m)
Insulator A	2,1	21,5	0,73	85,7
Insulator B	2,1	21,5	0,76	85,7
Insulator C	2,1	21,5	0,78	85,7
steel pilar A	2,05	27,2	0,15	36,8
steel pilar B	2,05	27,2	0,18	36,8
steel pilar C	2,05	27,2	0,21	36,8

there are plates between the steel pillar and the insulator : 35 kg

the clamps to fix the bus to the insulator are 0,16 m length and have a mass of 13,8 kg (A and C) and 18,2 kg (B)

boundary conditions :

the bus is clamped at B points and hinged at A and C.

3) short-circuit characteristics

kind of short-circuit (two or three-phase) : two phase, 50 Hz

	Irms (kA)	Ipeak (kA)	time constant (ms)	duration (s)
first fault	15,6	41,0	66	0,135
second fault	15,6	40,8	62	0,305

N.B. clearing time between the two fault : 0,445 s

design values :	measured before reclosure	measured after reclosure
max bending moment (insulator) N.m	5080	9710
max bending moment (steel support) N.m	10180	19610
max stress in the bus-bar (N/mm^2)	37,7	71,4

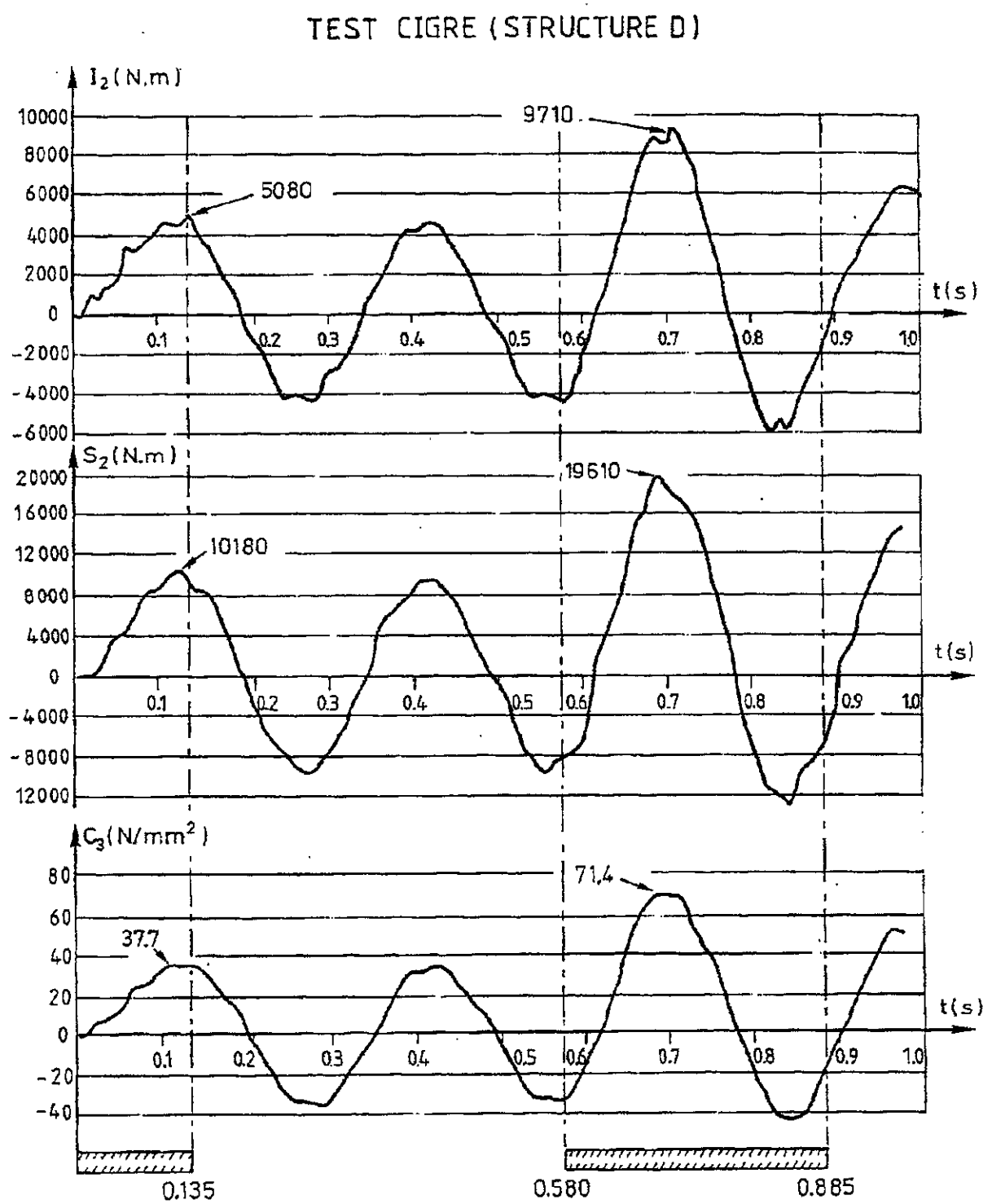

Fig. 1.2 Bending moment in the supporting structure and stress in the bus. Location of I2, S2 and C3 is indicated on fig. 1.1.

CASE 2

Test performed at FGH (Germany) in 1976
A parallel rigid bus with inclined parts
short-circuit current : 9,4 kA (25 kA peak)
without autoreclosure
inclined span length tested between two supports: 3,5 to 5 m

Bus-bar geometry (3 different configurations)

Test performed in Germany (FGH) in 1976

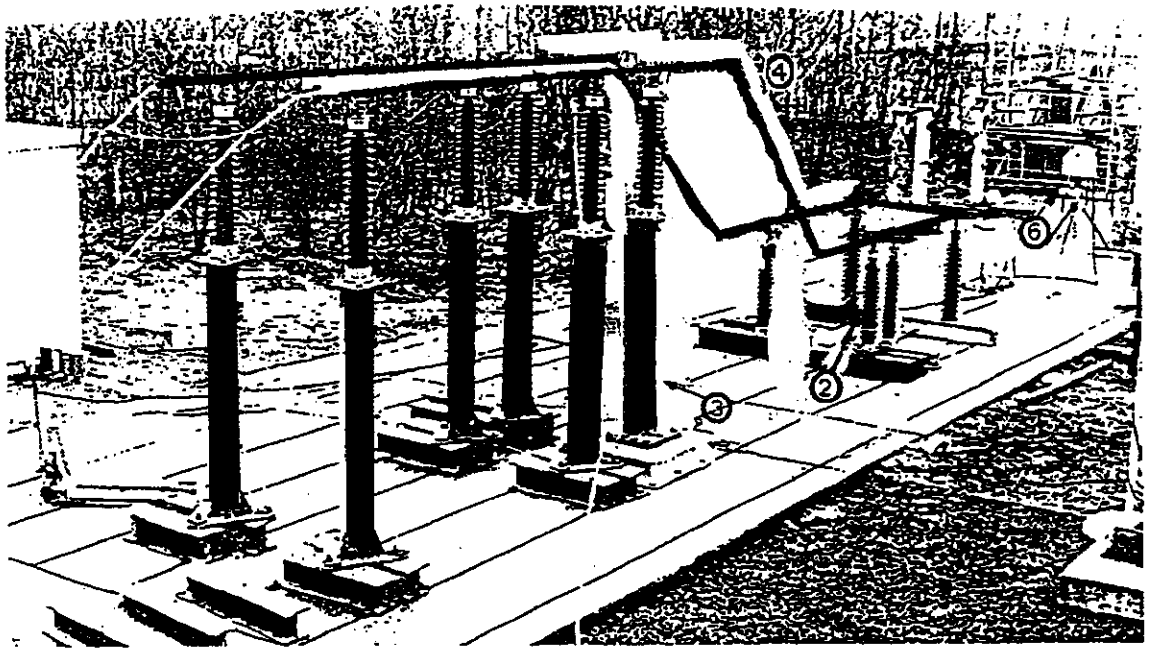

Fig. 2.1 A picture of the particular rigid bus tested in FGH with three different configurations. The upper part is supported by a steel pillar and a supporting insulator. The bus bar is not straight and connect the upper bus to lower bus by a tubular connection. The lower bus is supported by insulator.

Contact address : FGH Mannheim, Hallenweg 40, Postfach 810169, D 68201 Mannheim (Norbert Stein). Germany. Fax : + 49-621-8047112

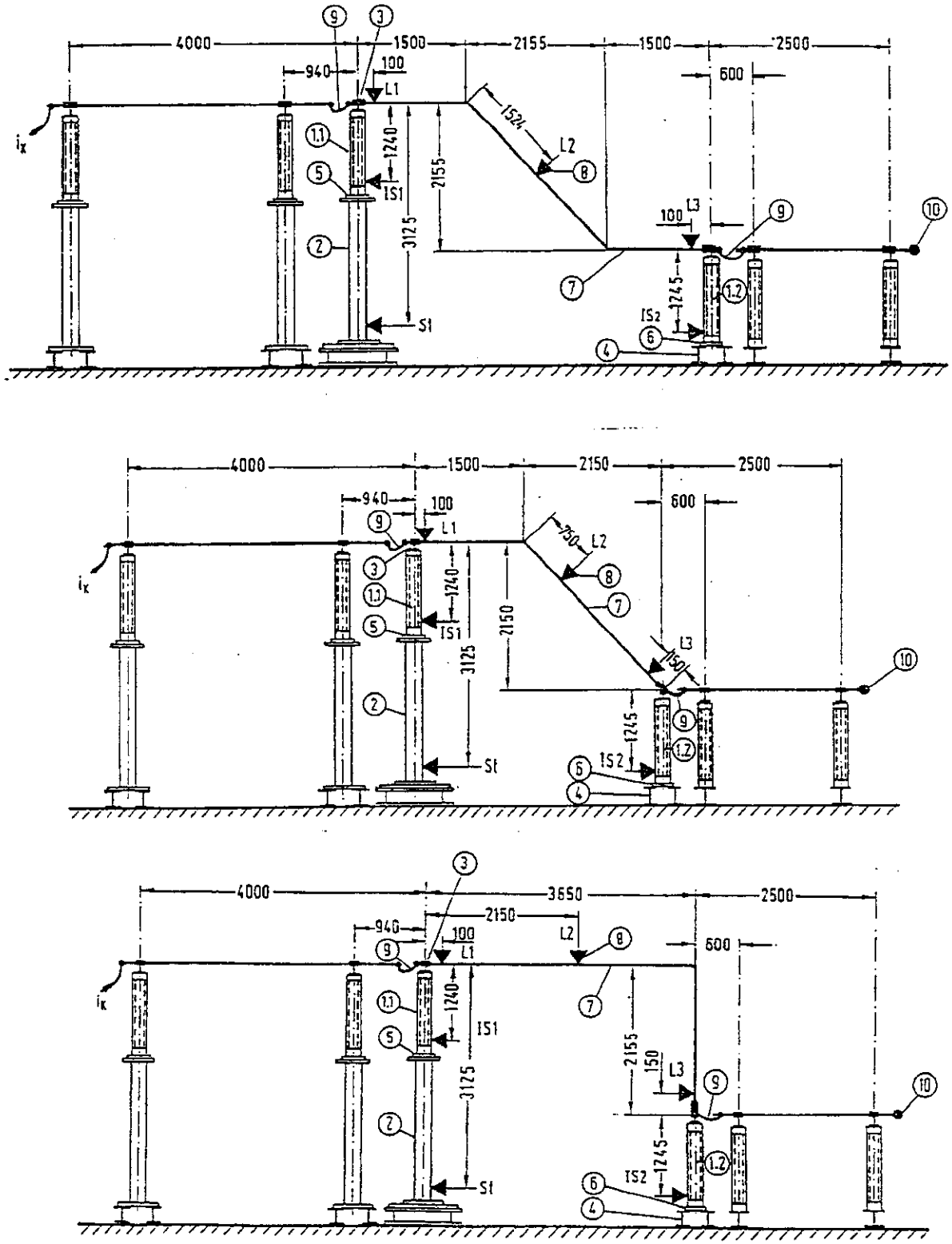

Fig. 2.2 The geometry of the three configurations, including measurement point (St for steel pillar bending moment, IS1 and IS2 for insulator support bending moment and L1, L2, L3 for bus-bar stress). Number 9 is a flexible connection, 10 is the point where short-circuit with other phase is done, other numbers are used in the data.

Basic data

1) bus-bar

	section (mm^2)	mass (kg/m)	Elasticity modulus	moment of inertia (mm^4)	wall thickness (mm)	outside diameter (mm)
bus-bar	424,1	1,145	$6,5\ 10^{10}$	39972,0	5	32

Centre line distance between phases : 1,4 m

2) Support

	length (m)	frequency (Hz)	stiffness (kN/mm)	mass (kg/m)
Insulators (1.1 and 1.2 on fig. 10.2)	1,215	55	2,6	71
steel pilar	2,06	25	2,5	35,6

between the steel pilar (number 2 on fig. 10.2) and the insulator (only for support 1), there is a plate of about 45 kg (number 5 on fig. 2.2).

between the top of the insulator and the busbars there is a fitting (about 3kg) which fix the level of the bus about 15 cm higher than the top of the insulator(number 3 on fig. 2.2)

boundary conditions :
the bus is clamped at both ends (free longitudinal movement at the top). There is a flexible connection to the other parts of the bus (number 9 on fig. 2.2). Clamps are reproduced on the next page.

3) short-circuit characteristics

kind of short-circuit (two or three-phase) : two phase, 50 Hz, bus-bar is number 7 on fig. 2.2

	Irms (kA)	Ipeak (kA)	time constant (ms)	duration (s)
first fault	9,4	25	75	0,3

Results

Configuration 1

design values for I_K=9,4kA (25kA peak)	measured
max bending moment (insulator) N.m	1000(STx)
max bending moment (steel support) N.m	1100(JS2x)
max stress in the bus-bar (N/mm^2)	42(L1)

N.B. the maximum displacement of the bus-bar has been evaluated to 7 cm

Configuration 2

design values for I_K=9,4kA (25kA peak)	measured
max bending moment (insulator) N.m	1050 (JS2y)
max bending moment (steel support) N.m	900(STx)
max stress in the bus-bar (N/mm^2)	36(L1)

Configuration 3

design values for I_K=9,4kA (25kA peak)	measured
max bending moment (insulator) N.m	1750(JS2x)
max bending moment (steel support) N.m	975(Stx)
max stress in the bus-bar (N/mm^2)	52(L3)

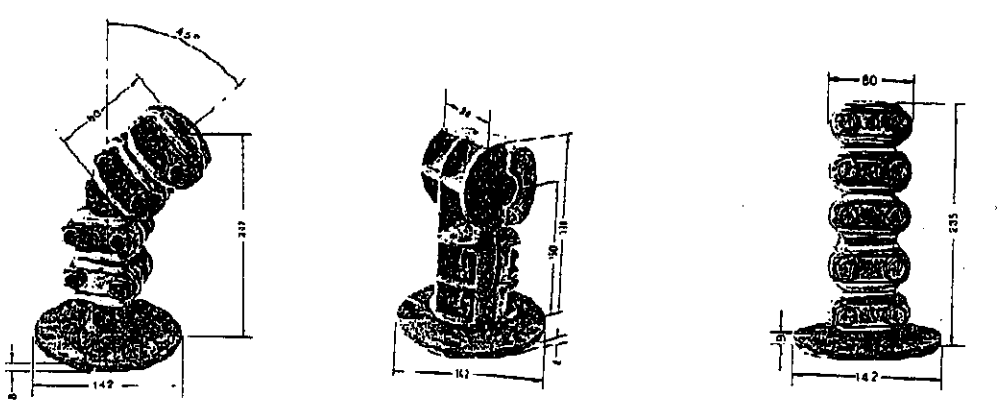

Fig. 2.3 clamps used to fix the bus to the insulators supports.

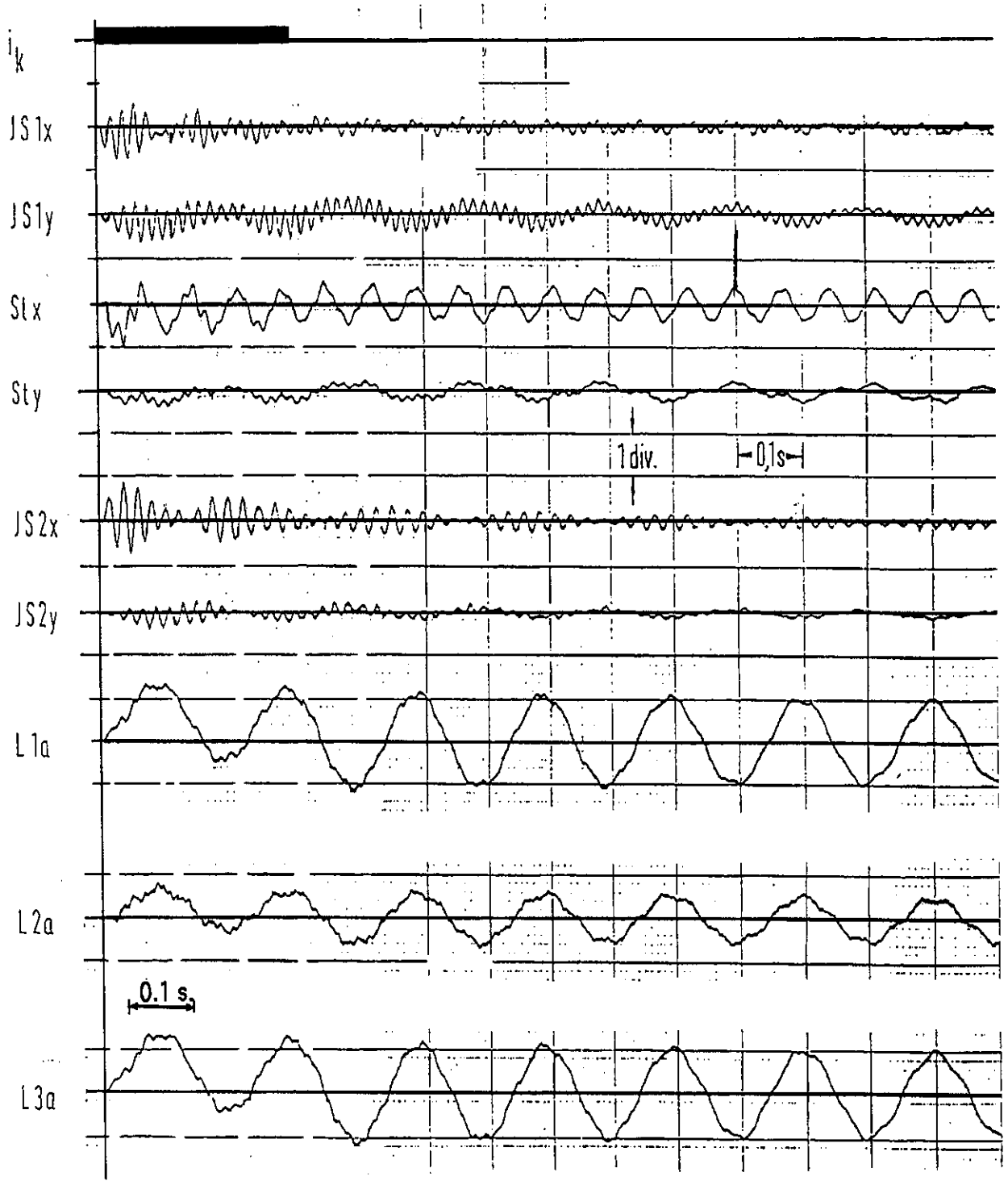

Fig. 2.4 Oscillograms for each measurement point (Structure configuation 1). x and y are used to give the measured values in the plane of the bus (x) or perpendicular to it (y). The scale of each curve is given by the values of 1 division shown in the graphic : (955 N.m for IS1x, 612 N.m for IS1y, 1188 N.m for Stx, 1539 for Sty, 1223 for IS2x and y, 31,5 N/mm^2 for L1a, L2a, L3a)

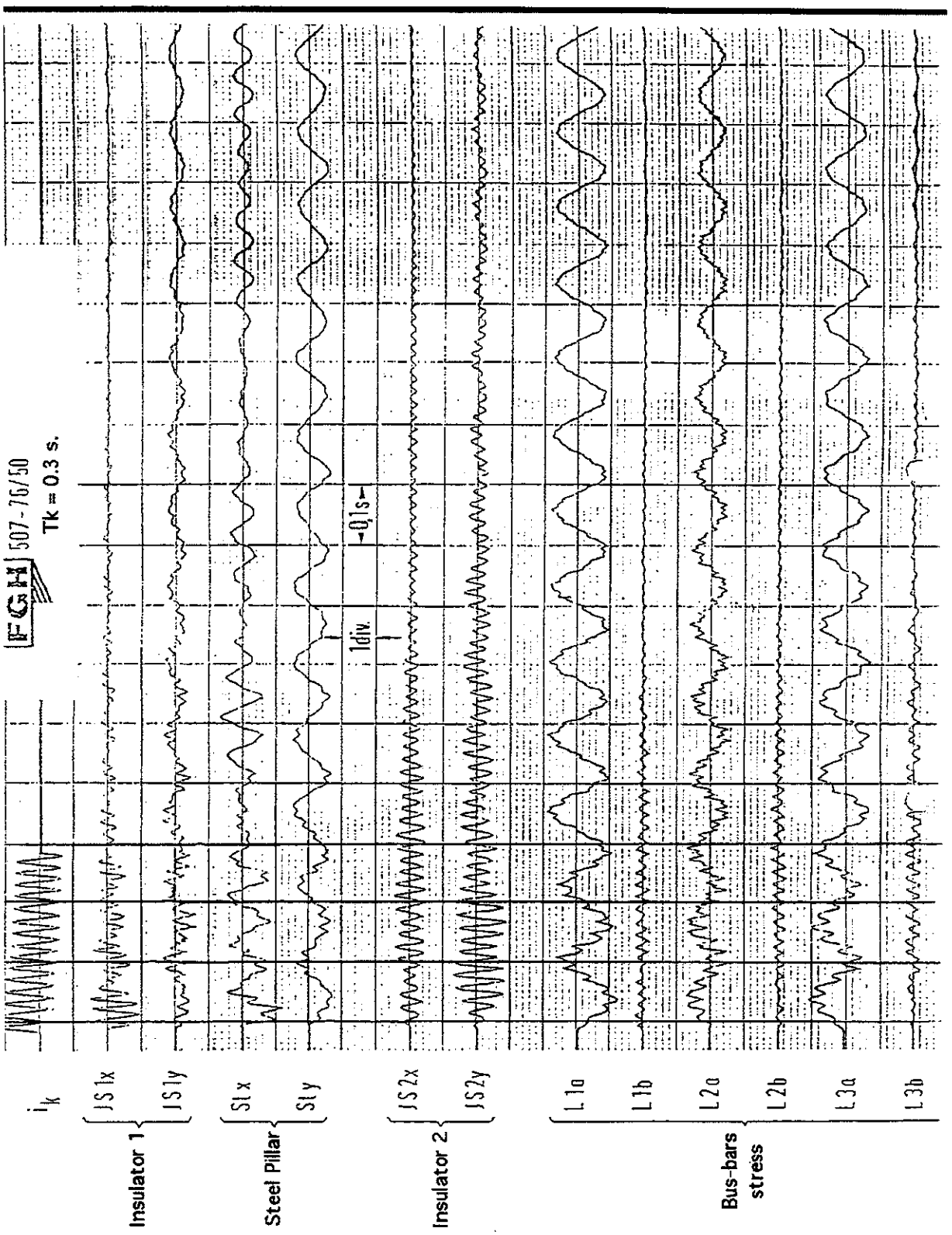

Fig. 2.5 Oscillograms for each measurement point (Structure configuation 2). x and y are used to give the measured values in the plane of the bus (x) or perpendicular to it (y). The scale of each curve is given by the values of 1 division shown in the graphic : (584 N.m for IS1x, 610 N.m for IS1y, 790 N.m for Stx and y, 1175 for IS2x and 1226 for IS2y, 31,5 N/mm^2 for L1a, L2a, L3a)

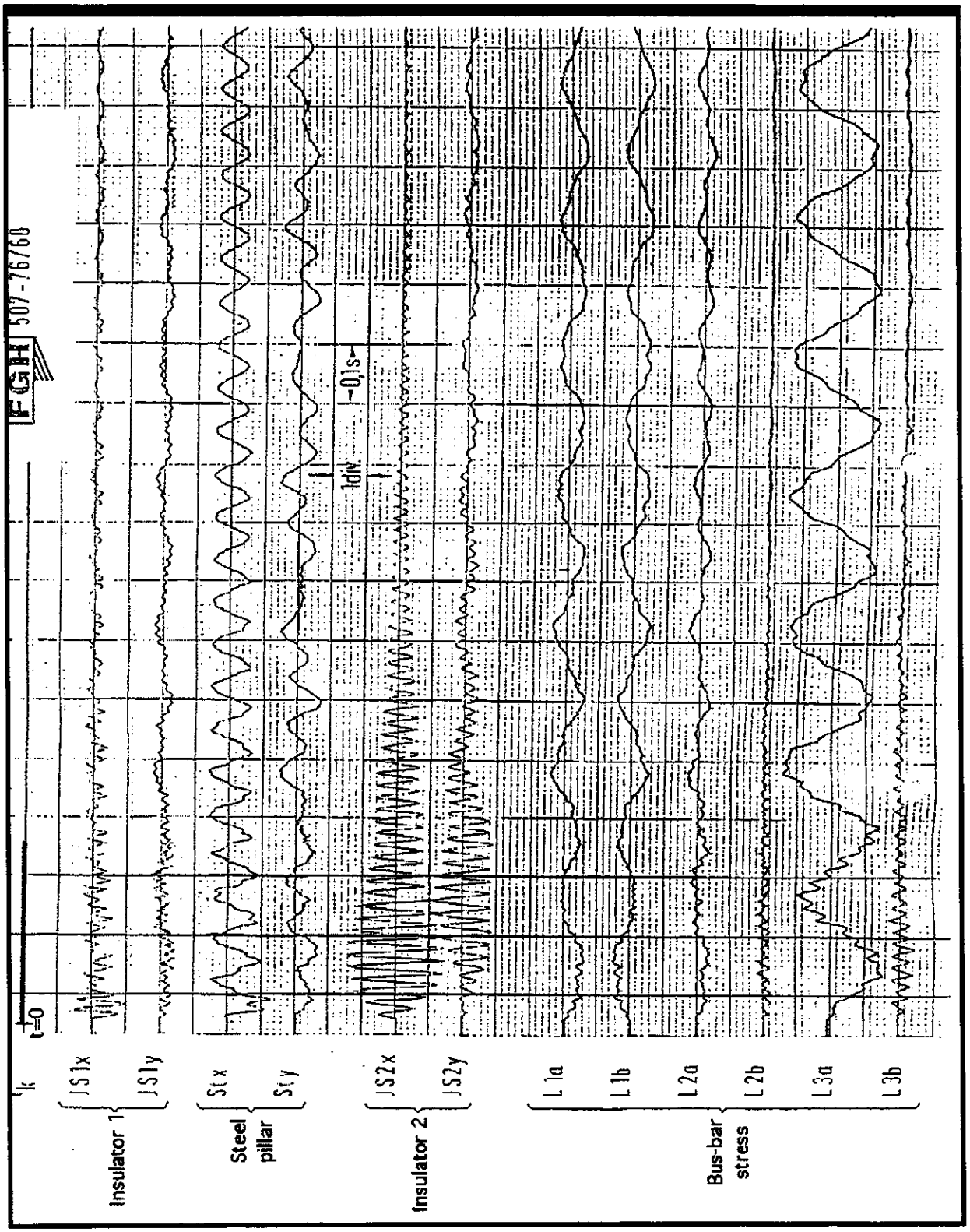

Fig. 2.6 Oscillograms for each measurement point (Structure configuation 3). x and y are used to give the measured values in the plane of the bus (x) or perpendicular to it (y). The scale of each curve is given by the values of 1 division shown in the graphic :
(593 N.m for IS1x, 603 N.m for IS1y, 790 N.m for Stx and 773 for Sty, 1213 for IS2x and 1241 for IS2y, 31,5 N/mm^2 for L1a, L2a, L3a)

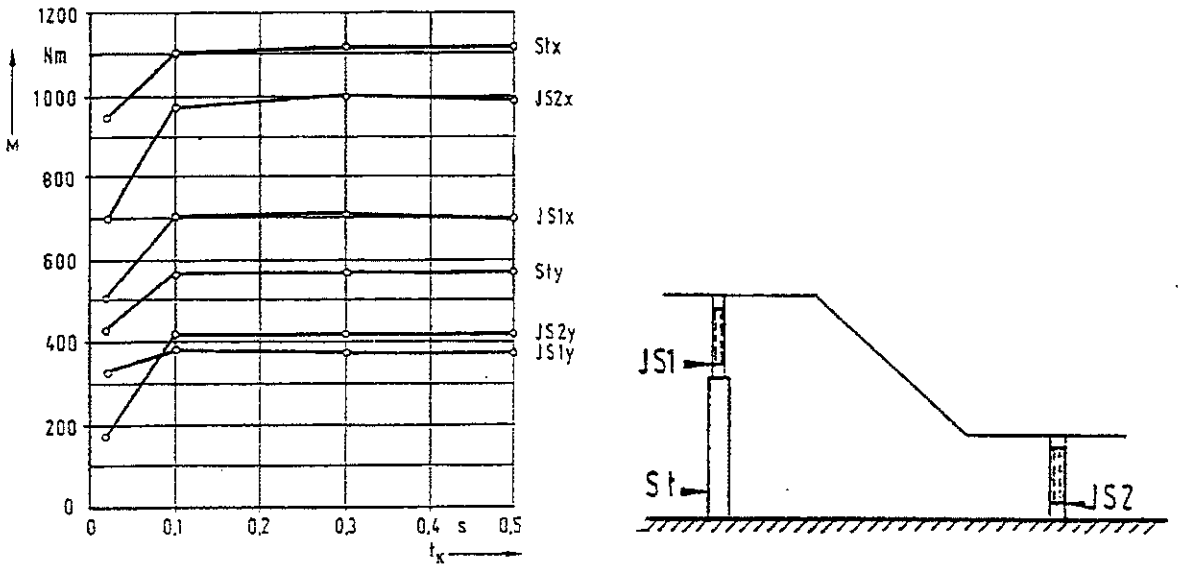

Fig. 2.7 Bending moments for structure configuration 1 and for different short-circuit time durations.

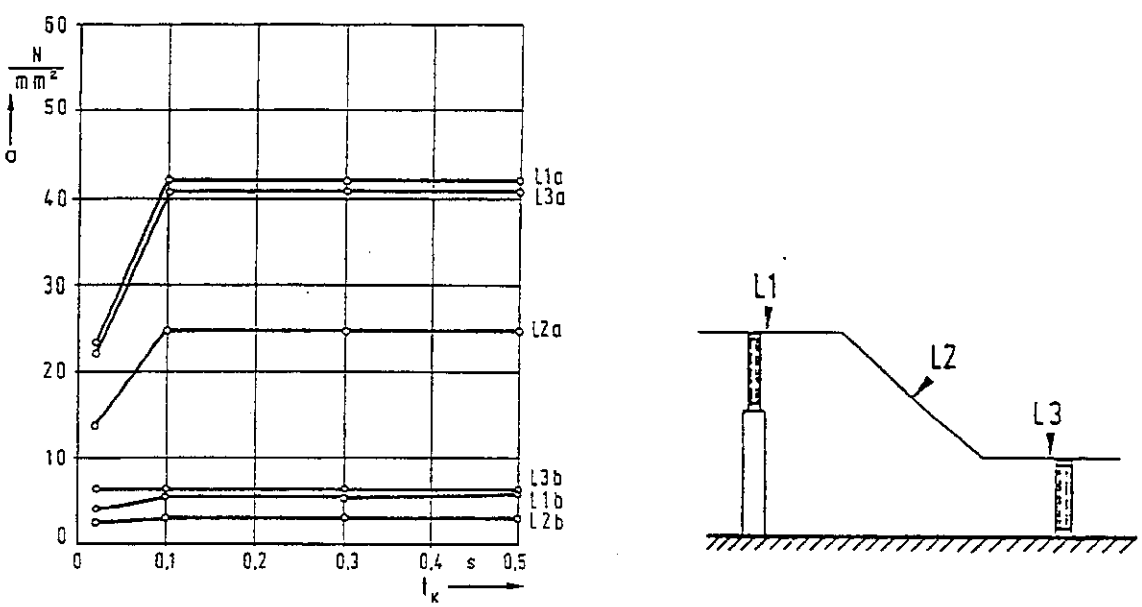

Fig. 2.8 Bus-bar stresses for structure configuration 1 and for different short-circuit time durations.

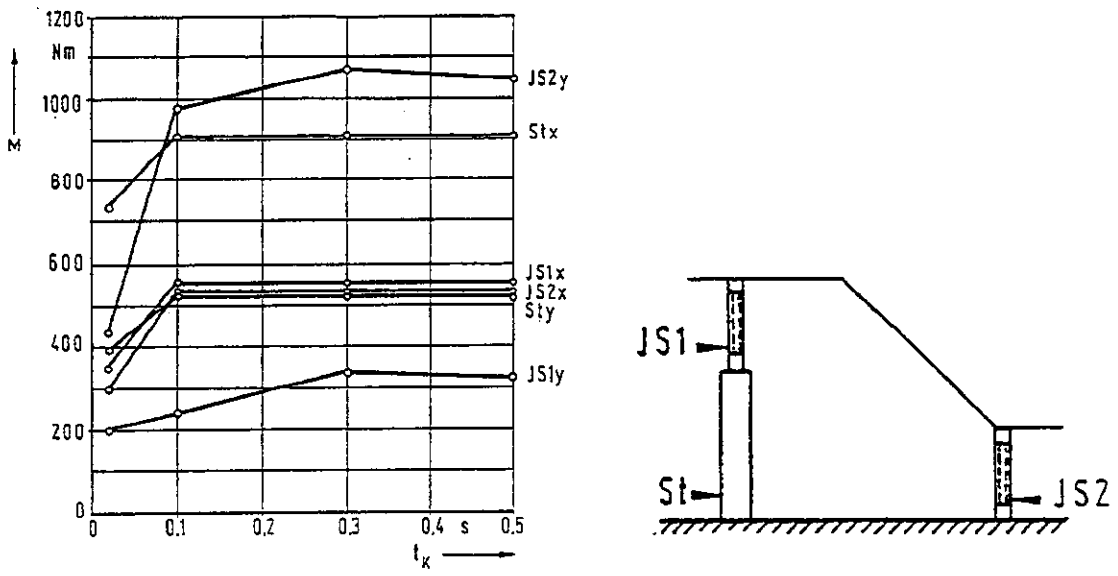

Fig. 2.9 Bending moments for structure configuration 2 and for different short-circuit time durations.

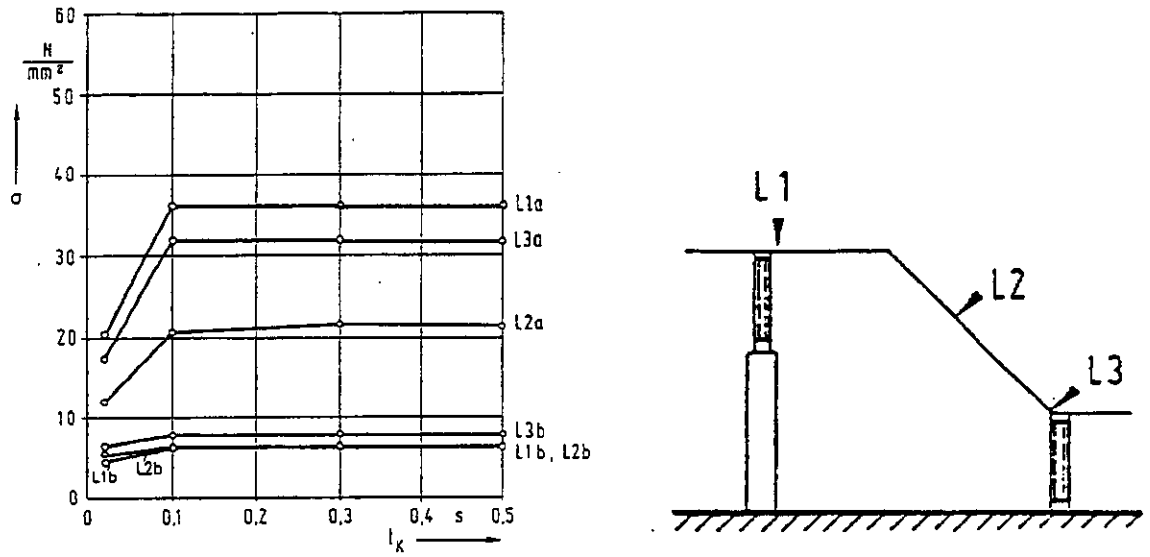

Fig. 2.10 Bus-bar stresses for structure configuration 2 and for different short-circuit time durations.

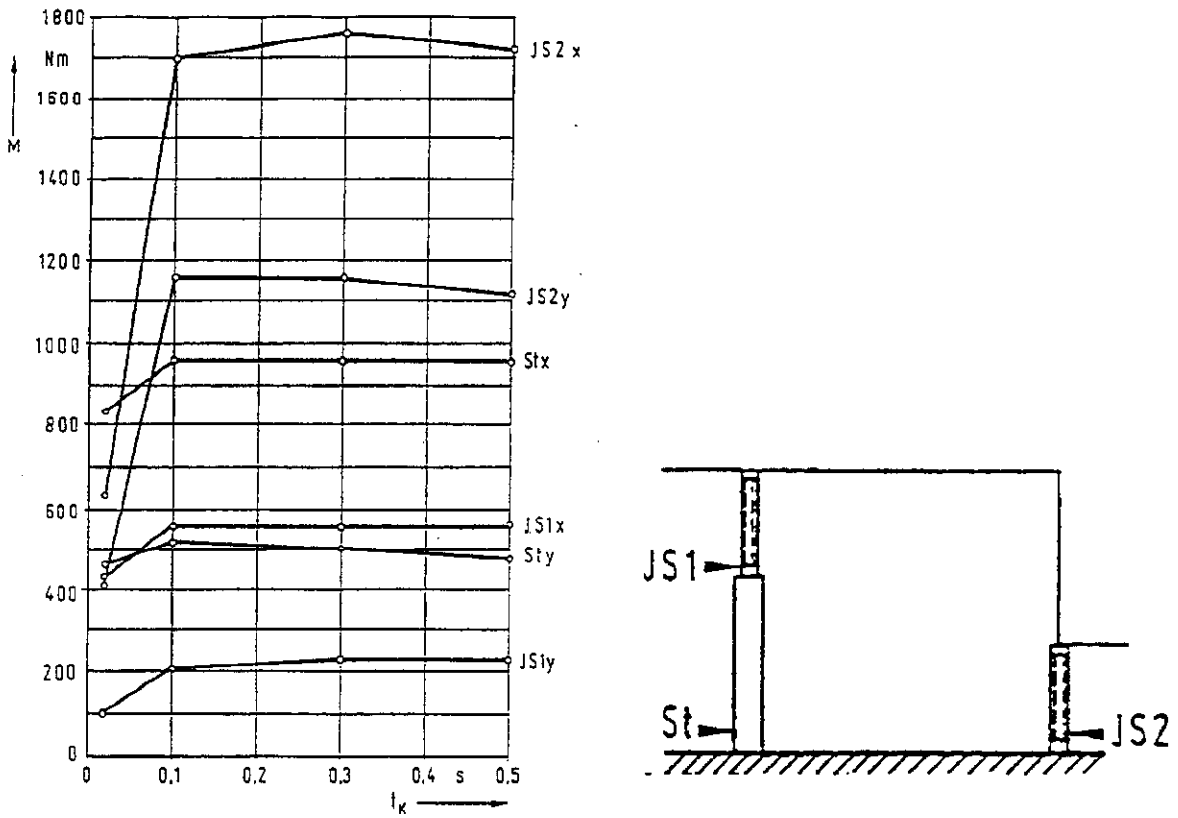

Fig. 2.11 Bending moments for structure configuration 2 and for different short-circuit time durations.

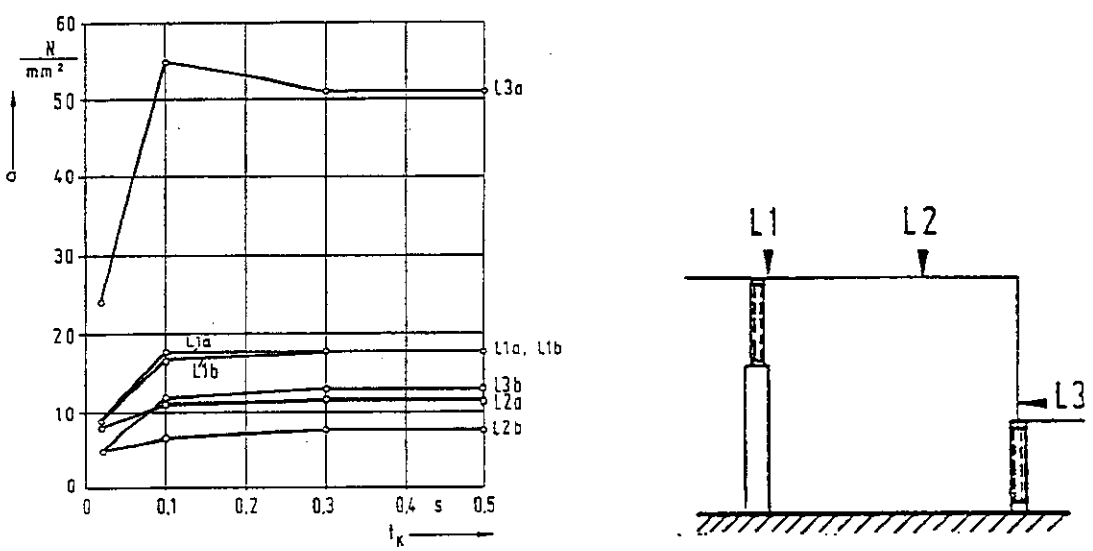

Fig. 2.12 Bus-bar stresses for structure configuration 2 and for different short-circuit time durations.

CASE 3

Test performed at Ontario Hydro (Canada) in 1976
A non- parallel rigid bus including A frame
short-circuit current : 36 kA (90 kA peak)
with autoreclosure

Bus-bar geometry

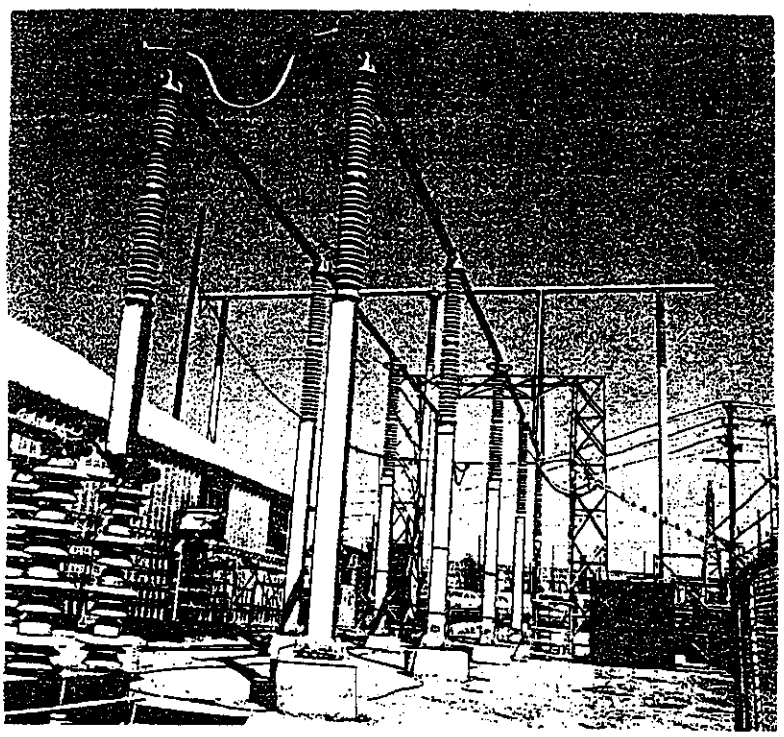

Fig. 3.1 A picture of the 500kV rigid bus-bar tested in Ontario Hydro.

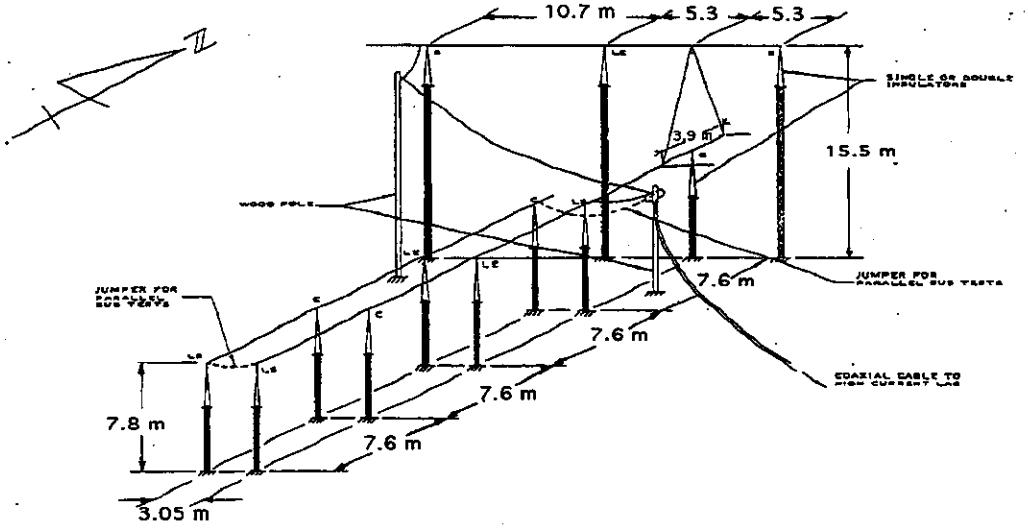

Fig. 3.2 500kV rigid bus-bar geometry.

Contact address : Ontario Hydro, 800 Kipling Av. KR151, Toronto, Ontario M8Z 5S4, Canada. (Gary Ford). Fax : +1-416-2075558 or e-mail (see preface)

Basic data

1) bus-bar

	mass (kg/m)	Elasticity modulus	wall thickness (mm)	outside diameter (mm)
upper bus-bar	29,3	$6,5\ 10^{10}$	12	300
lower bus and A frame	9,9	$6,5\ 10^{10}$	6	200

Centre line distance between phases : 3,05 m

2) Support

	length (m)	frequency (Hz)	stiffness (kN/mm)	mass (kg/m)
Insulator	3,3	2	0,539	unknown
steel pilar	4,5	unknown	unknown	unknown

boundary conditions :

the bus is clamped at C and LS points (free longitidinal movement at the top). There is a free vertical rotation at LE points.

3) short-circuit characteristics

kind of short-circuit (two or three-phase) : two phase, 60 Hz

	Irms (kA)	Ipeak (kA)	time constant (ms)	duration (s)
first fault	35,9	89,9	33	0,078
second fault	35,7	88,5	33	0,136

N.B. clearing time between the two fault : 0,7 s

Results

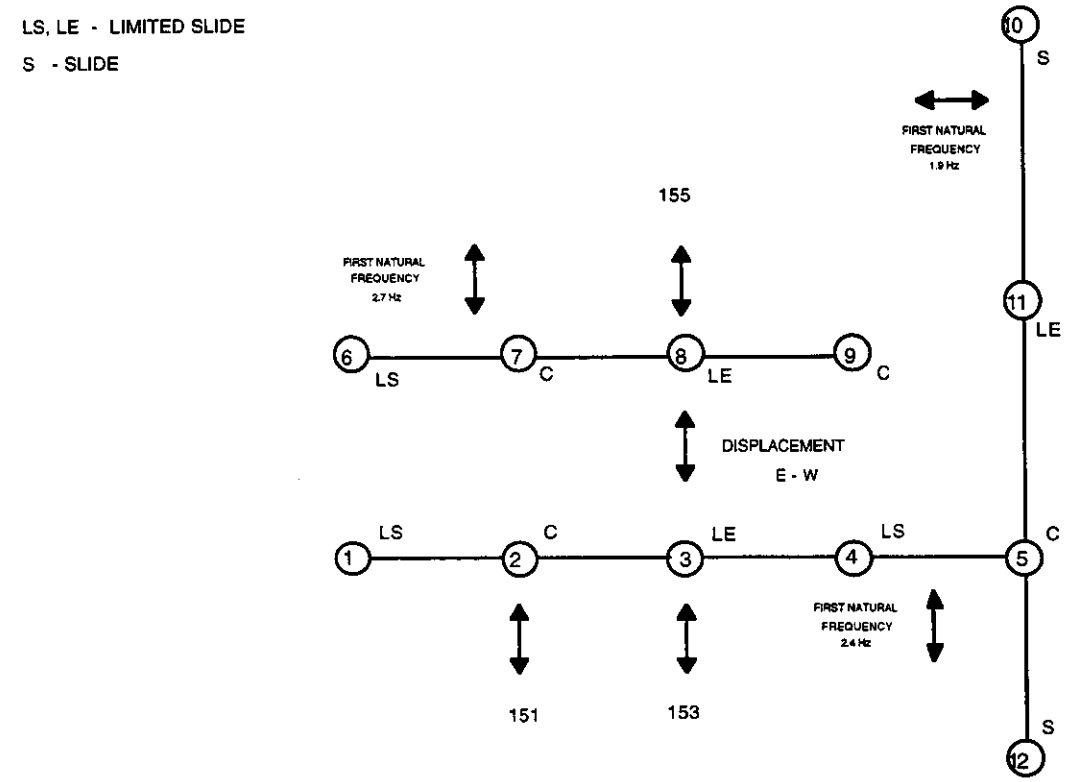

FIGURE 3.3 - LOCATION OF THE MEASURING POINTS

Current (kA)		151	153	155	Displacement E-W (mm)	
rms	peak	F (kN)	F (kN)	F (kN)	#3	#8
INITIAL FAULT						
35.9	89.9	0.73	0.627	0.783	9.1	9.7
		1.023	0.578	0.765	8.1	10.7
RECLOSING						
35.7	88.5	1.650	1.530	1.695	20.8	23.6
		2.122	1.481	1.713	19.8	23.6

Table 3.1 Some results for peak values. F are the forces measured on top of the insulators. #3 and #8 are displacement in mm on the same location. NOTE : for each fault there are two entries: the first and the second peak.

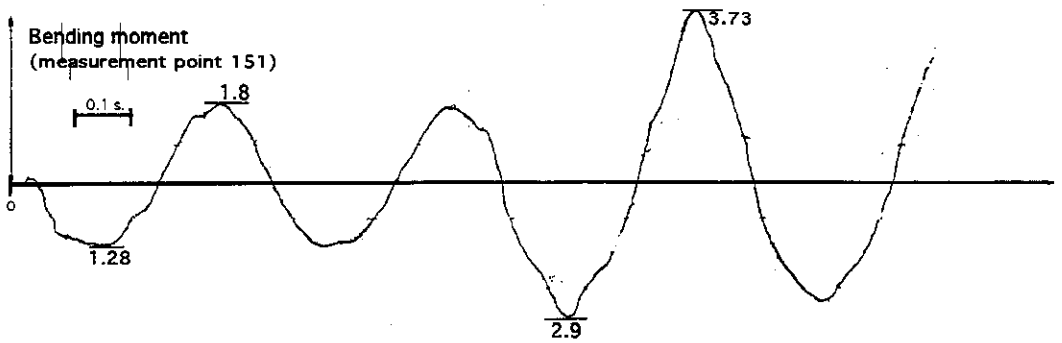

Fig. 3.4 Bending moment at the bottom of supporting insulator (location 151 on Fig. 3.3). For time scale see figure 3.8

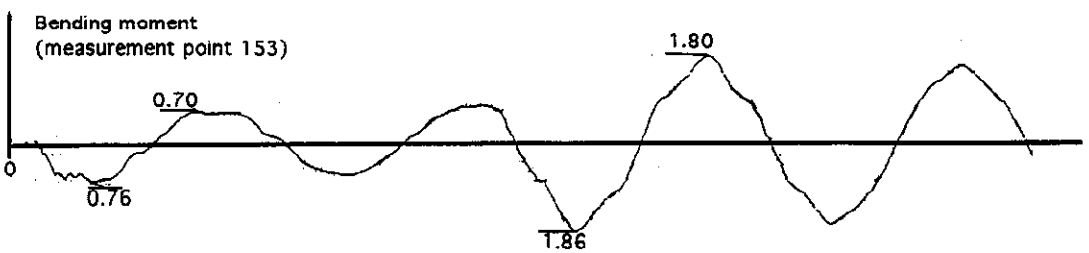

Fig. 3.5 Bending moment at the bottom of supporting insulator (location 153 on fig. 3.3). For time scale see figure 3.8

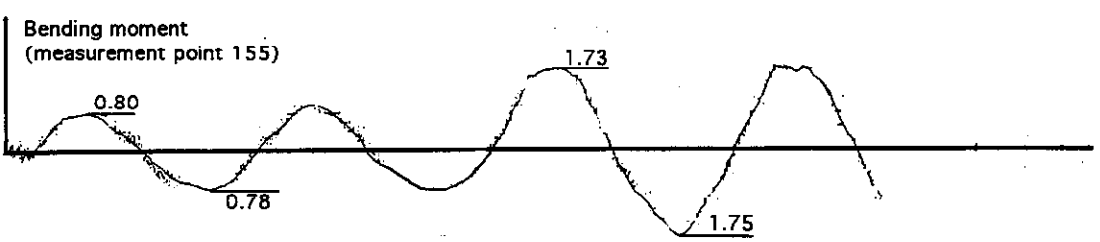

Fig. 3.6 Bending moment at the bottom of supporting insulator (location 155 on fig. 3.3). For time scale see figure 3.8

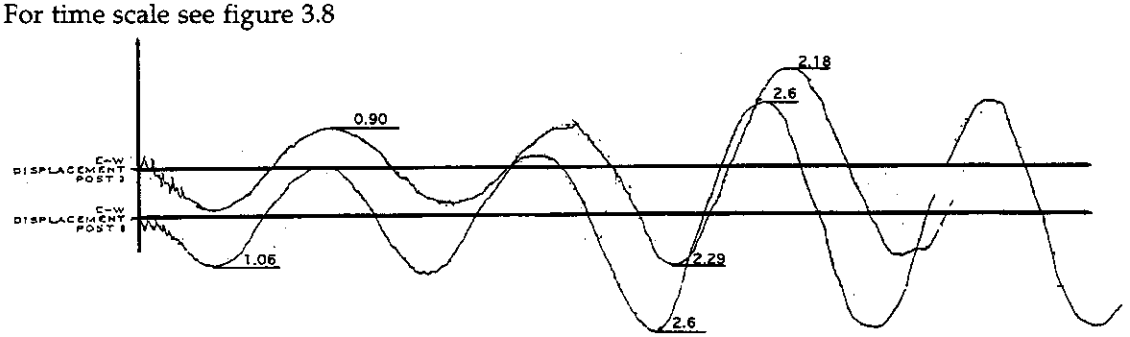

Fig. 3.7 Displacement in inches of the top of insulator 3 and 8 on Fig. 3.3. (converted in mm on table 3.1). For time scale see figure 3.8

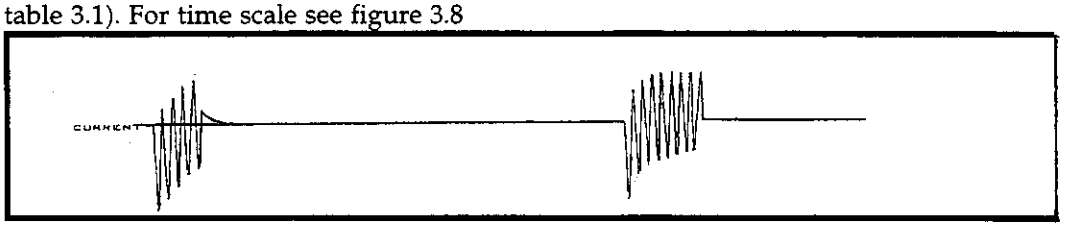

Fig. 3.8 Short-circuit wave shape (60 Hz) : 0.078s (35,9 kA rms, 89,9 kA peak), 0,7s.(dead time) , 0,136 s. (35,7 kA rms, 88,5 kA peak)

II) FLEXIBLE BUS CONFIGURATIONS

PART 1 :

SINGLE CONDUCTOR PER PHASE

Bus-bar geometry
(for case 4 to 7)

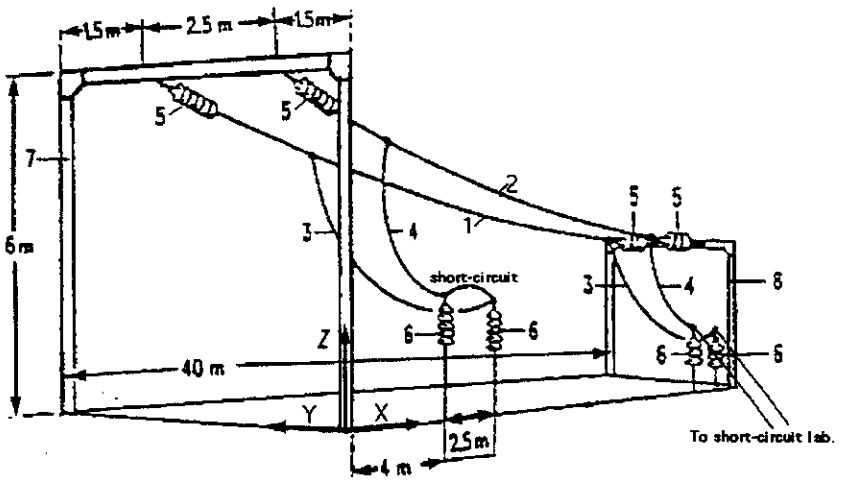

Fig. 4.1 Laborelec test geometry. See also fig. 1.2. Numbers 1 to 8 are used in the following data.

Supporting structure data :

Stiffness at cable fixation point (N/m) : about 3 10^5 N/m, details here under.

Frequencies (Hz) (measured on site) :

first symmetric mode :	4 Hz (% of critical damping 4%)
first antisymmetric mode :	5 Hz(% of critical damping 2%)
next symmetrical mode :	29 Hz
next antisymmetrical mode :	34 Hz

Remark : local additional masses of 62 kg each at the crossing between column and cross-arm.

details of the structure :
detailed static test made available corresponding equivalent bending and torsional stiffness (taking into account foundation effects): all are figure I beam in steel (density 7860 kg/m^3 and elasticity modulus of 21 10^{10} N/m^2).

	North column (number 7)	South column (number 8)	cross arm
EI max (Nm^2)	22,3 10^6	19,5 10^6	23,6 10^6
EI min(Nm^2)	10,7 10^6	10,7 10^6	8,2 10^6
GI (torsion)(Nm^2)	105,0 10^3	105,0 10^3	89 10^3
Section (m^2)	11,8 10^{-3}	11,8 10^{-3}	10,6 10^{-3}

the supporting insulator (number 6) is C8-750 (IEC standard) of 2,3 m height.

Contact address : LABORELEC , Rodestraat 125, B 1630 Linkebeek, Belgium, fax : +3223820241.

Other reference : W. Lehmann, J.L. Lilien,J. Orkisz. *The Mechanical effects of short-circuit currents in substations with flexible conductors. Numerical methods - computer approach.* CIGRE session 1982, report 23-08

CASE 4

Test performed at Laborelec (Belgium) in 1980
cross section : 324 mm^2
short-circuit current : 30 kA (73 kA peak)
span length : 40 m

1) all connections (number 1 to 5 on fig. 1)

	material	section (mm^2)	mass (kg/m)	diameter (mm)
bus-bar N° 1 and 2	copper (19 wires)	324	2,9	23,4

dropper (N° 3 and 4 on fig. 4.1) same as bus-bar

remarks : dropper length :
4 and 5,6 m. Shorter ones on west phase.

Insulating hardware (N° 5 on fig. 4.1) (length1 is the interface between portal and insulator itself and mass1 its mass. Length2 and mass2 are for insulator chain)

anchoring insulator	material	length 1 (m)	mass1 (kg)	length 2 (m)	mass2 (kg)
1 chain per phase	porcelain	1,4	8	1,54	52,3

remarks : extensional stiffness (Young modulus x cross section) of insulating hardware (measured) : EA = 11 10^6 N

2) initial conditions before testing :

wind speed (m/s)	ambiant temperature (°C)	cable	sag (m)	tension (N)
3,5	13	14,1	0,95	7800

3) short-circuit characteristics :

kind of short-circuit (two or three-phase) : two-phase fault (connection B)

	Irms (kA)	Ipeak (kA)	time constant (s)	duration (s)
first fault	29,4	72,7	0,033	0,8

available results

temperature effects :

initial temperature of the cable : 14,1 °C

cable temperature at the end of the first fault : 47,9 °C

design values :	measurement
initial static pull Fst(N) :	7800
swing out maximum Ft(N) :	16000
falling down maximum Ff(N) :	22500
max bending moment in supporting structure (daNxm) :	11000
min clearing distance (m) :	1,1

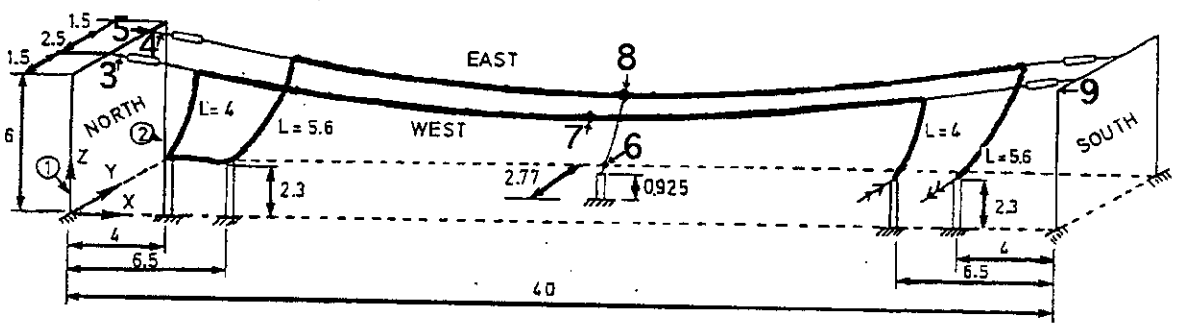

Fig. 4.2 Measuring points for case 1 to 4 (thick line for short-circuit current path) :
1 and 2) bending moment (at 5,2 m from the top of the portal),
3 and 4) traction in the cable,
5) displacement transducer for X movement of portal cable fixation point,
6) traction in the mid-span dropper - mid-span dropper only exists for tests cases 6 and 7,
7 and 8) the movement of these points in a vertical plane perpendicular to the cable have been recorded by high speed cameras located behind the south pillar,
9) displacement transducer for X movement of the top of south pillar column.

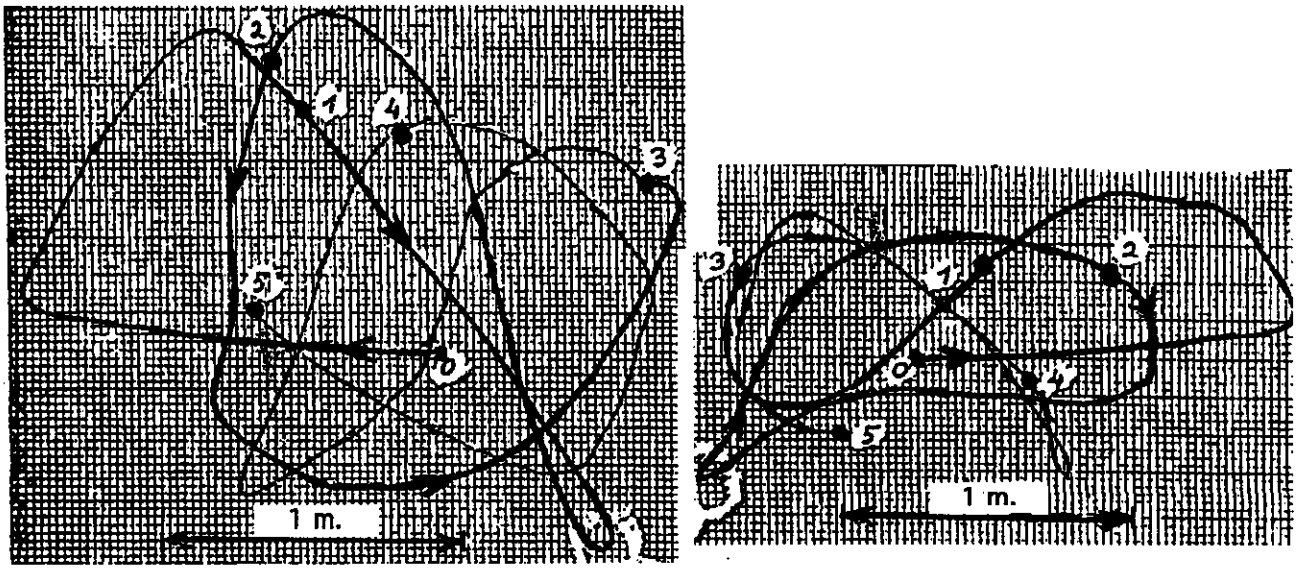

Fig. 4.3 and 4.4 : Mid-span displacement in a vertical plane perpendicular to the bus-bar. The left curve is the movement of point 7 on fig 4.2 and the right one is point 8 movement (there is no mid-span dropper in this case and point 8 is not connected to the ground. The two figures have not exactly the same scale and interphase distance is not respected.These curves have been obtained using two cameras situated behind the south portal.

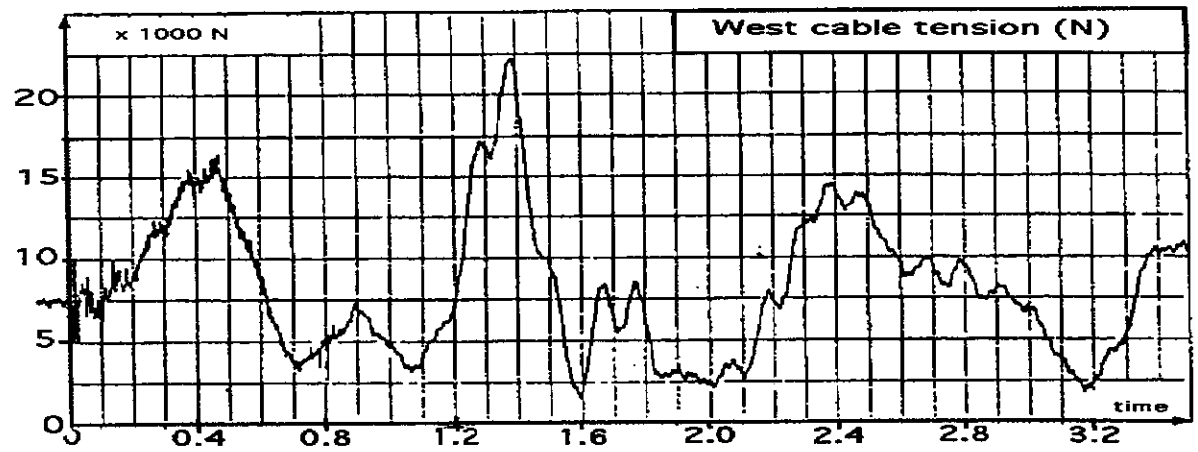

Fig. 4.5 West cable tension time evolution (measuring point 3 on fig. 4.2)

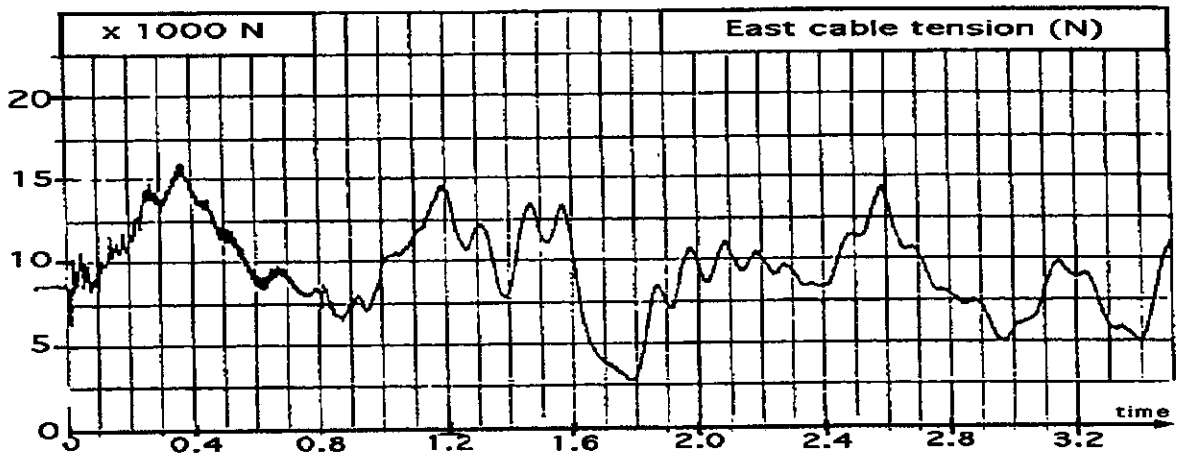

Fig. 4.6 East cable tension time evolution (measuring point 4 on fig. 4.2)

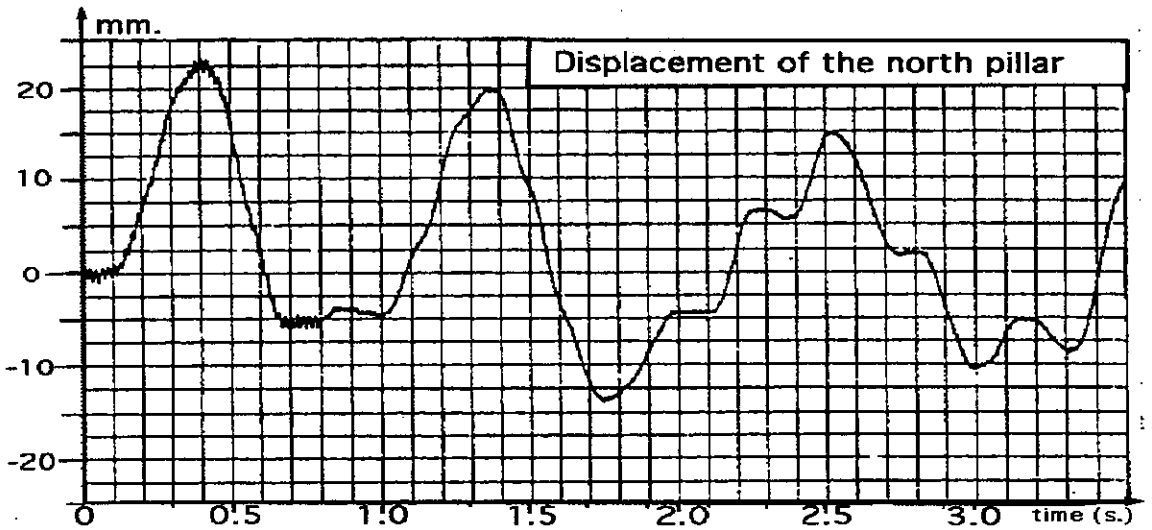

Fig 4.7 : Relative displacement of the North pillar (measuring point 5 on fig. 4.2 - anchoring point of east phase on the cross-arm).

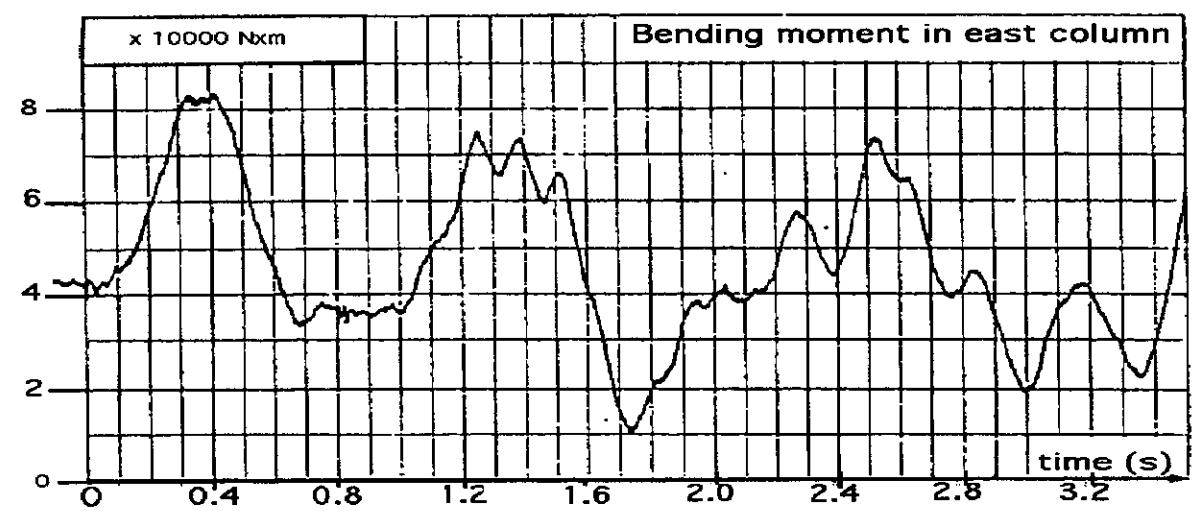

Fig. 4.8 : Bending moment in east column of north pillar (measuring point 2 in fig. 4.2)

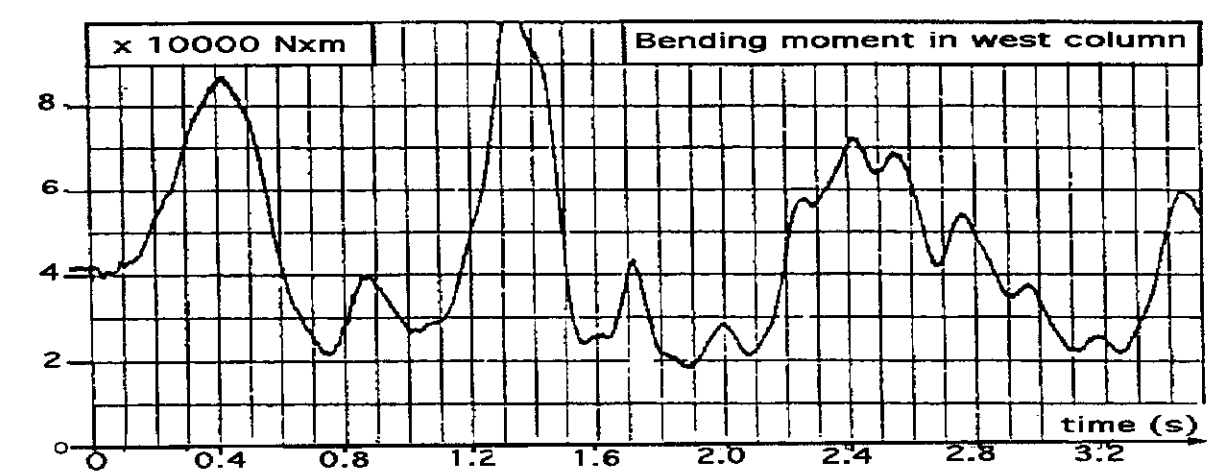

Fig. 4.9 : Bending moment in west column of north pillar (measuring point 1 in fig. 4.2)

CASE 5

Test performed at Laborelec (Belgium) in 1980
cross section : 105 mm^2
short-circuit current : 30 kA (65 kA peak)
span length : 40 m

1) all connections

	material	section mm^2	mass kg/m	diameter (mm)
bus-bar	copper	105	0,94	13,4

dropper same as bus-bar

remarks : dropper length :
4 and 5,6 m, Shorter ones on west phase.

bundle configuration : this is not a bundle configuration

Insulating hardware (length1(length) and mass1 (mass) is the interface between portal and insulator itself); length2 and mass2 are the same for cap and pin insulator only.

insulator	material	length 1 (m)	mass1 (kg)	length 2 (m)	mass2 (kg)
1 chain	porcelain	1,4	8	1,54	52,3

remark : extensional stiffness (Young modulus x cross section) of insulating hardware (measured) : EA = 11 10^6 N

2) initial conditions before testing :

wind speed (m/s)	ambiant temperature°C	cable	sag (m)	tension (N)
3,5	13	19,3	1,245	2560

3) short-circuit characteristics :

kind of short-circuit (two or three-phase) : two-phase fault (connection B)

	Irms (kA)	Ipeak (kA)	time constant (s)	duration (s)
first fault	28,8	65,4	0,019	0,5

Results

temperature effects :

initial temperature of the cable : 19,3 °C

cable temperature at the end of the first fault : 272,0 °C

design values :

initial static pull Fst(N) :	2560
swing out maximum Ft(N) :	8000
falling down maximum Ff(N) :	9200
max bending moment in supporting structure (daNxm) :	7000
min clearing distance (m) :	0,7

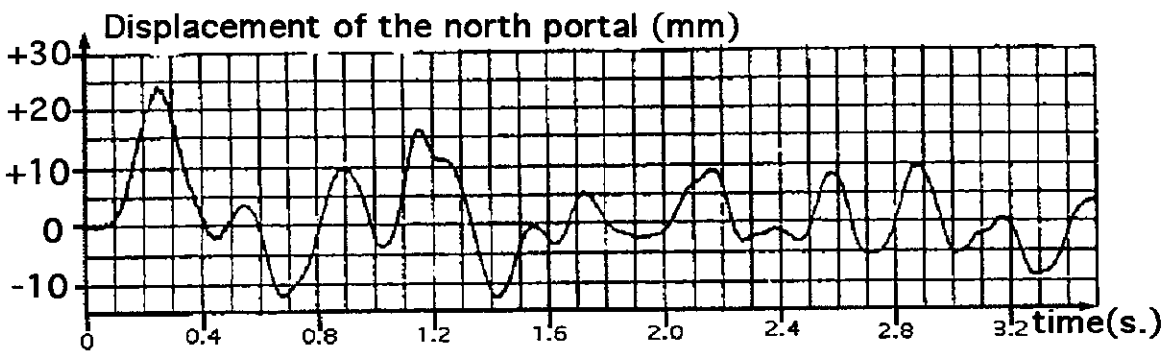

Fig. 5.1 : *Relative* displacement of the cross-arm of he north portal at the fixation of east phase (measuring point 5 on fig. 4.2).

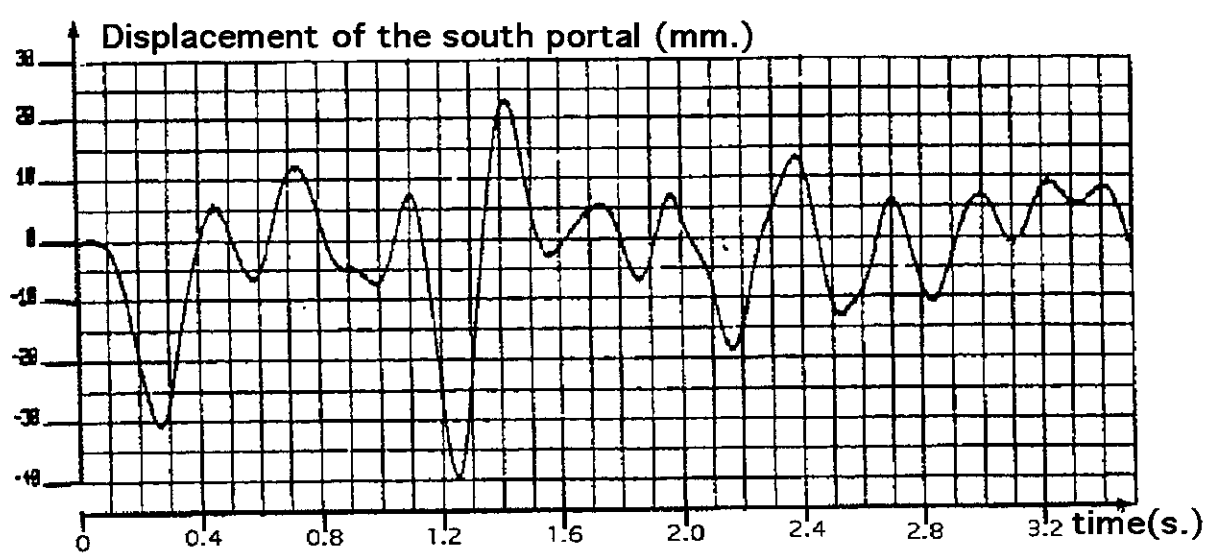

Fig. 5.2 : *Relative* displacement of the cross-arm of he south portal at the intersection of the west column with the cross-arm (measuring point 9 on fig. 4.2).

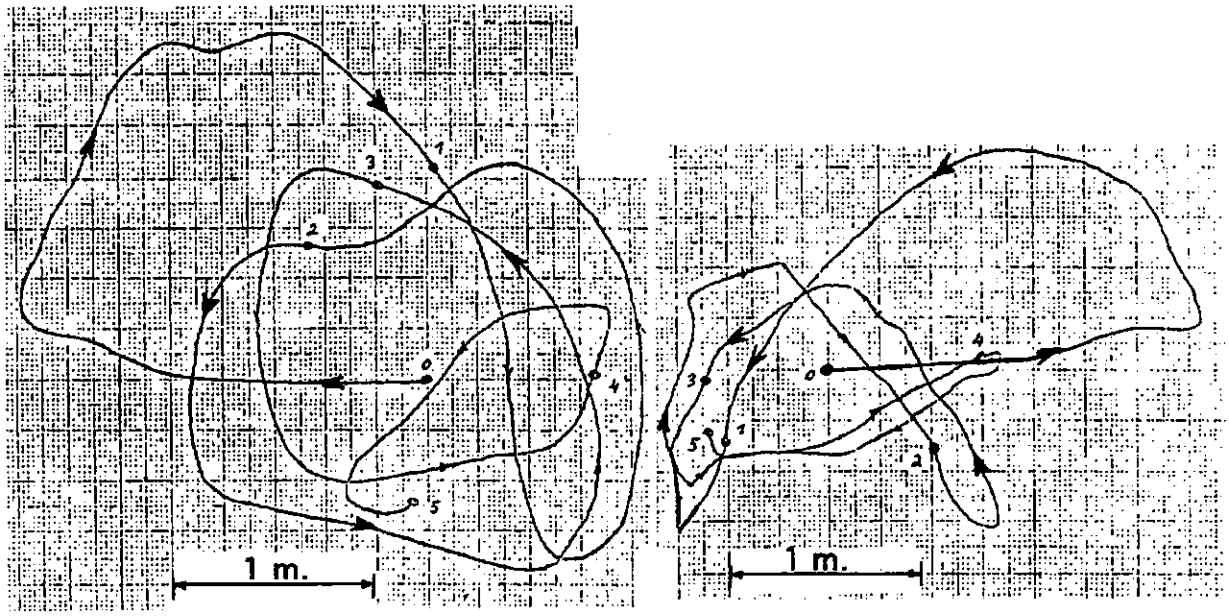

Fig. 5.3 and 5.4 : Mid-span displacement in a vertical plane of measuring points 7 (west phase, on the left) and 8 (east phase on the right). The scale is not exactly the same for the two figures and interphase distance is not respected on the drawing.

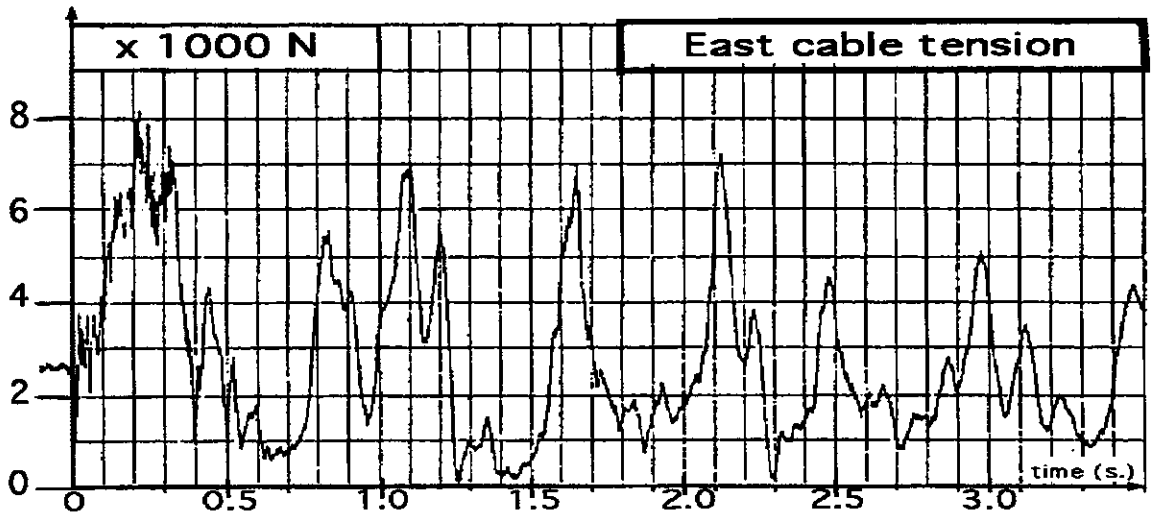

Fig. 5.5 : East cable tension-time evolution (measuring point 4)

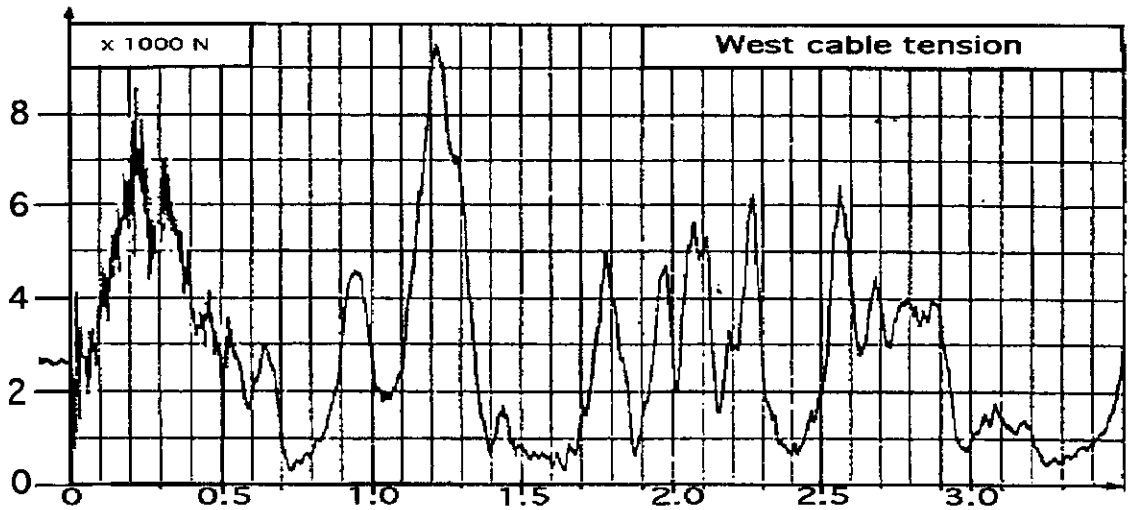

Fig. 5.6 : West cable tension-time evolution (measuring point 5)

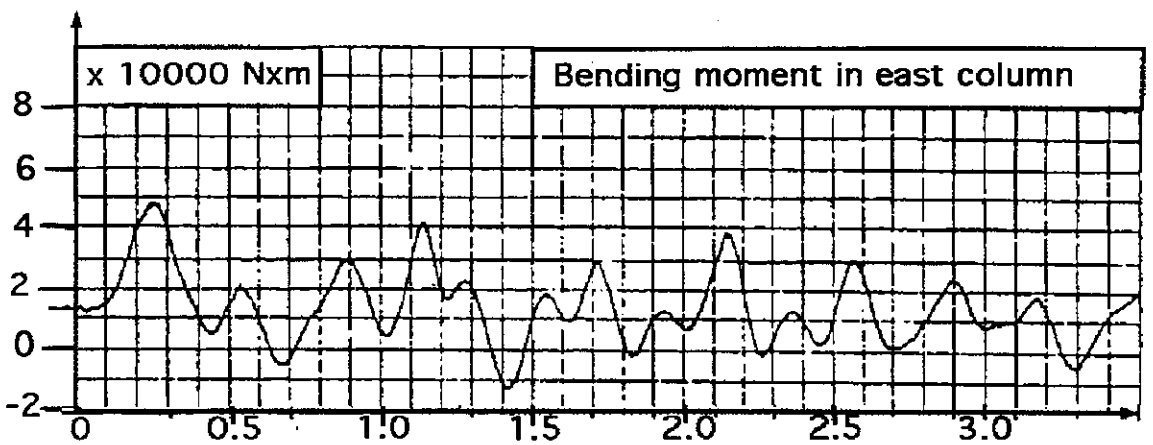

Fig. 5.7 : East column bending moment-time evolution (measuring point 2)

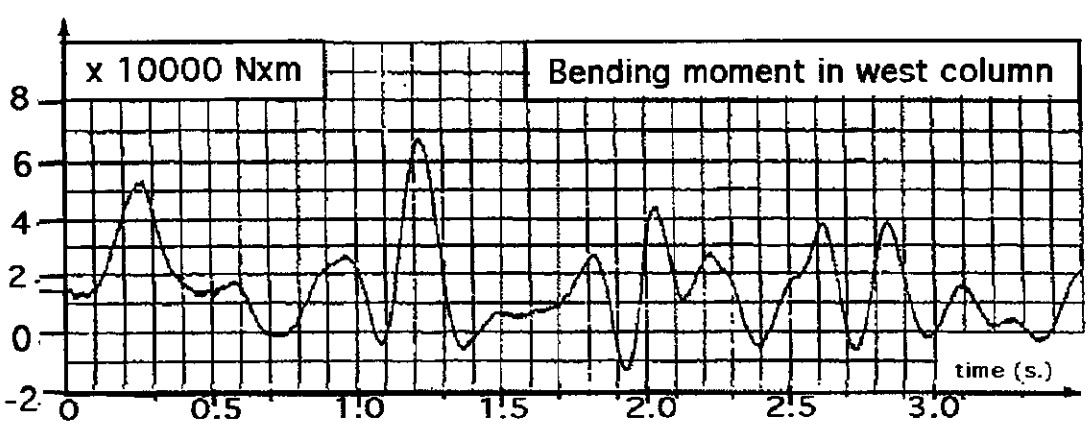

Fig. 5.8 : West column bending moment-time evolution (measuring point 1)

CASE 6

Test performed at Laborelec (Belgium) in 1980
cross section : 324 mm^2
short-circuit current : 30 kA (73 kA peak)
span length : 40 m
with added dropper (on east phase)

1) all connections

	material	section mm^2	mass kg/m	diameter (mm)
bus-bar	copper (19 wires)	324	2,9	23,4

dropper same as bus-bar

remarks : dropper length :
4 and 5,6 m. Shorter ones on west phase for basic arrangement
Compared to case 1, one more dropper at mid-span of east phase, global length : 4,4 m with a local mass on the bus bar: 5kg (clamp).The dropper is anchored at X=20m; Y=2,73m;Z=0,925m.

Insulating hardware
- length1 is the length of the interface between portal and insulator itself
- mass1 is the mass of the elements included in length1
- lengh2 is the length of the insulator itself, mass2 is the total mass of insulator chain

insulator	material	length 1 (m)	mass1 (kg)	length 2 (m)	mass2 (kg)
	porcelain	1,4	8	1,54	52,3

remark : extensional stiffness (Young modulus times cross section) of insulating hardware (measured) : EA = 11 10^6 N

2) initial conditions before testing :

wind speed (m/s)	ambiant temperature°C	cable	sag (m)	tension (N)
3,5 (NW)	13	19,0	1,1(east) 1,0(west)	8600 6800

3) short-circuit characteristics :
kind of short-circuit (two or three-phase) : two-phase fault (connection B)

	Irms (kA)	Ipeak (kA)	time constant (s)	duration (s)
first fault	29,7	73,3	0,033	0,81

Results

temperature effects :

initial temperature of the cable : 19,0°C

cable temperature at the end of the first fault : 55,1 °C

design values :	measurement
initial static pull Fst(N):	7800
swing out maximum Ft(N):	16000
falling down maximum Ff(N):	20000
max bending moment in supporting structure (daNxm)	10000
min clearing distance (m)	0,8
maximum stretch in mid-span dropper (N)	3250

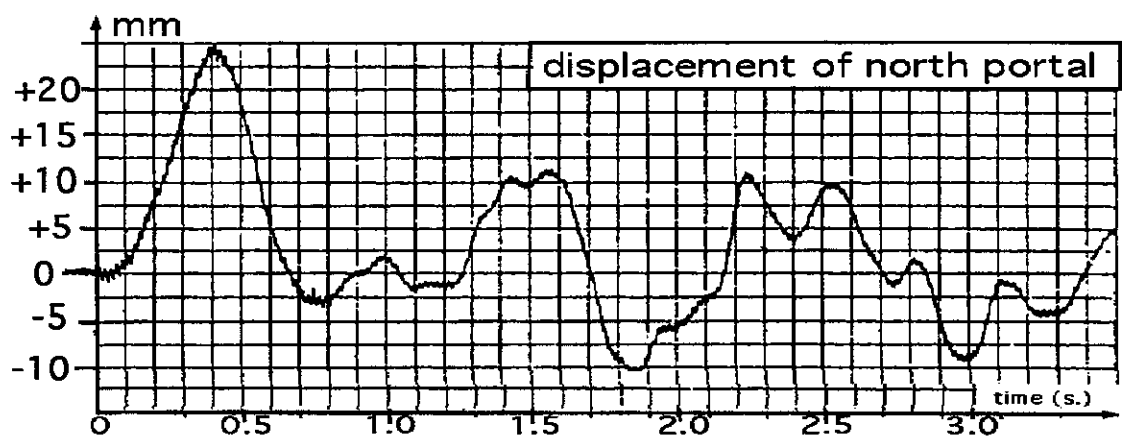

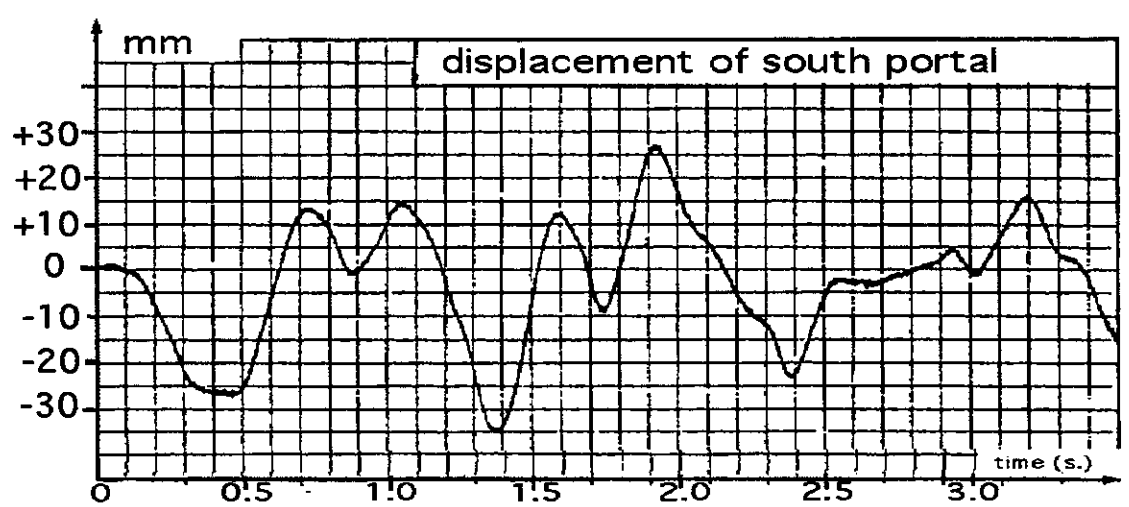

Fig. 6.1 and 6.2 : Relative displacement of norh and south portal (measuring point 5 for north cross-arm - upper curve- and 9 for south cross-arm - bottom curve)

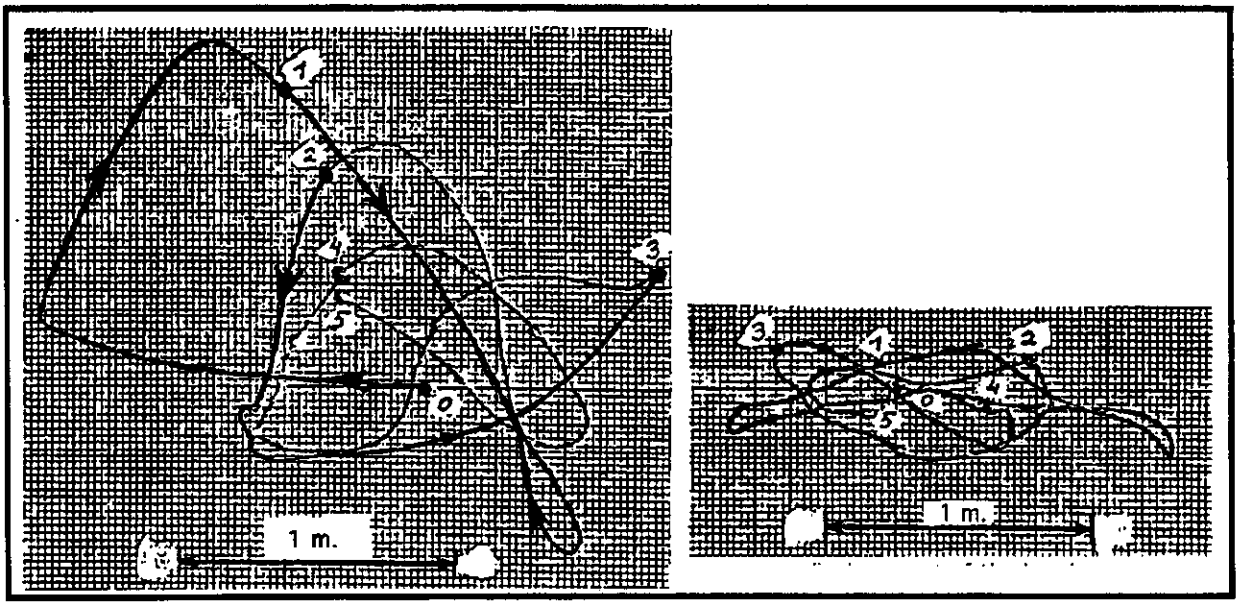

Fig. 6.3 and 6.4 : Mid-span displlacement of the bus-bar in a vertical plane. (measuring point 7 - on the left- and 8 -on the right- on fig 4.2). The scale is not the same for both figures and interphase distance is not respected.

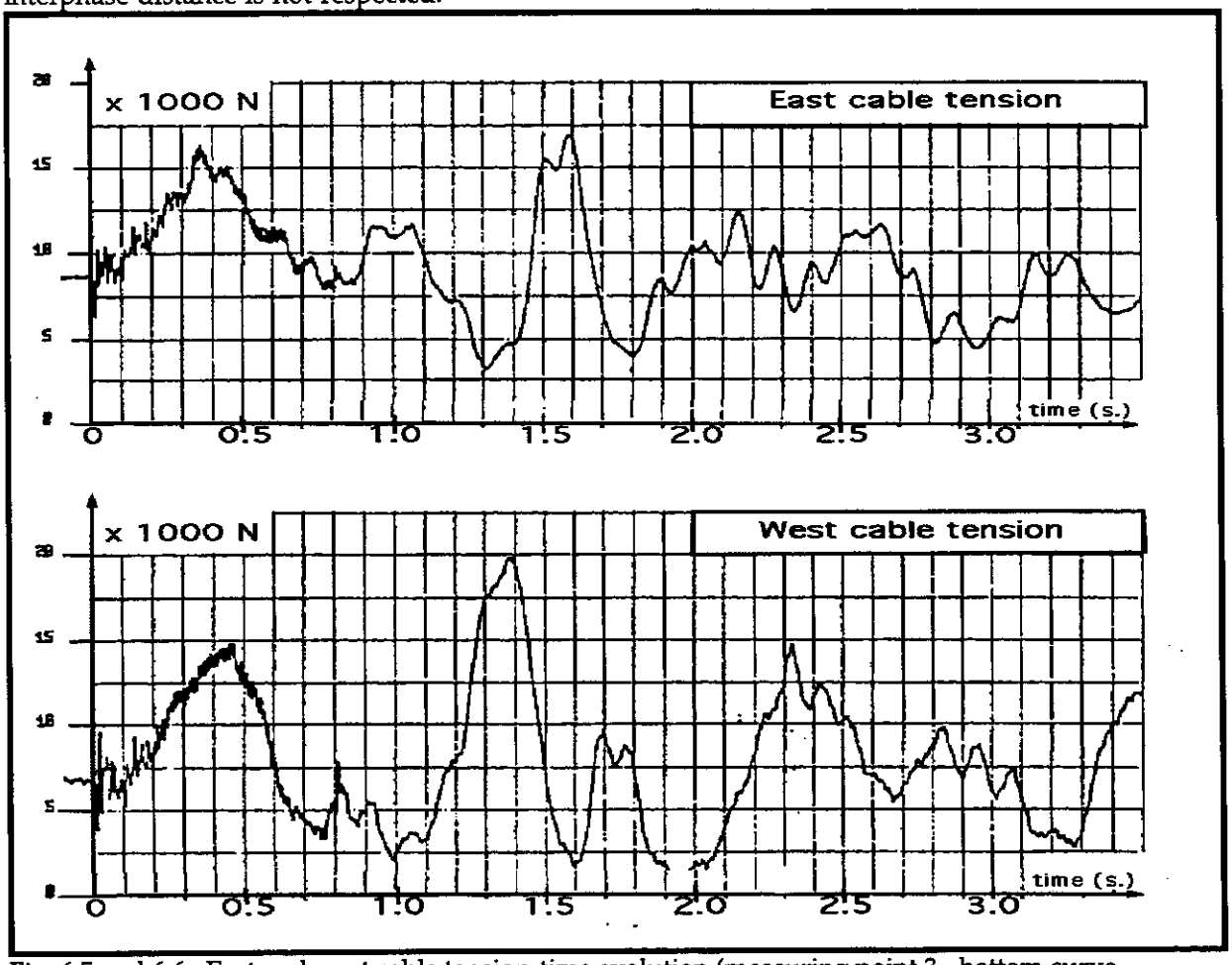

Fig. 6.5 and 6.6 : East and west cable tension-time evolution (measuring point 3 - bottom curve- and 4 - upper curve- of the fig. 4.2)

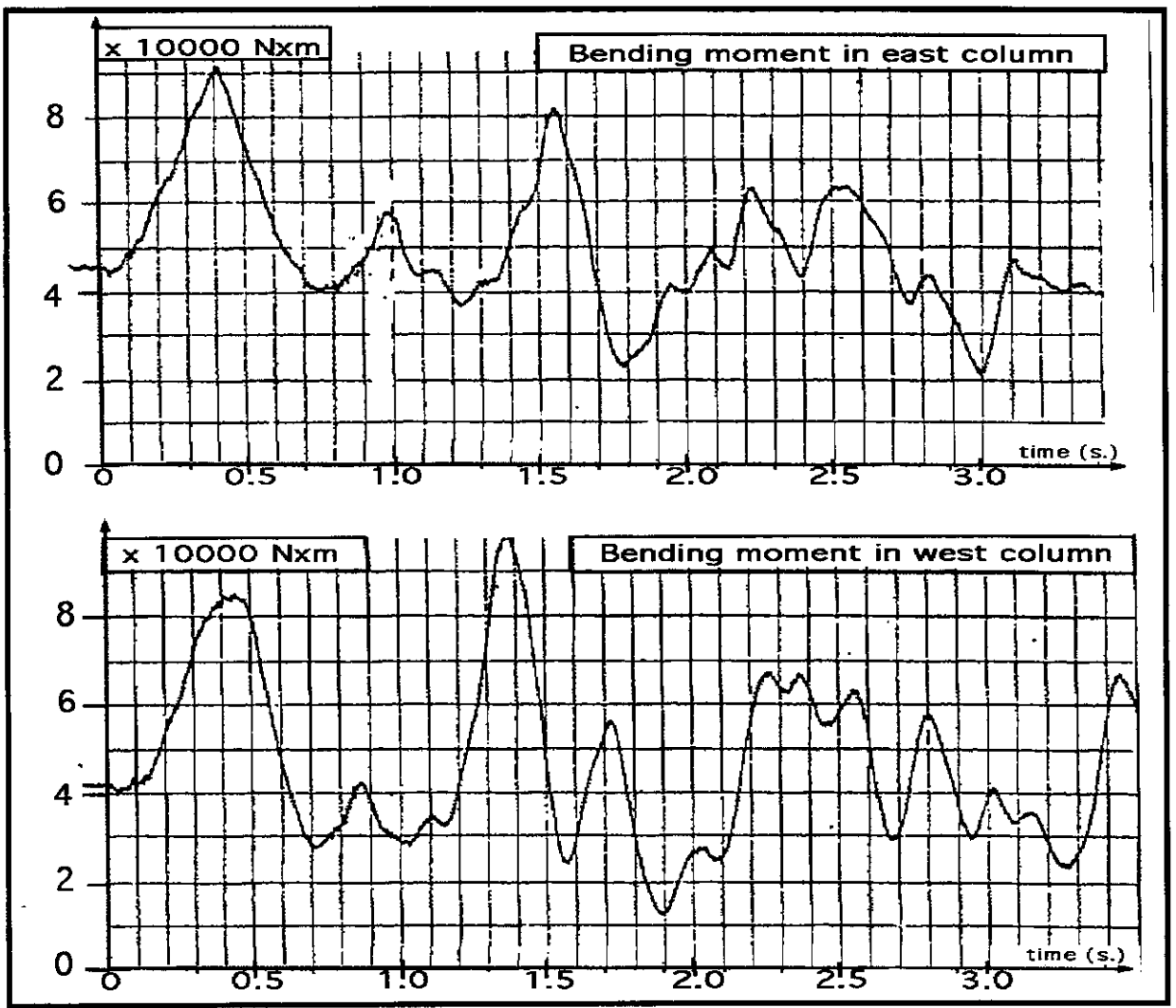

Fig. 6.7 and 6.8 : North-east and north-west portal bending moment-time evolution (measuring point 1 - bottom curve- and 2 - upper curve- of the fig. 4.2)

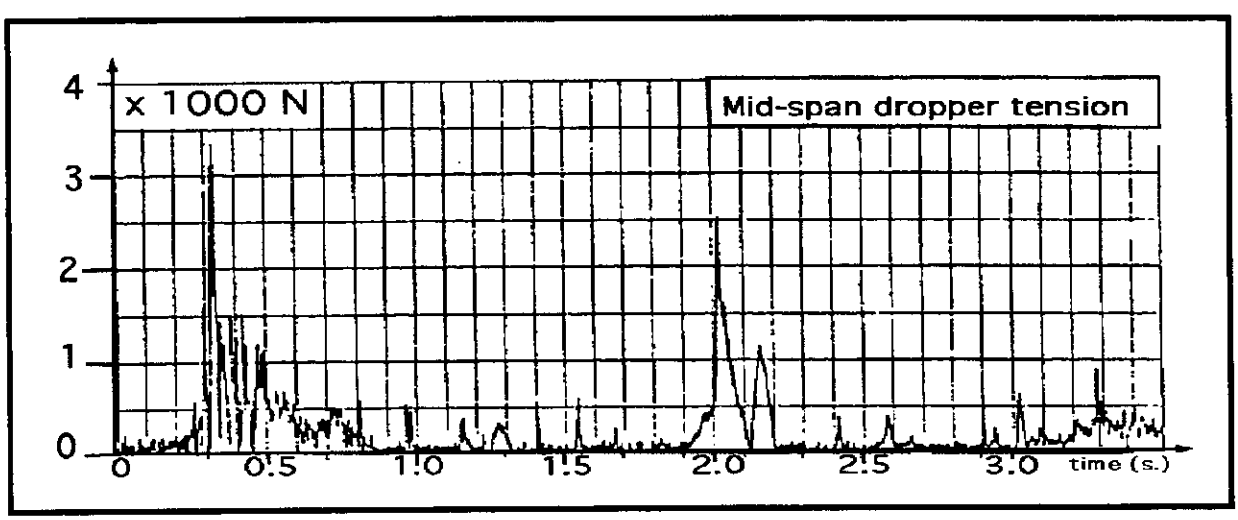

Fig. 6.9 Mid-span dropper tension-time evolution (measuring point 6 on fig. 4.2). The strain-gage is in the cable just before clamp on the supporting insulator.

CASE 7

Test performed at Laborelec (Belgium) in 1980
cross section : 105 mm^2
short-circuit current : 30 kA (73 kA peak)
span length : 40 m
with added dropper (on east phase)

1) all connections

	material	section mm^2	mass kg/m	diameter (mm)
bus-bar	copper	105	2,9	13,4

dropper same as bus-bar

remarks : dropper length : 4 and 5,6 m.
Shorter ones on west phase for basic arrangement
Compared to case 2, one more dropper at mid-span of east phase,
global length : 4,0 m with no local mass on the bus bar.
The dropper is anchored at X=20m; Y=2,73m;Z=0,925m.

Insulating hardware (length1 is the interface between portal and insulator itself)

insulator	length 1 (m)	mass1 (kg)	length 2 (m)	mass2 (kg)
1 chain	1,4	8	1,54	52,3

remark : extensional stiffness (Young modulus times cross section) of insulating hardware (measured) : EA = 11 10^6 N

2) initial conditions before testing :

wind speed (m/s)	ambiant temperature°C	cable	sag (m)	tension (N)
3,5	13	23,0	1,65(east) 1,73(west)	2500 2500

3) short-circuit characteristics :

kind of short-circuit (two or three-phase) : two-phase fault (connection B)

	Irms (kA)	Ipeak (kA)	time constant (s)	duration (s)
first fault	28,8	65,4	0,019	0,52

Results

temperature effects :

initial temperature of the cable : 23,0°C

cable temperature at the end of the first fault : 288,0 °C

design values :	measurement
initial static pull Fst(N):	2500
swing out maximum Ft(N):	7000
falling down maximum Ff(N):	7500
max bending moment in supporting structure (daNxm)	4000
min clearing distance (m)	0 (but no contact)
maximum stretch in mid-span dropper (N)	2200

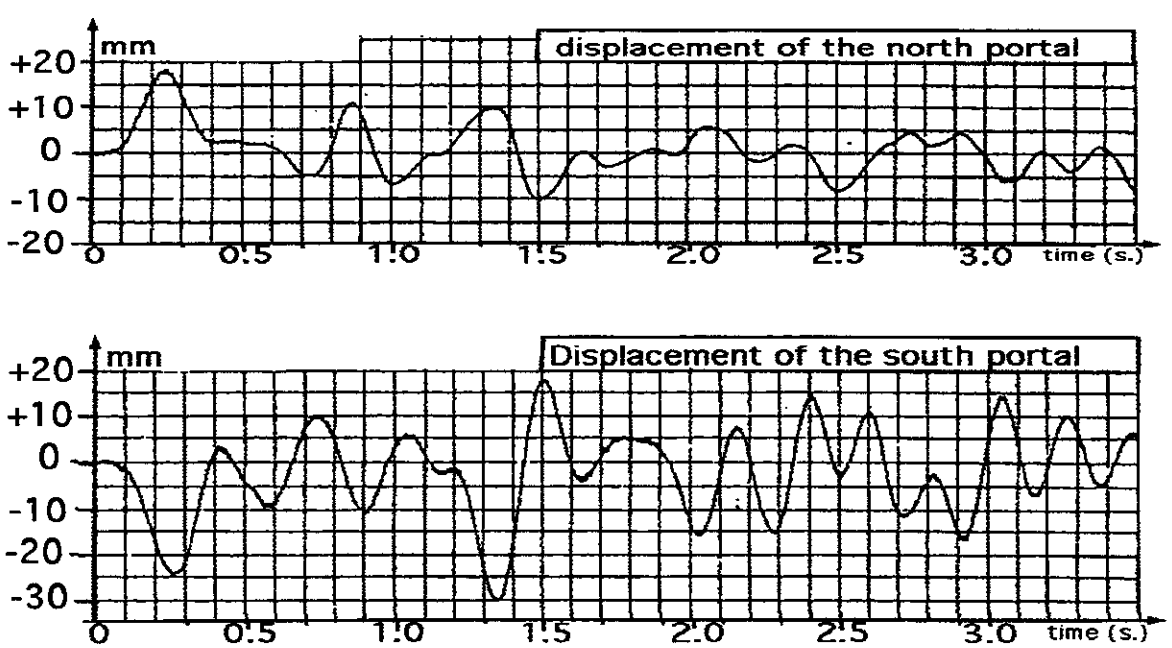

Fig. 7.1 and 7.2 : Cross-arm displacemment of north pillar (upper curve, measuring point 5 on fig. 4.2) and south pillar (bottom curve, measuring point 9 on fig. 4.2)

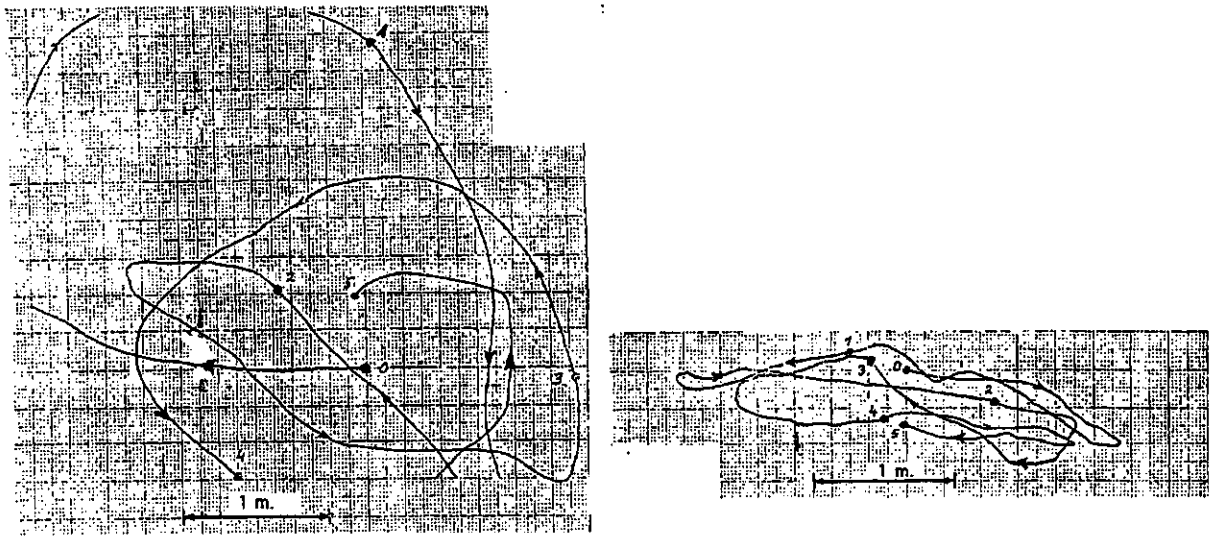

Fig. 7.3 and 7.4 : Mid-span displacement in a vertical plane (points 7 and 8 on fig 7.2). The scales of the two figures are not the same and the interphase distance is not respected.

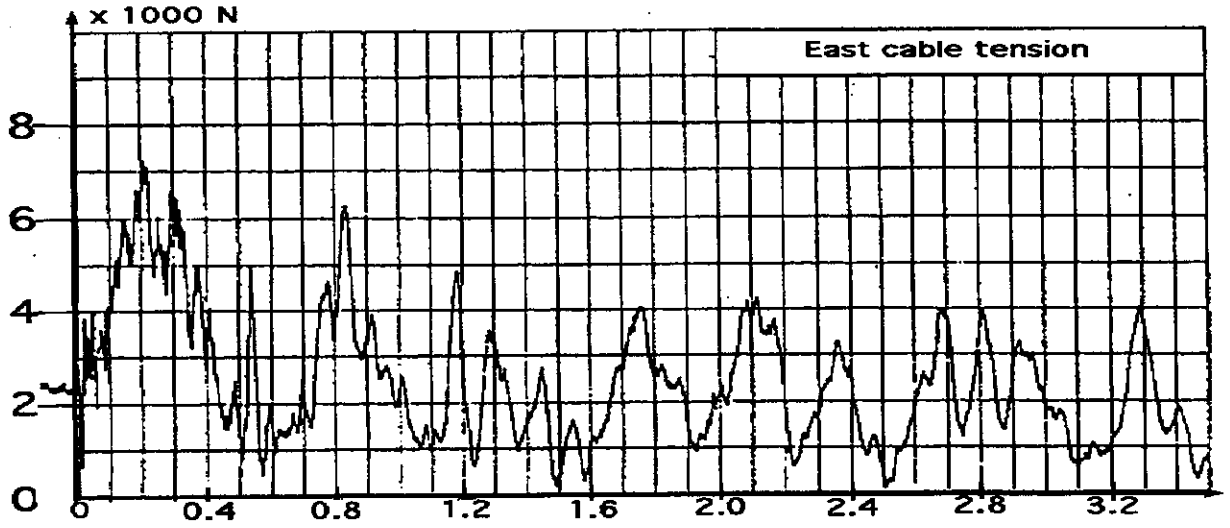

Fig. 7.5 : East cable tension-time evolution (measuring point 4 on fig. 4.2)

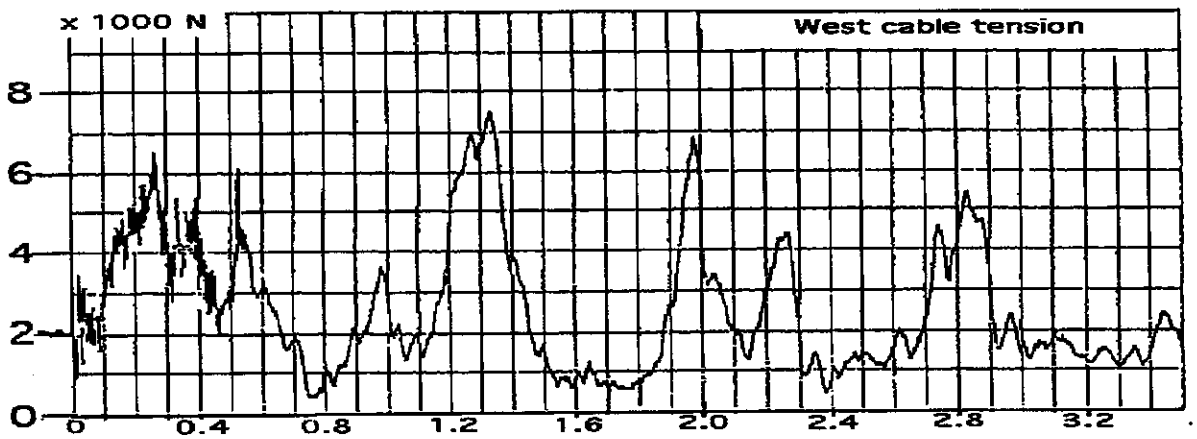

Fig. 7.6 : East cable tension-time evolution (measuring point 3 on fig. 4.2)

CASE 8

Test performed at FGH (Germany) in 1985
cross section : 590 mm^2
short-circuit current : 25 kA (64 kA peak)
span length : 40 m

Bus-bar geometry

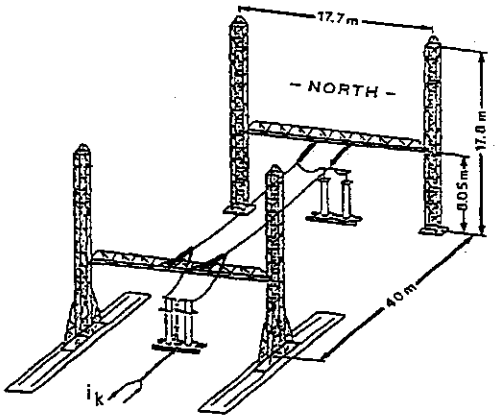

The high voltage open air substation testing arrangement at the FGH, Mannheim

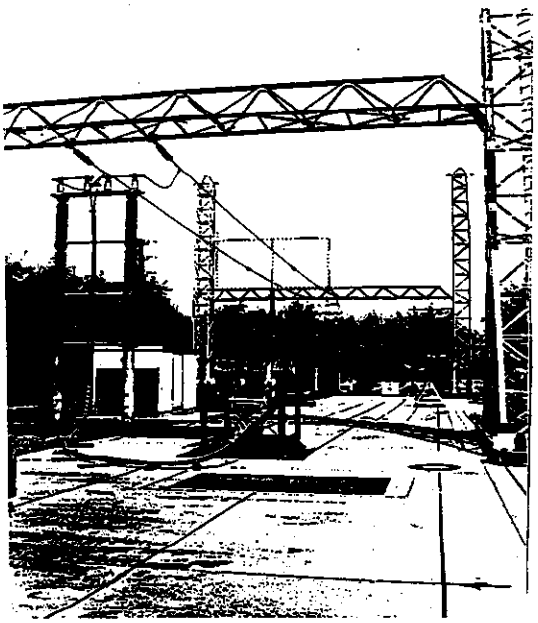

Supporting structure data :
stiffness : North : 2,45 10^6 N/m ; South : 3,35 10^6 N/m (measurement on the midpoint of the crossarm).

frequencies (Hz) :
the cross-arm alone : 8,8 Hz
One of the North column alone : 3,4 Hz
One of the South column alone : 5,0 Hz.

Contact address : FGH Mannheim, Hallenweg 40, Postfach 810169, D 68201 Mannheim (Norbert Stein). Germany. Fax : + 49-621-8047112

Basic data

1) all connections

	cable	section (mm^2)	mass (kg/m)	diameter (mm)
bus-bar	ACSR	537/57	1,97	32,1

jumper same as bus-bar, 2,86 m on South side and 3,03 m on North side.

centre line distance between main conductors : 2 m

bundle configuration : this is not a bundle configuration

Insulating hardware (insulator itself and other clamps, fittings, etc ...), On North side, the length is longer due to measuring devices.

insulator	material	length (m)	mass (kg)
1 chain cap and pin	porcelain	2,7 (North) 2,25 (South)	54,4 40,2

2) initial conditions before testing :

sag (m)	tension (N)
0,62	6400

3) short-circuit characteristics :

kind of short-circuit (two or three-phase) : two-phase fault /test LV 507-86/18

	Irms (kA)	Ipeak (kA)	time constant (s)	duration (s)
first fault	26,7	68,9	0,04	0,34

Results

coordinates in a vertical plane at mid-span :	X (m)	Z (m)
initial sag at coordinate :	0	0
Maximum horizontal displacement towards the outside, away from the other conductor :	1,15	0,34
Maximum vertical displacement upwards :	-0,08	1,17
Maximum horizontal displacement towards the other conductor :	-0,98	0,73
Maximum vertical displacement downwards :	0,55	-0,25
Horizontal displacement at he end of the short-circuit :	1,0	0,67

Table 1 : Mid-span displacement in a vertical plane perpendicular to the bus-bar (X for horizontal and Z for vertical)

design values :	measurement
initial static pull Fst(N):	6400
swing out maximum Ft(N):	27600
falling down maximum Ff(N):	22400
max traction in a bottom leg of one column (truss element) (daN)	14700
min clearing distance (m)	0,04

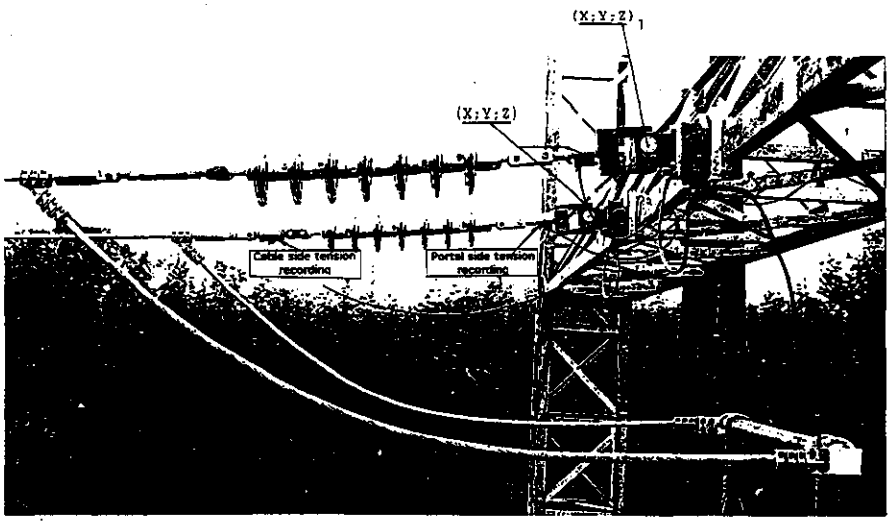

Fig, 8.1 Details of anchoring side including measurement devices for bus-bar tension recorder

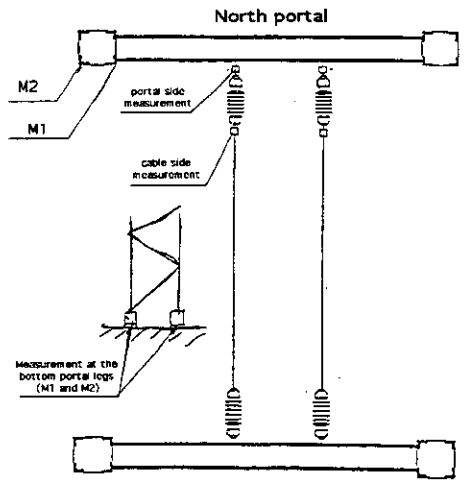

Fig. 8.2 Bus-bar geometry including the location of measurement next to the portal and immediately after anchoring chain

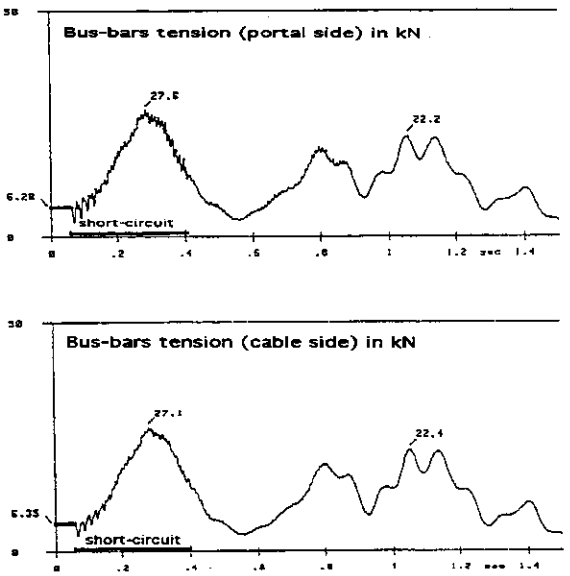

Fig. 8.3 and 8.4 Bus-bar tension (detail)

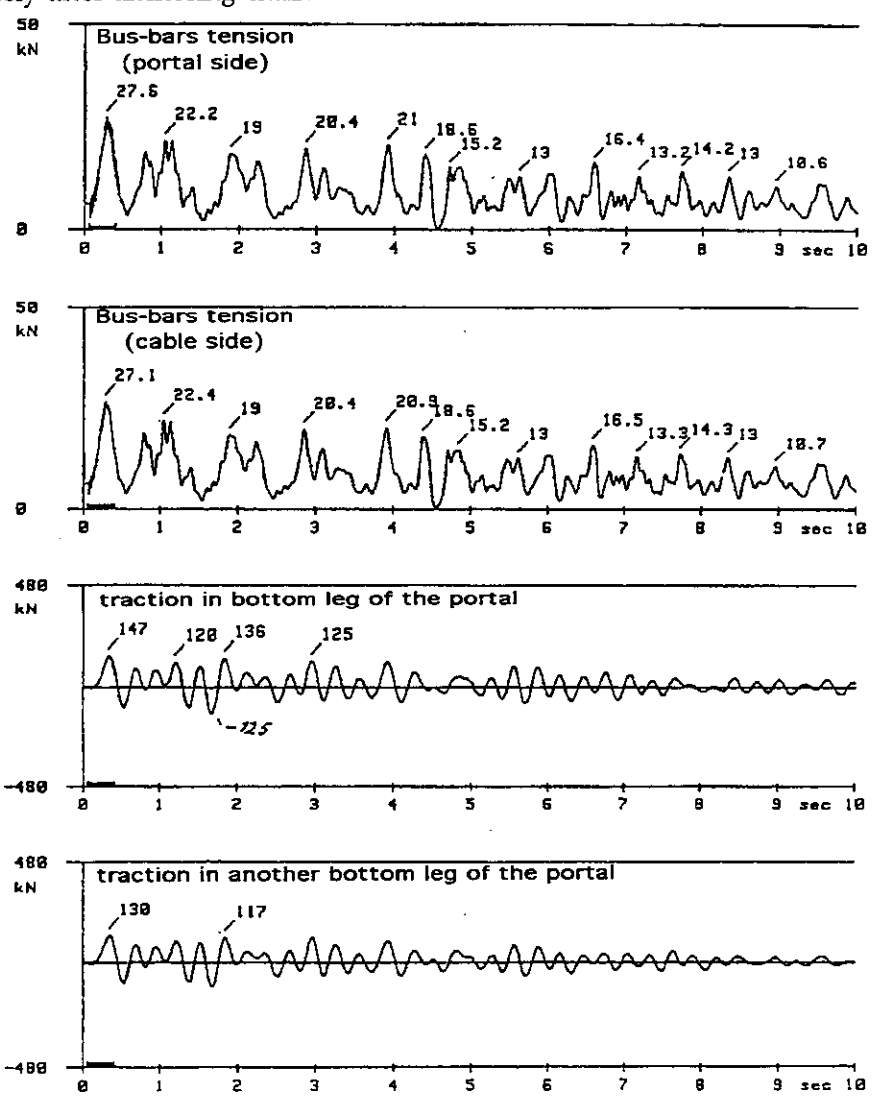

Fig. 8.5 to 8.8 Time evolution of each measured value during 10 seconds, test FGH 507-86/18

Configurations for case 9 to 11

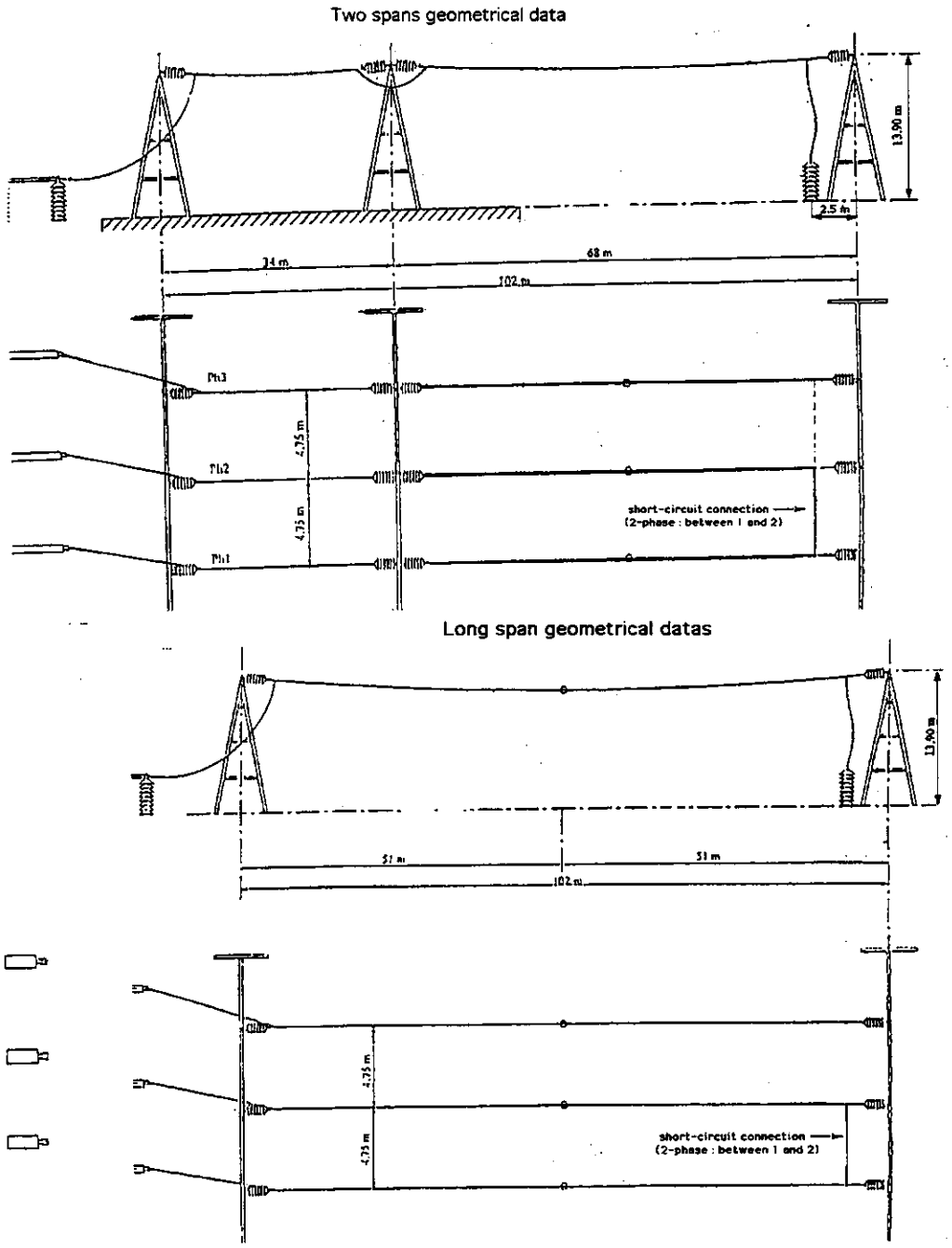

Supporting structure data :
stiffness at cable fixation point (N/m) : middle phase : 3,1 10^6 N/m, other phases : 5,3 10^6 N/m; first eigenfrequency : 2,75 Hz

Contact address : EDF/CERT Service Etudes, Immeuble Ampère, La Défense 6, 34-40 rue H. Régnault, F 92400 Courbevoie, France. (Guy Declercq). Fax + 33-1-41022757.

CASE 9

Test performed at EDF- Les Renardières (France) in 1990
cross section : 570 mm^2 ASTER
short-circuit current : 30 kA(80kA peak) 0,085 s,
with auto reclosure
span length : 68 and 34 m (test 1101)

Basic data

1) all connections

	cable	material	section (mm2)	mass kg/m	diameter (mm)
bus-bar	ASTER	Almelec	570	2,9	31,1
dropper	same as bus-bar				
jumper	same as bus-bar				

remarks :
dropper length : feeding : 13m; short-circuit : 10,3 m
(of limited influence due to their position, choosen slack to avoid stretching)

insulator	material	length 1 (m)	mass1 (kg)	length 2 (m)	mass2 (kg)
1 chain	porcelain	1,44	19,2	1,0	37,5

2) initial conditions before testing

ambiant temperature°C	cable	sag (m)	tension (N)
25	unknown	3%(45°C) 1 m (34 m) 1,9 m (68 m)	3400 N (34 m) 5400 N (68 m)

3) short-circuit characteristics

kind of short-circuit (two or three-phase) : two phase with autoreclosing after 2s deadtime.

	Irms (kA)	Ipeak (kA)	time constant (s)	duration (s)
first fault	30	79,8	0,081	0,085
second fault	30	78,6	0,081	0,095

Results

design values :	measurement span of 34 m	measurement span of 68 m
initial static pull Fst(N):	3400	5400
falling down maximum before reclosure Ff(N):	7000	13700
maximum after reclosure (N) :	9200	22000

N.B. We have only to consider the low frequency maxima. During short-circuit there are other instantaneous maxima; but at high frequency (50 Hz) which do not need to be taken into account for design.

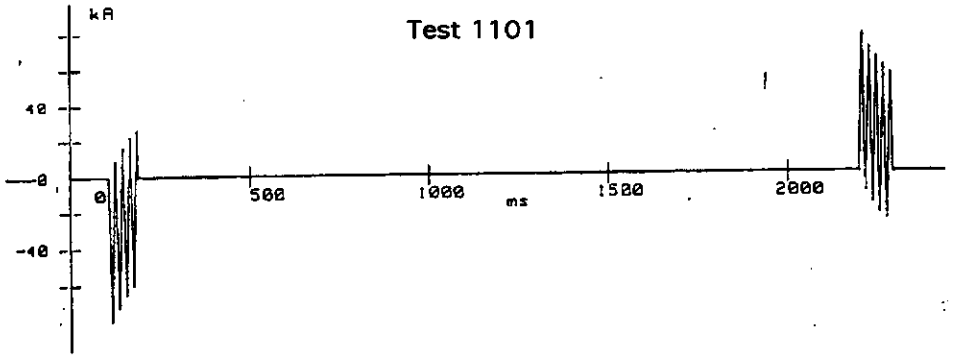

Fig. 9.1 Short-circuit current wave shape, time scale in ms.

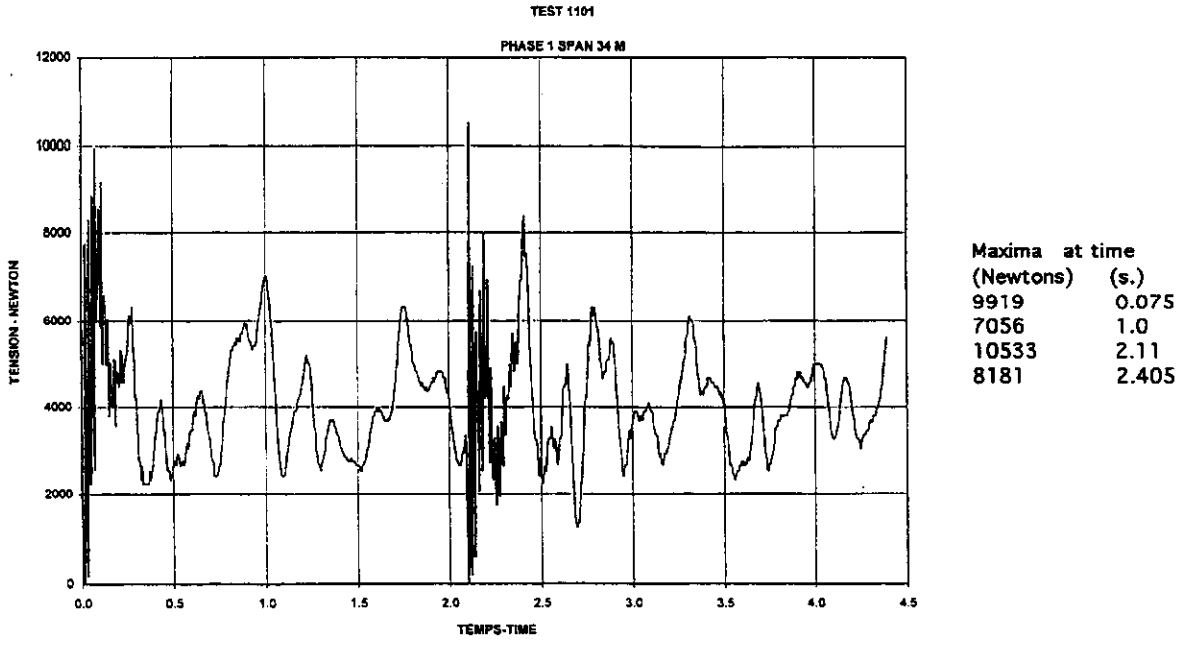

Fig. 9.2 Bus-bar tension-time evolution in phase 1 for the short span of 34 m.

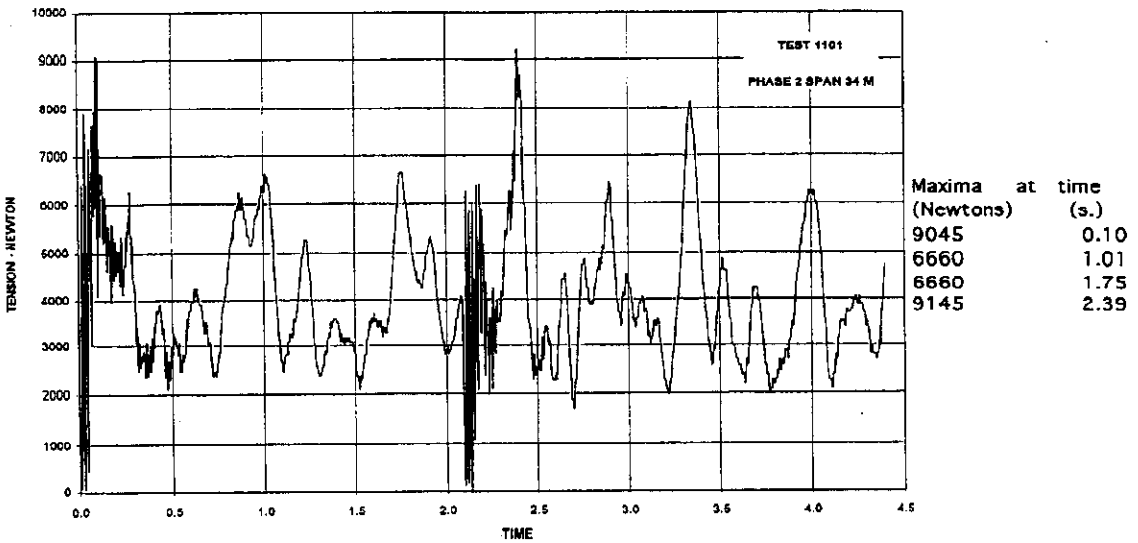

Fig. 9.3 Bus-bar tension-time evolution in phase 2 for the short-span of 34 m.

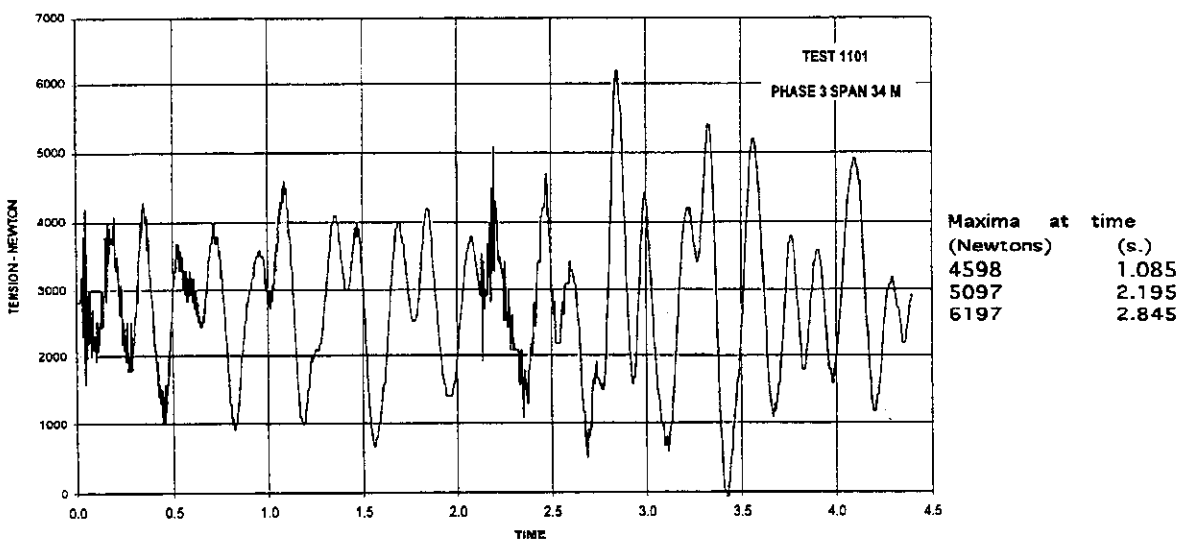

Fig. 9.4 Bus-bar tension-time evolution in phase 3 (test 1101 is a two-phase fault, the movement of phase 3 is only due to coupling due to the portal), for the short span of 34 m.

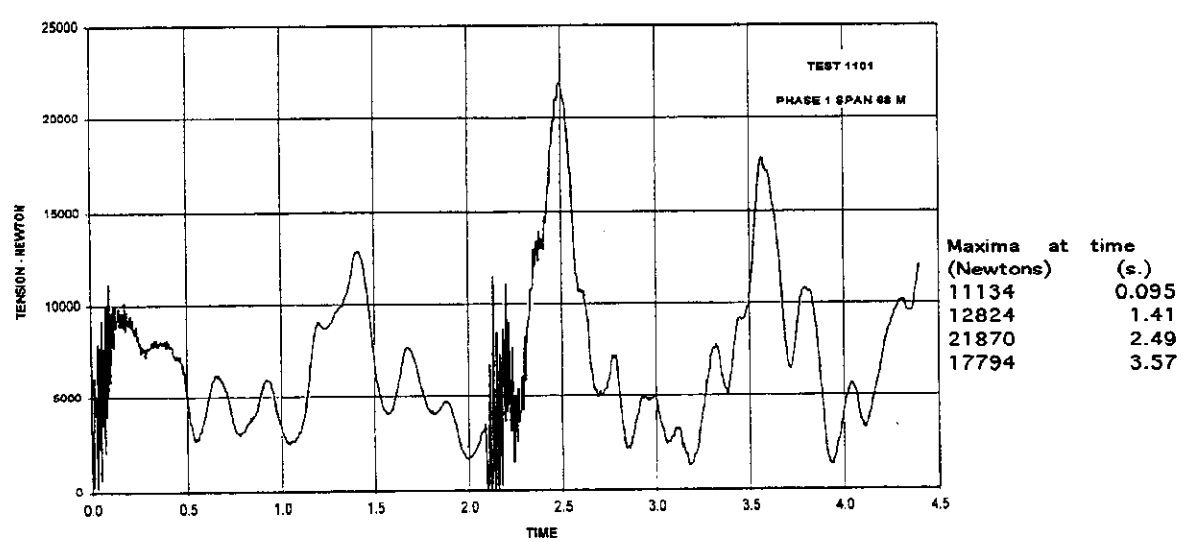

Fig. 9.5 Bus-bar tension-time evolution in phase 1 for the long span of 68 m.

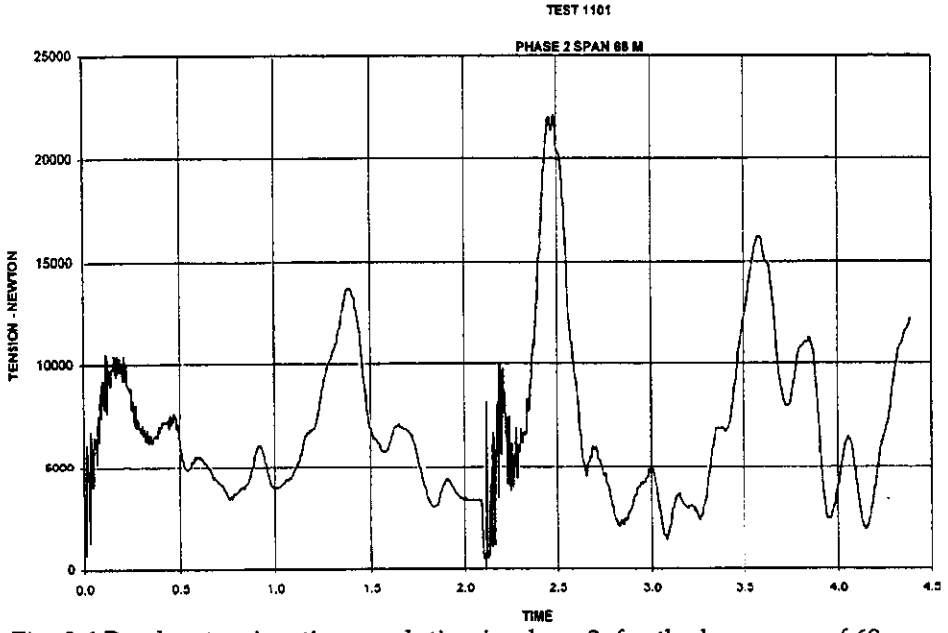

Maxima (Newtons)	at time (s.)
10472	0.115
13694	1.38
22051	2.48
16110	3.57

Fig. 9.6 Bus-bar tension-time evolution in phase 2 for the long-span of 68 m.

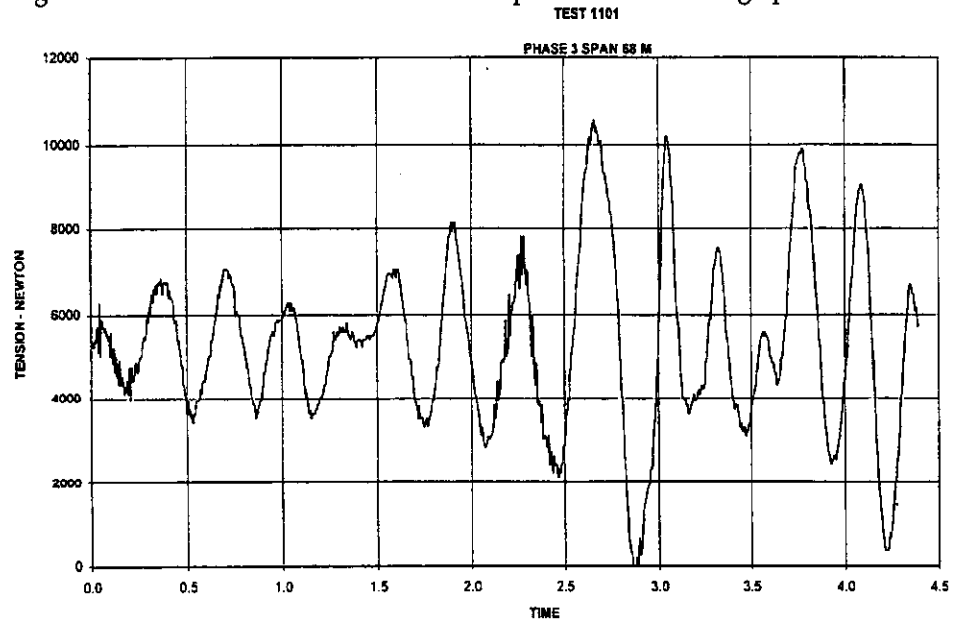

Maxima (Newtons)	at time (s.)
10583	2.665
10191	3.04

Fig. 9.7 Bus-bar tension-time evolution in phase 3 (test 1101 is a two-phase fault, the movement of phase 3 is only due to coupling due to the portal), for the long span of 68 m.

CASE 10

Test performed at EDF- Les Renardières (France) in 1990
cross section : 570 mm² ASTER
short-circuit current : 30 kA, 0,255 s
span length : 102 (test 1102)- 68 and 34 m (test 1003)

Basic data

1) all connections

	cable	material	section (mm^2)	mass kg/m	diameter (mm)
bus-bar	ASTER	Almelec	570	2,9	31,1
dropper	same cable as bus-bar				
jumper	same cable as bus-bar				

remarks :
dropper length : feeding : 13m; short-circuit : 10,3 m
(of limited influence due to their position, choosen slack to avoid stretching)

insulator	material	length 1 (m)	mass1 (kg)	length 2 (m)	mass2 (kg)
1 chain	porcelain	1,44	19,2	1,0	37,5

2) initial conditions before testing

ambiant temperature°C	cable	sag (m)	tension (N)
25	unknown	3%(45°C) 1 m (34 m) 1,9 m (68 m) 3 m (102m)	 3400 N (34 m) 5400 N (68 m) unknown

3) short-circuit characteristics

kind of short-circuit (two or three-phase) : two phase

	Irms (kA)	Ipeak (kA)	time constant (s)	duration (s)
first fault	29,7	79,2	0,081	0,255

Results

results on 68 and 34 m span lengths (test 1003) :

design values :	measurement span of 68 m	measurement span of 34 m
initial static pull Fst(N):	5400	3400
swing out maximum Ft(N):	15500	12000
falling down maximum Ff(N):	25000	15000

result on 102 m span length (test 1102):

design values :	measurement (test 1102)
initial static pull Fst(N):	8500
swing out maximum Ft(N):	22000
falling down maximum Ff(N):	34000

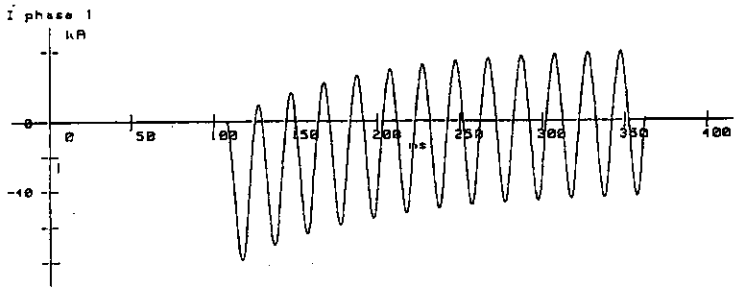

Fig. 10.1 Short-circuit current wave shape for the two-phase fault , test number 1003

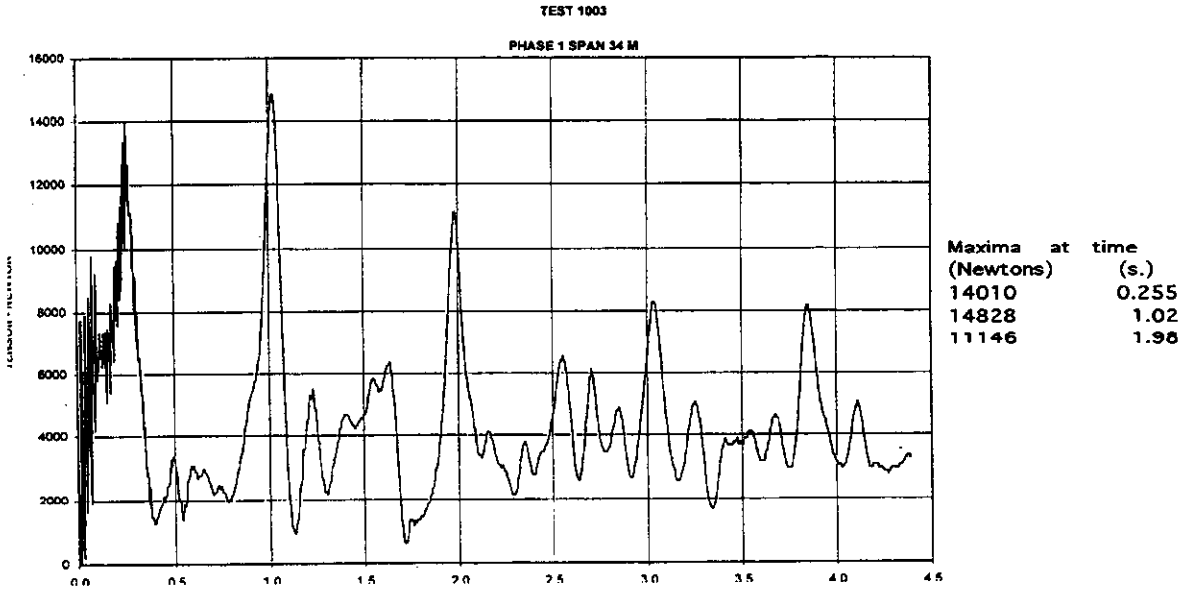

Fig. 10.2 Bus-bar tension-time evolution in phase 1 for the short span of 34 m.

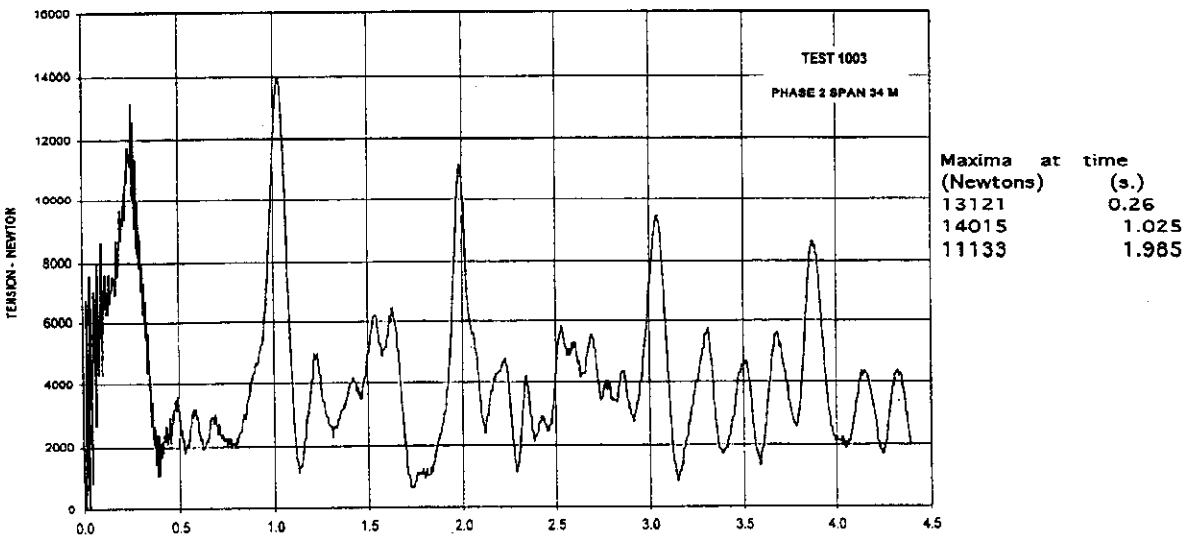

Fig. 10.3 Bus-bar tension-time evolution in phase 2 for the short span of 34 m.

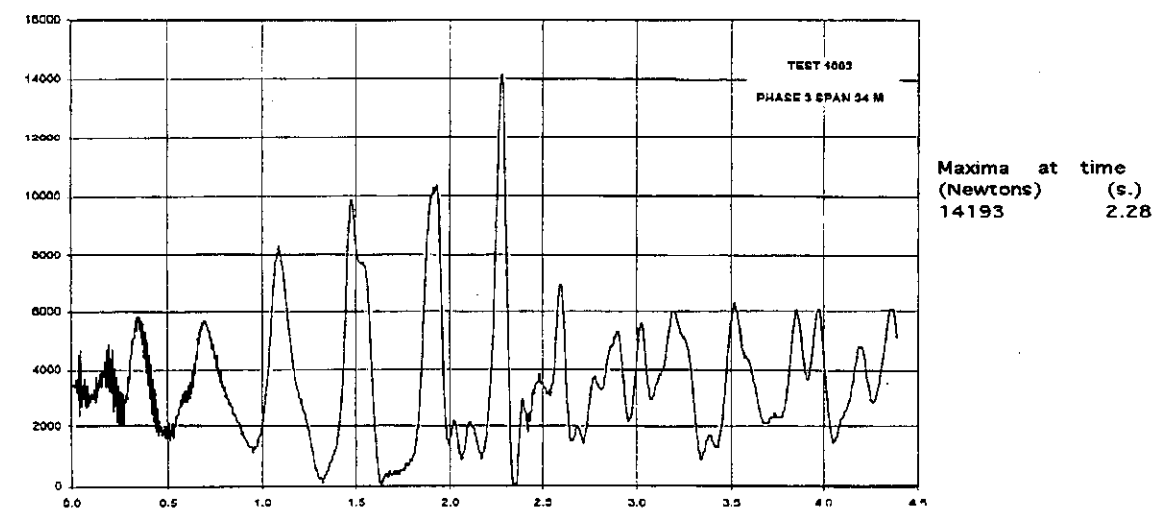

Fig. 10.4 Bus-bar tension-time evolution in phase 3 for the short span of 34 m. This phase is not carrying any current, the movement is induced due to coupling through the portal cross-arm.

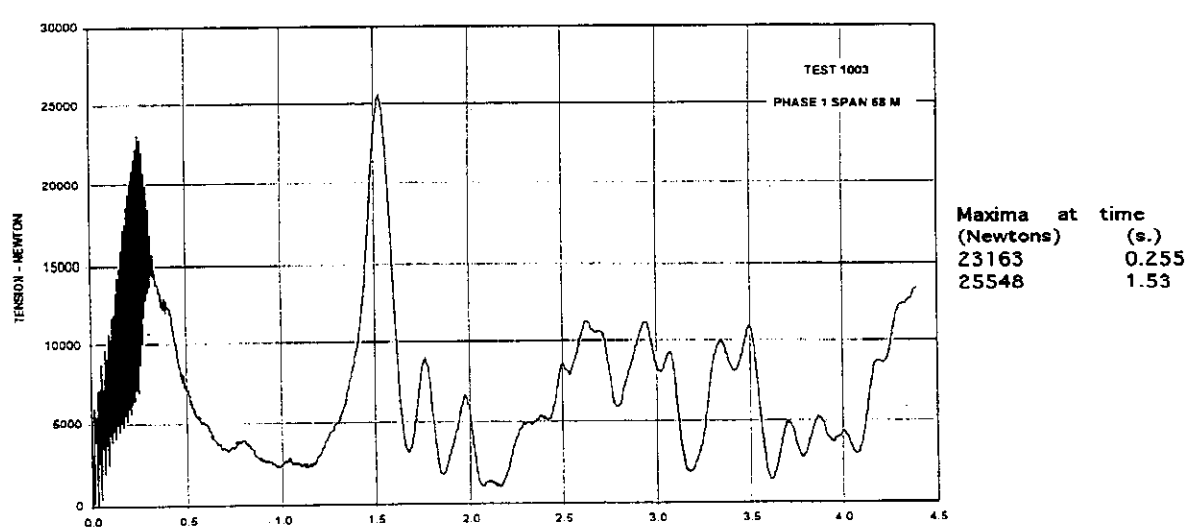

Fig; 10.5 Bus-bar tension-time evolution in phase 1 for the long span of 68 m.

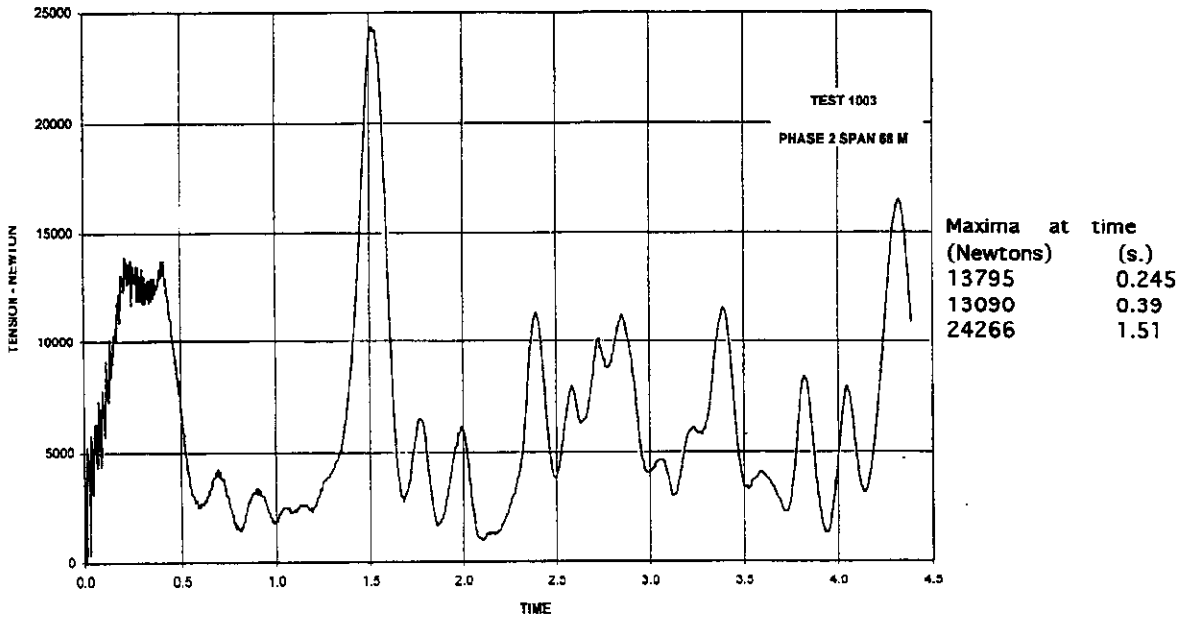

Fig; 10.6 Bus-bar tension-time evolution in phase 2 for the long span of 68 m.

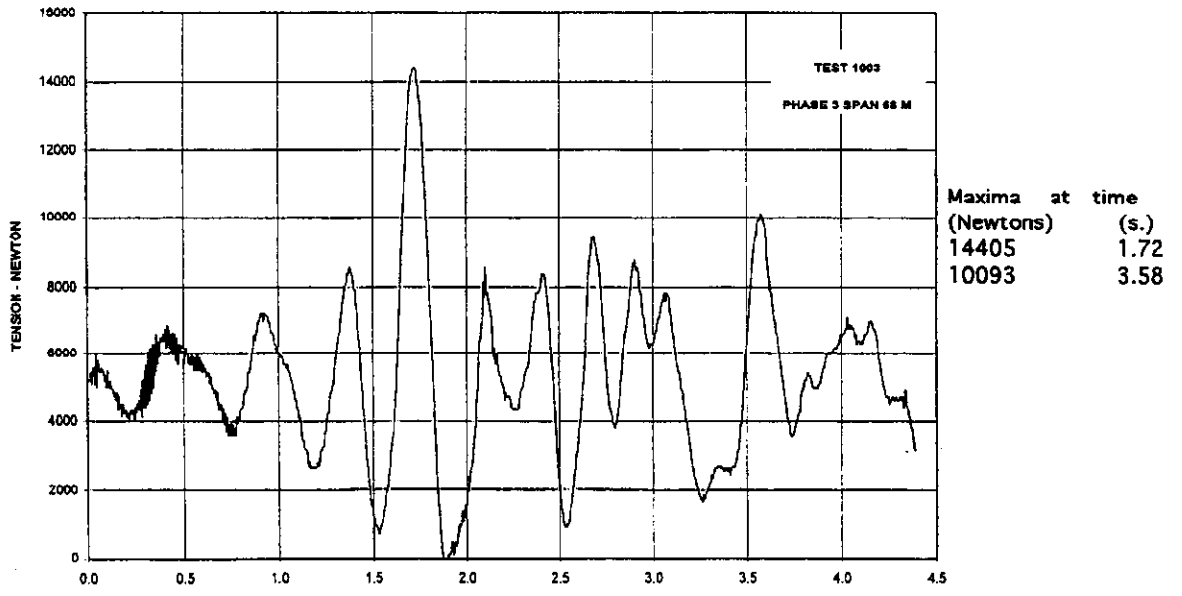

Fig. 10.7 Bus-bar tension-time evolution in phase 3 for the long span of 68 m. Same remark as fig. 10.4

Test 1102 : one very long span of 102 meters.

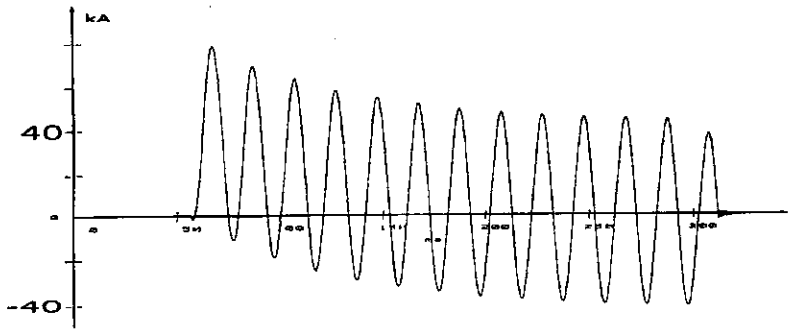

Fig. 10.8 Short-circuit current wave shape for two phase fault on very long span 102 m, test 1102.

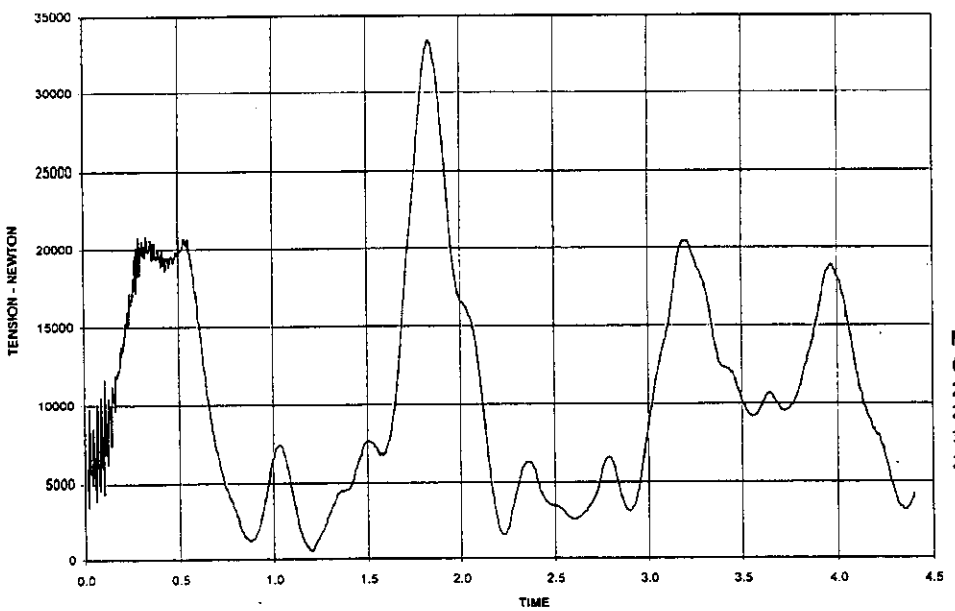

Maxima at time	
(Newtons)	(s.)
20749	0.29
20646	0.53
33320	1.835
20442	3.2

Fig. 10.9 Bus-bar tension-time evolution in phase 1 for the long span test (102 m).

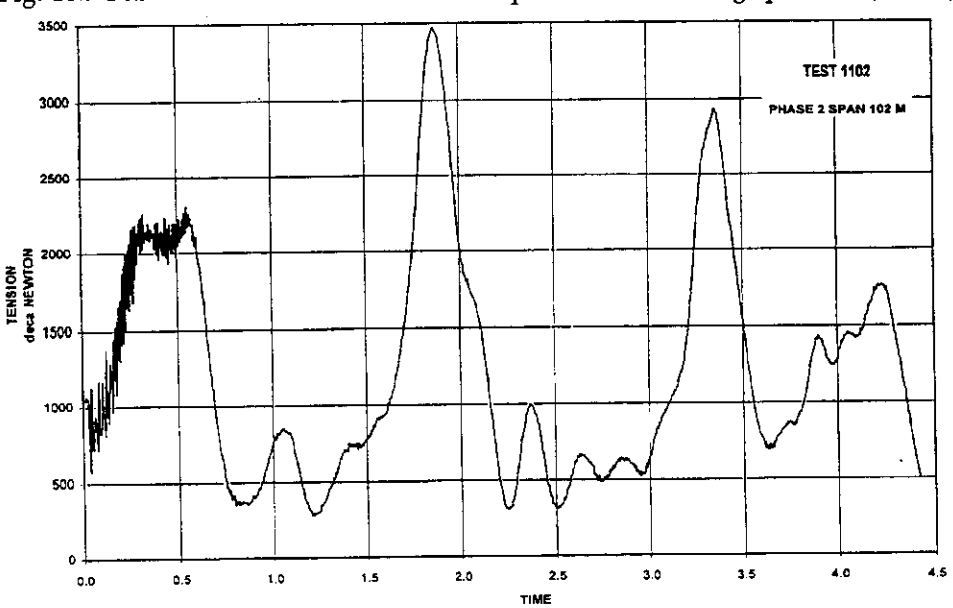

Maxima at time	
(Newtons)	(s.)
22681	0.56
34719	1.865
29347	3.355

Fig. 10.10 Bus-bar tension-time evolution in phase 2 for the long span test (102 m).

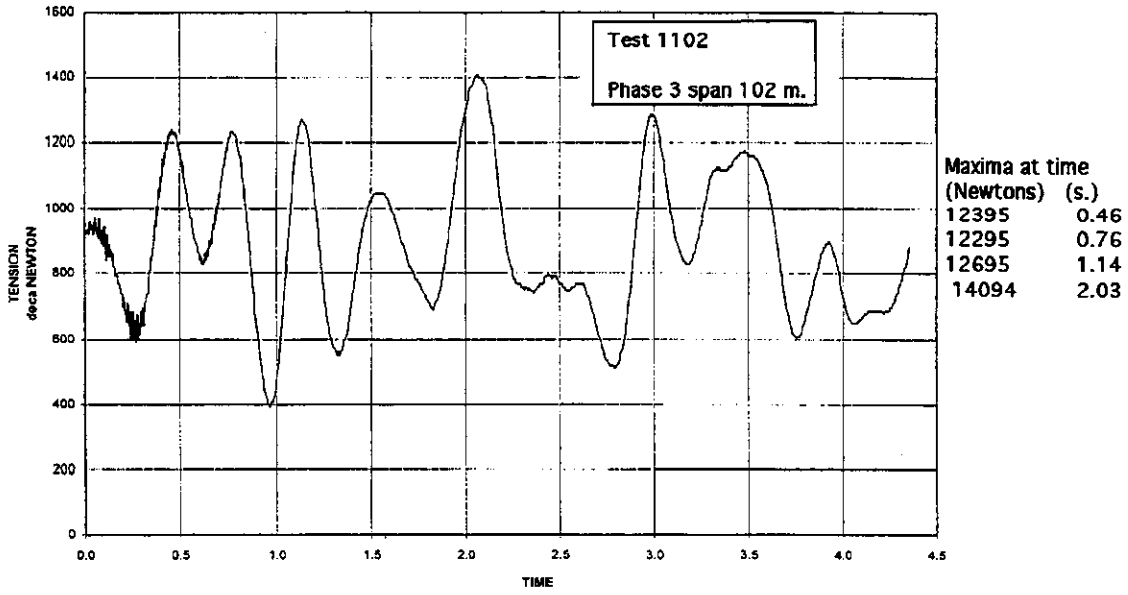

Fig. 10.11 Bus-bar tension-time evolution in phase 3 for the long span test (102 m). Same remark as fig. 10.4

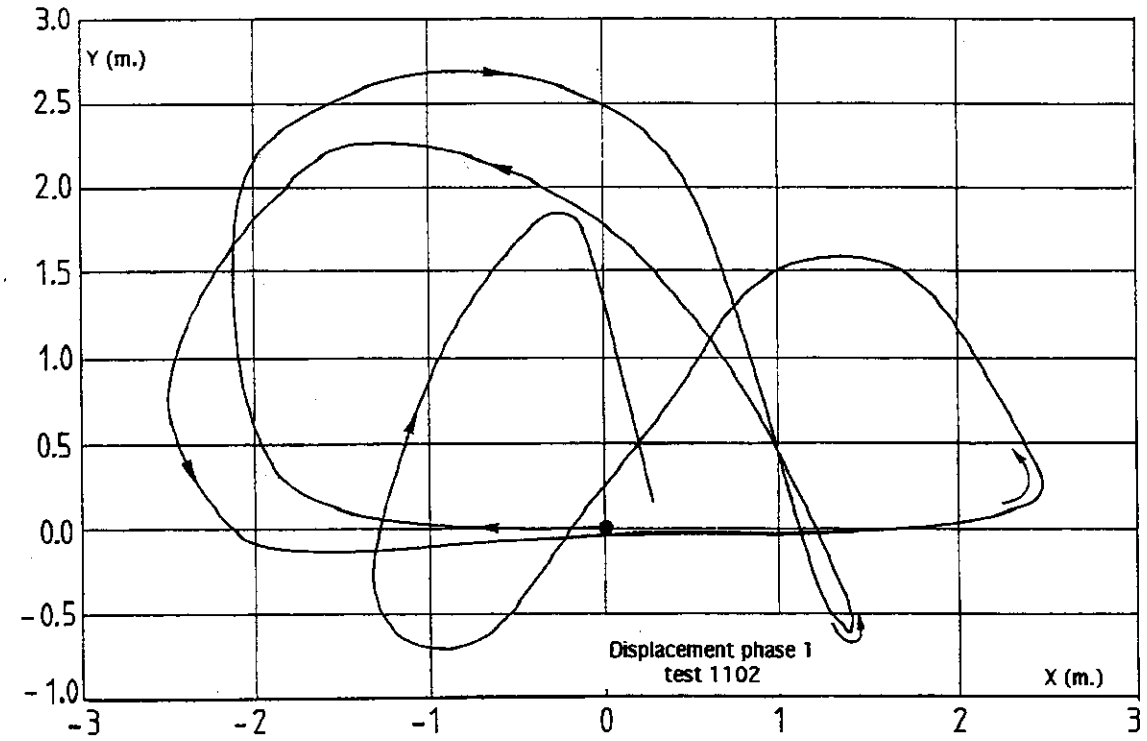

Fig. 10.12 Bus-bar movement in a vertical plane at mid-span, evolution for phase 1 for the long span test (102 m). This is the relative movement starting from (0,0) and following the arrow direction.

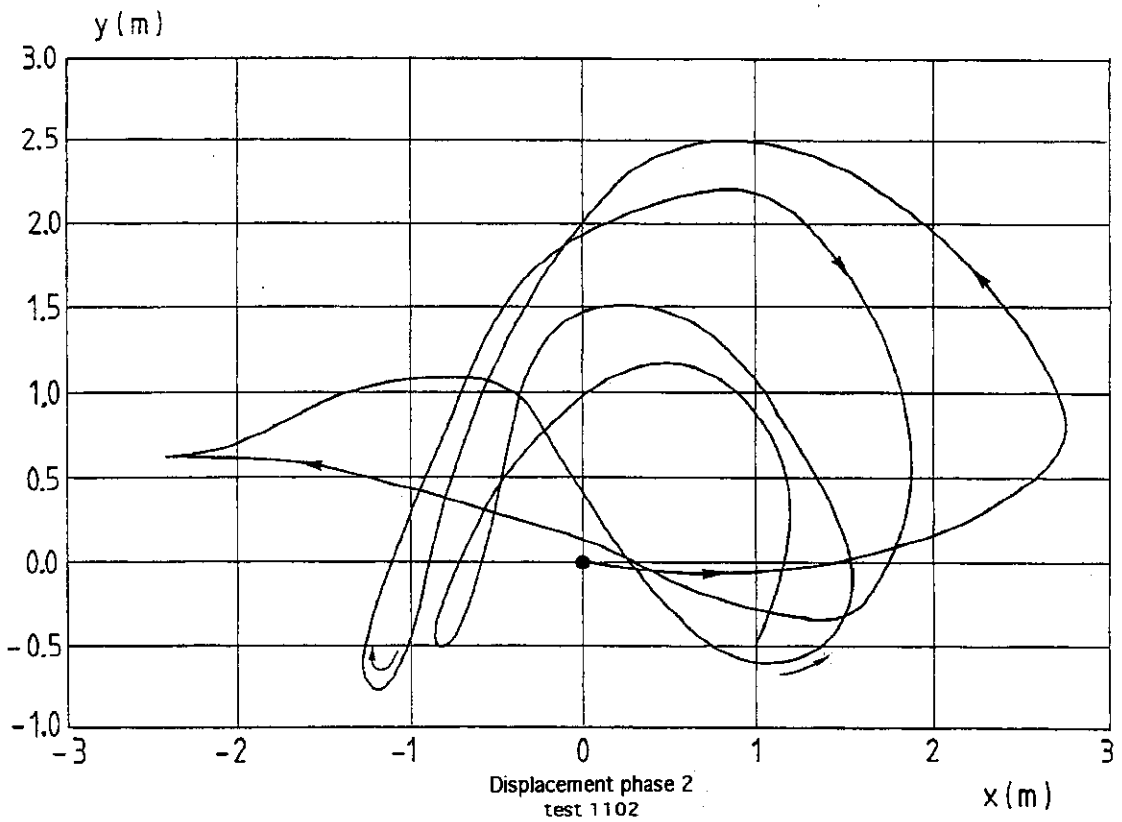

Fig. 10.13 Bus-bar movement in a vertical plane at mid-span, evolution for phase 2 for the long span test (102 m). This is the relative movement starting from (0,0) and following the arrow direction.

CASE 11

Test performed at EDF- Les Renardières (France) in 1990
cross section : 570 mm² ASTER
short-circuit current : three-phase, 35 kA; 0,245s
span length : 68 and 34 m (test 1202) - 102 m (test 1002)

Basic data

1) all connections

same cable as for cases 9 and 10

2) initial conditions before testing

test N°	ambiant temperature°C	sag (m)	tension (N)
1202 (68 and 34m)	19	3%(45°C) 1 and 1,9m	3400 and 5400
1002 (102 m)	17	3%(45°C) 2,6 m	8500

3) short-circuit characteristics : see also the oscillograms

test N°	Irms (kA)	Ipeak (kA) in each phase	time constant (s)	duration (s)
1202 (68 and 34m)	34,9	91,6 78,5 64	0,070	0,245
1002 (102 m)	34,8	72,9 93,5 71	0,070	0,245

Results

results on 68 and 34 m span lengths (test 1202) :

corresponding design values evaluated by :	measurement span of 68 m	measurement span of 34 m
initial static pull Fst(N):	5400	3400
swing out maximum Ft(N):	13000	15000
falling down maximum Ff(N):	27500	17000

result on 102 m span length (test 1002):

corresponding design values evaluated by	measurement (test 1002)
initial static pull Fst(N):	8500
swing out maximum Ft(N):	18000
falling down maximum Ff(N):	32200

1) Test 1202 : two spans of 34 and 68 meters.

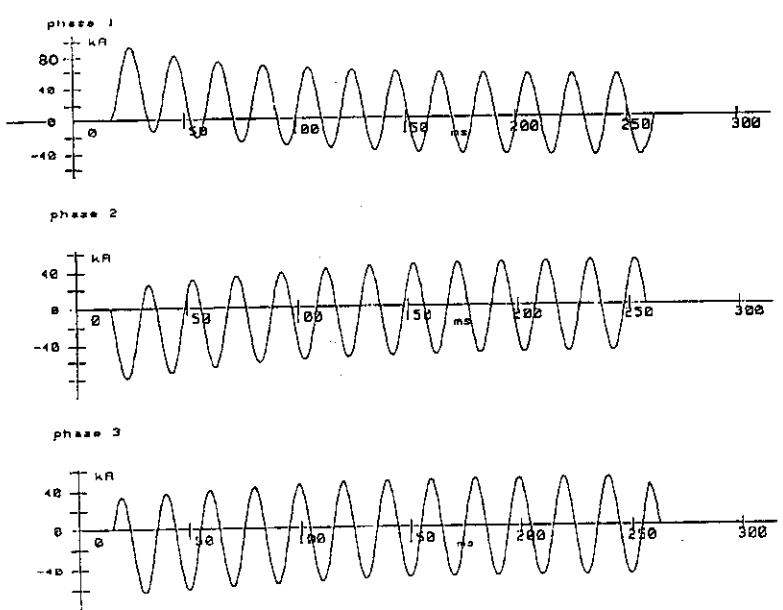

Fig. 11.1 Short-circuit current wave shape for three phase fault on two-span test number 1202.

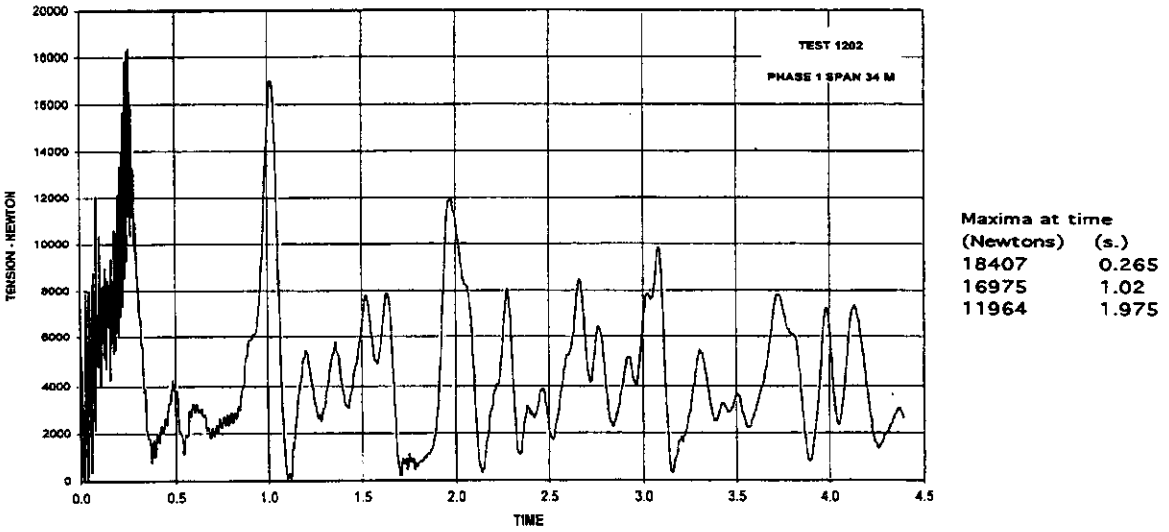

Fig. 11.2 Bus-bar tension-time evolution in phase 1 for the short span of 34 meters.

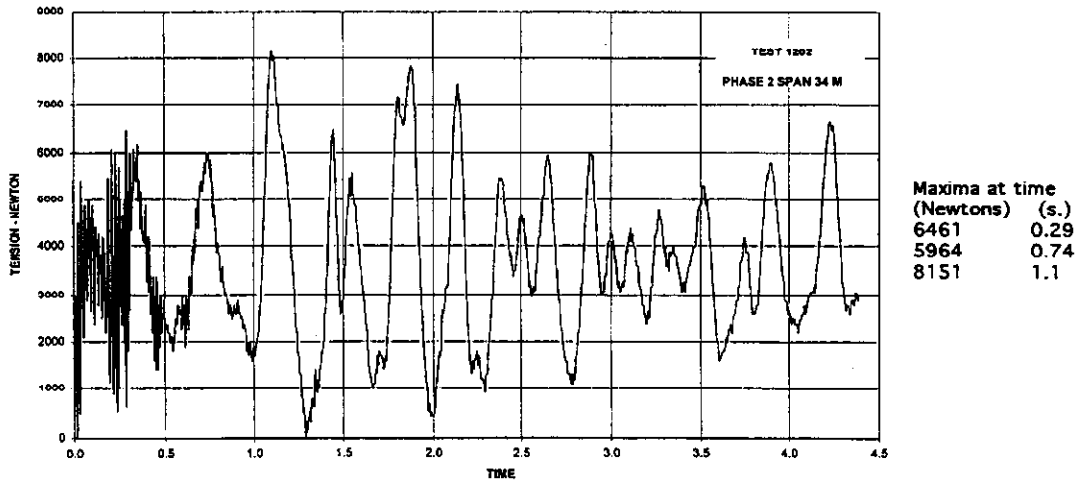

Fig. 11.3 Bus-bar tension-time evolution in phase 2 for the short span of 34 meters.

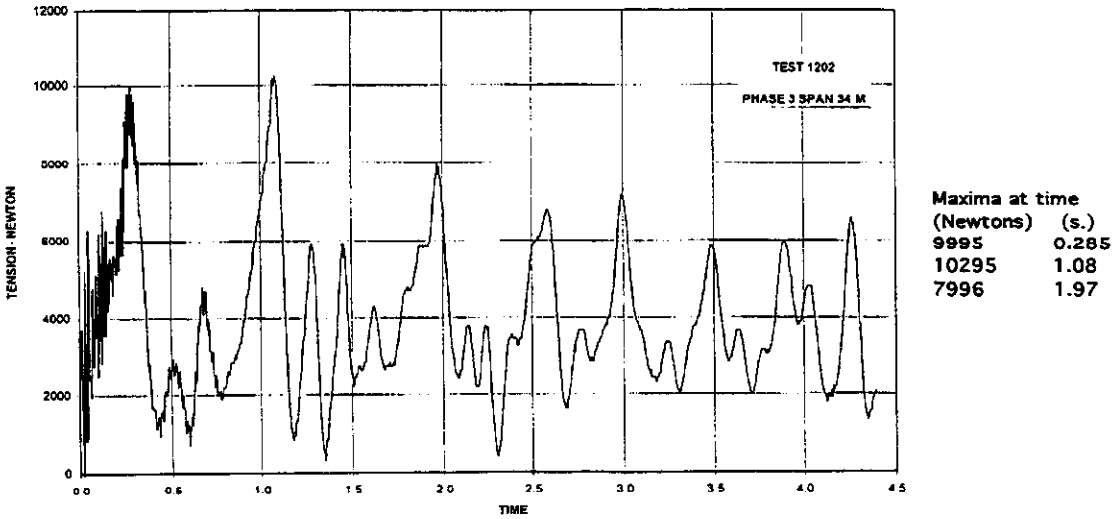

Fig. 11.4 Bus-bar tension-time evolution in phase 3 for the short span of 34 meters.

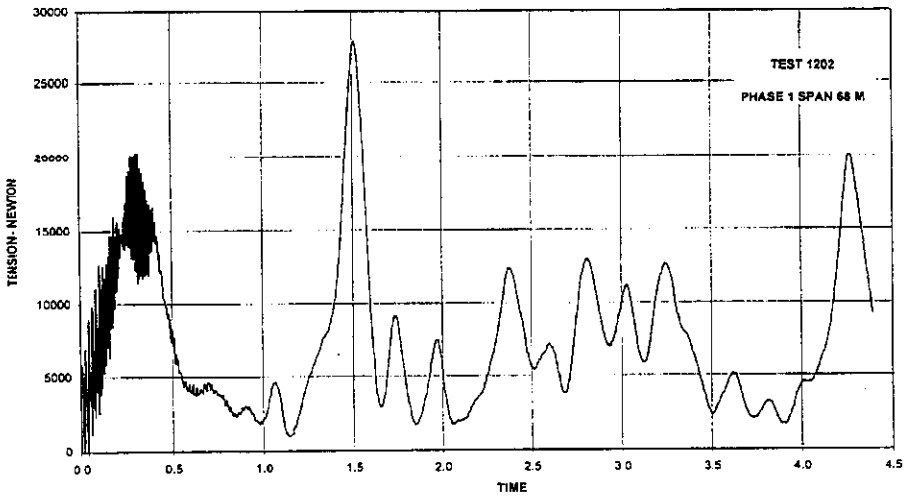

Fig. 11.5 Bus-bar tension-time evolution in phase 1 for the long span of 68 meters.

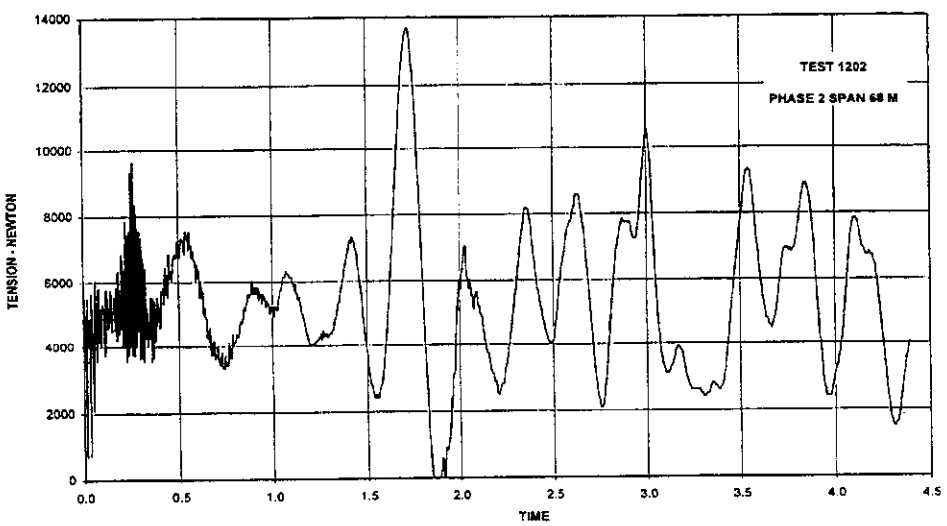

Fig. 11.6 Bus-bar tension-time evolution in phase 2 for the long span of 68 meters.

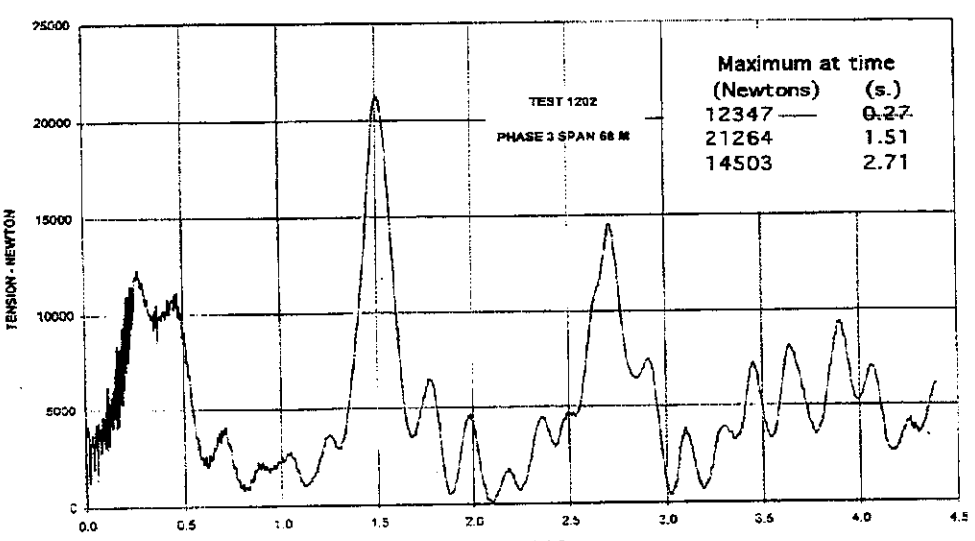

Fig. 11.7 Bus-bar tension-time evolution in phase 3 for the long span of 68 meters.

2) Three-phase tests on one very long span (102 m) , test number 1002.

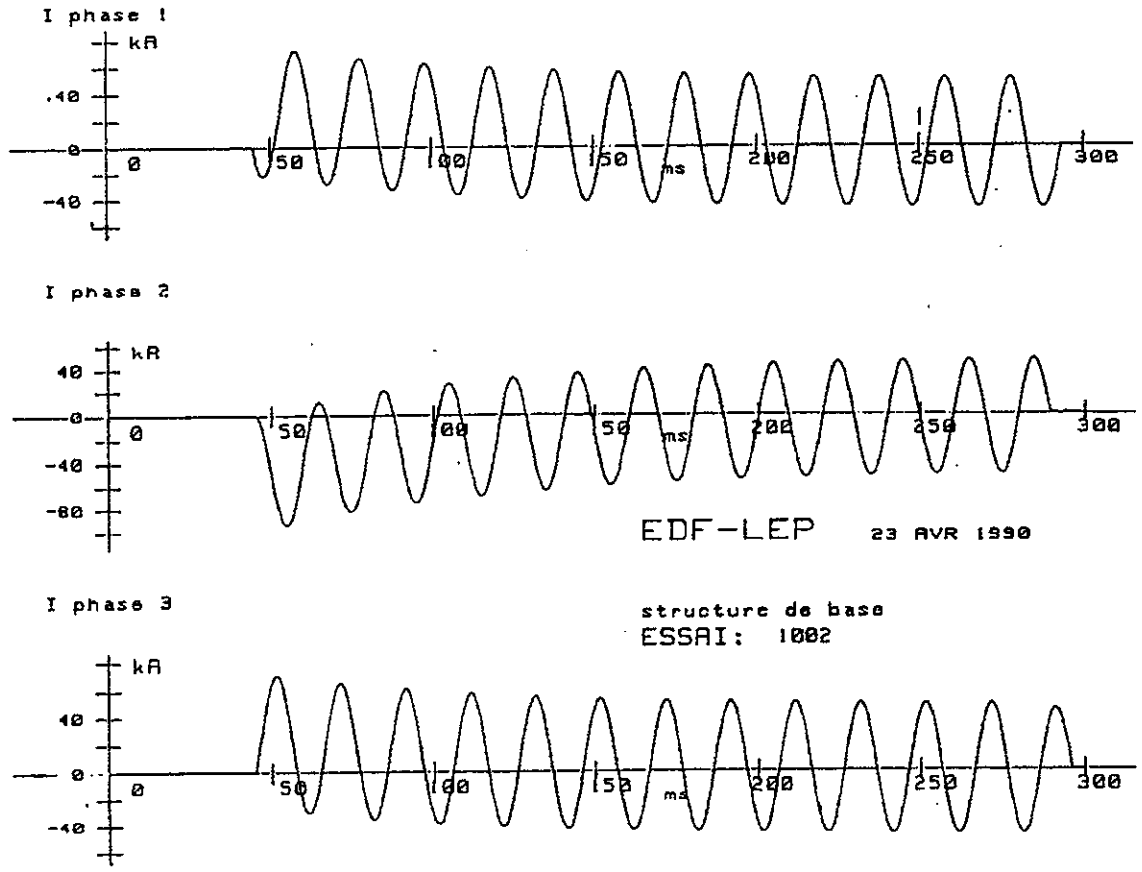

Fig. 11.8 Short-circuit wave shape for three phase test on one very long span of 102 m., test number 1002.

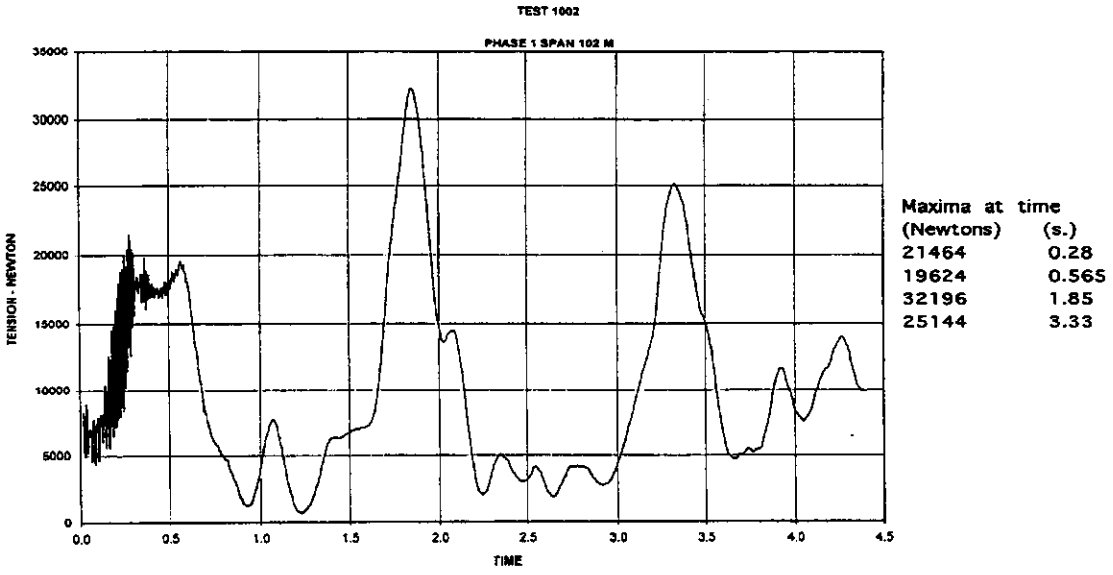

Fig. 11.9 Bus-bar tension-time evolution in phase 1.

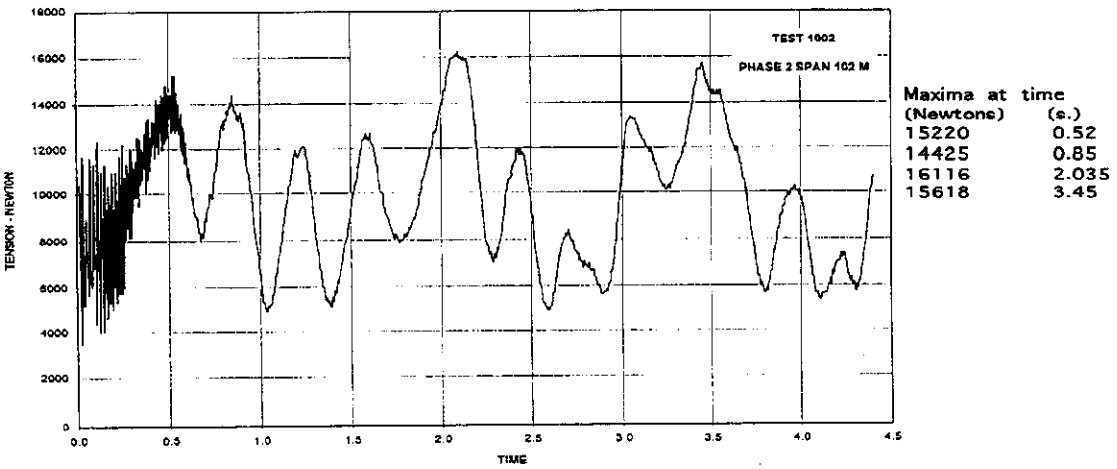

Fig. 11.10 Bus-bar tension-time evolution in phase 2.

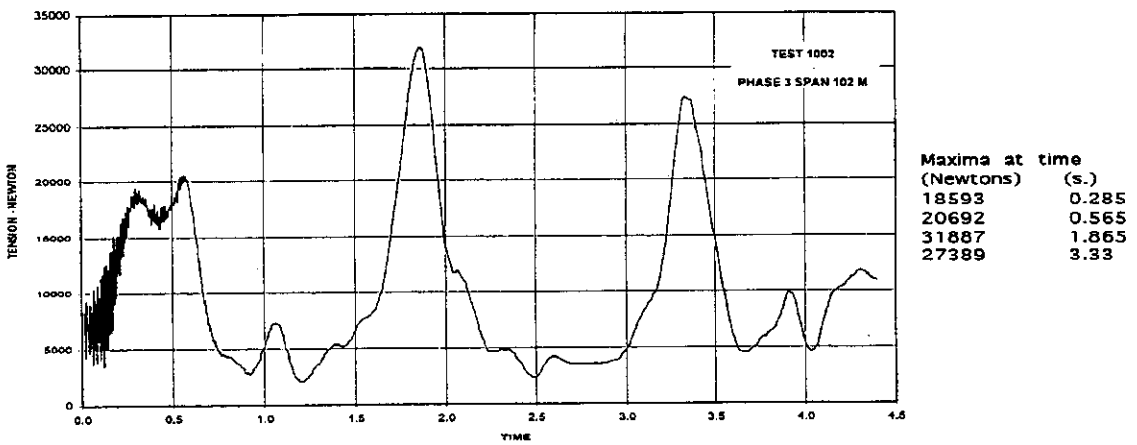

Fig. 11.11 Bus-bar tension-time evolution in phase 3.

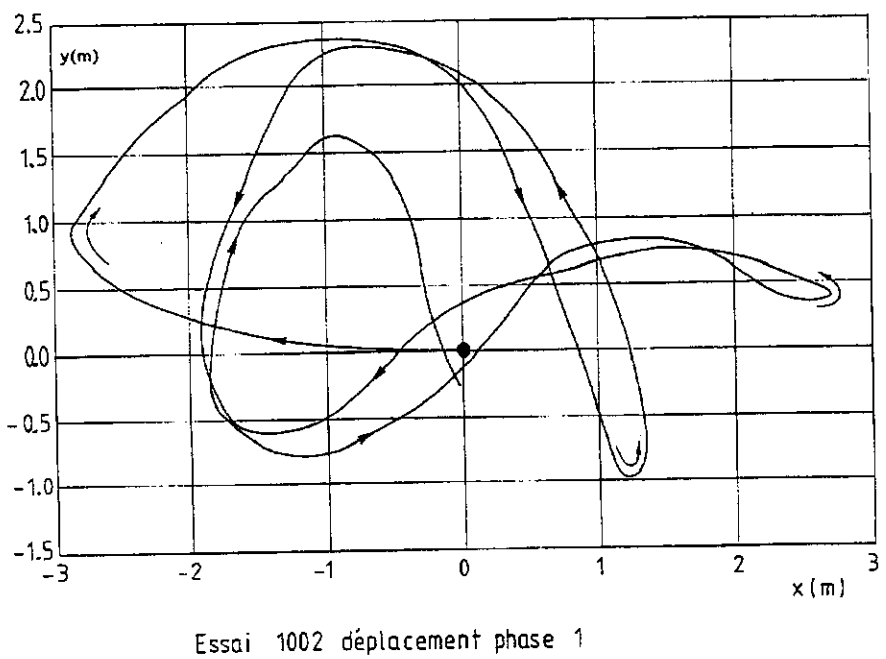

Fig. 11.12 Bus-bar movement in a vertical plane, phase 1 test 1002. This is the relative movement, starting from (0,0) (mid-span sag point) and following the arrow direction.

PART 2 :

BUNDLE CONDUCTOR

CASE 12

Test performed at ASEA- Ludvika (Sweden) in 1976
Case with bundle pinch (triple horizontal)
cross section : 3x772 mm^2 ACSR
short-circuit current : 30; 40 and 50 kA
span length : 70 m,subspan 12 m

Bus-bar geometry
(the same for case 12, 13 and 14)

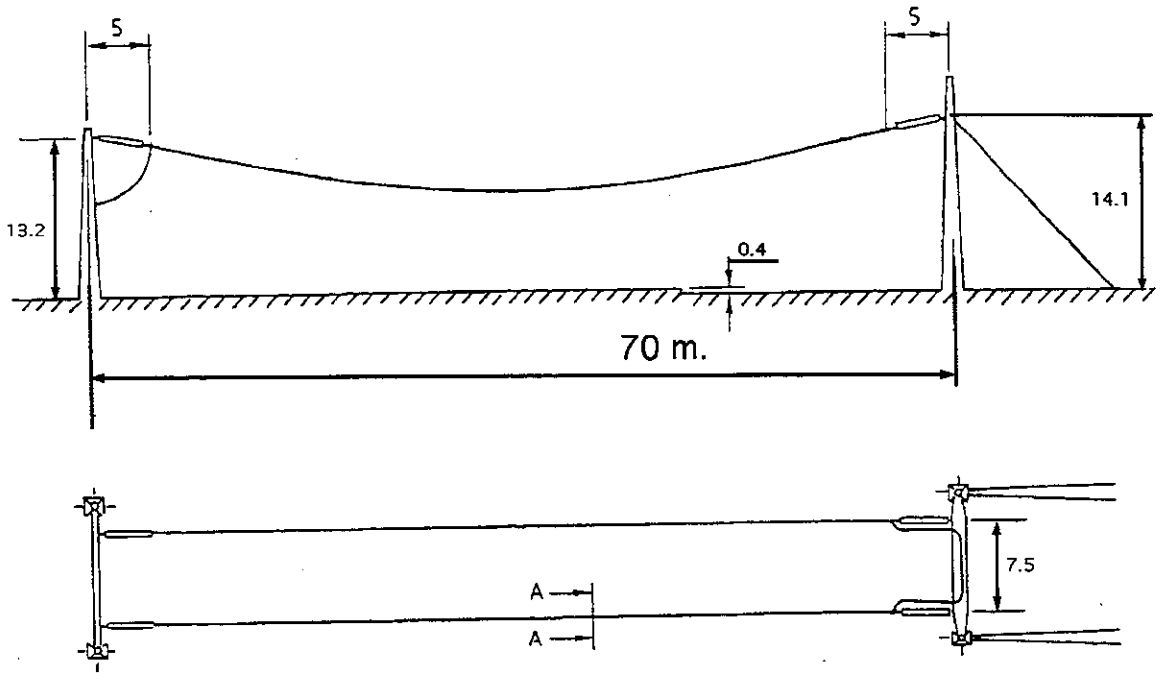

Fig. 12.1 Bus-bar geometry for ASEA tests on flexible bus with bundle configuration.

Supporting sructure data :
stiffness at cable fixation point (N/m) : 4,0 10^5 N/m; first eigen frequency : range 1.5 - 3,9 Hz
other details : cross-arm mass : 500 kg; one pole mass : 325 kg; global mass of the gantry : 1150 kg ; height : 13 m

Contact address :ABB Substations AB, S-721 82 Västeras, Sweden, (Jörgen Andersson), Fax : +46 21328013 or Vattenfall Utveckling AB, Power Generation & Distribution, S-162 87 Stockholm, Sweden (Rolf Nordin), Fax : +46 87396250.

Basic data

1) all connections

	material	section mm^2	mass kg/m	diameter (mm)
bus-bar	Al	3x772	2,9	36,2

bundle configuration :
spacing : 0,110 m; triple horizontal; sub-span length : 12 m.
Centre line distance between phases : 7.5 m

Insulating hardware (length1 is the interface between portal and insulator itself)

insulator	length 2 (m)	mass2 (kg)
1 chain	4	205

2) initial conditions before testing :

sag (m)	tension (N)
5,64	8750

3) short-circuit characteristics :

kind of short-circuit (two or three-phase) : two-phase fault

	Irms (kA)	Ipeak (kA)	time constant (s)	duration (s)	test number
first fault	31	78	0,07	1,0	16
first fault	40,3	106	0,07	1,0	17
first fault	50,5	138	0,07	1,0	18

corresponding design values evaluated by	measured
Maximum pinch load (test 16)	19000 N
Maximum pinch load (test 17)	38000 N
Maximum pinch load (test 18)	49500 N

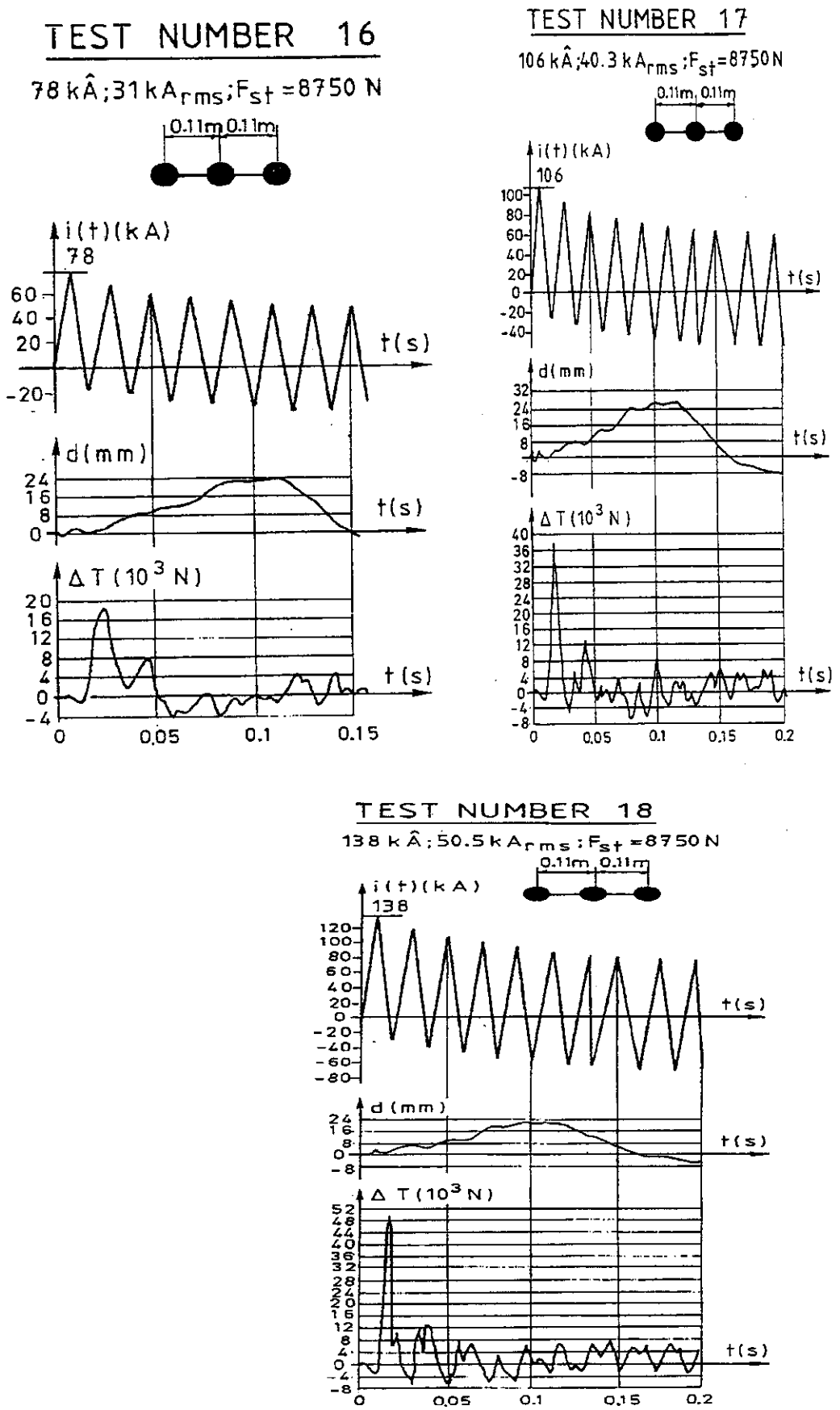

Fig. 12.2 to 12.4 Schematic short-circuit current wave shape, portal displacement and tension increase (pinch effect) in the bus.

CASE 13

Test performed at ASEA- Ludvika (Sweden) in 1976
Case with bundle pinch (triple triangle)
cross section : 3x772 mm^2 ACSR
short-circuit current : 30; 40 and 50 kA
span length : 70 m,subspan 30 m

Basic data

1) all connections

	material	section mm^2	diameter (mm)	mass kg/m
bus-bar	Al	3x772	36,2	3x 2,15

bundle configuration :
spacing : 0,450 m; triple triangle (peak downwards) ; one spacer at the middle of the span, sub-span length : 30m.

Insulating hardware :

insulator	length (m)	mass (kg)
1 chain	4	205

2) initial conditions before testing :

sag (m)	tension (N)
5,64	8750

3) short-circuit characteristics :
kind of short-circuit (two or three-phase) : two-phase fault

	Irms (kA)	Ipeak (kA)	time constant (s)	duration (s)	test number
first fault	30,5	78	0,07	0,5	68A
first fault	40,5	106	0,07	0,5	69A
first fault	50,5	138	0,07	0,5	70A

corresponding design values evaluated by	measured
Maximum pinch load (test 68A)	15000 N
Maximum pinch load (test 69A)	25000 N
Maximum pinch load (test 70A)	28500 N

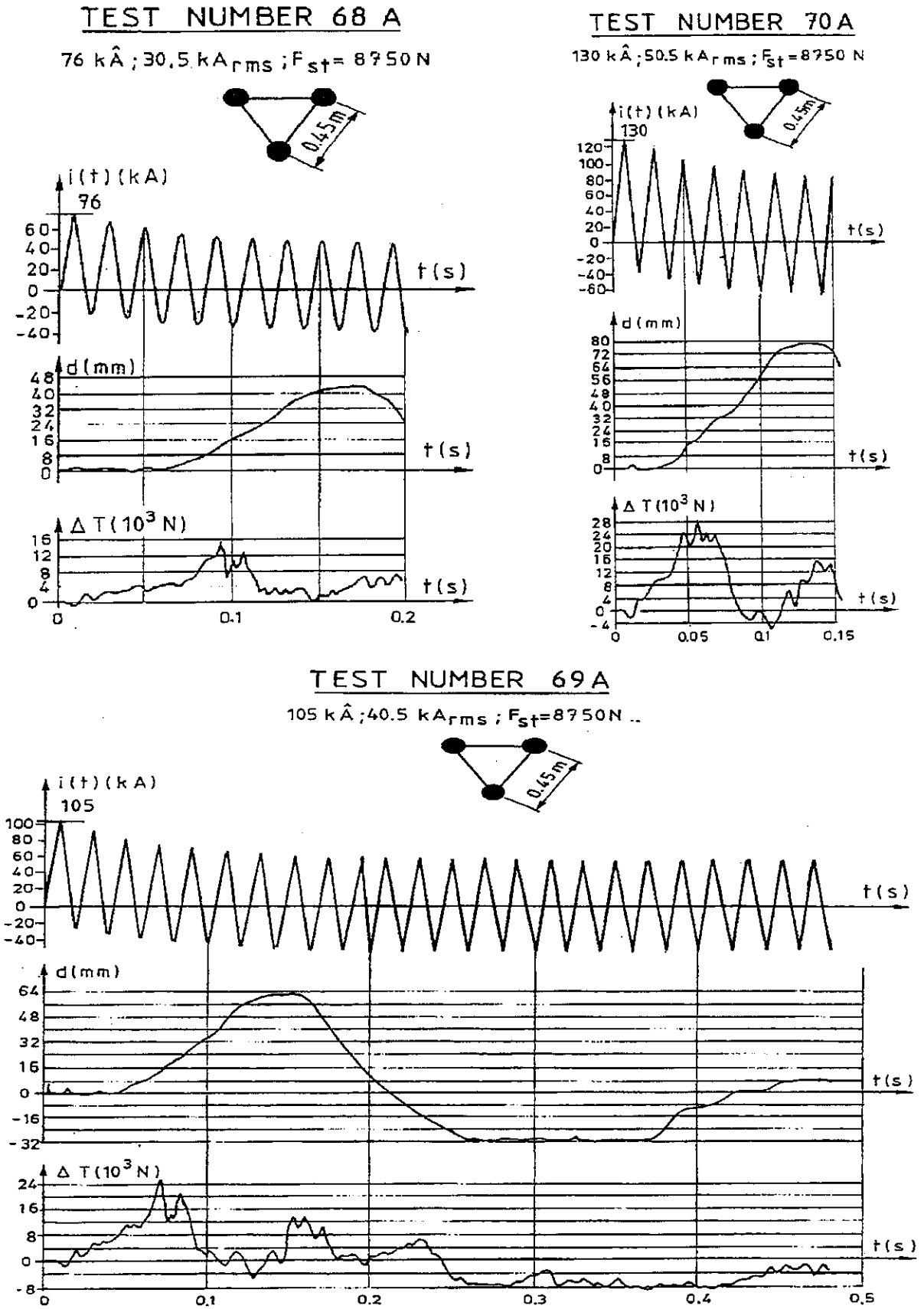

Fig. 13.1 to 13.3 Short-circuit wave shape, displacement of the support and pinch effect in the bus.

CASE 14

Test performed at ASEA- Ludvika (Sweden) in 1976
Case with bundle pinch (quad)
cross section : 3x772 mm^2 ACSR
short-circuit current : 30; 40 and 50 kA
span length : 70 m,subspan 30 m

Basic data

1) all connections

	material	section mm^2	diameter mm	mass kg/m
bus-bar	Al	4x772	36,2	4x 2,15

bundle configuration :
spacing : 0,600 m; quad bundle ; one spacer at the middle of the span, sub-span length : 30m.

Insulating hardware (length1 is the interface between portal and insulator itself)

insulator	length (m)	mass (kg)
1 chain	4	205

2) initial conditions before testing (per conductor):

sag (m)	tension (N)
5,64	8750

3) short-circuit characteristics :
kind of short-circuit (two or three-phase) : two-phase fault

	Irms (kA)	Ipeak (kA)	time constant (s)	duration (s)	test number
first fault	30	76	0,07	0,5	78A
first fault	40,5	106	0,07	0,5	79A
first fault	50,5	132	0,07	0,5	80A

Results

corresponding design values evaluated by	measured
Maximum pinch load (test 78A)	12000 N
Maximum pinch load (test 79A)	17500 N
Maximum pinch load (test 80A)	24000 N

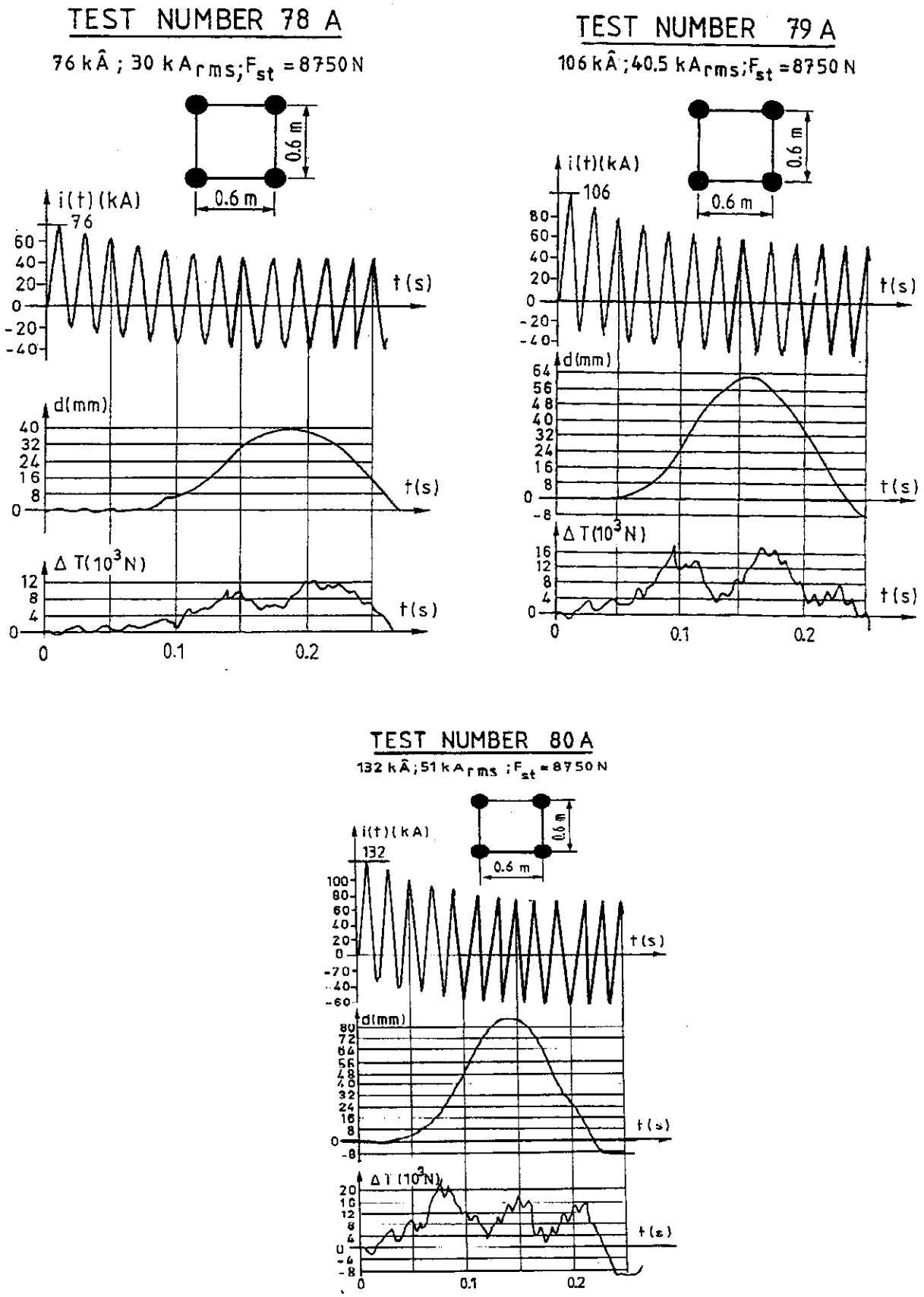

Fig. 14.1 to 14.3 Oscillograms of the short-circuit current, cross-arm displacement and pinch effect in the bundle.

CASE 15

Test performed at KEMA- Arnhem(The Netherlands)
in 1980
Case with bundle pinch (twin horizontal)
cross section : 2x1100 mm^2 ACSR
short-circuit current : 50 kA (137 kA peak)
span length : 30 m,subspan 6 m

Bus-bar geometry

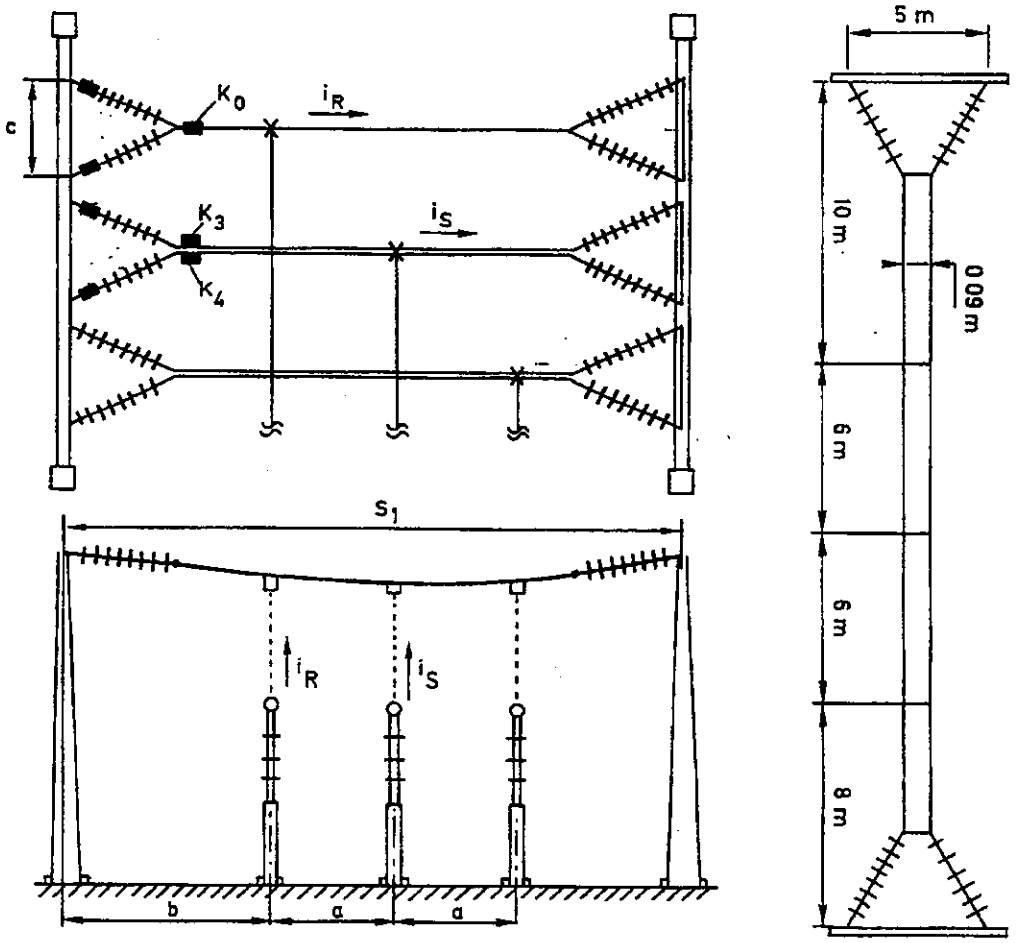

Fig. 15.1 Bus-bar geometry for Kema tests on bundle configuration.

data :
a = 6 m, b = 10 m, c = 5 m
Supporting sructure data :
stiffness at cable fixation point (N/m) : 5,0 10^5 N/m; first eigen frequency : 4 Hz
other reference : H. Adami, C.W.M. Vos. *Short-circuit tests and measurements of mechanical stresses on full-scale sections of 420 kV outdoor substations*. report 330-03 of the CIGRE symposium on « high currents in Power Systems under normal, emergency and fault conditions » held in Bruxelles in June 1985.

Basic data

1) all connections

	material	section mm^2	mass kg/m	diameter (mm)
bus-bar	ACSR	2x1100	2x3,2	43,2

bundle configuration :
spacing : 0,090 m; twin horizontal; three subspan (see the drawing) , shortest sub-span length : 6m.

Insulating hardware (V chain)

insulator	length 2 (m)	mass2 (kg)
2 chains in V	5,4	225 per chain

2) initial conditions before testing :

sag (m)	tension (N)
1,12	7500

3) short-circuit characteristics :

kind of short-circuit (two or three-phase) : two-phase fault , ATTENTION : the short-circuit current flow only in one half of the span.

	Irms (kA)	Ipeak (kA)	time constant (s)	duration (s)
first fault	48,8	137	0,065	0,5

results :

design values	measured
Maximum pinch load	23000 N

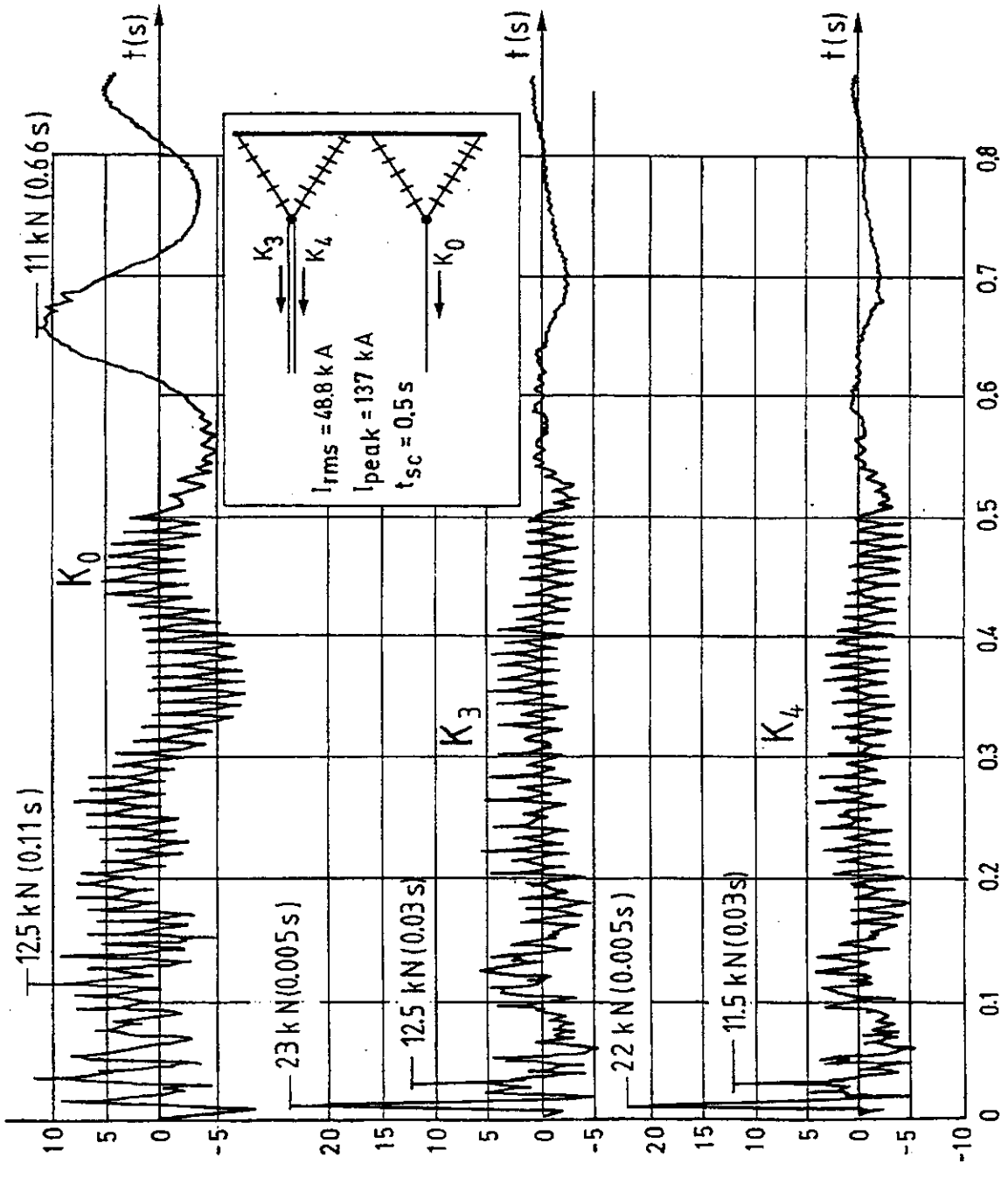

Fig. 15.2 Time response in each conductor of the bundle (K3 and K4) and in the single conductor (K0) during two-phase fault. Bus bar current i_R and i_S is only going through some part of the bus, fig. 15.1.

CASE 16

Test performed at Furukawa (Japan) in 1966 under supervision of Prof. Serisawa (Yokohama National University)
Case with tripple bundle pinch without contact
cross section : 3x1600 mm^2
short-circuit current : 63 kA (164 kA peak)
span length : 35 m (subspan length : 2m)

Bus-bar geometry

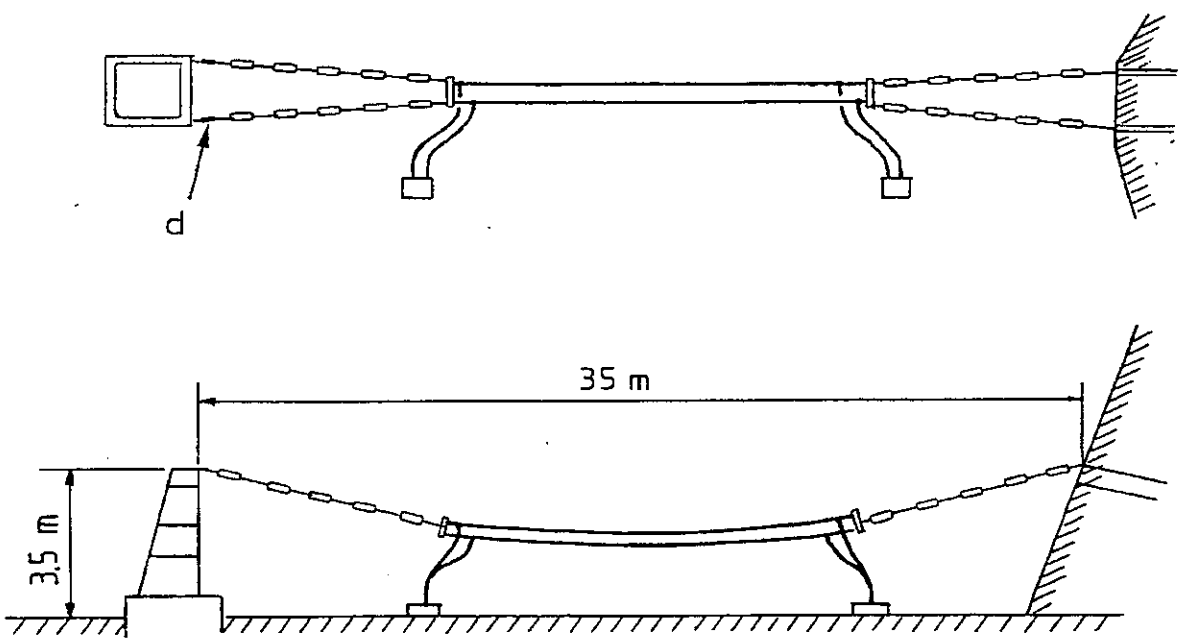

Fig. 16.1 Bus-bar geometry for bundle pinch test performed in Japan. d is a displacement transducer used in the results.

Supporting structure data :
stiffness at cable fixation point (N/m) : infinity (concrete bloc) ;
first eigen frequency : infinity.

contact address : The Furukawa Electric Electric Co. Ltd, Kiyotaki-Machi 500, Nikko City, Tochigi Pref., 321-14 , Japan (T. Yanagisawa, General Manager). Fax : +81-288-533572

Basic data

1) all connections

	material	section mm^2	mass kg/m	diameter (mm)
bus-bar	TAl (high temperature)	3x1600	3x4,44	52,1

bundle configuration :
spacing : 0,40 m; triple triangle (peak upwards); sub-span length : 2 m.

Insulating hardware (V chain)

insulator	length 2 (m)	mass2 (kg)
2 chains in V	7	320 per chain

2) initial conditions before testing :

sag (m)	tension (N)	test case
unknown	30000	3,2
unknown	15000	9

3) short-circuit characteristics :

kind of short-circuit (two or three-phase) : one-phase

	Irms (kA)	Ipeak (kA)	time constant (s)	duration (s)
first fault	63	164	0,060	very long

Results :

design values	measured	test case
Maximum pinch load	82000 after 20 ms	3,2
Maximum pinch load	60000 after 20 ms	9

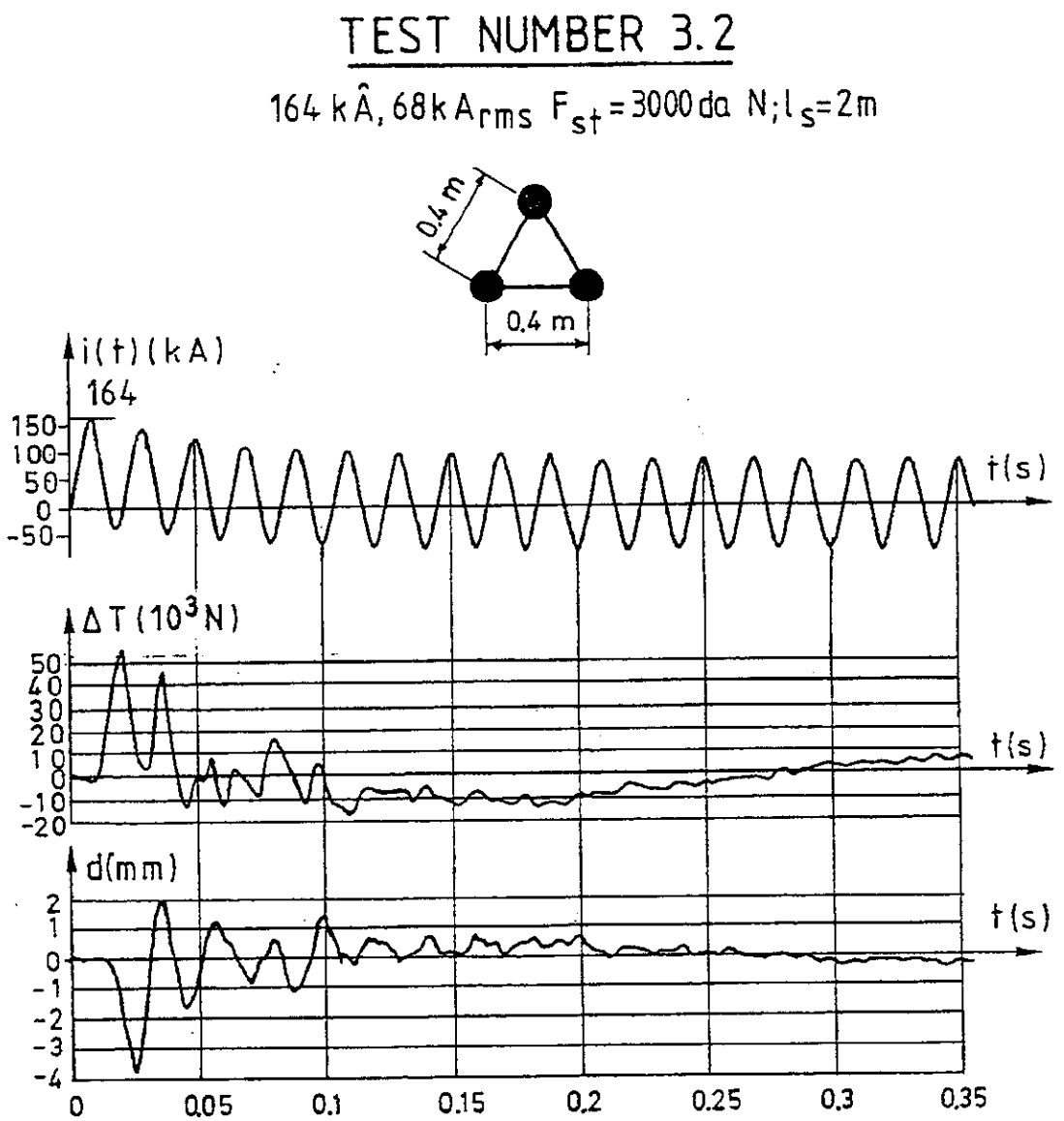

Fig. 16.2 Oscillograms for test results for Fst = 3000daN, ΔT for relative bundle pinch, d for relative displacement near anchoring level. (no contact observed)

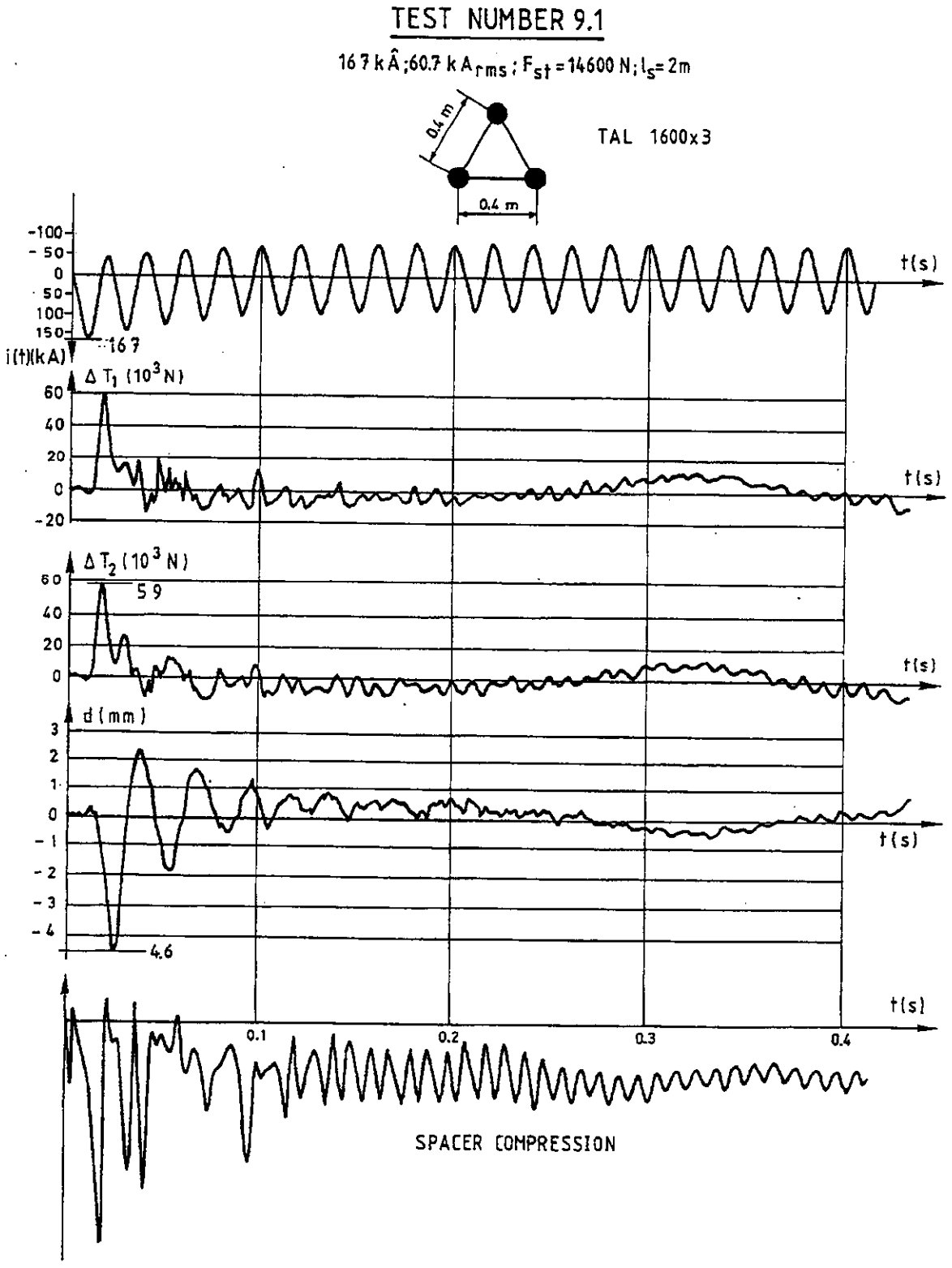

Fig. 16.3 Oscillograms of test results for 1460daN. ΔT in each subconductors, relative displacement near anchoring level and spacer compression (no scale available). (no contact observed)

PART 3 :

DROPPER CONFIGURATION

CASE 17

Test performed at FGH (Germany) in 1990
Case with end-dropper (single conductor)
cross section : ACSR 590 mm^2
short-circuit current : 20 ; 30 , 40 kA; 0,104 and 0,304 s
span length : 4 x 1,6 m (dropper length 4.9 m)

Geometry (the same for case 17 and 18)

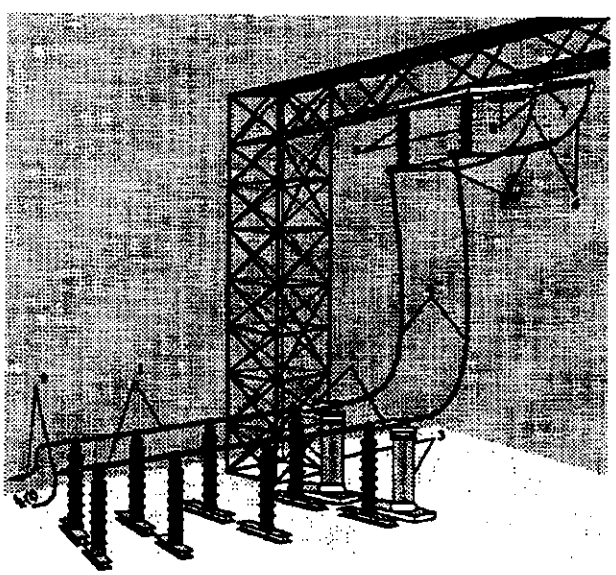

Fig. 17.1 Dropper geometry for FGH tests. 1. rigid pipe conductor, 2. mechanical decoupling, 3. post insulator, 4. dropper, 5. insulated spacer, 6. elliptical bow, 7. short-circuit connection, 8. rigid insulator, 9. feeder.

Supporting structure data :
stiffness at cable fixation point (N/m) : 2,1 to 2,5 10^6 N/m (Bottom insulator support, top one is supposed to be rigid)
frequencies (Hz) : 40 2,5 Hz ; logarithmic decrement of insulator support at 40 Hz : 5,5%
ATTENTION to angle bend at the top of the dropper. The connecting structure has been built as fully rigid.

contact address : FGH Mannheim, see case 5.
Other reference : G. Hosemann, A.M. Miri, N. Stein, E. Zeitler. *The behaviour of droppers in high voltage substations under short-circuit.* report 3.2 of the V th International Symposium on Short-circuit in Power Systems, held in Warsaw in 1992.

Basic data

1) all connections

	material	section mm^2	mass kg/m	diameter (mm)
bus-bar	ACSR	590	1,9	31,8

Insulating hardware : no insulator on the dropper.

dropper length : 4,9 meters
Centre line distance between phases : 2 m

2) initial conditions before testing : everything is defined by dropper length

3) short-circuit characteristics :

kind of short-circuit (two or three-phase) : two-phase

	Irms (kA)	Ipeak (kA)	time constant (s)	duration (s)	test number
first fault	20,2	52,3	0,050	0,104	74
first fault	20,2	52,3	0,050	0,304	75
first fault	28,2	71,5	0,050	0,104	80
first fault	28,3	71,7	0,050	0,304	82
first fault	39,8	98,9	0,050	0,104	86
first fault	39,8	98,5	0,050	0,304	87

Results :

design values

test case	74	75	80	82	86	87
Maximum force at the top of the insulator support where the dropper is fixed (X component) (kN)	1,0	0,95	1,84	1,87	3,37	3,66
Maximum force at the top of the insulator support where the dropper is fixed (Y component) (kN)	0,38	0,45	0,6	0,63	0,99	1,1

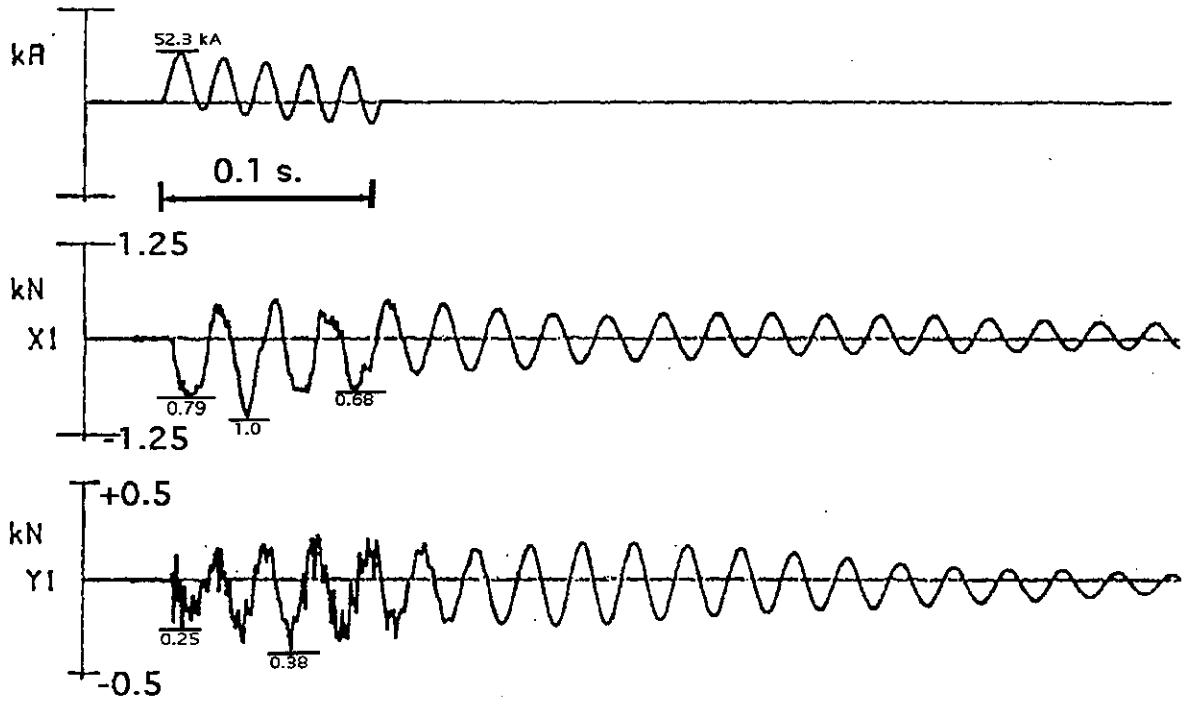

Fig. 17.2 Oscillograms of test number 74 (short-circuit wave shape, x and y components of the load applied to supporting insulator at thebottom side.

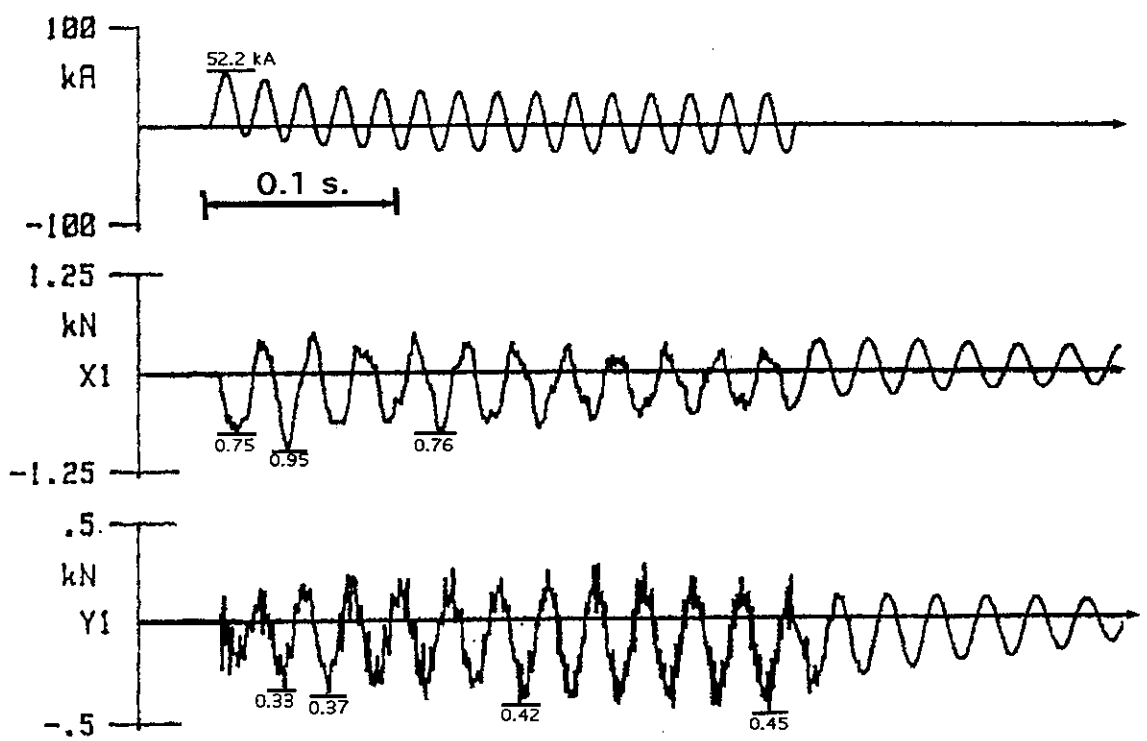

Fig. 17.3 Oscillograms of test number 75 (short-circuit wave shape, x and y components of the load applied to supporting insulator at the bottom side.

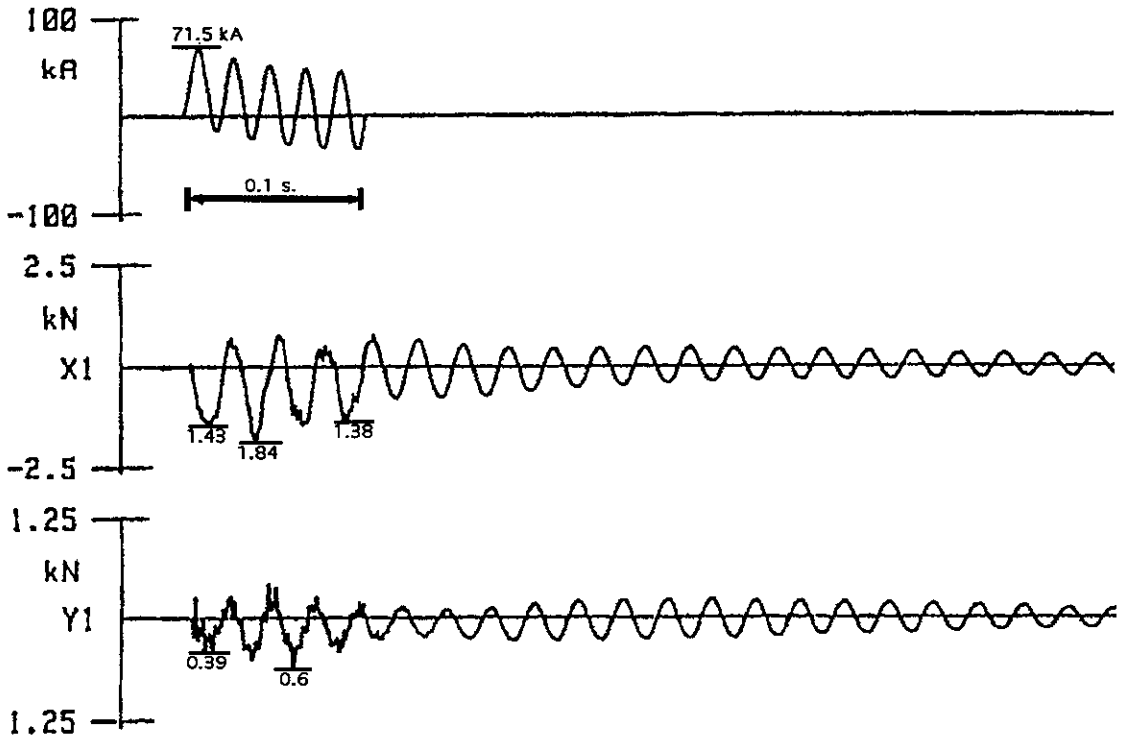

Fig. 17.3 Oscillograms of test number 80 (short-circuit wave shape, x and y components of the load applied to supporting insulator at the bottom side.

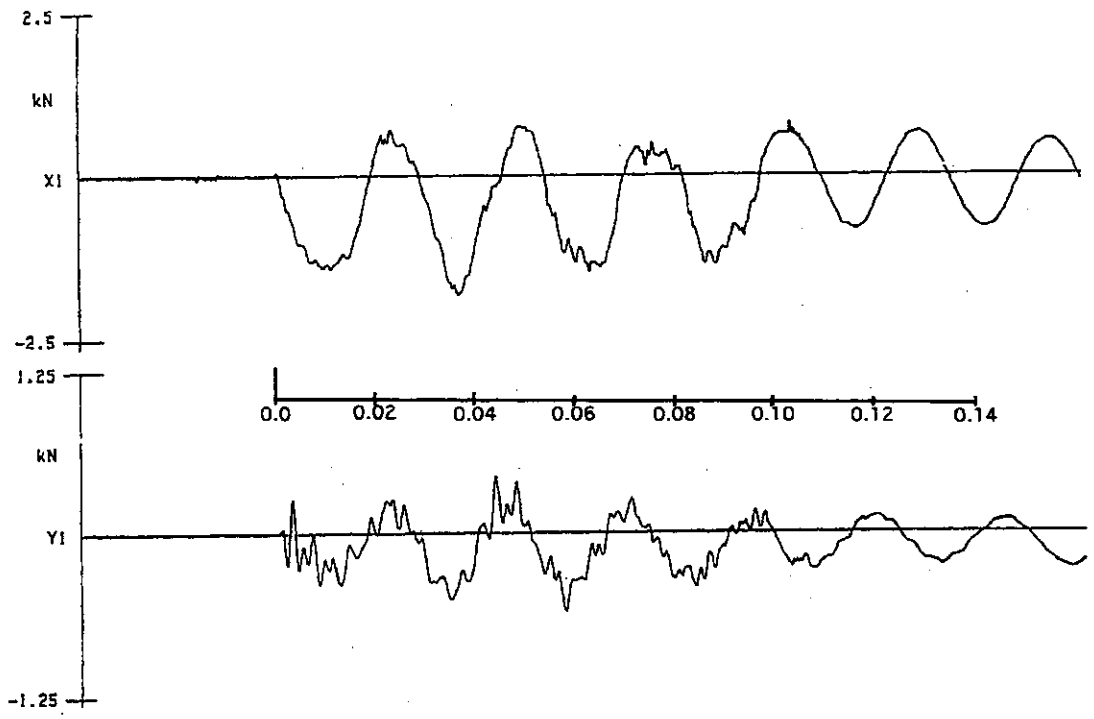

Fig. 17.4 Oscillograms of test number 80 - details of fig. 17.3- (x and y components of the load applied to supporting insulator at the bottom side.

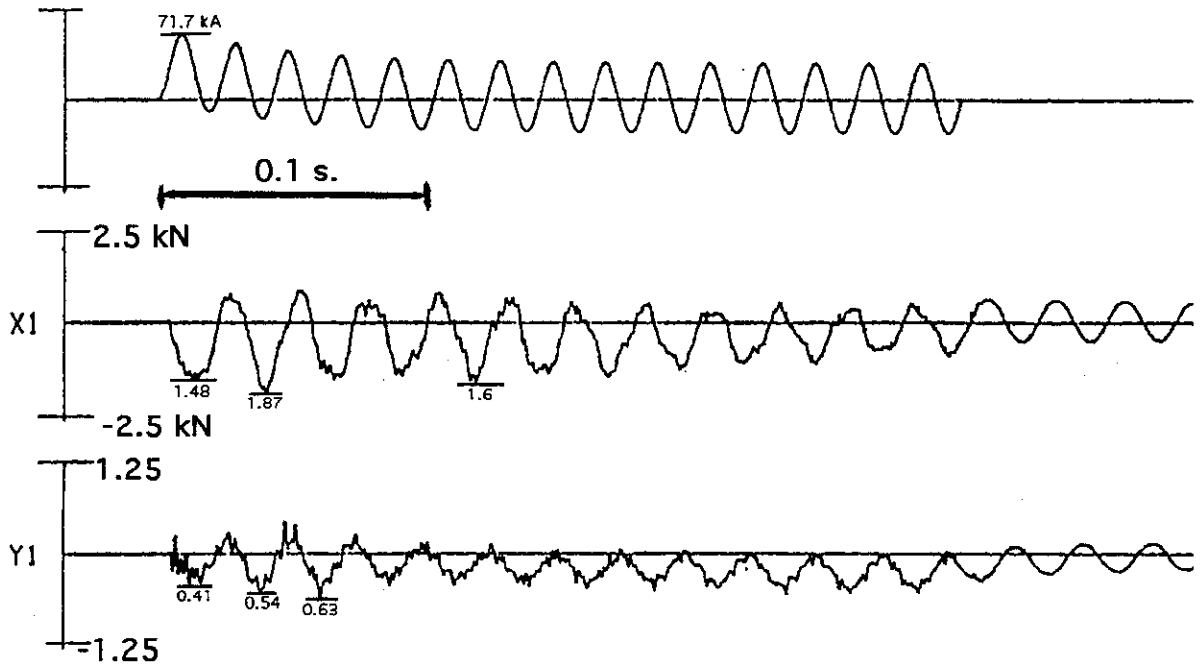

Fig. 17.5 Oscillograms of test number 82 - (short-circuit wave shape, x and y components of the load applied to supporting insulator at the bottom side.

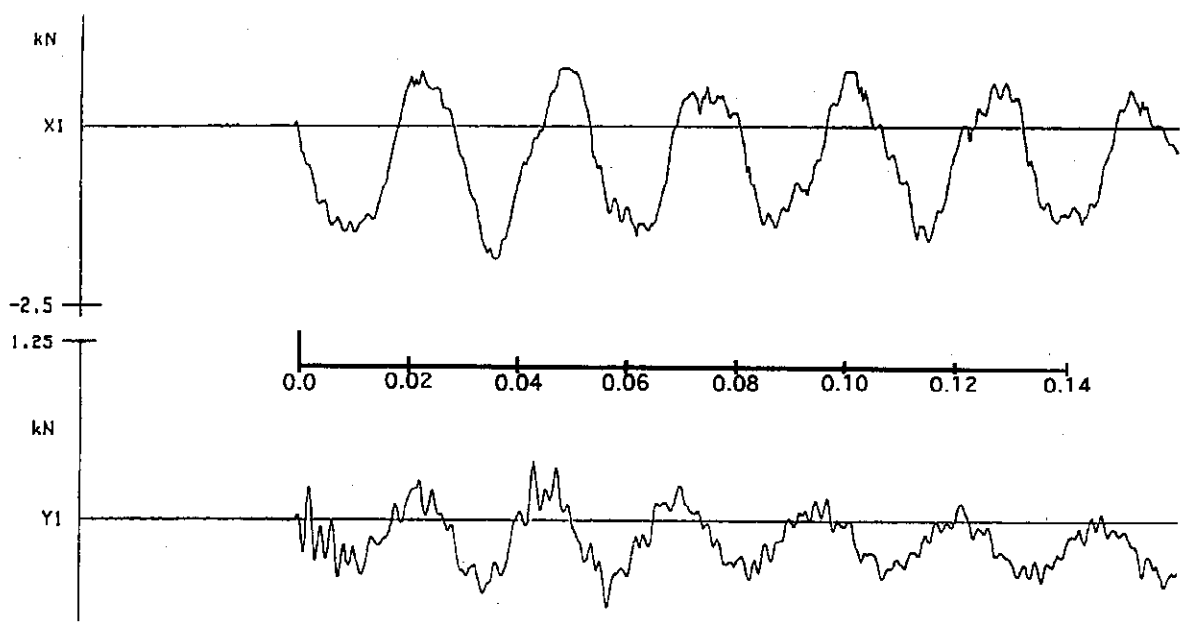

Fig. 17.6 Oscillograms of test number 82 - details of fig. 17.5- (x and y components of the load applied to supporting insulator at the bottom side.

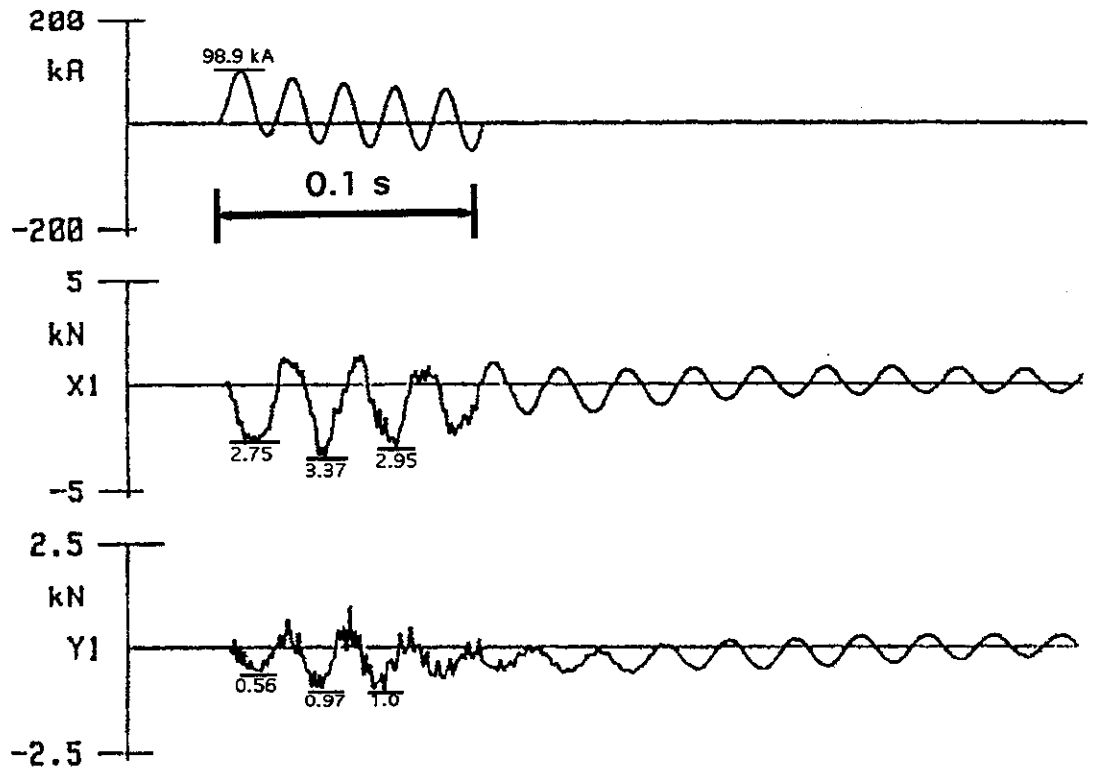

Fig. 17.7 Oscillograms of test number 86 - (short-circuit wave shape, x and y components of the load applied to supporting insulator at the bottom side.

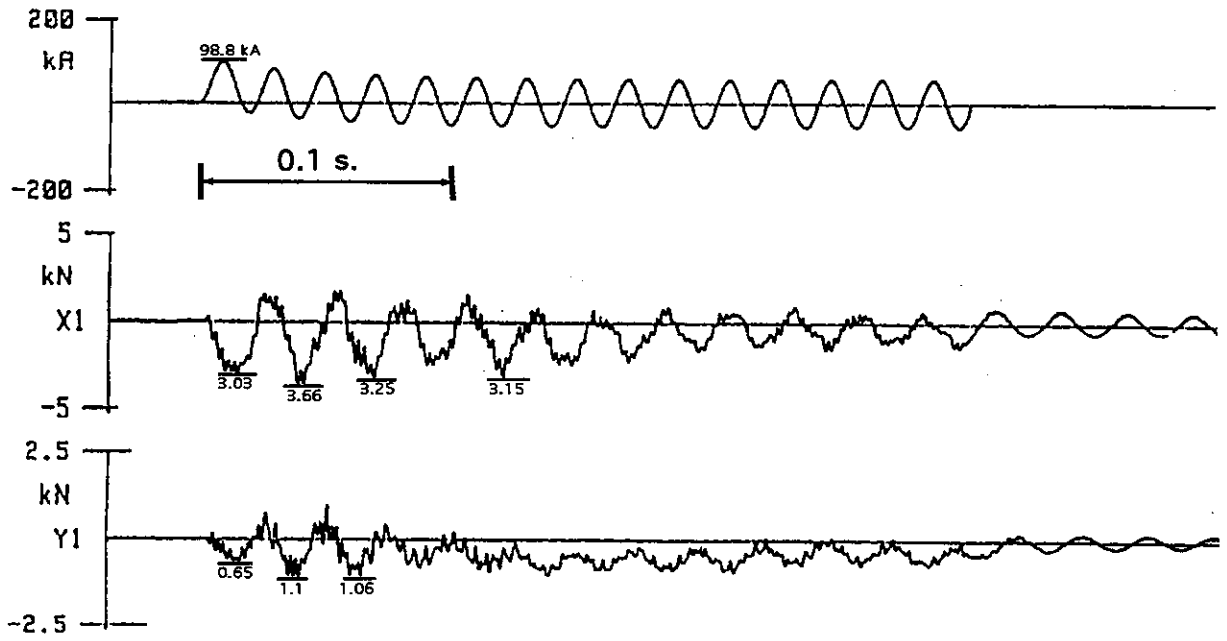

Fig. 17.7 Oscillograms of test number 87 - (short-circuit wave shape, x and y components of the load applied to supporting insulator at the bottom side.

CASE 18

Test performed at FGH (Germany) in 1990
Case with end-dropper (twin bundle)
cross section : ACSR 2x590 mm^2
short-circuit current : 20 ; 30 and 40 kA ; 0,104 and 0,304 s
span length : 7 x 3,2 m (dropper length 9 m)

Basic data

1) all connections

	material	section mm^2	mass kg/m	diameter (mm)
bus-bar	ACSR	2x590	2x1,9	31,8

Insulating hardware : no insulator on the dropper,

dropper length : 9,0 0,1 meters

bundle characteristics :
spacing : 0,06 m; twin horizontal bundle; two series of tests :
a) no spacer on phase 1, no spacer on phase 2 (tests 355, 358, 375)
b) no spacer on phase 1, 1 spacer on phase 2 (0,75 kg, at the middle of the dropper) (tests 351, 365, 372)

2) initial conditions before testing : everything is defined by dropper length

3) short-circuit characteristics :

kind of short-circuit (two or three-phase) : two-phase

	Irms (kA)	Ipeak (kA)	time constant (s)	duration (s)	test number
first fault	20,1	52,3	0,050	0,5	355 (no spacer)
first fault	28,2	71,8	0,050	0,5	358 (no spacer)
first fault	39,9	99,6	0,050	0,3	375 (no spacer)
first fault	20,1	52,2	0,050	0,1	351 (one spacer)
first fault	28,3	71,5	0,050	0,1	365 (one spacer)
first fault	40,0	100,4	0,050	0,1	372 (one spacer)

Results :

test case	355	358	375	351	365	372
Maximum force at the top of the insulator support where the dropper is fixed (X component) (kN)	1,8 after 18 ms	3,0 after 17 ms	4,2 after 15 ms	3,1 after 19 ms	3,4 after 17 ms	6,9 after 16 ms
Maximum force at the top of the insulator support where the dropper is fixed (Y component) (kN)	0,54 after 29 ms	0,6 after 18 ms	1,16 after 300 ms	0,57 after 30 ms	0,56 after 46 ms	1,1 after 16 ms

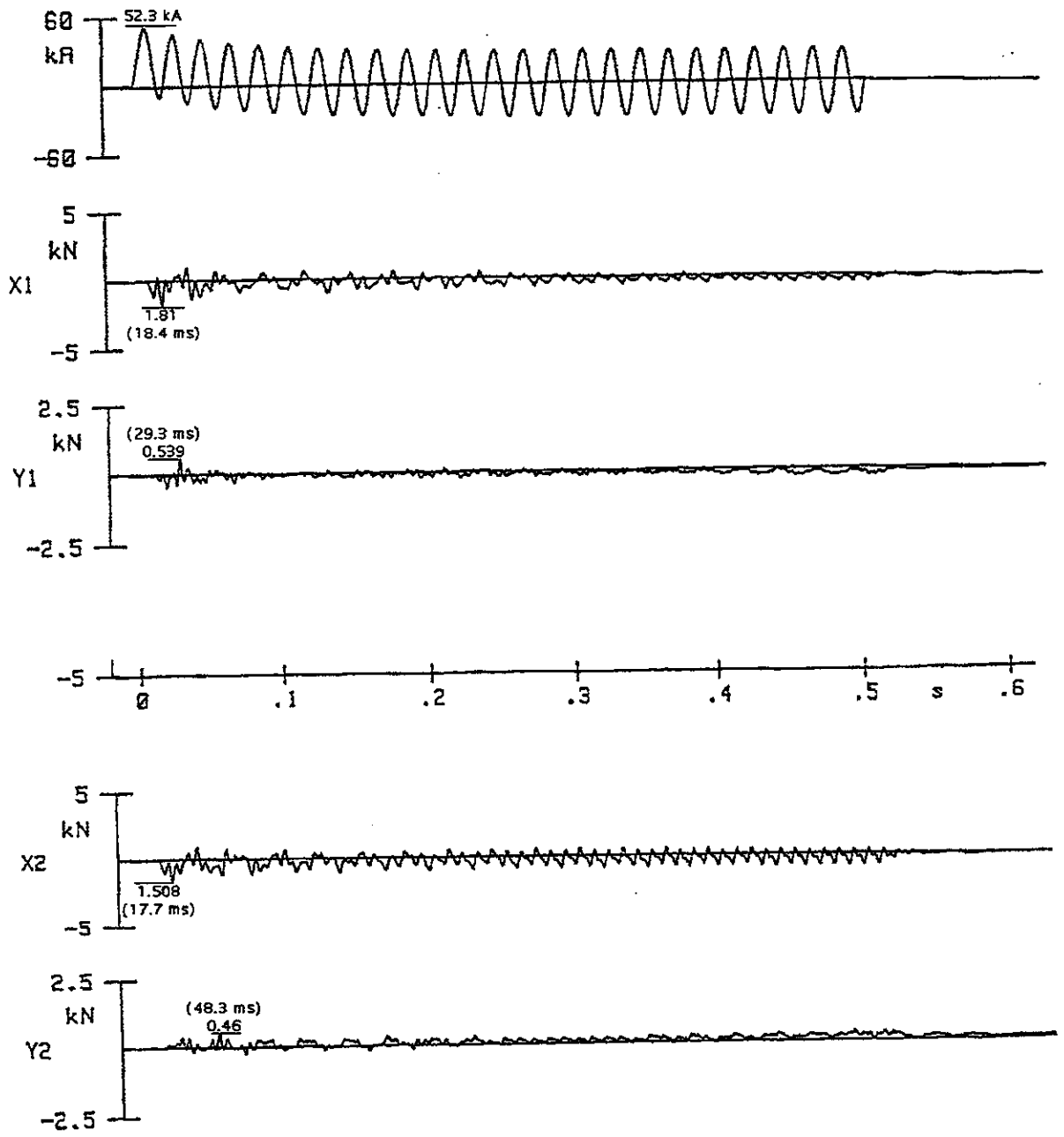

Fig. 18.1 Oscillograms of test number 355 - (short-circuit wave shape, x and y components of the load applied to supporting insulator at the bottom side for both phase.

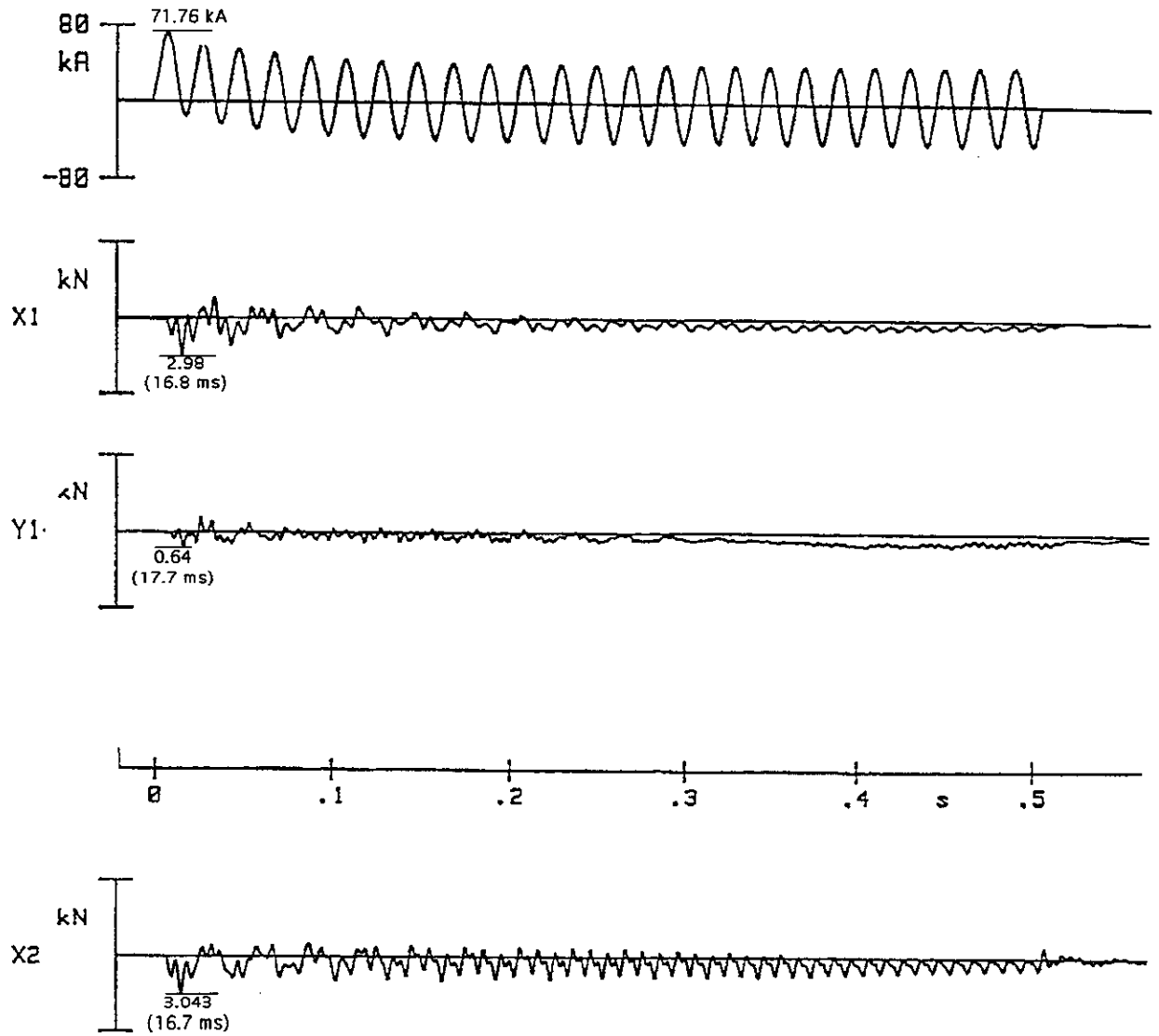

Fig. 18.2 Oscillograms of test number 358 - (short-circuit wave shape, x and y components of the load applied to supporting insulator at the bottom side for both phase.

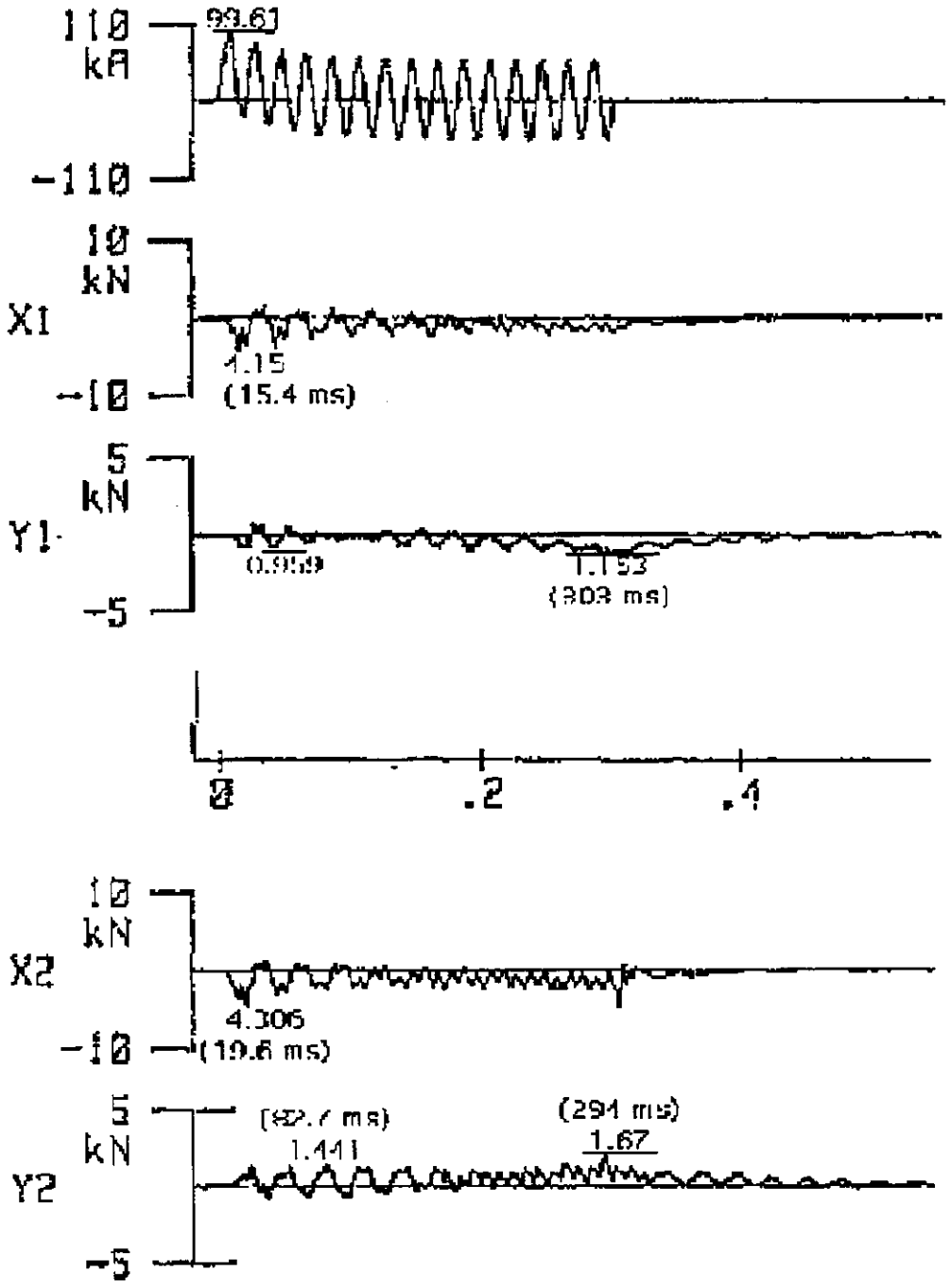

Fig. 18.3 Oscillograms of test number 375 - (short-circuit wave shape, x and y components of the load applied to supporting insulator at the bottom side for both phase.

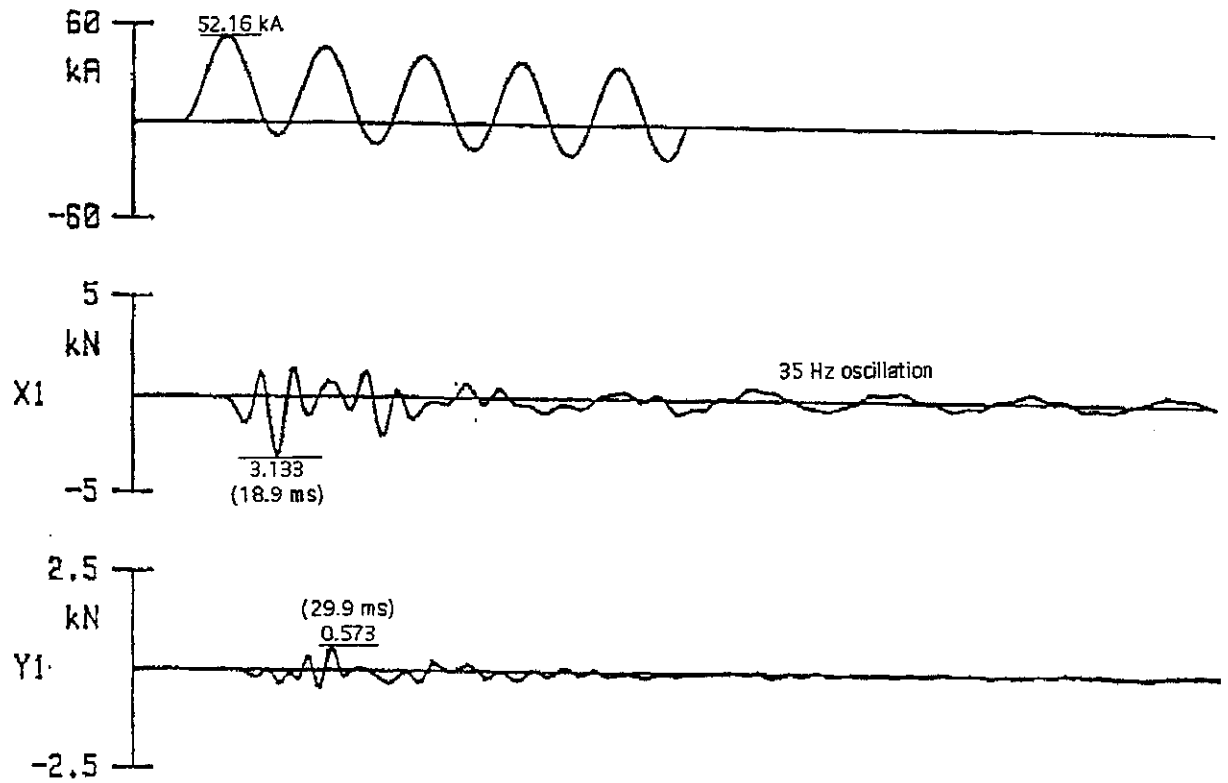

Fig. 18.4 Oscillograms of test number 351 - (short-circuit wave shape, x and y components of the load applied to supporting insulator at the bottom side for both phase.

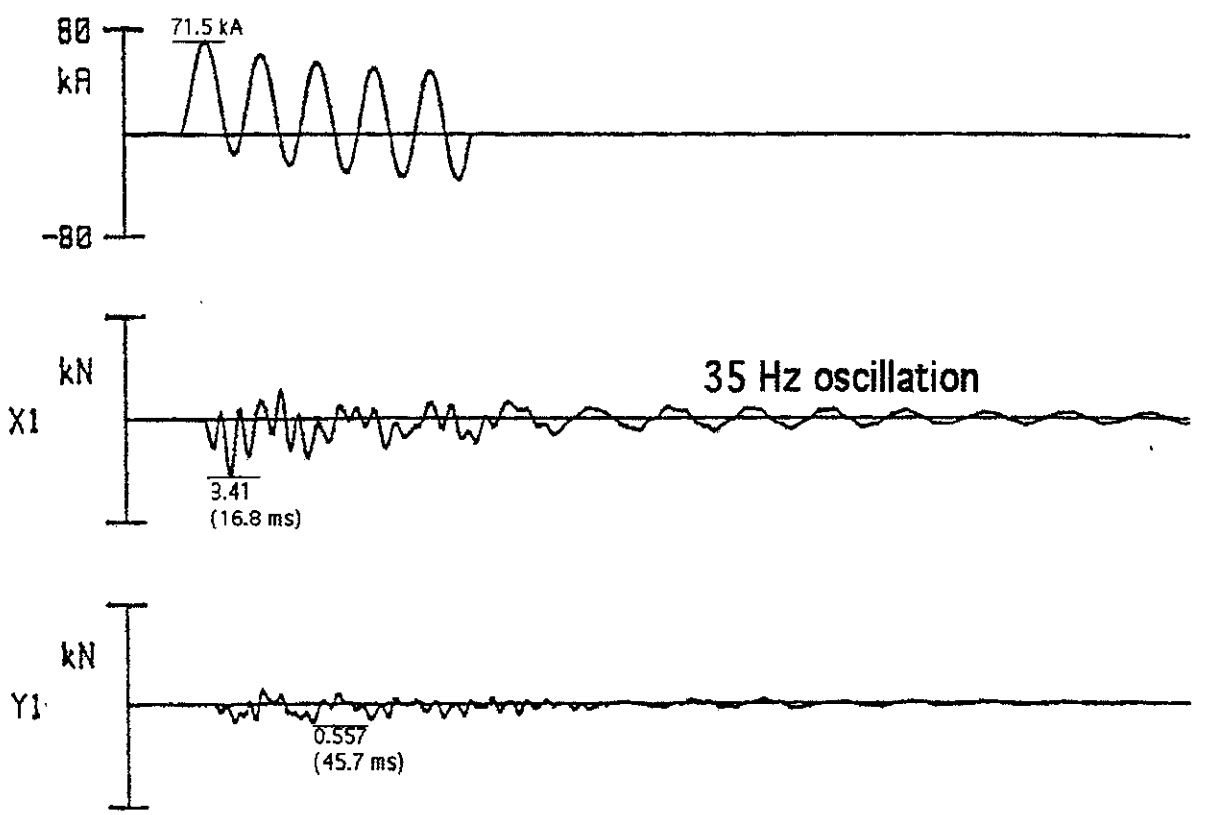

Fig. 18.5 Oscillograms of test number 365 - (short-circuit wave shape, x and y components of the load applied to supporting insulator at the bottom side for both phase.

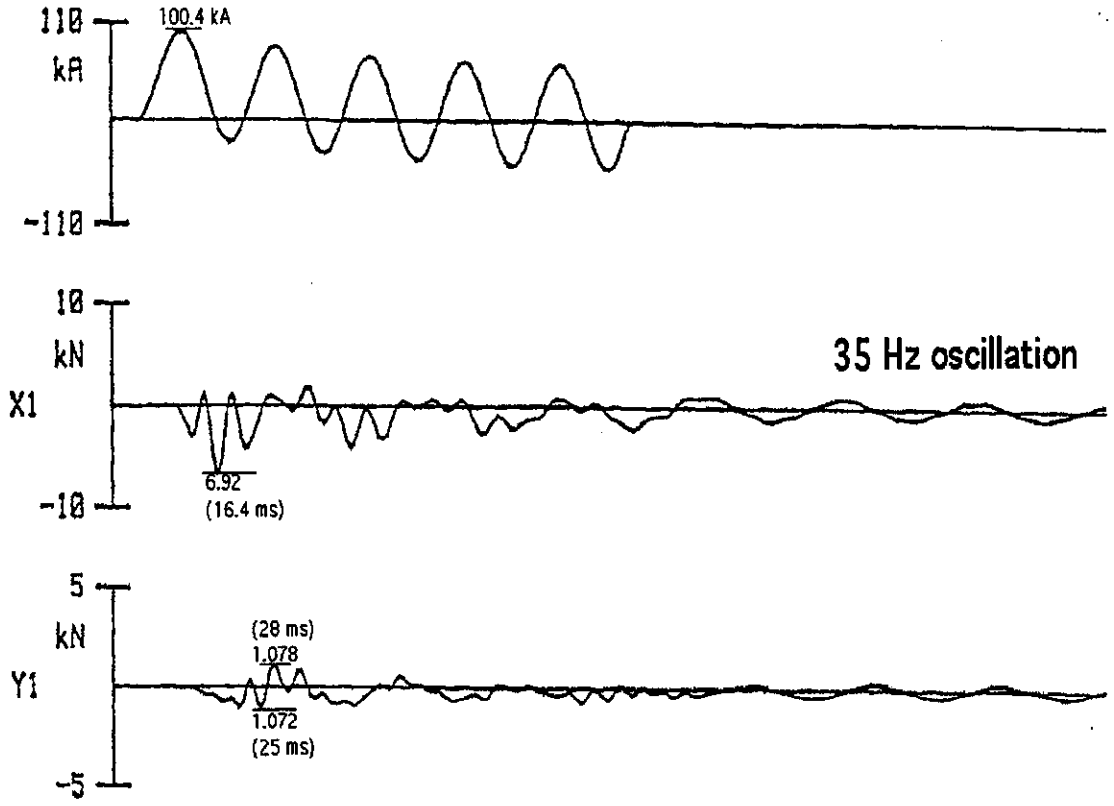

Fig. 18.6 Oscillograms of test number 372 - (short-circuit wave shape, x and y components of the load applied to supporting insulator at the bottom side for both phase.

ANNEX : TYPICAL DATA (CU, AL, ASTER, ACSR)

	Copper	Aluminium-alloy	ASTER and ACSR
resistivity 20°C (Ωxm)	$1{,}7\ 10^{-8}$	$3{,}4\ 10^{-8}$	$2{,}9\ 10^{-8}$
specific heat 20°C (J/kg/°C)	389	900	900
specific mass (kg/m^3)	8920	2700	2760
coeff. of resistivity variation with temp. ($°C^{-1}$)	0,00393	0,004	0,004
linear coefficient of expansion ($°C^{-1}$)	$16{,}8\ 10^{-6}$	$23{,}0\ 10^{-6}$	$23{,}0\ 10^{-6}$
typical Young modulus (N/m^2) for stranded cable	$12\ 10^{10}$	$6\ 10^{10}$	$6\ 10^{10}$

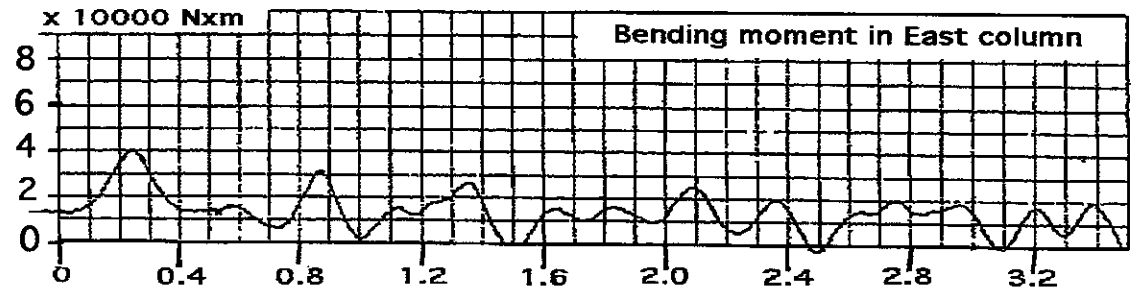

Fig. 7.7 : Bending moment in north-east column (measuring point 2 on fig. 4.2)

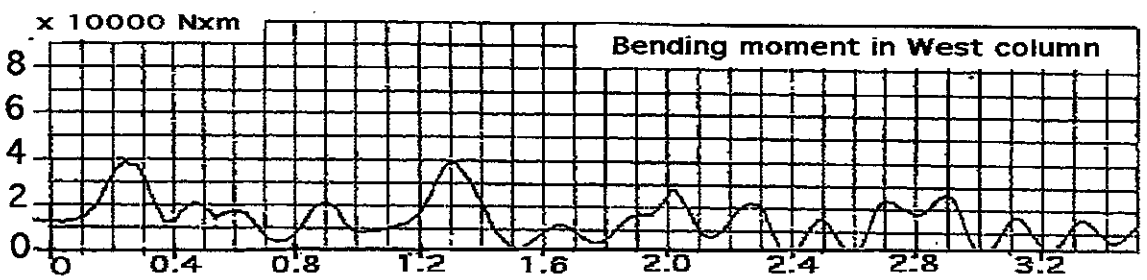

Fig. 7.8 : Bending moment in north-west column (measuring point 1 on fig. 4.2)

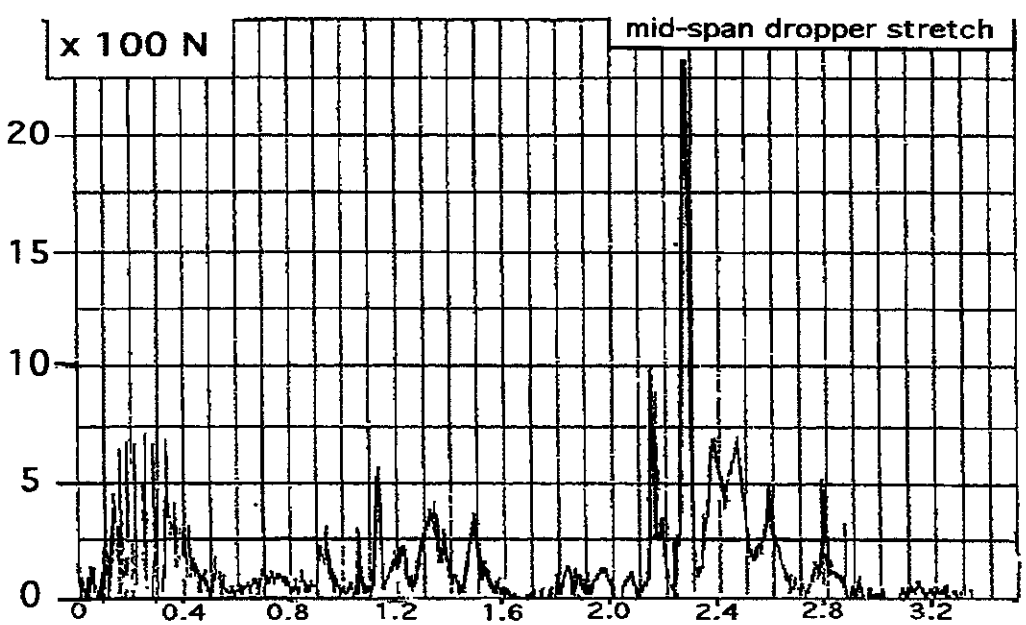

Fig. 7.9 : Mid-span dropper, tension-time evolution (measuring point 6 in fig. 4.2)

Le CIGRÉ a apporté le plus grand soin à la réalisation de cette brochure thématique numérique afin de vous fournir une information complète et fiable.

Cependant, le CIGRÉ ne pourra en aucun cas être tenu responsable des préjudices ou dommages de quelque nature que ce soit pouvant résulter d'une mauvaise utilisation des informations contenues dans cette brochure.

Publié par le CIGRÉ
21, rue d'Artois
FR-75 008 PARIS
Tél. : +33 1 53 89 12 90
Fax : +33 1 53 89 12 99

The greatest care has been taken by CIGRE to produce this digital technical brochure so as to provide you with full and reliable information.

However, CIGRE could in any case be held responsible for any damage resulting from any misuse of the information contained therein.

Published by CIGRE
21, rue d'Artois
FR-75 008 PARIS
Tel : +33 1 53 89 12 90
Fax : +33 1 53 89 12 99